California Solar Initiative

RD&D: Research, Development, Demonstration and Deployment Program

GO solar CALIFORNIA

Final Project Report:

Development and Analysis of a Progressively Smarter Distribution System

Grantee:

Advanced Power and Energy Program

University of California, Irvine

March 2013

www.CalSolarResearch.ca.gov

PREPARED BY

Advanced Power and Energy Program

University of California
Irvine, CA 92697-3550
949-824-5468

Principal Investigator:
Professor Scott Samuelsen, Director
gss@apep.uci.edu

Professor Jack Brouwer, Associate Director
jb@apep.uci.edu

Project Partners:
Pacific Gas & Electric

PREPARED FOR

California Public Utilities Commission
California Solar Initiative: Research, Development, Demonstration, and Deployment Program

CSI RD&D PROGRAM MANAGER

Itron CSI RD&D Program Manager

Program Manager:
Ann Peterson
Ann.Peterson@itron.com

Project Manager:
Jonathan Wanjiru
Jonathan.Wanjiru@itron.com

Additional information and links to project related documents can be found at
http://www.calsolarresearch.ca.gov/Funded-Projects/

Preface

The goal of the California Solar Initiative (CSI) Research, Development, Demonstration, and Deployment (RD&D) Program is to foster a sustainable and self-supporting customer-sited solar market. To achieve this, the California Legislature authorized the California Public Utilities Commission (CPUC) to allocate **$50 million** of the CSI budget to an RD&D program. Strategically, the RD&D program seeks to leverage cost-sharing funds from other state, federal and private research entities, and targets activities across these four stages:

- Grid integration, storage, and metering: 50-65%
- Production technologies: 10-25%
- Business development and deployment: 10-20%
- Integration of energy efficiency, demand response, and storage with photovoltaics (PV)

There are seven key principles that guide the CSI RD&D Program:

1. **Improve the economics of solar technologies** by reducing technology costs and increasing system performance;
2. **Focus on issues that directly benefit California**, and that may not be funded by others;
3. **Fill knowledge gaps** to enable successful, wide-scale deployment of solar distributed generation technologies;
4. **Overcome significant barriers** to technology adoption;
5. **Take advantage of California's wealth of data** from past, current, and future installations to fulfill the above;
6. **Provide bridge funding** to help promising solar technologies transition from a pre-commercial state to full commercial viability; and
7. **Support efforts to address the integration of distributed solar power into the grid** in order to maximize its value to California ratepayers.

For more information about the CSI RD&D Program, please visit the program web site at www.calsolarresearch.ca.gov.

Table of Contents

1. Abstract 4
2. Executive Summary 4
3. Introduction 6
4. Project Objectives 7
   - 4.1 Task 1: Project Management 7
   - 4.2 Task 2: Model Development and Evaluation 8
   - 4.3 Task 3: Quantify PV Integration Limits 8
   - 4.4 Task 4: Advanced Inverter Control 8
   - 4.5 Task 5: Integrated Distribution Grid Control 8
   - 4.6 Task 6: Practical Feasibility and Outreach 8
5. Project Approach 8
   - 5.1 Task 1: Project Management 9
   - 5.2 Task 2: Model Development and Evaluation 10
   - 5.3 Task 3: Quantify PV Integration Limits 11
   - 5.4 Task 4: Advanced Inverter Control 12
   - 5.5 Task 5: Integrated Distribution Grid Control 13
   - 5.6 Task 6: Practical Feasibility and Outreach 14
6. Project Outcomes 14
   - 6.1 Task 2: Model Development and Evaluation 14
     - 6.1.1 Distribution Circuits 15
     - 6.1.2 Circuit Model Methodology 19
     - 6.1.3 Circuit Model Development 47
   - 6.2 Task 3: Quantify PV Integration Limits 55
     - 6.2.1 Conceptual Background 56
     - 6.2.2 Results 82
     - 6.2.3 Summary 115
   - 6.3 Task 4: Advanced Inverter Controls 116
     - 6.3.1 Inverter-Based Generation 116
     - 6.3.2 Approach 122

6.3.3 Results 142
6.4 Task 5: Integrated Distribution Grid Control 150
6.4.1 Steady State Results to T3 Fixes 151
6.5 Task 6: Practical Feasibility and Outreach 173
7. Conclusions 173
8. Public Benefits to California 176
9. Acknowledgements 177
10. References 178
11. Appendices 179
11.1 Appendix A: Sub-Station Supervisory Control and Data Acquisition (SCADA) Measurement Evaluation for Cayetano and Menlo Circuits 179
11.2 Appendix B: Commercial (Cayetano 2111) Model Settings 183
11.3 Appendix C: Residential (Menlo 1102) Model Settings 203
11.4 Appendix D: Acronyms 218

1. Abstract

This project is collaboration between the Advanced Power and Energy Program (APEP) at the University of California, Irvine (UCI) and Pacific Gas & Electric (PG&E). The goals of the project are to utilize modeling and simulation to:

- Quantify PV integration limitations.
- Develop and evaluate progressively smarter distribution systems.

Five tasks have been established to meet the project goals:

1. Develop, tune, and verify distribution circuit models with monitored field data,
2. Quantify PV integration limits for typical distribution circuits,
3. Evaluate the feasibility to utilize advanced PV inverters to alleviate PV integration limits,
4. Develop and evaluate integrated control strategies to support the increased penetration of PV in the distribution system, and
5. Evaluate the practical feasibility of the relevant standards, hardware, and communications needed to enable progressively smarter distribution systems.

This research provides the needed information and understanding regarding (1) modeling methodology to evaluate PV installation on distribution circuits, (2) PV penetration limitations and tradeoffs, (3) control strategies and communication advances that may be required to achieve different levels of PV penetration, and (4) regulatory and technology barriers. The project evaluates the control and integration of existing major components on both the primary and secondary distribution system. Two specific distribution system configuration scenarios are evaluated; one with many smaller PV installations, and a second with fewer larger PV installations. The project identifies PV integration limitations of standard operating procedure and develops a progressively smarter distribution system to mitigate distribution circuit limitations that might otherwise hinder the California Solar Initiative goal of installing 3,000 MW of new electricity generation from solar energy by 2017.

2. Executive Summary

This research aims to quantify PV integration limitations and develop and evaluate progressively smarter distribution systems. Five tasks have been established to meet the project goals:

1. Develop, tune, and verify distribution circuit models with monitored field data,
2. Quantify PV integration limits for typical distribution circuits,
3. Evaluate the feasibility to utilize advanced PV inverters to alleviate PV integration limits,
4. Develop and evaluate integrated control strategies to support the increased penetration of PV in the distribution system, and
5. Evaluate the practical feasibility of the relevant standards, hardware, and communications needed to enable progressively smarter distribution systems.

A collection of experts has been established to provide the necessary guidance and engineering insights to successfully and practically quantify PV integration limitations as well as to develop and evaluate progressively smarter distribution systems. The APEP project team is led by Professor Scott Samuelsen in collaboration with Professor Keyue Smedley. Both Professor Scott Samuelsen and Professor Keyue

Smedley co-advise graduate students and staff. PG&E provides professional guidance and a practical perspective and the overall relevance of the distribution system models are assessed through regular communication and feedback with PG&E. Identifying the operation limitations and characteristics of a commercial (Cayetano) and a residential (Menlo) circuit with high penetration PV is the primary objective of this research. Each circuit was evaluated using a three phase balanced feeder model developed and calibrated using circuit description and measurement information. High-Pen PV was evaluated by varying PV generation on the circuit in penetration and distribution.

Studies have yielded interesting and informative results. Important highlights of results are summarized below. With regard to primary feeder voltage profile evaluation:

1. The majority of the simulation scenarios did not feature out of standard voltages at the primary feeder as penetrations increased with the exception of the Menlo End and Menlo Beginning generation distribution scenarios.
    - **a.** The Menlo End distribution scenarios demonstrated out-of-standard high voltages induced by PV generation for all evaluated PV penetrations.
    - **b.** The Menlo Beginning distribution scenarios demonstrated out-of-standard low voltage conditions for evaluated penetrations greater than 40%.
2. The out-of-standard voltages issue may be remedied by addressing circuit impedance, bus siting evaluation, and the application of voltage regulation equipment.

Regarding high penetration PV interactions with existing voltage regulation and substation equipment:

1. High-Pen PV had a marginal impact on capacitor switching. Only two of the 160 simulated Cayetano circuit scenarios showed a change in capacitor switching in the PV region.
2. PV generation in the circuit causes the sub-station LTC with LDC control to lower the circuit voltage via tapping. The LDC operation was simulated for the entire year, and both the Cayetano and Menlo circuits show increases in yearly tap position changes increase with penetration.
3. It was observed in both the Cayetano and Menlo simulation scenarios that sub-station power factor decreases (leading or lagging) as PV penetration increases.
4. Unnecessary capacitor switching for reactive power or voltage regulation by Time-Clock switching controls aggravated the decrease in sub-station power factor. Capacitor switching controls that utilize system feedback could prevent the unnecessary capacitor switching aggravating the sub-station power factor.

The incorporation of advanced inverter controls has been shown to improve grid reliability, operation, and stability by implementing ancillary features utilizing existing inverter technology.

1. Volt/VAR control has been shown to improve the transient voltage regulation performance of distribution circuits with high penetration PV in the presence of load and insolation transients.
2. Multi-inverter instabilities among closely coupled volt/VAR enabled inverters at the distribution level may occur. This may be remedied through the use of communications systems.
3. Active power filtering may prove beneficial in reducing distribution level harmonic distortion.
4. Advanced control inverters show minimal detrimental interaction with hard-switched voltage regulation equipment.

The Menlo Beginning generation distribution scenario was observed to have non-standard low voltages in the PV region for penetration greater than 40%. The low voltage occurred on a 4.16kV section of the Menlo circuit. To address the voltage issue three approaches were proposed:

1. By raising the system voltage from 4.16kV to 12.47kV for the low voltage prone section, the low voltage condition was improved from 40% to 90% penetration.
2. The fixed step-down transformer was replaced with a Line Regulator.
3. The LDC controls of the Load Tap Changing (LTC) transformer were modified using LDC Current Compensation controls.

This research contributed to the development and understanding of a proposed progressively smarter distribution system. Smarter distribution systems will improve the economics of solar PV implementation by (1) reducing the need for costly ad hoc load flow studies to determine whether the PV installation creates unacceptable circuit conditions, (2) increasing the value of PV installations by enabling ancillary services such as active power filtering and controlled reactive power support, and (3) improving circuit efficiency and equipment lifetime as a result of those services.

3. Introduction

The project approach is designed to evaluate and develop the requirements for interconnecting a high penetration of solar PV with a progressively smarter distribution system. A major California research center (APEP), in close collaboration with a major California utility (PG&E), will develop realistic and comprehensive models of distribution systems and systematically apply various PV installation scenarios using different levels of communication and control. Two distribution system configuration scenarios will be modeled that each considers both primary and secondary circuits: (1) a residential circuit with many small PV installations, (2) a commercial circuit with a few large PV installation. In the cases without control, this method will identify PV limits and barriers to widespread implementation by quantifying changes in voltage and power flow, as well as power quality concerns, such as harmonics and voltage sags and swells. The resultant fundamental understanding of the constraint violations and instigating phenomena will then lead to a progressive series of control strategies that start with advanced inverter control and then expand to integrated distribution system controls with communication. Potential problems will be documented, and minimum requirements to enable any control strategies will be evaluated for each scenario evaluated at different PV penetration levels. Guidelines for the progressive deployment of distribution systems with increased PV penetration will be suggested. The practical feasibility of developed concepts will be evaluated both in terms of technology and policy.

Major insights of the projects are projected in four major areas: modeling methodology, understanding of PV penetration limits, inverter and integrated system advances, and the identification of regulatory and technology barriers. No new technology will be physically developed or demonstrated, instead, the project will provide understanding and knowledge required to adequately address increased PV penetration on distribution systems. The proposed effort will evaluate the challenge of integrating PV distributed generation from a fundamental perspective, but the collaborative team will maintain a strong and essential focus on practical reality and feasibility of concepts proposed.

The net result of the approach is to (1) develop strategies needed to accommodate an increased penetration of renewable resources, (2) identify the pathways to facilitate an efficient and more rapid deployment of renewables than will otherwise occur, and (3) provide a paradigm shift in understanding

the challenges and needs on both the utility and academic research cornerstones associated with an enhanced deployment of renewables in the State of California.

4. Project Objectives

Project performance objectives are established based on feedback and distribution system performance requirements. The primary criterion for success is whether the PV implementation causes an adverse effect, no effect, or a beneficial effect on the primary and secondary distribution system. The adverse effect will create a PV penetration limit, and this condition should be avoided where possible and increased where inevitable. Cases with no effect are fine, but cases with a beneficial effect are the most desirable as they not only allow PV, but increase the economic benefit by providing utility and customer services.

These distribution system requirements have performance objectives implications for each of the project tasks as follows:

4.1 Task 1: Project Management

The purpose of this task is to ensure that all products and deliverables in the statement work are complete.

A collection of experts has been established to provide the necessary guidance and engineering insights to successfully and practically quantify PV integration limitations as well as to develop and evaluate progressively smarter distribution systems. The budgeted amount of time of each individual reflects the amount of daily work.

The APEP project team is led by Professor Scott Samuelsen in collaboration with Professor Keyue Smedley. Both Professor Scott Samuelsen and Professor Keyue Smedley co-advise graduate students and staff. Professor Samuelsen manages the project and interactions between APEP, PG&E and the CPUC and makes sure the project remains on time, with proper resources and outreach. Professor Smedley provides electrical engineering expertise and ensures the use of appropriate resources, up-to-date standards. A principal research staff on the team is Dr. Fabian Mueller, an expert in energy system controls and complex energy system integration and a lead in the APEP Renewable-Based Energy Secure community project. He provides leadership in the control development and assures that the results are relevant to future energy scenarios that will integrate diverse renewable and supporting advanced energy resources to meet the states renewable portfolio standards. Two graduate students complete the APEP project team. The graduate students are responsible for the APEP modeling and bring the combination of mechanical and electrical engineering expertise to evaluate the management of distribution circuit with high penetration of distributed generation.

PG&E will provide professional guidance and a practical perspective on progressively smarter distribution circuit control strategies to be developed. Through PG&E participation the practical feasibility and usefulness of the project will be ensured.

4.2 Task 2: Model Development and Evaluation

This performance objective is to accurately capture the behavior of the realistic distribution circuits: residential and commercial. The circuit voltage magnitude, frequency and imbalance as well as load imbalance and power factor are modeled within 10% of distribution standards. For example, if a 5% overshoot on voltage is acceptable, then the model voltage accuracy must be within 0.5% of the measured voltage or within 0.6 volts on a 120 volt secondary. The overall relevance of the distribution system models are assessed through regular communication and feedback with PG&E.

4.3 Task 3: Quantify PV Integration Limits

All phenomena that can directly or indirectly cause a distribution system to operate outside operating requirements at high PV penetrations are identified. PV penetration levels that cause the distribution system to violate operating requirements are quantified for the specific distribution configuration scenarios under current standard operating conditions as follows: (1) many small PV installations, (2) few large PV installations.

4.4 Task 4: Advanced Inverter Control

The effectiveness of advanced inverter control is assessed based on the ability to increase PV penetration limits while maintaining acceptable system conditions. Each capability—active power filter, reactive power control, and real power control—are evaluated individually to understand their fundamental effect. Inverter control strategies that can expand PV integration limits are quantified and evaluated in the scenarios previously discussed.

4.5 Task 5: Integrated Distribution Grid Control

Advanced inverter control strategies along with communication and simultaneous control of other circuit resources such as capacitors are progressively evaluated to enable 0 to 100% PV penetration for the scenarios identified. Performance improvements of proposed strategies are progressively quantified with cost and complexity.

4.6 Task 6: Practical Feasibility and Outreach

Guidelines for the progressive deployment of smarter distribution system with increased PV penetration are developed for each of the scenarios proposed to maintain the entire circuit within operating requirements. The practical feasibility, complexity, and required technology upgrade for each progressive improvement suggested are evaluated. Technology and regulatory barriers and suggested modifications are identified and explained.

4.7 Project Approach

The project approach is designed to evaluate and develop the requirements for interconnecting a high penetration of solar PV with a progressively smarter distribution system. A major California research center (APEP), in close collaboration with a major California utility (PG&E), have developed realistic and

comprehensive models of distribution systems and systematically applied various PV installation scenarios using different levels of communication and control. Two distribution system configuration scenarios are modeled that each consider both primary and secondary circuits: (1) a residential circuit with many small PV installations, (2) a commercial circuit with a few large PV installations. In the cases without control, this method identifies PV limits and barriers to widespread implementation by quantifying changes in voltage and power flow, as well as power quality concerns, such as harmonics and voltage sags and swells. The resultant fundamental understanding of the constraint violations and instigating phenomena then leads to a progressive series of control strategies that start with advanced inverter control and then expands to integrated distribution system controls with communication. Potential problems are documented, and minimum requirements to enable any control strategies are evaluated for each scenario evaluated at different PV penetration levels. Guidelines for the progressive deployment of distribution systems with increased PV penetration are suggested. The practical feasibility of developed concepts is evaluated both in terms of technology and policy.

Major insights of the projects are projected in four major areas: modeling methodology, understanding of PV penetration limits, inverter and integrated system advances, and the identification of regulatory and technology barriers. No new technology are physically developed or demonstrated, instead, the project provides understanding and knowledge required to adequately address increased PV penetration on distribution systems. The effort evaluates the challenge of integrating PV distributed generation from a fundamental perspective, but the collaborative team maintains a strong and essential focus on practical reality and feasibility of concepts proposed.

The net result of the approach is to (1) develop strategies needed to accommodate an increased penetration of renewable resources, (2) identify the pathways to facilitate an efficient and more rapid deployment of renewables than will otherwise occur, and (3) provide a paradigm shift in understanding the challenges and needs on both the utility and academic research cornerstones associated with an enhanced deployment of renewables in the State of California.

4.8 Task 1: Project Management

APEP will conduct the modeling and simulation in collaboration with PG&E. The collaboration is anchored by quarterly leadership meetings and recurrent and sustained communication between PG&E and APEP project staff. PG&E provides (1) insight into standard utility methods, (2) operational and model data, and (3) designs and practice in order to assure that the APEP analyses are based on accurate assumptions and that the proposed control methods and communications strategies are viable and practical, and can be implemented within the existing electric utility industry.

The project is a two-year study estimated at a cost of $400K with $20K UCI and $80K PG&E match fund. PG&E's match funding are provided in the form of in-kind contributions (e.g., employee time) and the support associated with the provision of data. A summary of the project technical and proposal scoring criteria can be found in the appendix. The net result of the project is to (1) develop strategies needed to accommodate an increased penetration of renewable resources, (2) identify the pathways to facilitate an efficient and more rapid deployment of renewables than will otherwise occur, and (3) a provide a paradigm shift in the understanding of the challenges and needs on both the utility and academic research cornerstones associated with an enhanced deployment of renewables in the State of California.

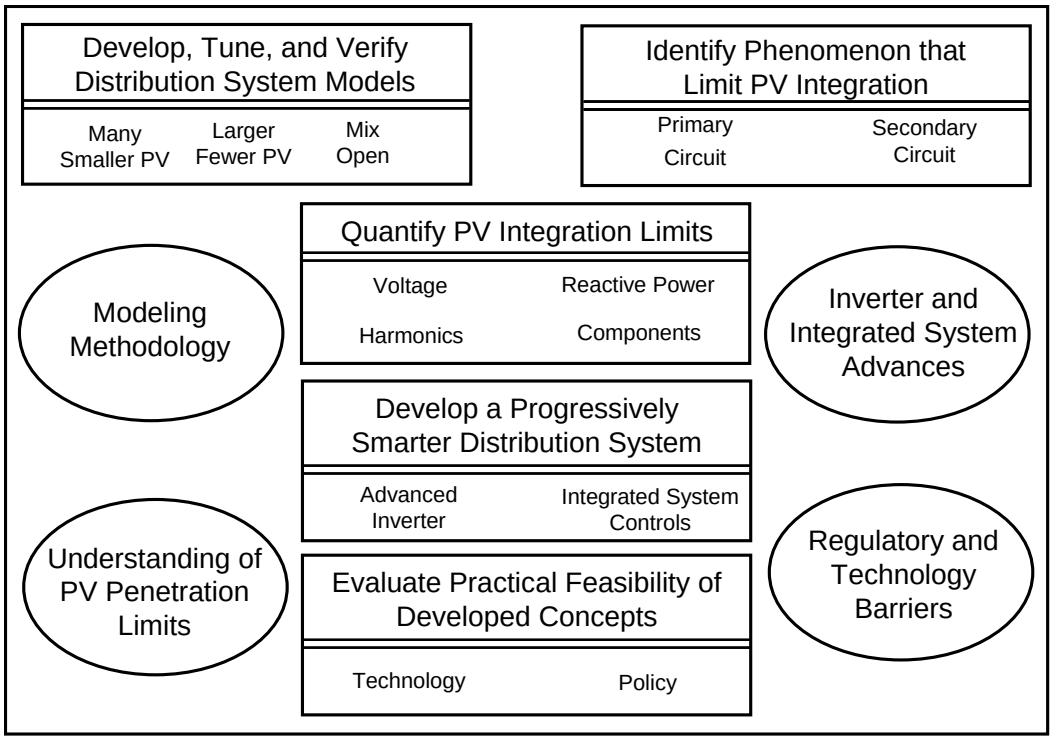

Figure 1. Project approach and projected major insights.

4.9 Task 2: Model Development and Evaluation

Goal: Develop, tune, and verify distribution circuit models with monitored field data.

Task Summary: In this task, two specific circuit model configurations are created: (1) a residential circuit, (2) a commercial circuit. The scenarios represent several of the common distribution circuit types within the PG&E territory, and include both a generic version of the circuit primary, as well as common potential configurations for the distribution secondary. The models are developed by APEP in collaboration with PG&E, using established models and circuit modeling capability resident at APEP. This modeling capability has been previously used to investigate the load flow and circuit voltage impacts of high distributed generation penetration (primarily fuel cell type) on the primary circuit in [1] and to analyze the power quality impacts of solid oxide fuel cells and nearby loads on the distribution secondary in [2], [3] and [4]. This approach is capable of evaluating PV influences local to the installation site, along the distribution circuit, and on neighboring circuits. It is essential that the distribution system requirements are met for all customers along the distribution system. Where possible, these models are based on monitored data provided by PG&E and the data are used to further tune and verify the modeling methodologies. Information regarding distribution circuit design and typical sizing of equipment from PG&E will greatly add value and practicality of the modeling.

Model Development: The model will capture the myriad of effects relevant to the primary and secondary distribution system by using two modeling strategies. The specific list of modeled parameters is

developed as part of this task, but includes real/ reactive power flow, voltage regulation, capacitor switching, and protection coordination for the primary circuit, and, in addition, voltage and current harmonics, phase imbalance, voltage sags and swells, and other power quality related concerns in the secondary circuit. The primary distribution circuit modeling capability utilizes a modified iterative ladder technique that is implemented in Matlab/Simulink to capture both steady-state and transient effects. The flexibility of the Matlab/Simulink platform, along with the extensive APEP library of compatible DER and power electronics models, enables the circuit to represent nearly any installation and/or future control and communication scenario. The secondary distribution circuit presents a critical challenge for power quality issues, and will therefore be focused on with a more detailed model to allow for the power quality impacts as well. The two models will be used in conjunction to ensure that both local parameters and circuit-wide concerns are adequately addressed.

The primary circuit modeling methodology has been previously validated against the steady-state load flow simulator, PowerWorld, as well as against analytical calculations where feasible. The secondary circuit modeling methodology has been validated using experimental data along with theoretical analysis. Power monitoring is more easily accomplished at the secondary, due to the lower voltage and relatively easier access, as compared to the higher voltage primary. Extended validation will be performed by modeling a sample circuit secondary of each of the two types: residential and commercial. Then the relevant circuit parameters are measured and compared to the associated model results. The modeling methodology will then be iterated and refined until the results are consistently accurate to within 10% of the allowable parameter range. Where possible and circuit monitoring equipment exists, the same procedure will be accomplished for the circuit primary as well.

Deliverable: Modeled scenarios and comparisons to grid monitored data.

4.10 Task 3: Quantify PV Integration Limits

Goal: Quantify PV integration limits for typical distribution circuits.

Task Summary: Phenomena that limit PV penetration with standard inverters and distribution circuit operation are identified for the scenarios described. The models from Task 2 are used to parametrically evaluate PV grid impacts in a variety of conditions. The specific parameters for investigation are developed through the PG&E/APEP partnership, but include the sensitivity of distributed generation (DG) PV array size on integration limit along with temporal/stochastic effects, such as diurnal and cloud cover dynamics, on the distribution system. Guidelines for PV integration limits and performance tradeoffs are developed for typical distribution circuits that have neither communication nor advanced inverter topologies.

Parametric Methodology: Realistic PV installation scenarios will be applied to the models from Task 2. The number and location of the PV installations will be spanned to gain insight into the range of effects on the circuit. The scenarios are:

(1) few large PV arrays (commercial),
(2) many small PV arrays (residential)

Representative residential and commercial PV array sizes are assumed and installed at different locations along the circuit. For low penetration, this includes both scattered and grouped residential arrays, and a commercial array at different locations. High penetration cases will likely include uniformly distributed residential PV and multiple large arrays that can be either scattered or grouped. In all cases, representative diurnal profiles are generated for the entire primary distribution circuit. The main power quality effects of the secondary will be localized around the DG, and these circuits can be analyzed independent of the rest of system.

Deliverable: PV integration limits in typical distribution circuits.

4.11 Task 4: Advanced Inverter Control

Goal: Evaluate advanced PV inverters controls that can increase PV integration limits.

Task Summary: Potential control strategies for the inverter ancillary services, such as active power filter (APF) and reactive power compensation (STATCOM) capability are applied to the PV installations from Task 2 and simulated in the distribution system model. Recent advances in inverter technology have enabled these ancillary services, yet the lack of an established protocol for implementing these functions in practice has caused these advanced smart inverters to default to providing only real power. Much of the research on applying power electronics to power systems has been pioneered at APEP, such as an active power filter (APF) with reactive power control that is designed, built, and tested [5] and a universal control strategy that is validated for inverter, APF, and STATCOM functions [6]. These smart inverters can not only provide real power, but can be controlled to use excess capacity to provide active power filtering and reactive power compensation without supplementary inverter hardware (i.e., only control logic). These control strategies, which use only local measurements, are evaluated for a wide range of DG penetration levels for each developed circuit scenario. Existing net-metering limitations are exceeded to understand potential sensitivities on both the primary and secondary distribution circuit to ensure that both the end-user and utility benefit from high PV penetrations. Any potential interactions with other inverters or capacitors on the line are identified and evaluated.

Active Power Filter: An active power filter (APF) is an existing solution that achieves a combination of harmonics compensation, phase balancing, and power factor correction capabilities. An APF essentially turns an unbalanced non-linear “troublesome” load into one that appears extremely “clean” from the utility perspective. Harmonic currents, which arise from non-ideal loads, are undesirable because they cause voltage distortion and increase rms neutral current. Real loads are also rarely balanced and cause a neutral current in three phase-four wire systems. Harmonics compensation and phase balancing cause the utility to see a non-balanced, non-linear load as a balanced, linear one, which substantially reduces the neutral line current and increases the overall efficiency and improves component lifetime. Power factor correction (PFC) monitors a load and injects reactive power locally, so that the utility sees the load/ PFC combination as having a power factor of unity.

Reactive Power Control: The ability to produce or consume reactive power is often called a STATCOM capability. The STATCOM creates a sinusoidal current that is 90° out of phase with the voltage. An existing DG voltage control strategy that utilizes reactive power control is called local voltage regulation

(LVR). This strategy attempts to regulate the local voltage by generating reactive power when the local voltage is low, and consuming it when local voltage is high.

Deliverable: Risks and benefits of advanced inverter control.

4.12 Task 5: Integrated Distribution Grid Control

Goal: Develop and evaluate integrated control strategies to support the increased penetration of PV in the distribution system.

Task Summary: The voltage spatial behavior and power quality of a distribution system depends on load characteristics, generation dynamics, and installed equipment along the circuit. As are identified in Task 2, certain PV installation scenarios may not be manageable without external communication to other locations on the distribution circuit/ substation. Integrated distribution grid controls are evaluated in this task to determine the extent and complexity needed to address these PV installation cases. The goal is to develop a simple integrated distribution grid control strategy that utilizes communication between available monitoring points (i.e. smart meters and substation) and actuators (PV inverters) to increase PV integration flexibility. PG&E will provide insights into components that can be practically controllable (i.e., transformers, capacitors) in addition to PV inverters. Since each substation autotransformer typically feeds multiple circuits, the voltage cannot be manipulated independently for each circuit and will require communication among adjacent circuits. On the other hand, it may be possible to manipulate circuit capacitors as long as the whole circuit remains within operating requirements. Developed control strategies are tuned and evaluated through implementation in developed grid system models for each of the three scenarios. Integrated distribution grid control can be a gateway to future smart circuits where the distribution circuit performance can be optimized from a central location.

Progressive Improvement: The control strategy design process assumes different levels of communication in the distribution system to provide insight into the limitations of a wide variety of possible control strategies. The communication levels represent the evolution from a present-day standard distribution system into a highly automated smart grid distribution system in the future. In addition to providing the optimal benefit for each development stage, the integration strategy should be sufficiently flexible to adapt to future circuit upgrades and additional equipment, communication, and controls. The overall control strategy provides guidelines that describe what communication should be considered under each scenario.

Concept Validation: The concept of progressively implementing local and extended controls and communication is illustrated through an example of a large PV installation at the end of radial distribution circuit. Sample diurnal real and reactive loads for the circuit, in addition to real power output of the PV, are generated from monitored PV irradiation and load. These data are input into a radial distribution circuit model, and the voltage at each bus is measured and analyzed throughout the 24-hour period. Three levels of control are shown: (1) no control, (2) local-only real power curtailment, and (3) local-only real power curtailment with reactive power load-following.

Deliverable: Progressively smarter integrated distribution system controls.

4.13 Task 6: Practical Feasibility and Outreach

Goal: Evaluate the practical feasibility of the relevant standards, hardware, and communications needed to enable advanced inverter and integrated distribution system control strategies.

Task Summary: Maintaining practical viability of the developed control strategies is critical for the project, and is addressed through constant communication between the utility industry (PG&E), an academic institution (UCI), and oversight by a policy/ regulatory commission (CPUC). All three of these sectors must be aligned for widespread PV implementation and deployment. The practical feasibility of controls developed at APEP is evaluated throughout the project directly by PG&E and through periodic progress reports with the CPUC. The final project task is to specifically quantify the feasibility of the control strategy and implementation method by evaluating hardware, communication, computational modifications, and other necessary upgrades. The required basic hardware components, engineering expertise, and design layouts are assessed to provide general insight into the cost of a potential upgrade.

Developed control strategies may require changes in standards including IEEE 1547 and UL 1741. The extent to which each control strategy can be implemented with existing standards is clearly identified. Further, the simulation results may provide insights and data that can guide and justify the development of new standards. Along with the potential benefits and sensitivity from the simulations, the practical feasibility of the developed control strategy is quantified.

Deliverables: Practical feasibility of the proposed integrated distribution grid controls.

5. Project Outcomes

5.1 Task 2: Model Development and Evaluation

In this task, two specific circuit model configurations will be created: (1) a residential circuit, (2) a commercial circuit.

The scenarios will represent several of the common distribution circuit types within the PG&E territory, and will include both a generic version of the circuit primary, as well as common potential configurations for the distribution secondary. The models will be developed by APEP in collaboration with PG&E, using the established modeling capability resident at APEP. This approach is capable of evaluating PV influences local to the installation site, along the distribution circuit, and on neighboring circuits. It is essential that the distribution system requirements are met for all customers along the distribution system. Where possible, these models will be based on monitored data available from PG&E and the data will be used to further tune and verify the modeling methodologies. Information regarding distribution circuit design and typical sizing of equipment from PG&E will greatly add value and practicality of the modeling.

5.1.1 Distribution Circuits

The circuits under evaluation of the effects High Penetration PV (High-Pen PV) are a commercial and a residential circuit. Both circuits are located in northern California in PG&E territory. PG&E provided connectivity and measurement information used to model both circuits. The details of both circuits are discussed in the following sections.

5.1.1.1 Commercial Circuit (Cayetano 2111)

The first circuit, the Cayetano, is selected as a commercial circuit for this analysis. The sub-station supporting the Cayetano supports two feeders, Cayetano 2111 and 2109.The Cayetano 2111 is the feeder of interest in this study. The circuit is located in Livermore, CA and is operated by PG&E. Figure 2 is the average load demand profile for a weekday and weekend for both the summer and winter seasons. The load demand profiles are typical of a commercial circuit with a peak at approximately 3:00 PM on a weekday [1, Ch. 1.7].

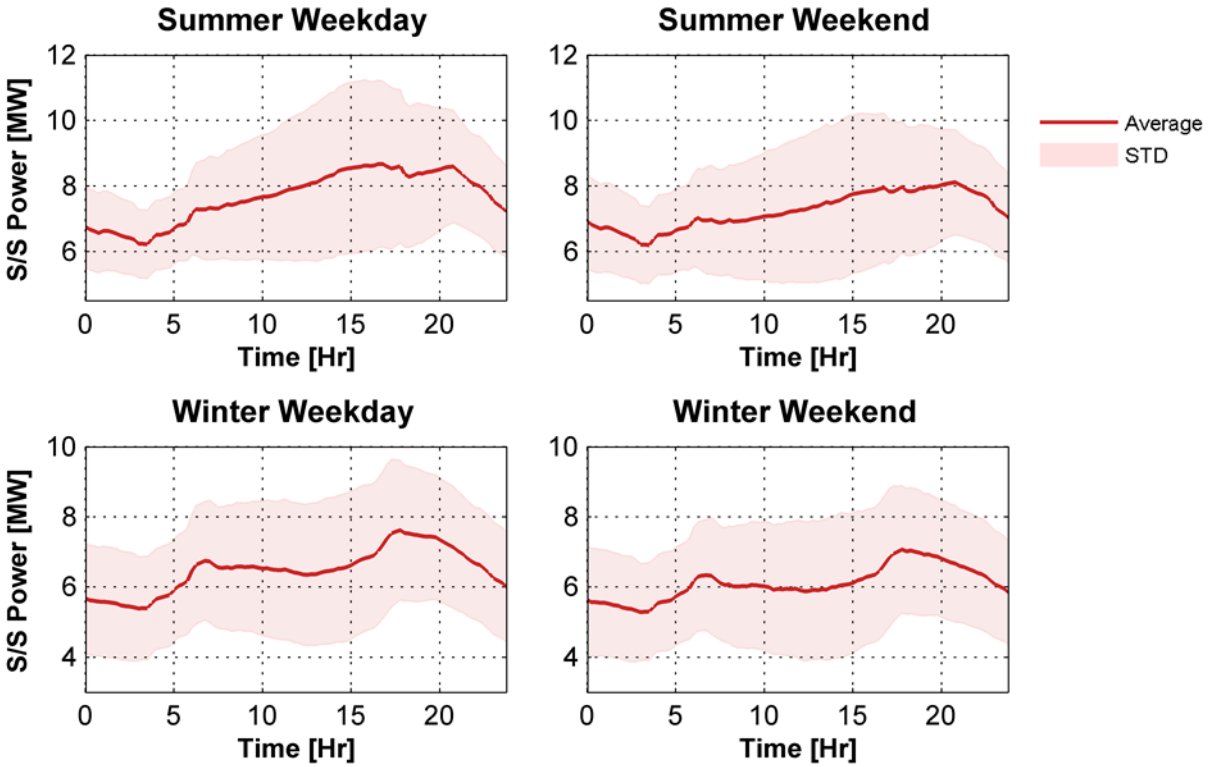

Figure 2. Cayetano seasonal sub-station real power load demand.

The geographic plot of the Cayetano 2111 circuit's construction is shown in Figure 3. The feeder is a typical radial feeder constructed as a 21kV three phase wye system. The sub-station transformer is a Load Tap Changing (LTC) transformer with Load Drop Compensation (LDC) rated at 45 MVA. The sub-station LTC regulates the Cayetano circuit with a ±10% range. The circuit also features 7 three phase switching capacitor banks which provide a total amount of 9.6MVAR of reactive power support to the circuit. The capacitor controls used are Time-Clock, Temperature, and Voltage Override controls.

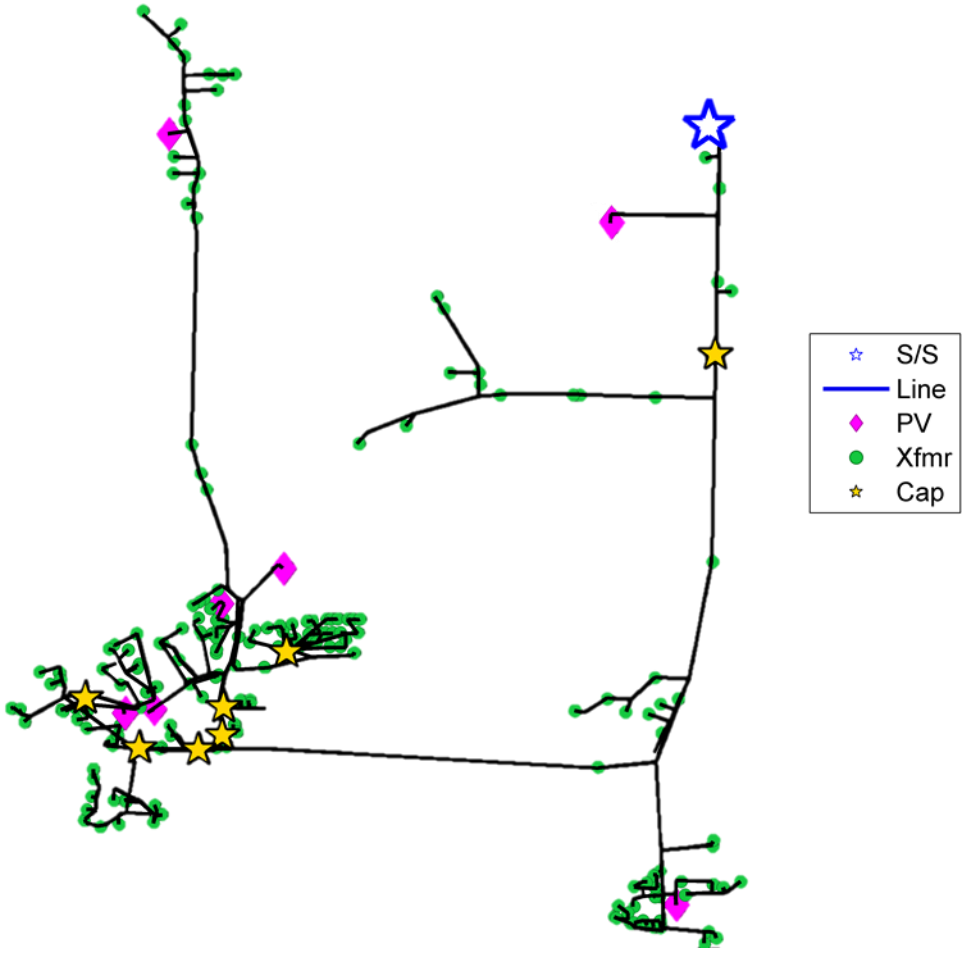

Figure 3. Commercial circuit (Cayetano 2111).

As indicated above the, the load demand profile is typical of a commercial circuit. The Cayetano 2111 services a total of 1202 customers varying from domestic to industrial customers. Table 1 is a break of the customer types found in the Cayetano 2111, as classified by PG&E. The majority (~ 92%) of the total August and January energy of the circuit is consumed by industrial and commercial customers.

Customer Type	Customers	August Feeder Energy Demand	January Feeder Energy Demand
Agriculture	4	0.05%	0.02%
Commercial	193	9.53%	10.27%
Domestic	886	8.80%	8.46%
Industrial	110	81.55%	81.18%
Other	9	0.07%	0.07%
Grand Total	1202	100.00%	100.00%

Table 1. The Cayetano 2111 customer distribution.

A commercial circuit with High-Pen PV is expected to feature few, but large, PV installations. As of 2010, the Cayetano had a PV penetration of 15.6% (12 MW peak load demand) totaling to 1873 MW of PV generation. The circuit only featured six PV installations: three less than 50 kW, 1 between 50kW and 500kW, and 2 larger than 500 kW. The largest PV installation is 1 MW.

An objective of this research is to model a representative commercial distribution circuit featuring High-Pen PV and voltage regulating equipment. The Cayetano 2111 circuit features voltage regulation equipment, such as a sub-station LTC with LDC and switching capacitors. The majority of the energy demand on the circuit is from commercial and industrial customers and the circuit features few, but very large, PV installations. As of 2010, the Cayetano featured a PV penetration of 15.6%. Because of these factors, the Cayetano 2111 distribution feeder circuit was selected for this research as a representative commercial distribution circuit

5.1.1.2 Residential Circuit (Menlo 1102)

The second circuit, the Menlo, was selected as a residential circuit for this analysis. The sub-station supporting the Menlo supports two feeders, Menlo 1101 and 1102. The Menlo 1102 is the feeder of interest in this study. The circuit is located in West Menlo Park, CA and is operated by PG&E. Figure 4 is the average load demand profile for a weekday and weekend for the summer seasons. The load demand profiles are typical of a commercial circuit with a peak in the evenings (approximately 8:00 PM) on both weekdays and weekends [1, Ch. 1.7].

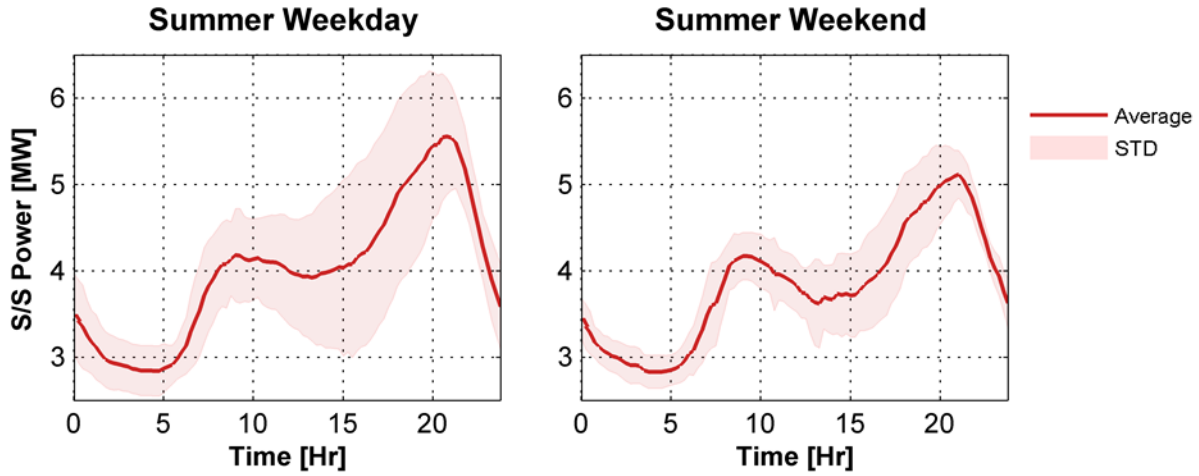

Figure 4. Menlo summer sub-station real power load demand.

The geographic plot of the Menlo 1102 circuit's construction is shown in Figure 5. The feeder is primarily a 12.47kV three phase delta system, but also supports two small 4.16kV three phase wye legacy sections. The design of the distribution is that of a typical radial feeder. The sub-station transformer is a Load Tap Changing (LTC) transformer with Load Drop Compensation (LDC) rated at 16MVA. The sub-station LTC regulates the Menlo circuit with a ±10% range. Along the primary feeder, a 3% low impedance Booster transformer (5.16MVA) and two 12.47 to 4.16kV grounded wye Step-down transformers (1MVA and 750kVA) are present. The circuit also features 6 three phase switching capacitor banks providing a total amount of 3.6 MVAR of reactive power support to the circuit. The capacitor controls used are fixed, Time-Clock, Voltage Override controls.

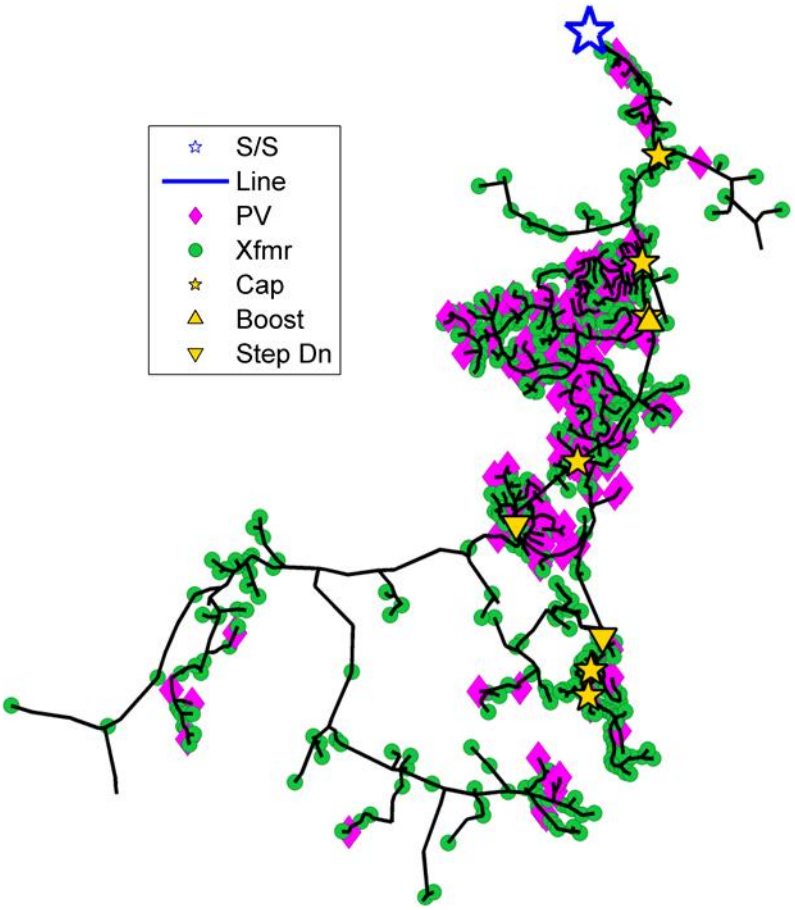

Figure 5. Residential Circuit (Menlo 1102).

As indicated above, the load demand profile is typical of a residential circuit. The Menlo 1102 services a total of 2681 customers varying from domestic to industrial customers. Table 2 is a summary of the customer types found in the Menlo 1102, as classified by PG&E. The majority of the total August (69.4%) and January (78%) energy of the circuit is consumed by domestic customers.

Customer Type	Customers	August Feeder Energy Demand	January Feeder Energy Demand
Agriculture	**10**	**0.5%**	**0.4%**
Commercial	**178**	**8.5%**	**7.1%**
Domestic	**2435**	**69.4%**	**78.0%**
Industrial	**40**	**21.5%**	**14.4%**
Other	**18**	**0.1%**	**0.1%**
Grand Total	**2681**	**100.00%**	**100.00%**

Table 2. Menlo 1102 customer distribution.

A residential circuit with High-Pen PV is expected to feature numerous small (less than 50 kW) PV installations. As of 2010, the Cayetano had a PV penetration of 12.1% (9.1MW peak load demand)

totaling to 1105MW of PV generation. The circuit featured 171 PV installations: 170 less than 50 kW, 1 between 50kW and 500kW, and none larger than 500 kW.

An objective of this research is to model a representative residential distribution circuit featuring high penetrations of PV voltage regulating equipment. The Menlo 1102 circuit features voltage regulation equipment such as a sub-station LTC with LDC and switching capacitors. The majority of the energy demand on the circuit is from domestic customers and the circuit features many small PV installations. As of 2010, the Cayetano featured a PV penetration of 12.1%. Because of these factors, the Menlo 1102 distribution feeder circuit was selected for this research as a representative residential distribution circuit.

5.1.2 Circuit Model Methodology

The objective of this research is to understand the effects of High-Pen PV on distribution circuits. This research focuses on two aspects of distribution circuits: 1) the voltage regulation equipment and 2) the primary line voltage. Distribution circuits are typically constructed as radial feeder circuits; circuits stemming from the sub-station. Typically, the distribution line wire is thicker (low impedance, high ampacity), closer to the sub-station, and gradually decreases in width as the distance increases to the sub-station. Thin wire (high impedance, low ampacity) is typically found at the end of a radial circuit. Radial distributions are normally constructed so that a primary run (primary feeder) of thick line conductor runs from the sub-station to the general center of the load and a lateral run of thin line (laterals) stem from the primary feeder to the load. Since the majority of voltage regulation equipment is installed at the primary feeder, only the voltage along the primary feeder is necessary to characterize the effect of High-Pen PV on voltage regulation equipment.

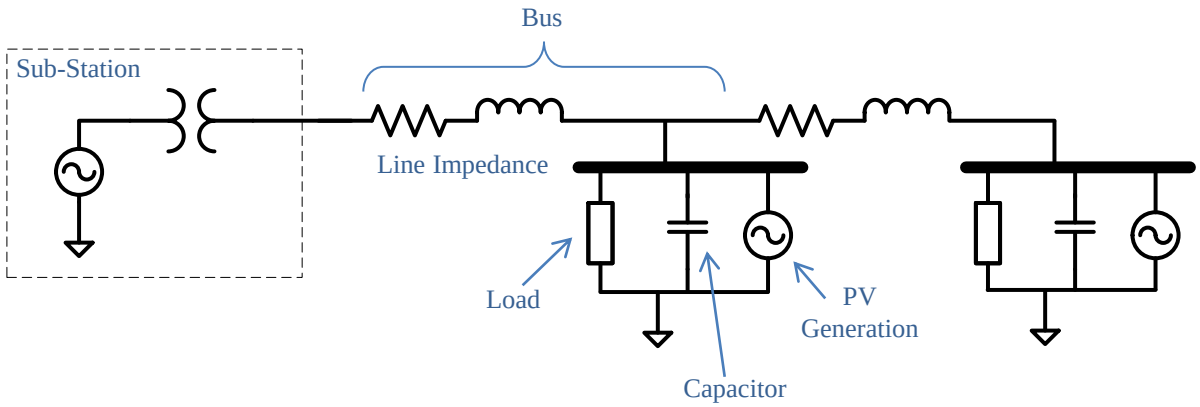

Figure 6 Balanced three phase feeder model.

In this research, the primary feeder of the commercial and residential distribution circuits are modeled as a balanced three phase feeder model, as shown in Figure 6. The transmission system is modeled as an infinite voltage source on the high side of the sub-station transformer. The sub-station transformer impedance is modeled as a series impedance (winding impedance), but the shunt magnetizing impedance is neglected. For large transformers, the magnetizing impedance is typically marginal in comparison to the series winding impedance.

A balanced three phase model assumes that the load and generation found at each bus is balanced so that 1) there is not a return current found on the neutral and 2) the phase current and voltage are the equal. A balanced load and generation may be made if the load and generation in the same vicinity are aggregated together to form a balanced bus. For this research, the load and generation are aggregated to the primary feeder, forming balanced buses directly on the feeder. The voltage drop is modeled using the primary feeder line impedance between the buses. A bus in this research is the aggregated load and generation and immediate upstream line impedance.

Voltage regulation equipment is also modeled within a bus. Examples of voltage regulation equipment include Load Tap Changing transformers and switching capacitors. Special attention is made to accurately describe the location of the voltage regulation equipment on the primary feeder since many use local measurements in its operation control. If a piece of voltage regulation equipment is located away from the load demand, a bus is created for the equipment to accurately represent its location on the circuit.

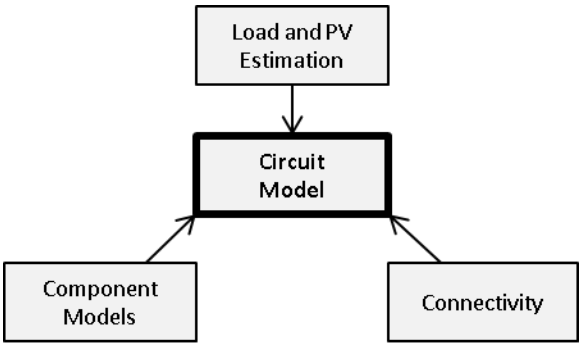

Figure 7. Model development architecture.

The three phase model development of the commercial and residential circuits occurred in three stages: 1) component model development, 2) circuit connectivity reduction, and 3) PV generation and load demand estimation. The component models used to describe the components of distribution circuit vary from load demand models to generation capacitor switching models. The circuit connectivity reduction step involves using the geographical information of the circuit construction to define the bus structure of the three phase balanced circuit model. The final step is to estimate the aggregated PV generation and load demand at each bus. These steps are explained in the following sub-sections.

5.1.2.1 Component Models

The balanced three phase models of the Cayetano and Menlo circuits are comprised of a collection of component models organized to represent the construction and operation of the circuit. The modeling platform used in this research is Matlab/Simulink, with the SimPowerSystems toolbox. Two types of component models were developed in this research: bus and voltage regulating transformers. Bus component models included line impedance, load, capacitors, and PV generation and are combined in series or parallel arrangements to describe the radial construction of circuits. Voltage regulating transformer component models include the sub-stations Load Tap Changer with Load Drop Compensation and Line Regulators. Below are descriptions of the component models developed in the Matlab/Simulink environment.

A. Bus

Figure 8 is a diagram of the bus model used as part the three phase balanced modeling approach. Assuming the bus is balanced at its point of connection with the feeder, only a single phase of the three phase system is necessary to the bus voltage. At each bus model, there is a series impedance connected to a shunt bus with load, capacitor, and/or PV components. The series impedance models the line impedance of distribution line interconnecting busses on a distribution circuit. The shunt bus is modeling an aggregated bus connected to a distribution feeder that may contain multiple customer loads, capacitor installations, and/or PV installations that are lumped into, respectively, a load, capacitor, and/or PV constant power elements. Details of each of the elements are described in the sub-sections below.

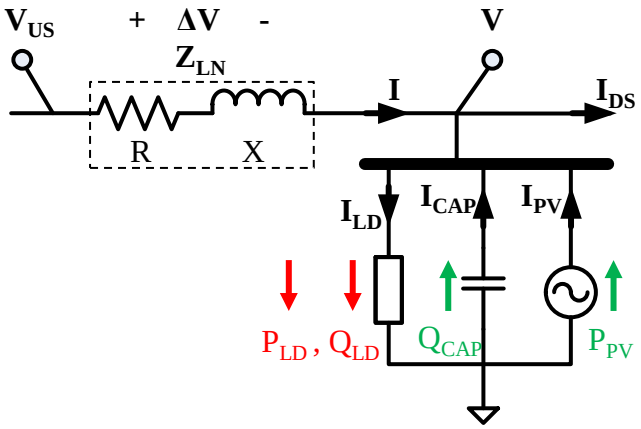

V_{US}	→	*Upstream Voltage*
V	→	*Load Voltage*
ΔV	→	*Voltage Drop*
I	→	*Line Current*
I_{DS}	→	*Downstream Line Current*
I_{LD}	→	*Load Current*
I_{CAP}	→	*Capacitor Current*
I_{PV}	→	*PV Generation Current*
Z_{LN}	→	*Line Impedance*
R	→	*Line Resistance*
X	→	*Line Reactance*

Figure 8. Bus Model.

The following equations describe how the bus voltage is calculated. The bus voltage is calculated by applying Kirchoff's Voltage Law; the bus voltage (**V**) is the difference of the upstream bus voltage ($\mathbf{V_{US}}$) and the voltage drop ($\mathbf{\Delta V_{LN}}$) across the distribution line, as shown in equation 5-1. The line drop is approximated using Ohm's Law and is the product to line impedance and line current. The line impedance (equation 5-3) is a comprised of two components: a resistance (R) and a reactance (X). The resistive component impedes "in-phase" current and the reactive component impedes "out-of-phase" current. In distribution circuits, an in-phase current is consumed or generated as real power and an out-of-phase current is consumed or generated as reactive power [2, Ch. 2.2]. Applying Kirchoff's current law at the point of the shunt bus provides an equation of the line current, as shown in equation 5-4. The line current is composed on four elements: local bus components of load ($\mathbf{I_{LD}}$), capacitor ($\mathbf{I_{CAP}}$), PV ($\mathbf{I_{PV}}$) current and the downstream current ($\mathbf{I_{DS}}$). The currents drawn at the bus ($\mathbf{I_{LD}}$, $\mathbf{I_{CAP}}$, and $\mathbf{I_{PV}}$) are dependent on the load, capacitor, and PV elements are described in detail in the preceding sub-sections. The downstream current is dependent on the current draw of all the buses downstream of the bus; this is calculated iteratively.

$$V = V_{US} - \Delta V_{LN} \quad \textbf{5-1}$$

$$\Delta V_{LN} = I \cdot Z_{LN} \quad \textbf{5-2}$$

$$Z_{LN} = R + jX \quad \textbf{5-3}$$

$$I = I_{LD} - I_{CAP} - I_{PV} + I_{DS} \quad \text{5-4}$$

Using equations 5-1 through 5-4, the feeder voltage is calculated for each bus, where each calculation is interdependent. Bus voltage is dependent on the upstream voltage and line drop. Line drop is dependent on line current. Line current is dependent on the local and downstream current draw. The local and downstream current is dependent on the bus voltage, and so on. In order to calculate feeder voltage, the system is solved iteratively from an initial estimate of bus voltage to calculate line current, then line drop, and so on. The Matlab/Simulink modeling environment optimizes the steps in this iterative process to a solution within a relative tolerance. The parameters of the solver used in this research are detailed in Table 3.

Model Environment	Matlab/Simulink
Block Set	SimPowerSystems
Type	Variable-Step
Solver	ODE23tb (stiff/TR-BDF2)
Relative Tolerance	10^{-4}

Table 3. Iterative Solver Parameters.

A.1 Load

At each bus, the aggregate load demand is modeled as a single real power load element; equivalent of a three-phase balanced wye load. The load element consumes both real and reactive power with a lagging power factor. Starting with the voltage and current definition of the load demand complex power ($\boldsymbol{S_{LD}}$) (equation 5-5) and the quadrature definition (equation 5-6), an equation of the complex load demand current ($\boldsymbol{I_{LD}}$) draw is formed, as shown in equation 5-7. Real power (P_{LD}) and reactive power (Q_{LD}) load demand is an external input into the model, while the bus voltage ($\boldsymbol{V}$) is internal feedback of the model. How the inputs of P_{LD} and Q_{LD} are derived for the Cayetano and Menlo models is detailed in section 5.1.2.4.

$$\boldsymbol{S_{LD}} = \boldsymbol{V} \cdot (\boldsymbol{I_{LD}})^* \quad \text{5-5}$$

$$\boldsymbol{S_{LD}} = P_{LD} + jQ_{LD} \quad \text{5-6}$$

$$\boldsymbol{I_{LD}} = \frac{P_{LD} - jQ_{LD}}{(\boldsymbol{V})^*} \quad \text{5-7}$$

Capacitor

If a switching or fixed capacitor is within an aggregated bus, it is modeled as a single switched capacitor on the bus. As is the case with the Cayetano and Menlo circuits, distribution feeders typically only feature large switched or fixed capacitor banks sparingly spaced on the primary feeder for efficiency and voltage control purposes. Just as the load model, the capacitor is modeled as a constant power source, but operates as a source, rather than a sink, of reactive power. The capacitor model is the equivalent of a three-phase WYE connected capacitor bank. Starting the various definitions of the capacitor's complex power (equations 5-8 and 5-9), an equation of the complex capacitor current ($\boldsymbol{I_{CAP}}$) is formed. The bus voltage ($\boldsymbol{V}$) is an internal feedback, but the reactive capacitive power (Q_{CAP}) is derived from the nameplate and bus voltage.

$$\boldsymbol{S_{CAP}} = \boldsymbol{V} \cdot (\boldsymbol{I_{CAP}})^* \quad \textbf{5-8}$$

$$\boldsymbol{S_{CAP}} = -jQ_{CAP} \quad \textbf{5-9}$$

$$\boldsymbol{I_{CAP}} = \frac{jQ_{CAP}}{(\boldsymbol{V})^*} \quad \textbf{5-10}$$

A capacitor installation is typically described by a nameplate indicating the rated reactive power at a rated voltage, but not the actual capacitance of the capacitor bank. Equation 5-11 is the definition of a capacitors reactive power in terms of bus voltage and reactance. It is evident that the reactive power of a capacitor installation is a function of bus voltage, so the capacitance (C) of the bank should be de-coupled to model this fluctuation. Using the definition of capacitance in terms of reactance (equation 5-12) and equation 5-11, we can calculated C given the nameplate information of the capacitor installation as shown in equation 5-13. Since capacitors installations vary from the single phase and three phase configurations, an equivalent definition for both is provided. Now that C is calculated for the installations, we can form equation 5-14 to calculate Q_{CAP} using internal bus voltage and the bank capacitance derived from nameplate information.

$$Q_{CAP} = \frac{\boldsymbol{V}^2}{X_{CAP}} \quad \textbf{5-11}$$

$$C = \frac{1}{w \cdot X_{CAP}}, \qquad w = 2\pi f = 120\pi \quad \textbf{5-12}$$

$$C = \frac{Q_{NP}}{w \cdot V_{NP}^2} = \frac{Q_{NP,3\varphi}}{w \cdot V_{NP,LL}^2} \quad \textbf{5-13}$$

$$Q_{CAP} = w \cdot C \cdot \boldsymbol{V}^2 \quad \textbf{5-14}$$

A critical aspect of capacitor banks in distribution feeders is to provide improved system efficiency and voltage regulation. This is accomplished by switching the capacitors on and off depending on the situation. Types of switching controls are time-clock, temperature, voltage override, and VAR switching controls. Figure 9 illustrates the orientation of the switching control models in relation to the capacitor models used in this research. In the proceeding sub-sections, time-clock, temperature, voltage override, and VAR controls are described.

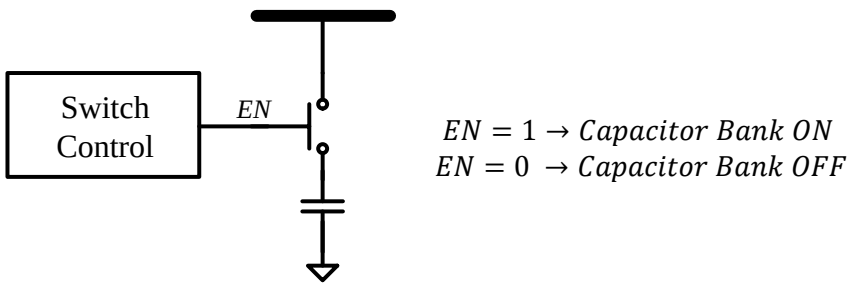

Figure 9. Switched Capacitor Model.

A.1.1 Time-clock (TC) and Temperature (Temp) Control

The time-clock (TC) control is time controller that is configured by two thresholds: time-on and time-off. The time-on threshold is the time of day the capacitor switches on-line or "banks on". Likewise, the time-off threshold is the time of day the capacitor switches off or "banks off". Figure 10 is an illustration of TC control of a capacitor bank. An aspect of TC control is night versus day operation. In night operation, the capacitor is bank is on-line during the night; this is indicated by the time-off threshold set to an earlier time of day than time-on. For day operation, the capacitor bank on during the day and the time-on threshold is set to an earlier time than time-off. The TC controls are developed based on the S&C Electric Company IntelliCAP controls series [3, p. 14].

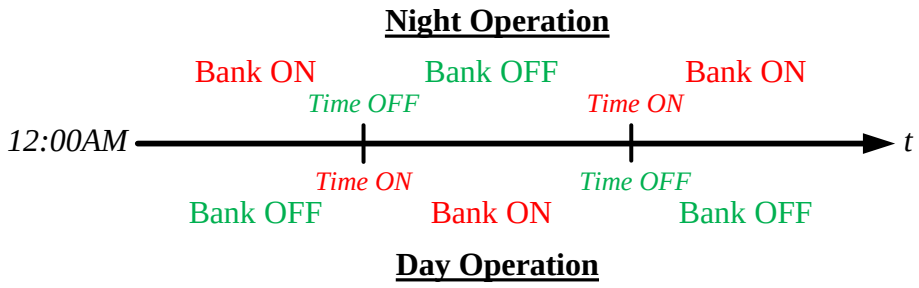

Figure 10. Time Clock Capacitor Controls Switching Diagram.

For this research, a temperature controlled switching model was not developed. Since the methodology is not using stochastic load demand models, representative circuit high and low demand days are simulated instead. Since the days are selected, the capacitor switching events due to temperature can be empirically found and simulated using TC switching controls, as discussed in section C. Since the ambient temperature is not influenced by the distribution circuits operation state, it is appropriate to use TC controls to simulate capacitor switching from temperature based controls.

B.1.1 Voltage Override Control (VO)

Voltage override (VO) switching control operates in conjunction with another type of capacitor switching control such as time-clock and VAR switching controls. In Figure 11, this conjunctive control is labeled as "Normal Control". The VO controls that were developed are based on the S&C Electric Company IntelliCAP controls series [3, p. 15].

VO controls monitors the bus voltage in parallel to the normal control and intervenes in high or low voltage conditions as specified by the high voltage threshold and low voltage threshold parameters, respectively. The voltage is measured at the capacitors (on the distribution circuit side of the switch) by a potential transformer. The turns-ratio of the potential transformer is selected step the distribution circuit voltage down to a 120 volt scale. The high and low voltage thresholds are specified on a 120V scale. The control does not operate immediately; the high or low voltage condition must be maintained for a period of time. This period of time is specified by the override hold-out threshold parameter: specified in minutes. If it is a high voltage condition maintained past the override hold-out time limit, the VO control will switch off the capacitor bank, or bank off. Likewise, in a low voltage condition extending past the hold-out time, the VO control will bank on.

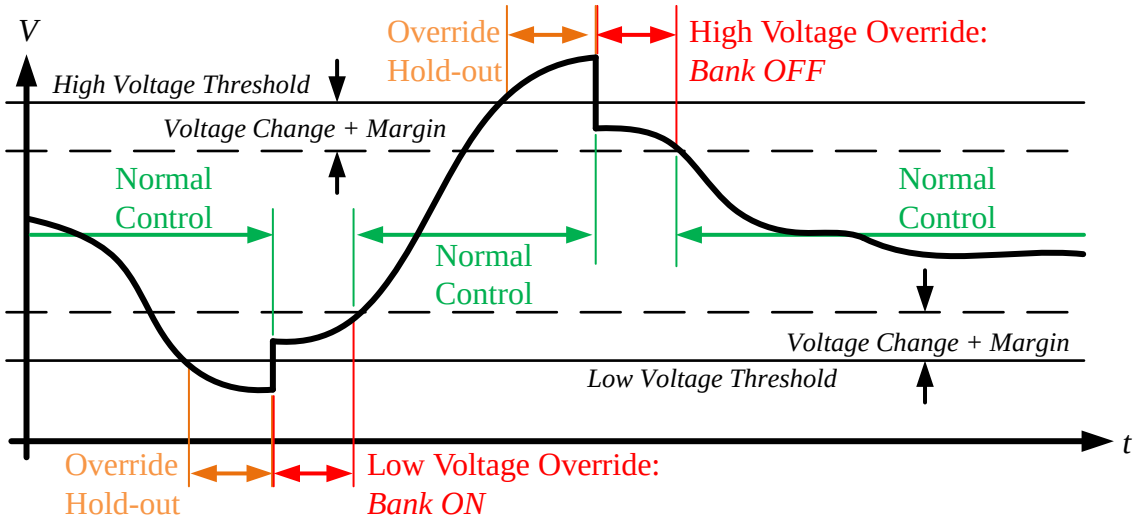

Figure 11. Voltage Override Capacitor Controls Switching Diagram.

The VO control will continue to override the normal control until the voltage has returned to normal levels past a buffer region. Since capacitor installations are typically large, the voltage will discretely rise/fall by a magnitude of volts on a 120 volt scale [1, Ch. 6.3]. An estimation of the amount of voltage change caused by a capacitor banking on can be calculated using equation 5-15 or can simply be estimated heuristically. When the voltage returns to normal levels, it must return to a point beyond the estimated voltage change caused by the capacitor to avoid rapidly returning back to an out-of-bounds state. An example is a TC with VO control. The TC control has the capacitor switch on, but the voltage goes past the high voltage threshold of the VO controls. The VO control intervenes and banks off. When the voltage returns to normal bounds, the VO control will return to the TC control, resulting in the capacitor banking on. If the voltage is not lower than the buffer below the threshold, the voltage will return to a high voltage condition. By establishing this margin, excess capacitor switching is prevented. The buffer is specified by configuring the voltage change and margin parameters in 120 based volts. Therefore, in a high voltage override condition (bank off), once the voltage has decreased below the high voltage threshold minus the voltage change and margin, the VO controls will return normal controls. Likewise for a low voltage condition, VO controls will concede to normal control when the voltage has increases past the low voltage threshold plus the voltage change and margin.

$$V_{rise} = \frac{Q_{CAP} \cdot X_L}{10 \cdot V_{LL}^2} \text{ ([1, Ch. 6.3])} \qquad \textbf{5-15}$$

V_{rise} → *The estimate percentage voltage rise from capacitor [%]*
Q_{CAP} → *3-phase rating of capacitor bank [kVAR]*
X_L → *Positive Sequence impedance from source to capacitor [Ω]*
V_{LL} → *Line-to-Line voltage [kV]*

C.1.1 VAR Control

VAR capacitor switching controls switches the capacitor bank based on the measured reactive power at the distribution feeder. VAR controls are typically more expensive than other types of controls since it requires both a potential and current transformer to operate. The VAR controls that were developed are based on the S&C Electric Company IntelliCAP controls series [3, p. 15].

The reactive power is measured utilizing a potential transformer and current transformer. The current transformer is positioned on the upstream (towards the sub-station) side of the capacitor bus so that the reactive power measurement includes the capacitor bank [1, Ch. 6.6]. VAR control banks on when the reactive power rises past the high VAR threshold for a period longer than the hold-out time. A capacitor bank will decrease the amount of measured reactive power when on-line. When the reactive power drops below the low VAR threshold for a period longer than the hold-out time, the VAR controls bank off the capacitor. For typical commercial and residential distribution circuits, the reactive profile will start low in the morning, rise during the day and fall in the evening. An example the described VAR switching controls is shown in in Figure 12.

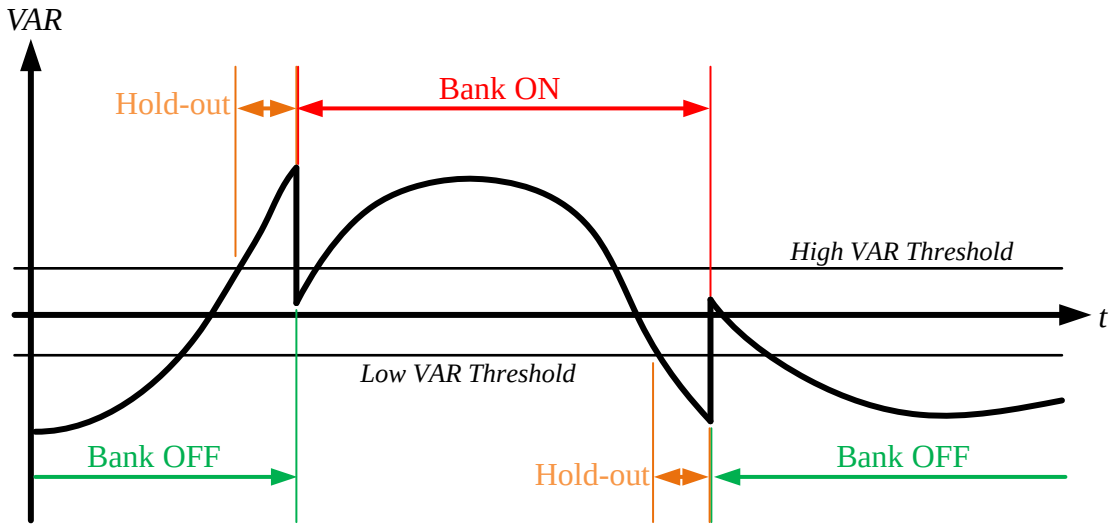

Figure 12. VAR Capacitor Controls Switching Diagram.

The high and low VAR threshold values are selected using the following equations (5-16 and 5-17). Since VAR control feedback is heavily influenced by the presence of on-line capacitor banks, multiple capacitor banks with VAR controls have to be coordinated in order to prevent excessive switching. This is accomplished through the holdout parameter. As a rule of thumb, capacitors farther on the line from the sub-station will have a shorter holdout time than upstream installations [1, Ch. 6.6].

$$Thr_{High\,VAR} = \frac{2}{3} \cdot Q_{CAP} \quad \text{[1, Ch. 6.6]} \qquad \textbf{5-16}$$

$$Thr_{Low\,VAR} = Thr_{High\,VAR} - \frac{5}{4} \cdot Q_{CAP} \qquad \textbf{5-17}$$

$Thr_{High\ VAR}$ → *High VAR threshold [kVAR]*
$Thr_{Low\ VAR}$ → *Low VAR threshold [kVAR]*
Q_{CAP} → *3-phase rating of capacitor bank [kVAR]*

B. PV Generation

At each bus, the aggregate PV generation of the bus is modeled as a single real power load element; equivalent of a three-phase balanced WYE connection. Since PV installations are not allowed to regulate voltage [4], the PV element generates real power at local bus voltage with a unity power factor. Starting with the voltage and current definition of the PV generation complex power ($\mathbf{S_{PV}}$) (equation 5-18) and the quadrature definition (equation 5-19), an equation of the complex PV current ($\mathbf{I_{PV}}$) draw is formed, as shown in equation 5-20. Real power (P_{PV}) of the PV element is an external input into the model, while the bus voltage ($\mathbf{V}$) is internal feedback of the model. How P_{PV} is derived for the Cayetano and Menlo models is detailed in section 5.1.2.4.

$$\boldsymbol{S_{PV}} = \boldsymbol{V} \cdot (\boldsymbol{I_{PV}})^* \quad \textbf{5-18}$$

$$\boldsymbol{S_{PV}} = -P_{PV} \quad \textbf{5-19}$$

$$\boldsymbol{I_{PV}} = \frac{-P_{PV}}{(\boldsymbol{V})^*} \quad \textbf{5-20}$$

5.1.2.2 Voltage Regulation Transformers

Transformers are a critical component in an AC distribution circuit. A transformer is essentially two coils of wire that are magnetically coupled in an AC system. The voltage and current between the coils are related by the ratio of turns between the coils, as seen in equation 5-21. Every distribution circuit features a sub-station transformer and many service transformers. A sub-station transformer is a very large transformer located at the sub-station to step sub-transmission level voltages (ex. 230kV) to distribution level (ex. 21kV) voltages. Service transformer are located throughout the circuit to step distribution voltages to service levels (ex. 120/207 V). There are also transformers that are located directly on the primary feeder of distribution circuits to assist in voltage regulation: booster and step-down transformers are examples.

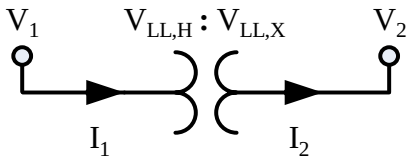

Figure 13. Ideal Transformer Model.

$$\frac{V_1}{V_2} = \frac{V_{LL,H}}{V_{LL,X}} = \frac{I_2}{I_1} \qquad \textbf{5-21}$$

$V_{LL,H}$ → Transformer high-voltage line-to-line nameplate voltage rating [V]
$V_{LL,X}$ → Transformer low-voltage line-to-line nameplate rating [V]

An important aspect to capture in the modeling of a transformer is its impedance. Figure 14 is a simplified model of the transformer impedance; the shunt magnetizing impedance is neglected since, on a loaded transformer, the series impedance is dominant [5, p. 111]. The impedance of a transformer is derived from the nameplate. In the literature, the equations developed to derive a transformer impedance require transformers VA rating ($S_{3\phi}$), voltage (VLL), impedance drop (Z%), and finally power loss during open-circuit and closed-circuit tests [1, Ch. 4–3] [2, p. 105]. From the author's personal experience, typically only the VA rating, voltage, and impedance drop information is available on the nameplate. Using only this nameplate information, the magnitude of the impedance (Z) is calculated using equation 5-22. To decompose Z into is resistive (R) and reactive (X) components, the power loss during the open-circuit and short-circuit transformer tests is useful, but unavailable. To overcome this short-coming, a "K" factor is used to estimate R and X. The K factor an estimate of the ratio of transformer reactance (X) to resistance (R). A K factor of 6 is appropriate for transformers ranging between 1-3MVA [5, pp. 100–101]. For very large transformers, such as sub-station transformers (5-50MVA), the reactance is dominant and a large K factor may be used (K→∞, R→0) [5, pp. 111–112].

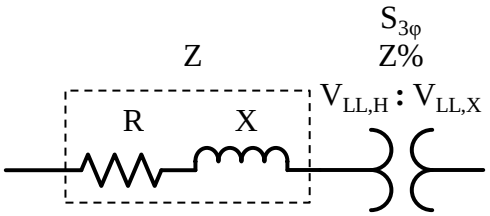

Figure 14. Simple Transformer Impedance Model

$$Z = \frac{Z\%}{100} \cdot \frac{V_{LL,H}^2}{S_{3\varphi}} \qquad \textbf{5-22}$$

$$R = \frac{Z}{\sqrt{1 + K^2}} \qquad \textbf{5-23}$$

$$X = \sqrt{Z^2 + R^2} \qquad \textbf{5-24}$$

$S_{3\phi}$ → Three-phase nameplate transformer rating [VA]
$V_{LL,H}$ → Transformer high-voltage line-to-line nameplate voltage rating [V]
$V_{LL,X}$ → Transformer low-voltage line-to-line nameplate rating [V]
Z% → Percentage transformer voltage drop at full load
Z → Transformer impedance magnitude [Ω]
R → Transformer resistance [Ω]
X → Transformer reactance [Ω]
K → X/R transformer impedance ratio

In this research, a distribution circuit is reduced to a three-phase balance model. By doing so, only a single phase of the entire system has to be simulated. Therefore, only transformers directly appearing on the primary feeder are modeled: this includes load tap changers, booster, and step-down transformers. Service transformers are not directly modeled, but are aggregated into the load models at each bus. The transformers that are modeled are reduced to an ideal transformer with a series high-side impedance. The details of the LTC transformer are detailed in the proceeding sub-section.

A. Load Tap Changing (LTC) Transformers with Load Drop Compensation (LDC)

One form of voltage regulation is the use of tap changing transformers, also called a Load Tap Changer (LTC). LTCs can be located at the sub-station or on the primary feeder of the distribution circuit. The basic operation premise of LTCs is to raise (tap up) or lower (tap down) the voltage control the voltage drop at the end of the circuit, as assumed in radial distribution circuits. A controller on the LTC controls the tapping. A common controller is Load Drop Compensation (LDC). A LDC control estimates the voltage down the line and taps the LTC accordingly (Figure 15). Other types of controls exist, but LDCs are used in the two circuits under analysis and are the only type of control considered in this research.

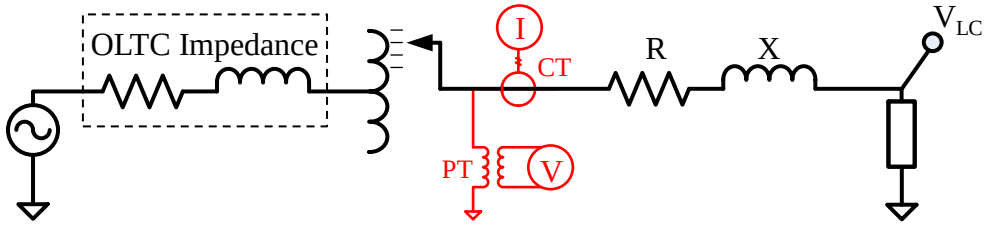

Figure 15. Load Tap Changer Transformer with Load Drop Compensation Model.

$$V_{ideal} = V_{LC} + \frac{I}{CT}(R + jX) \quad \text{5-25}$$

$$\frac{V}{PT}\begin{cases} > V_{ideal} + \dfrac{Band}{2} & \rightarrow Tap\ Down \\ < V_{ideal} - \dfrac{Band}{2} & \rightarrow Tap\ Up \end{cases} \quad \text{5-26}$$

$$Tap_{Range} = \left[\frac{Steps}{2}, -\left(\frac{Steps}{2} - 1\right)\right] \quad \text{5-27}$$

$$V_{Step} = \frac{120 \cdot \left(\frac{Regulation}{100}\right)}{Steps} \qquad \textbf{5-28}$$

Measurement

V	→	Measured line-to-neutral voltage at LTC [V]
I	→	Measured line current at LTC [A]
CT	→	Current transformer turns-ratio
PT	→	Potential Transformer turns-ratio

Load Drop Compensation Parameters

V_{LC}	→	Load Center Voltage [V_{120}]
R	→	Resistance to load center [Ω]
X	→	Reactance to load center [Ω]
Band	→	Regulation bandwidth around V_{ideal} [$\pm V_{120}$]

Load Tap Changer Parameters

Regulation	→	Total voltage regulation percentage [±%]
Steps	→	Total allowable taps of LTC
Tap	→	Regulation coil tap position in LTC

Calculation

V_{ideal}	→	Ideal LTC voltage to achieve VLC [V_{120}]
Tap_{Range}	→	Tap range of LTC
V_{Step}	→	Voltage per tap step [V_{120}]

The controls of the LDC are summarized in the above system of equations and parameter definitions. The LDC controller adjusts the LTC voltage to maintain a constant potential at the load center across the line drop. The load center voltage (VLC) and line impedances are input parameters of the LDC control. Starting with a local measurement at the LTC via a potential transformer (PT) and a current transformer (CT), an ideal LTC voltage set-point (V_{ideal}) is estimated using equation 5-25. Now the controller compares the measured voltage to V_{ideal}; if the LTC voltage is outside the band surrounding the V_{ideal}, the LTC either taps up or down. The LTC specifications determine the range of tap positions (equation 5-27) and the step voltage change from a single tap position change (equation 5-28). The LDC control is implemented by calculating the ideal voltage and bands over a range of currents. Figure 16 is an example of such a chart, referred to a VI chart, for the parameters specified in Table 4.

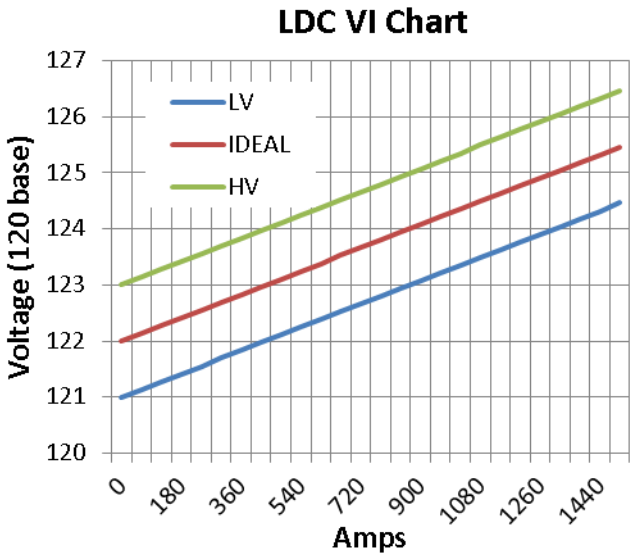

Figure 16. LDC VI Chart Example.

Parameter	Value
Regulation	±10%
Steps	32
V_{LC}	122V
R	3Ω
X	0Ω
Band	±1V
CT ratio	1300:1
PT ratio	100:1

Table 4. LDC Parameters Example.

In this research, two types of LTCs are modeled: sub-station and regulator transformers. Both LTCs use LDC for tap control, but are different in size and location. A sub-station LTC is located at the sub-station with an ideal voltage source (to model a stiff grid) on the high-side. Regulators are located on a feeder and use the feeder voltage on the side. The sub-station LTC is typically much larger in VA rating and has a larger K factor than the regulator.

5.1.2.3 Connectivity

To develop the distribution feeder models, Pacific Gas & Electric (PG&E) provided geospatial information for each circuit of interest, referred to as circuit connectivity data in this document. The connectivity data includes information for distribution lines, transformers, capacitors, and PV generation equipment. Table 5 provides of overview of the type of information provided for each piece of equipment.

Component	Information
Distribution Line	Location, impedance, construction, phase count, length
Distribution Transformers	Location, sizing, configuration
On-Load Tap Changing Transformer with Load Drop Compensation	Location, sizing, connection, compensator controls
In-Line Boost Transformer	Location, sizing, configuration
Photo-Voltaic Generation	Location, sizing
Switched Capacitors	Location, sizing, switching control
Customer	Location, Seasonal Energy

Table 5. Connectivity Data information.

An important aspect of the connectivity data is the geospatial information for each piece of equipment in the circuit provided as geographical coordinates. Plotting the information provides valuable insight into the construction of the circuit: the location of the sub-station, load inter-connection, capacitors, etc. Figure 17 is a sample of the connectivity information provided for the Menlo 1102 distribution circuit. Visualizing geospatial connectivity information aids in the reduction of the circuit and in the production of an equivalent 3-phase model representation.

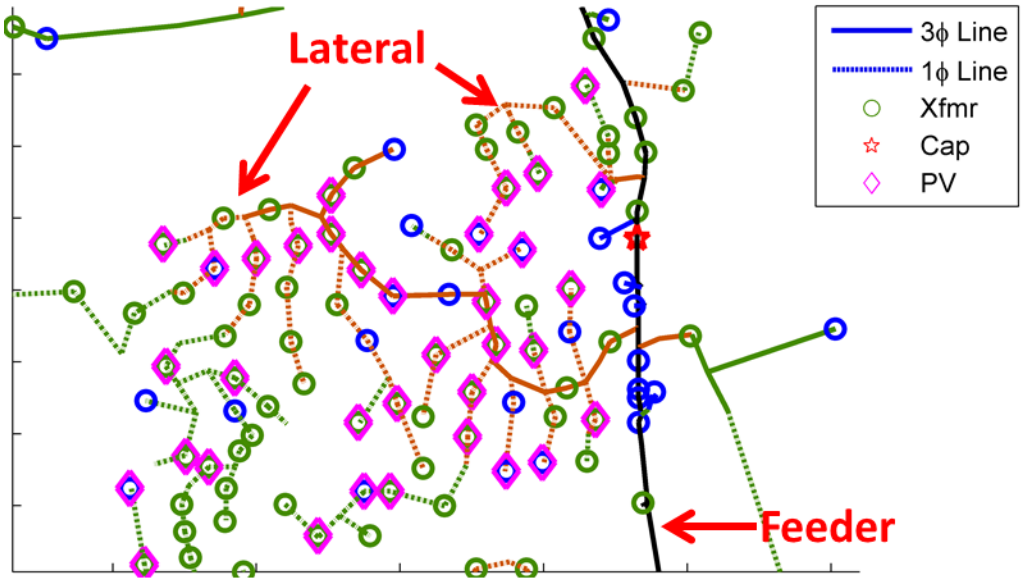

Figure 17. Geospatial plot example of connectivity data.

Typical distribution circuit construction consists of a single run of a large, low impedance conductor, known as the feeder, with smaller conductors radiating from the feeder, known as laterals. To form a

balanced 3-phase model of the distribution circuit, the existing laterals must be reduced to a bus on the feeder. This process is referred as the Bus Reduction Process in this document and is illustrated in Figure 18. The steps in this process are as follows:

1) Using the geospatial plots of the circuit, the feeder and laterals are identified
2) The laterals are reduced to the feeder. Single phase and dual phase laterals are aggregated to together to neighboring laterals in order to the keep the balanced three phase load and generation assumption valid at each bus. Voltage control equipment is reduced to its own bus to maintain the location along the feeder. Examples of voltage control equipment include capacitors, boosts, step-downs, and OLTC w/ LDC.
3) Once the bus locations are identified along the feeder, impedance, aggregate load/generation, and other equipment parameters are collected from the connectivity data.
4) The bus reduction information is used to construct an equivalent model in Matlab/Simulink.

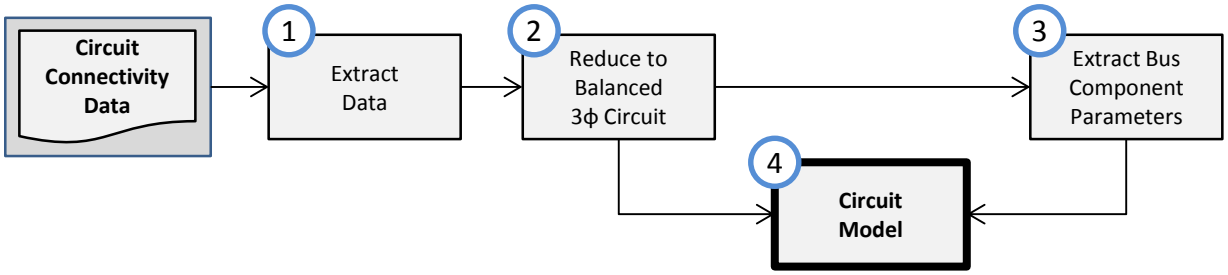

Figure 18. Bus Reduction Process.

5.1.2.4 PV and Load Demand Estimation

The purpose of this study is characterizing the effects of High-Pen PV in distribution circuit equipment. The approach taken to evaluate High-Pen PV is the analysis of characteristic extreme days, so the distributed load demand used in the simulations should representative. Figure 19 shows the process used to derive the load demand, PV generation, and capacitor operation for characteristic extreme days in both the Cayetano 2111 and Menlo 1102 circuits.

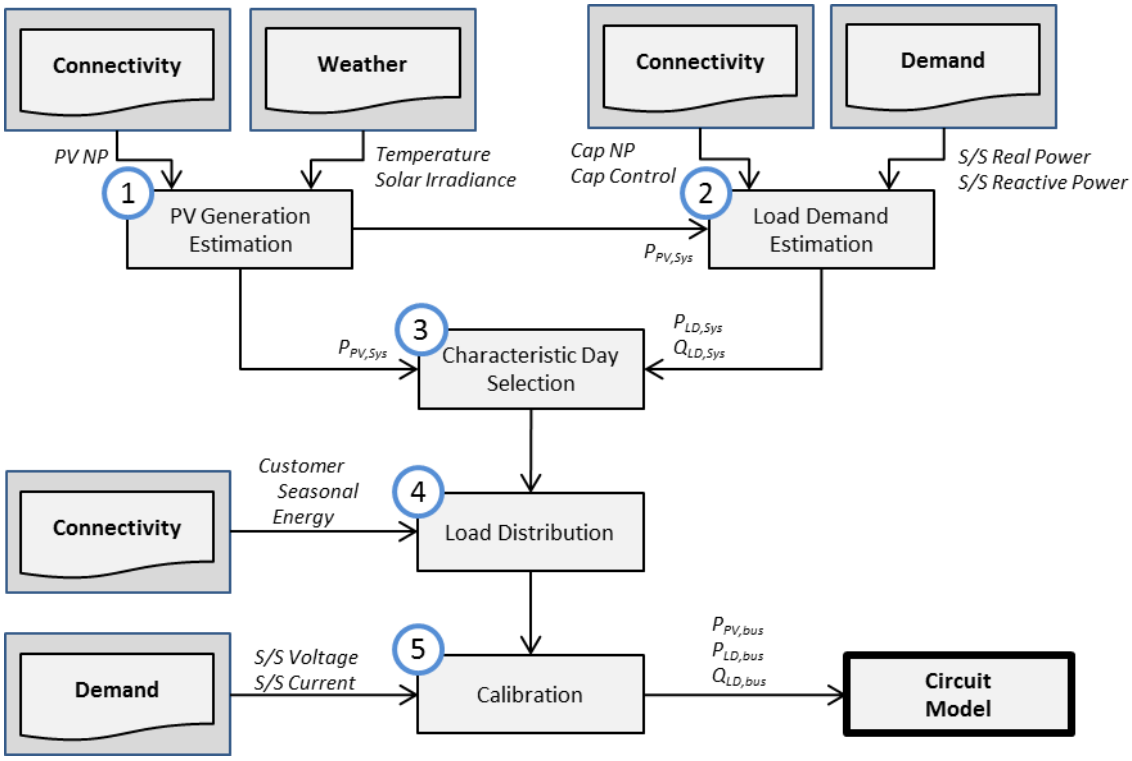

Figure 19. Bus Load/PV/Capacitor estimation and distribution process.

In distribution circuits, the load demand, DG, and capacitor operation are physically independent components on the circuit. To accurately simulate a distribution circuit, these components are simulated as physically independent entities at each bus. Initially, real and reactive power generation of (1) PV generation and consumption of (2) real and reactive load demand is estimated using the available connectivity, weather, and SCADA information for each circuit. Once the load demand is estimated, a statistical analysis is performed to (3) identify characteristic high and low demand days for use in simulation. Using available energy consumption at each bus, the estimated system demand is (4) distributed across the entire circuit. Finally, the estimated load demands are (5) calibrated against sub-station current and voltage measurements adjust for unaccounted system losses. Each step in this process, 1 through 6 is detailed in the sections below.

A. Data Sets

To develop the estimations described in this section, two primary types of data sets are used: 1) sub-station load demand measurements and 2) weather data including solar insolation and temperature. The collection, processing, and analysis of both data sets are described in detail below.

A.1 Demand

To conduct the evaluation of PV penetrations limitations, PG&E provided sub-stations demand measurements from their Supervisory Control and Data Acquisition (SCADA) system for both the Cayetano 2111 and the Menlo 1102 feeders. The data was collected on 15 minute intervals over the course of an entire year (2010); the signals measured are listed in Table 6. It is important to note that the Cayetano 2111 and Menlo 1102 feeders did not have do not have identical measurement quantities; voltage measurements were not recorded for the Menlo feeder.

Feeder	Real Power (P)	Reactive Power (Q)	Line-to-Neutral Voltage			Line Current		
			Phase A ($V_{LN,A}$)	Phase B ($V_{LN,B}$)	Phase C ($V_{LN,C}$)	Phase A (I_A)	Phase B (I_A)	Phase C (I_A)
Cayetano 2111	Yes	Yes	Yes	Yes	Yes	Yes	Yes	Yes
Menlo 1102	Yes	Yes	No	No	No	Yes	Yes	Yes

Table 6. Recorded Measurements at Feeder Sub-Station.

The quantities measured are interdependent and can be used to derive a quantity called apparent power (S) with units of volt-amperes (VA). This interdependent relationship between real power, reactive power, voltage and current is expressed in 5-29. With this relationship, the sub-station SCADA data is used in the modeling effort in two ways: as an input into the model and as a comparison for the output. The 3-phase balanced circuit model uses bus demand as an input and iteratively derives the bus voltage and current for the circuit. As an input to the model, SCADA data real and reactive power measurements are distributed to the various buses in the model. The process of bus demand distribution is detailed in the Load/Generation Distribution section (E). After the simulation is complete for the given input, the output bus voltage and current is compared to the SCADA data voltage and current. This process is referred to as calibration in this document and is detailed in Calibration section (G).

$$S = \sqrt{P^2 + Q^2} = V_{ln} * I_{a+b+c}\ [VA] \qquad \text{5-29}$$

5-29 is also used to assess the consistency of the SCADA data collected. If the data collected is consistent, then the equation will hold true; if not, then the data is flawed and not used in this work. The results of the assessment are summarized in Table 7 with 94% valid days the Cayetano 2111 SCADA data and only 38% for the Menlo 1102 SCADA data. The winter season (November through March) did not feature enough valid days to consider in the analysis, as evident in Figure 20. The process used validate the SCADA data is detailed in Appendix A.

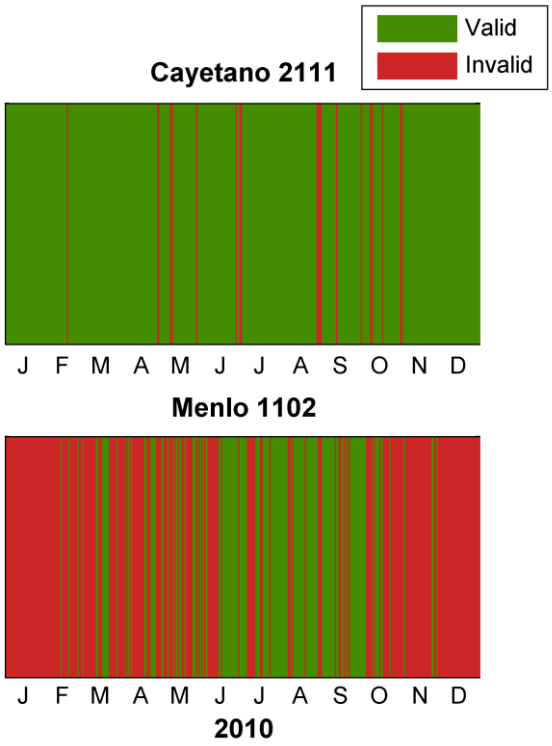

Figure 20. SCADA data validation.

	Cayetano 2111	Menlo 1102
Valid days	344 (94%)	138 (38%)
Invalid days	20 (6%)	227 (62%)

Table 7. SCADA data validation.

B.1 Weather

Before high penetrations of PV can evaluated on the Cayetano 2111 and Menlo 1102 circuit, the balanced three phase model must first be calibrated. Since the circuits have an existing high penetration of PV, knowledge of the amount of generation contribution from the PV installations is critical. Since direct measurement is not available for the majority of the PV installations in the Cayetano and Menlo circuit, it is necessary to estimate the generation through available solar irradiance and temperature. Both solar insolation and temperature signals were attained from SolarAnywhere and from the Quality Controlled Local Climatology Database (QCLCD), respectively. The application of the insolation and temperature to estimate PV generation is described in PV Generation Estimation section (B).

SolarAnywhere is a website run by the Clean Power Institute that provides geospatial and time-resolved solar irradiance for the continental United States [6]. The solar irradiance is estimated using satellite imagery and the SUNY model [7]. The model has been validated in the continental United States to estimate steady-state energy production of a PV system [8]. The datasets contain estimates of Global Horizontal Irradiance (GHI), Direct Normal Irradiance (DNI), and Diffused Horizontal Irradiance (DHI) on thirty minute intervals with a spatial resolution of 1km^2; a single spatial sample is referred to as SolarAnywhere tile in this document. The data collected for use in PV generation estimation is summarized in Table 8.

		SolarAnywhere	**QCLCD**
Cayetano 2111	*Parameter [Units]*	GHI [Wh/m^2] DNI [Wh/m^2] DHI [Wh/m^2]	Temperature [˚C]
	Range	1/1/2010 – 12/31/10	1/1/2010 – 12/31/10
	Resolution	30 min at 1 km	60 min
	Site	Lat: 37.69 to 37.73 Long: -121.81 to -121.77	Livermore Municipal ARPT (23385) Lat: 37.694 Long: -121.817
Menlo 1102	*Parameter [Units]*	GHI [Wh/m^2] DNI [Wh/m^2] DHI [Wh/m^2]	Temperature [˚C]
	Range	1/1/2010 – 12/31/10	1/1/2010 – 12/31/10
	Resolution	30 min at 1 km	60 min
	Site	Lat: 37.42 to 37.33 Long: -122.26 to -122.17	SF International ARPT (23234) Lat: 37.620 Long: -122.398

Table 8. Weather Data.

The temperature data used in the PV estimation was gathered from the Quality Controlled Local Climatology Database (QCLCD) managed by National Climatic Data Center. The QCLCD is a collection of 1600 sites across the United States collecting and processing local climate measurements on hourly intervals [9]. The parameter of interest for the estimation of PV generation is temperature, as summarized in Table 8.

B. PV Generation Estimation

The PV Generation Model is used to estimate the PV generation using insolation, temperature, and PV installation data as inputs. Spatial and temporal insolation data is gathered from SolarAnywhere (Clean Power Institute). SolarAnywhere estimates direct normal, direct horizontal, and diffused horizontal irradiance via satellite imagery. 2010 data is available gratis for the state of California. Temperature information is gathered and processed from the Quality Controlled Local Climatology Database (QCLCD), measured at a local weather station in proximity to the circuit feeder.

To estimate the power production from the local PV installations, an in-house PV estimation model, developed at the Advanced Power and Energy Lab, was used. This model is referred to as the MGH model in this document. The MGH model takes solar irradiance, ambient temperature, and PV installation characteristics as input parameters and estimates the power production of a fixed PV

installation. The model takes into consideration the azimuth and tilt angle of the installation, the ambient temperature and thermal de-rating factors, such as Normal Operations Temperature Celsius (NOTC) and a power de-rating temperature coefficient (P_{max} %/^{o}C), and the estimated inverter/installation losses. The MGH model was verified to be within 5% of the NREL PVWATTS model for California for PV tilt angles ranging from 0 to 45 degrees; the validation was carried out in 2008 [10, p. 240].

As presented in section 5.1.2.3, in the circuits under investigation, neighboring laterals are aggregated to a point bus on the feeder. The PV nameplate capacity located on the aggregated laterals are summed and simulated as a single PV installation. For the majority of the PV installation, the geographic coordinates were available, through the connectivity data, and used to select the appropriate SolarAnywhere tile. In some cases, numerous PV installations spanning an area larger than 1 km^2 were aggregated into a single bus. In these cases, the tile containing the most sites was used. Very few installations had installation information, such as azimuth and tilt angle. When available, the installation was used, otherwise the optimal parameters were used: 0^{o} south facing azimuth and between 10^{o} to 50^{o} tilt angle [11, p. 719]. In the case of aggregate busses featuring multiple PV installations, the average azimuth and tilt angle was used. The thermal de-rating coefficients used are typical for crystalline silicon PV modules; the values used for NOTC and P_{max} coefficients are 47^{o}C and -0.38 %/^{o}C, respectively [11, p. 719]. The ambient temperature input parameters came from QCLCD data, detailed in Table 8 of section B.1. Table 9 below details the input parameters used for each bus to estimate the PV generation at each bus.

Circuit	Bus	Solar Anywhere Tile Centroid		STC NP[kW]	Azimuth	Tilt
		Latitude	Longitude			
Cayetano 2111	3	37.735^{o}	-121.775^{o}	14	0^{o}	20^{o}
Cayetano 2111	8	37.695^{o}	-121.775^{o}	4	0^{o}	20^{o}
Cayetano 2111	16	37.705^{o}	-121.815^{o}	623	-30^{o}	10^{o}
Cayetano 2111	23	37.705^{o}	-121.815^{o}	235	61^{o}	15^{o}
Cayetano 2111	27	37.735^{o}	-121.815^{o}	6	-7^{o}	18^{o}
Cayetano 2111	29	37.715^{o}	-121.805^{o}	1000	-25^{o}	5^{o}
Menlo 1102	2	37.425^{o}	-122.195^{o}	12.4	0^{o}	37^{o}
Menlo 1102	3	37.425^{o}	-122.195^{o}	6.5	0^{o}	37^{o}
Menlo 1102	4	37.425^{o}	-122.195^{o}	10.9	0^{o}	37^{o}
Menlo 1102	9	37.405^{o}	-122.195^{o}	16.3	0^{o}	37^{o}
Menlo 1102	11	37.405^{o}	-122205^{o}	135.7	0^{o}	37^{o}
Menlo 1102	15	37.395^{o}	-122.195^{o}	312.2	0^{o}	37^{o}
Menlo 1102	16	37.385^{o}	-122.205^{o}	34.3	0^{o}	37^{o}
Menlo 1102	17	37.385^{o}	-122.205^{o}	101.9	0^{o}	37^{o}
Menlo 1102	18	37.375^{o}	-122.205^{o}	10.1	0^{o}	37^{o}
Menlo 1102	19	37.375^{o}	-122.195^{o}	77.6	0^{o}	37^{o}
Menlo 1102	20	37.635^{o}	-122.205^{o}	20.3	0^{o}	37^{o}
Menlo 1102	24	37.345^{o}	-122.215^{o}	69.1	0^{o}	37^{o}

Circuit	Bus	Solar Anywhere Tile Centroid		STC NP[kW]	Azimuth	Tilt
		Latitude	Longitude			
Menlo 1102	26	37.345°	-122.195°	3.8	0°	37°
Menlo 1102	28	37.345°	-122.215°	3.8	0°	37°
Menlo 1102	29	37.345°	-122.205°	2.8	0°	37°
Menlo 1102	31	37.335°	-122.195°	13.6	0°	37°
Menlo 1102	32	37.335°	-122.215°	4.3	0°	37°
Menlo 1102	33	37.365°	-122.215°	94.7	0°	37°
Menlo 1102	34	37.635°	-122.215°	23.8	0°	37°
Menlo 1102	35	37.635°	-122.215°	49.4	0°	37°
Menlo 1102	38	37.355°	-122.265°	7.4	0°	37°
Menlo 1102	39	37.335°	-122.205°	20.4	0°	37°
Menlo 1102	41	37.375°	-122.205°	18.6	0°	37°

Table 9. Input parameters into MGH model for PV estimation.

C. Load Demand Estimation

In Figure 21, the plots show the Cayetano circuit demand (P_{SS}, Q_{SS}) sub-station measurement for 10-14-10, the estimations of the local PV (P_{PV}) and capacitor (Q_{CAP}) power contributions, and the estimation of the real and reactive load demand (P_{LD}, Q_{LD}). By observation, it is evident the real and reactive power sub-station measurements in the SCADA data are actually a composite of the circuit load demand and the existing PV and capacitor installations on the circuit. To correctly simulate the circuit with different penetrations and distributions of PV, the load demand must first be estimated in the baseline case.

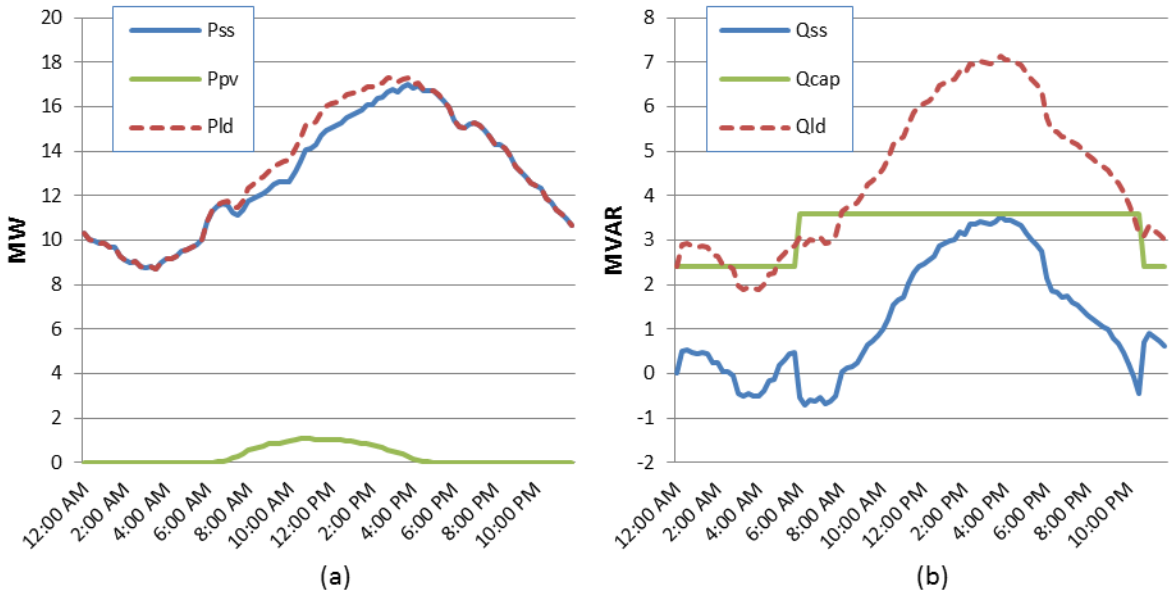

Figure 21. Cayetano 2111 10-14-10 Demand with adjustment.

(a) S/S Real Power vs Time and (b) S/S Reactive Power vs Time.

A stated before, the sub-station real and reactive power is a composite of the load demand and local generation in the circuit. The PV installed in the circuit only accounts for real power generation as according to [4] and the switching capacitors are the source of reactive power support. Capacitance and inductance are 180° out of phase to one another. Distribution line is characteristically inductive (Q > 0), so a capacitor acts as a reactive power generation (Q < 0).

$$P_{SS} = P_{LD} - P_{PV} + P_{loss}\ [W]$$
$$Q_{SS} = Q_{LD} - Q_{CAP} + Q_{loss}\ [var] \qquad \textbf{5-30}$$

5-30 is the set power balance equations for real and reactive power relating the sub-station power to the load demand, generation sources, and loss components. To estimate the load demand, the estimated contributions of the installed PV (P_{PV}) and capacitors (Q_{CAP}) are summed with the sub-station measurement (P_{SS}, Q_{SS}), as shown in 5-31. This step does not account for the power consumed by system losses, such as line loss. The system loss are accounted for in the calibration step detailed in section G.

$$P_{LD} \approx P_{SS} + P_{PV}\ [W]$$
$$Q_{LD} = Q_{SS} + Q_{CAP}\ [var] \qquad \textbf{5-31}$$

The power generation from the installed PV is estimated using the process discussed in section A. Given the availability of irradiance data for the entire year 2010, the load demand real power is estimated for the entire year for both circuits.

On the other-hand, the reactive power profile of the switched capacitors cannot be estimated by an indirect measurement, as P_{PV} is estimated using weather data. The reactive power profile is estimated empirically using capacitor switching control information provided in the connectivity information. The switched controls featured in the Cayetano and Menlo circuits include: 1) time, 2) time with voltage override (VO), 3) temperature, and 4) temperature with VO. Models for these control strategies are detailed in the component model section 5.1.2.1, with exception of temperature based controls. Since only characteristic days are used to evaluate High-Pen PV on distribution circuits and not a stochastic model, it was decided that empirically estimating the operations of the temperature based controls was satisfactory for this analysis. Temperature based switching events are implemented in the simulation using time based control modules.

The switching due to time based controls was easily identifiable, but this was not case for controls featuring voltage override and/or temperature based on controls. Voltage override and temperature controls are dependent dynamic variables (voltage and temperature) that are tightly coupled with the operation of the distribution circuit. Since this step is to achieve an approximate estimate of the load demand, signals such as power and temperature are used to advise the author in the estimation of the switching pattern of the distribution capacitors.

To emphasize the empirical process used to estimate the reactive power profile, the 10-14-10 capacitor reactive power estimate for the Cayetano 2111 is provided as an example. Table 10 is a summary of the

capacitor controls for the six installations in the Cayetano circuit. The control featured in the circuit includes time, time with VO, temperature, and temperature with VO. The switching thresholds indicate the point at which the switching controls will switch the capacitor on, or off, based on time, temperature, or voltage. In the case of capacitor controls with VO, the voltage threshold will supersede either the time or temperature thresholds.

			Temp Thr [^oF]		Time Thr		Voltage Thr [V_{120}]	
Bus	**NP (MVAR)**	**Control**	**Low (On)**	**High (Off)**	**On**	**Off**	**Low (On)**	**High (Off)**
4	0.3	Temp	115	125				
10	1.2	Temp	115	125				
15	1.2	Temp	120	130				
20	1.2	Time w/ VO			9:00 PM	5:00 AM	120	126
21	1.2	Time w/ VO			9:30 PM	5:30 AM	118	125
22	1.2	Time			6:45 AM	10:45 PM		
30	1.8	Temp w/ VO	125	115			118	125

Table 10. Cayetano 2111 Summer Capacitor Controls.

Since time controls are certain to activate, the initial capacitor reactive power profile includes only the capacitor switched on by time controls, as illustrated in Figure 22(a). By observing the resulting load demand estimate (a) and power factor (c), a discrete drop in the reactive power profile is indicative of either (1) a capacitive load coming online or (2) a large drop in load. Load demand is characteristically inductive by nature, making this scenario (1) very unlikely. The Cayetano 2111 is a commercial circuit in the summer and it is more likely that air conditioning would come on-line rather off-line, so scenario (2) is also unlikely. Instead, the logical explanation is that the capacitor support did not drop off but actually increased at 6:00 AM to support the probable air conditioning load, as shown in Figure 22 (b). This indicates that either (1) a voltage override scenario keeps the capacitor on-line or (2) a temperature switching event occurred at 6:00 AM. It is important to note that identifying whether the source of the reactive power support is due to VO or temperature control is important since a predictive model for temperature is not used in this research. In order for a temperature event to occur at 6:00 AM, the capacitor's internal temperature would have crossed the high temperature threshold (>125^oF). This is extremely unlikely since ambient temperature is below 75^oF for the entire morning, as observed in Figure 22(c). The most likely scenario is that a low voltage condition prevented the capacitors from switching off. At this point, an estimate of a reasonable reactive power load demand is reached based on the logic above.

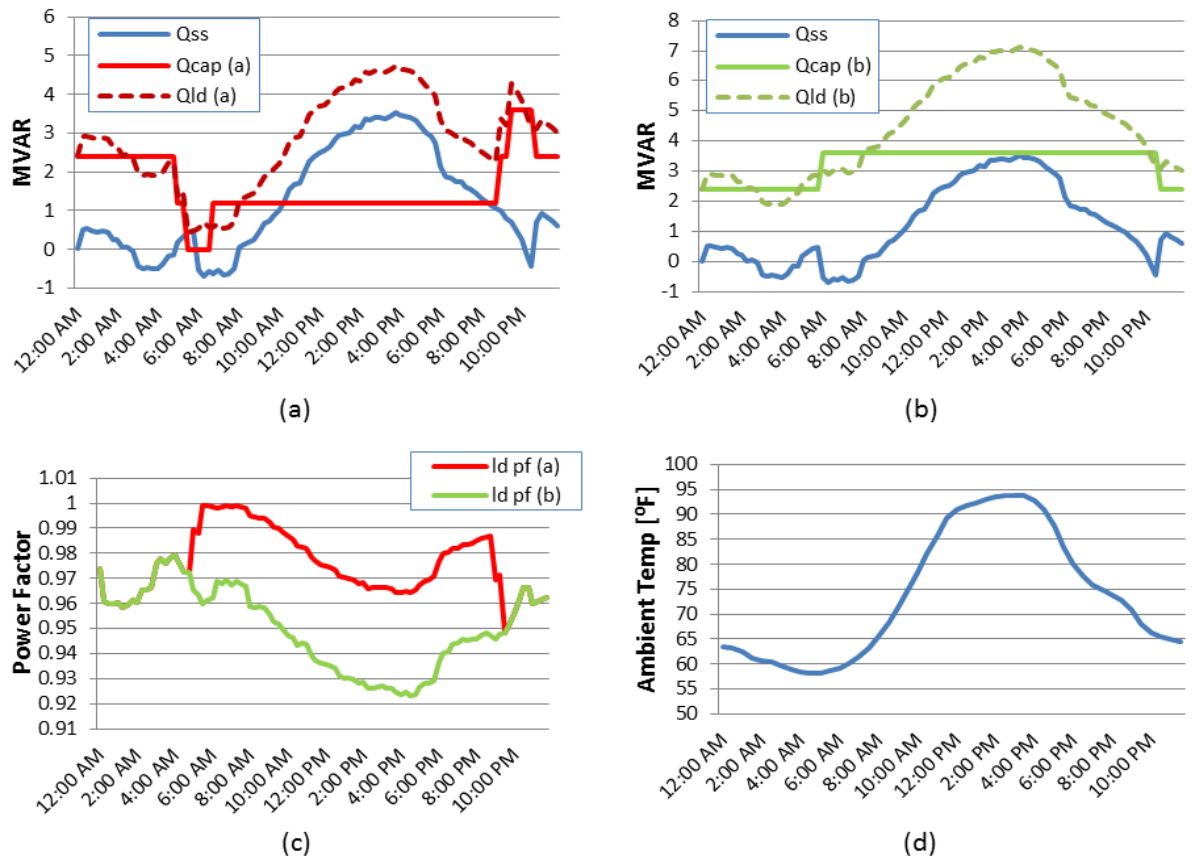

Figure 22. Cayetano 2111 10-14-10 capacitor estimation with (a) time controls only and (b) with time and voltage override controls. (c) The resulting load demand power factor. (d) the local ambient temperature.

The empirical process, described previously, was repeated for each characteristic day under consideration for the both circuits. Since the capacitor switching is not monitored in either circuit, this methodology was justified in providing an initial estimate of the reactive power load demand. The process is error prone, but that is acceptable as it is just an initial estimate the reactive load demand.

The processes described in this section details the methodology used to produce an initial estimate load demand. Since irradiance estimates are available for the entire year, the real power load demand is estimated for the entire year. The empirical process used to estimate the reactive power demand is as efficient, and is only applied to candidate characteristic days. The process of selecting candidate days for simulation is detailed in section 5.1.2.4D. After an initial load demand estimate is produced, the power consumed by line loss is accounted for in the calibration step. The calibration step is explained in the section 5.1.2.4G.

D. Day Selection

The purpose of this research is to identify the effects of High-Pen PV on the distribution system. For safety and reliability concerns, utilities size distribution equipment and control parameters are sized to maintain the system in bounds even in extremes. For this reason, it was decided to approach the characterization of High-Pen PV by simulating the circuit for seasonal low and high days.

To select the characteristic high and low days, a set of criteria was created to identify potential candidate days. The criteria based approach is as follows:

Seasonal high day selection criteria

A. The day's load profile is (mostly) one standard deviation or more above the average.
B. The day's PV estimated generation profile is within one standard deviation of the average.
C. A characteristic day will satisfy both (a) and (b) criteria, but an exception can be made if (a) or (b) is satisfied and sound reasoning is provided for the exception.

Seasonal low day selection criteria

A. The day's load profile is (mostly) one standard deviation or more below the average.
B. The day's PV estimated generation profile is within one standard deviation of the average.
C. A characteristic day will satisfy both (a) and (b) criteria, but an exception can be made if (a) or (b) is satisfied and sound reasoning is provided for the exception.

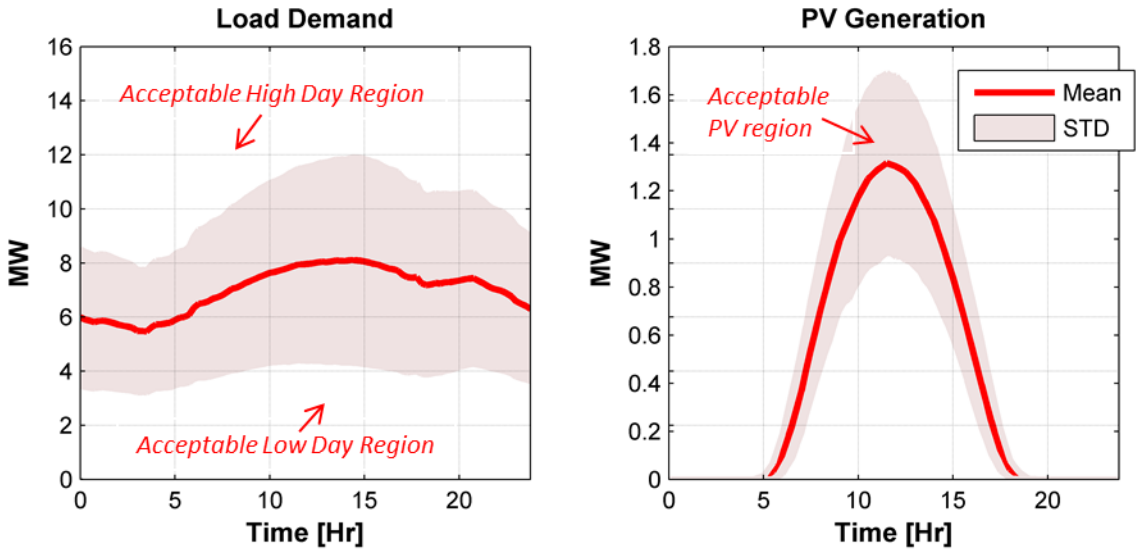

Figure 23. Cayetano 2111 Load Demand and PV Generation Average.

Essentially, a high day is a load demand profile greater than a one standard deviation above the seasonal day mean and a low day is less than a standard deviation below the mean. The seasons under consideration are summer and winter, as defined by PG&E. The summer season is defined to span 4/1 to 10/31 and a winter season to span 11/1 to 3/31. A second criteria applied is to choose a day with an estimated PV generation profile within one standard deviation of the seasonal day mean. The intention of the second criteria (B) is to mitigate the error in the de-coupled load demand stemming from the estimated PV generation. Figure 23 is an example of acceptable regions that meet the criteria defined above.

E. Load/Generation Distribution

Once the circuit-wide load demand has been estimated, the LD is distributed between the buses in the circuit model. To distribute the load, the seasonal customer energy measurements were used to derive a Load Demand Allocation Factor (LDAF). For each aggregate bus, the seasonal energy usage for each customer ($E_{bus\ customer}$ [kWh]) is summed to form a total bus energy usage (E_{bus} [kWh]), as shown in 5-32. Using the total bus energy, a scalar of the whole system energy usage is found, forming the LDAF, as shown in 5-33. Properties of the LDAF include: (1) each bus LDAF is less than 1 and (2) the sum of all the circuit bus LDAFs will equate to 1. To distribute the load demand to each bus, the LDAF is multiplied to the total system LD (P_{LD} [W], Q_{LD} [var]) to form the LD for each bus ($P_{LD,bus}$ [W], $Q_{LD,bus}$ [var]), as shown in 5-34. At this point, the LD has been distributed to each bus for the circuit simulation.

$$E_{bus} = \sum_i E_{bus\ customer,i} \qquad i = 1,2,\dots, bus\ customer_{max} \qquad \textbf{5-32}$$

$$LDAF = \frac{E_{bus}}{\sum_i E_{bus,i}} \qquad i = 1,2,\dots, bus_{max} \qquad \textbf{5-33}$$

$$P_{LD,bus} = LDAF \cdot P_{LD}$$

$$Q_{LD,bus} = LDAF \cdot Q_{LD} \qquad \textbf{5-34}$$

The total PV generation does not require this allocation process. Since the PV generation is estimated for each bus, as detailed in section A, it is already distributed for each and ready for simulation.

F. Post-Processing

As described above , the inputs into the balanced 3 phase feeder model are real and reactive bus load demand, and PV generation. The output of the model is complex voltage (**V**) and current (**I**). The equations below are used to derive real power (P), reactive power (P), per unit voltage (V_{pu}), and phase angle (δ).

$$\boldsymbol{V} = V_R + jV_X = V\ /\underline{\delta} \quad [V] \qquad \textbf{5-35}$$

$$\boldsymbol{I} = I_R + jI_X \quad [A] \tag{5-36}$$

$$P = 3 \cdot Re\{\boldsymbol{V} \cdot \boldsymbol{I}^*\} \quad [W] \tag{5-37}$$

$$Q = 3 \cdot Im\{\boldsymbol{V} \cdot \boldsymbol{I}^*\} \quad [VAR] \tag{5-38}$$

$$V_{pu} = \frac{\sqrt{{V_R}^2 + {V_X}^2}}{V_{base}} \quad [p.u.] \tag{5-39}$$

$$\delta = \tan\frac{V_X}{V_R} \quad [degrees] \tag{5-40}$$

V	→	*Complex voltage [V]*
V_R	→	*Real voltage component [V]*
V_I	→	*Reactive voltage component [V]*
V_{base}	→	*System Voltage [V]*
V_{pu}	→	*Per Unit voltage [p.u.]*
I	→	*Complex current [A]*
I_R	→	*Real current component [A]*
I_X	→	*Reactive current component [A]*
P	→	*Real Power[W]*
Q	→	*Reactive Power [VAR]*
δ	→	*Phase angle [degrees]*

In terms of the bus components in the balanced three phase feeder model, the above equations are used to derive bus load demand for real (P_{ld}) and reactive (Q_{ld}) power, bus capacitors real (P_{CAP}) and reactive (Q_{CAP}) power, and PV generation real (P_{PV}) and reactive (Q_{PV}) power using the component current (**I_{LD}**, **I_{CAP}**,or **I_{PV}**) and the bus voltage (**V**). The per unit voltage (Vpu) and voltage phase angle (δ) is also calculated. The values calculated during post processing are used in the calibration and analysis of the model.

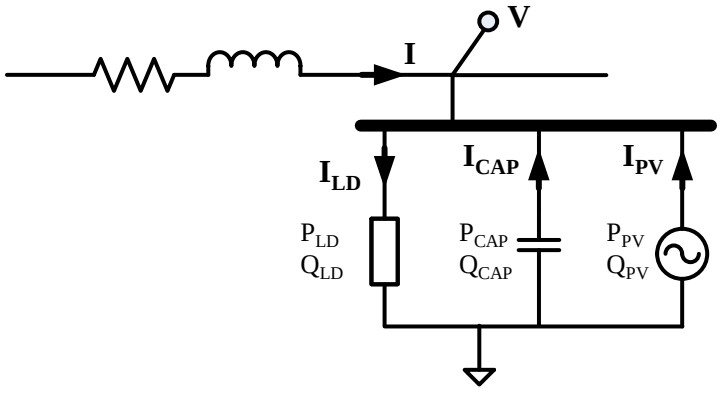

Figure 24. Bus Post Processing.

G. Calibration

The final step in developing the model baseline is calibrating the model inputs to account for system losses, primarily line-losses. The inputs into the three phase balanced model for calibration are: (1) the capacitor and OLTC with LDC model parameters, and (2) the load demand.

Before the load demand is calibrated, the parameters for the capacitor switching and LDC models are calibrated in a two-step process: (1) the LDC is adjusted, then (2) the switching capacitors. During the calibration of the LDC and the switching capacitors, the initial LD (section C) is used with the distribution discussed in section E. Initially, using the settings provided from the connectivity data, the LDC parameters are adjusted so that model output voltage and current match the SCADA voltage and current measurements. While the LDC parameters are under calibration, the estimated capacitor switching is used (section C). Next, the capacitors switching controls are calibrated to approximately match the estimated capacitor switching profile (section C). As with the LDC calibration, initially the settings from the connectivity data are used. Only the switching controls with VO require adjustment. Once the LDC and switching capacitors are calibrated, the LD is addressed.

$$P_{LD} = P_{SS} + P_{PV} - P_{loss}\ [W] \quad \textbf{5-41}$$

$$P_{LD,init} = P_{SS} + P_{PV}\ [W] \quad \textbf{5-42}$$

$$P_{LD,init} \cdot DF = P_{LD}\ [W] \quad \textbf{5-43}$$

$$DF = \frac{P_{LD,init} - P_{loss}}{P_{LD,init}} \quad \textbf{5-44}$$

$$P_{loss} = -\int e \cdot dt\ [W] \quad \textbf{5-45}$$

In section C, the process to develop the first initial load demand is presented. From 5-41, a variant of 5-30, the actual load demand contains a loss component (P_{loss}), but the initial estimate ($P_{LD,init}$) does not, as shown in 5-42. The loss component is attributed to line loss during the transmission of energy on the circuit and is dependent on the bus LD and voltage. Since the line loss is tightly coupled with the operation of the system, an iterative process is used to adjust the input LD to the model in order to account for the line loss, as shown in Figure 25.

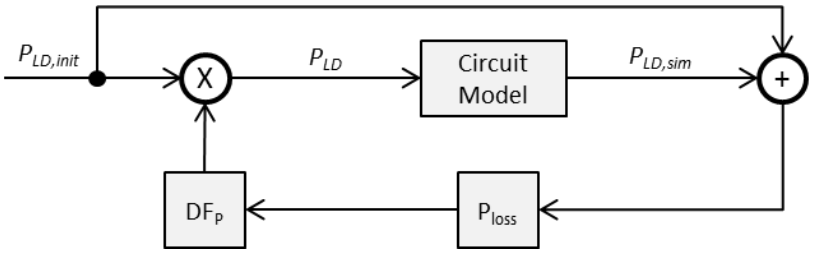

Figure 25. Load Demand Calibration.

To adjust the initial LD, a Deficit Factor (DF) is used to scale the initial estimate to the actual LD, as shown in 5-43. We can solve for the DF, as represented by 5-44, with P_{loss} appearing directly in the DF equation. P_{loss} is estimated by integrating the error between the simulation LD ($P_{ld,sim}$) and the initial LD estimate ($P_{ld,init}$). The process described above is identical for calibrating the reactive power LD, which is done in parallel to the real power LD. In implementation, the process only required three iterations to arrive to a final DF that corrects the initial LD estimate. Continuing forward, it should always be assumed that the LD estimate (found in section C) is adjusted using the DF found in calibration. Following the calibration of the LD, the baseline model is complete. This process is repeated for each characteristic day, on both the Cayetano and Menlo circuits.

5.1.3 Circuit Model Development

Utilizing the modeling methodology described in section 5.1.2, balanced 3 phase models of the Cayetano and the Menlo circuit primary feeder were derived using connectivity data and measured information (provided by PG&E). Below is the description of the resulting models.

5.1.3.1 Commercial Circuit (Cayetano 2111) Three-Phase Balanced Feeder Model

The balanced 3 phase model of the commerical circuit (Cayetano 2111) comprises of thirty buses: 1 bus representing the sub-station, 1 bus representing the Cayetano 2109 feeder, and 28 buses representing the Cayetano 2111. The Cayetano 2111 is the circuit of interest in this study, but the current draw from the adjacent feeder (Cayetano 2109) impacts the tapping behavior of the Load Tap Changing transformer found at the sub-station and is simulated as a lumped load. The operatino voltage of the model is 21kV. Figure 26 is a diagram of the commercial (Cayetano) circuit model.

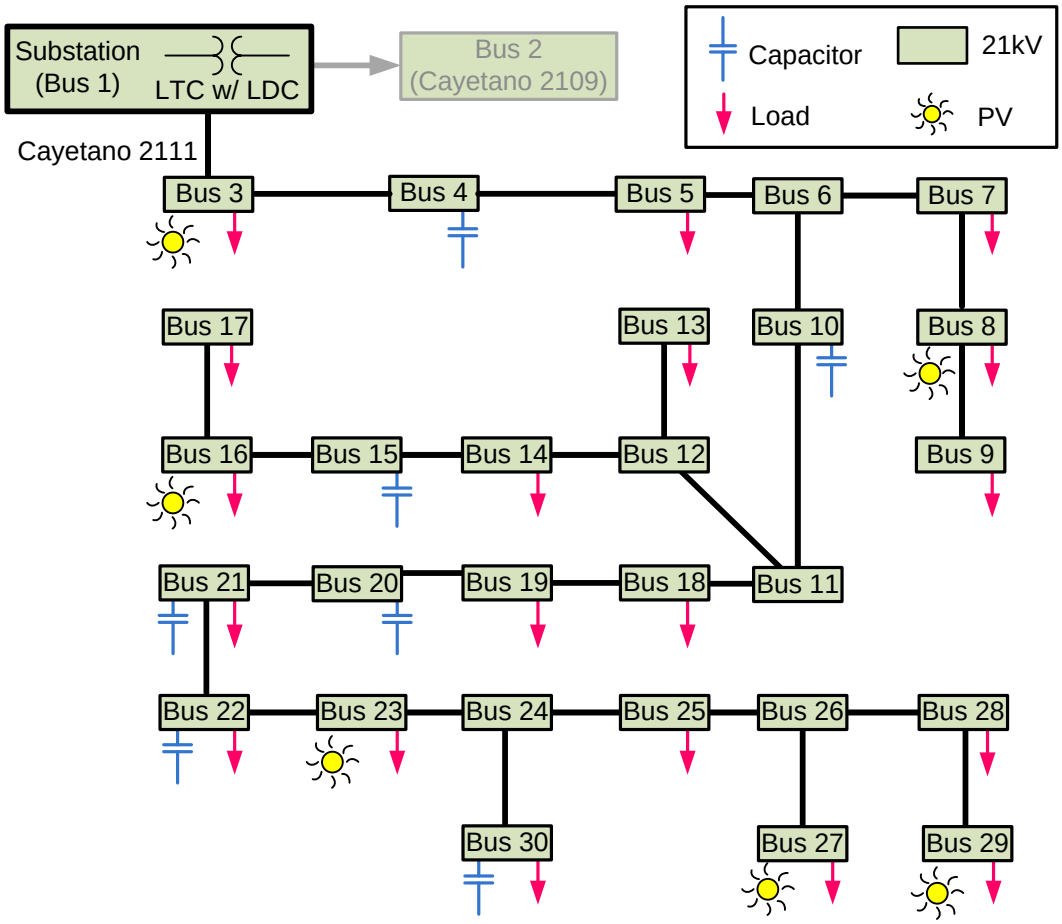

Figure 26. The commercial circuit (Cayetano 2111) balanced three phase model block diagram.

The Cayetano 2111 model represents the load demand distribution via 19 buses. The distribution value at each bus is derived using the method presented in section (E). The 7 capacitors and 7 PV installations in the circuit are each represented with a bus to maintain the spatial postion within the circuit. The line impedance between each bus is the aggragated series positive sequence resistances and reactances. The values used for each bus line impedance, load demand, capacitor, and PV rating are listed in Table 11.

Bus	Line Length [ft]	Line Resistance [Ω]	Line Reactance [Ω]	Load Demand Distribution	Capacitor Rating [kVAR]	PV Rating [kW]
3	4340	0.1141	0.3051	0.25%	-	14
4	1708	0.0475	0.1361	-	1800	-
5	6963	0.1936	0.5550	0.18%	-	-
6	2026	0.0563	0.1615	-	-	-
7	1810	0.0380	0.0679	0.81%	-	-
8	1344	0.0316	0.0715	7.32%	-	4
9	1617	0.0281	0.0243	3.59%	-	-
10	11642	0.2817	0.6671	-	1200	-
11	20	0.0003	0.0003	-	-	-
12	95	0.0017	0.0014	-	-	-

Bus	Line Length [ft]	Line Resistance [Ω]	Line Reactance [Ω]	Load Demand Distribution	Capacitor Rating [kVAR]	PV Rating [kW]
13	2915	0.0507	0.0437	5.72%	-	-
14	2375	0.0413	0.0356	1.66%	-	-
15	500	0.0087	0.0075	-	1200	-
16	1095	0.0191	0.0164	13.77%	-	623
17	446	0.0123	0.0168	5.25%	-	-
18	909	0.0158	0.0136	2.84%	-	-
19	309	0.0054	0.0046	2.58%	-	-
20	149	0.0026	0.0022	-	1200	-
21	1151	0.0200	0.0173	1.72%	1200	-
22	675	0.0117	0.0101	23.57%	1200	-
23	650	0.0113	0.0098	13.86%	-	235
24	427	0.0074	0.0064	-	-	-
25	1414	0.0246	0.0212	4.42%	-	0
26	510	0.0089	0.0077	-	-	-
27	421	0.0073	0.0063	1.41%	-	6
28	172	0.0417	0.0085	0.03%	-	-
29	1253	0.5864	0.1516	8.36%	-	1000
30	1970	0.0343	0.0296	2.66%	1800	-

Table 11. Cayetano 2111 model bus configuration.

The Cayetano circuit features a Load Tap Changing (LTC) transformer with Load Drop Compensatation (LDC) at the sub-station and various capacitor switching controls at the capacitor installation. The capacitor controls switching present on the circuit include Time-Clock (TC), Temperature (Temp), Time-Clock with Voltage Override (TC w/ VO), and Temperature with Voltage Override (Temp w/ VO). Table 12 includes the list of switching controls found at each bus for each characteristic day. As stated in previous sections, this research did not develop a predictive temperature switching control model, so temperature based controls are approximated with TC controls. The detailed control settings for the LTC and capacitor installation are found in Appendix B.

Bus	Equip.	Rating	Summer High	Summer Low	Winter High	Winter High
1	LTC	27 MVA	LDC	LDC	LDC	LDC
4	Cap	1.8 MVAR	Temp	Temp	Off	Off
10	Cap	1.2 MVAR	Temp	Temp	Off	Off
15	Cap	1.2 MVAR	Temp	Temp	Temp	Temp
20	Cap	1.2 MVAR	TC w/ VO	TC w/ VO	TC w/ VO	TC w/ VO
21	Cap	1.2 MVAR	TC w/ VO	TC w/ VO	TC w/ VO	TC w/ VO
22	Cap	1.2 MVAR	TC	TC	TC	TC
30	Cap	1.8 MVAR	Temp w/ VO	Temp w/ VO	Off	Off

Table 12. Cayetano 2111 model voltage regulation controls.

As described in section D, the Cayetano circuit model is calibrated to seasonal characteristic extreme high and low days. The evaluation of the characteristic days selected for the Cayetano model is described in Table 13 and the characteristic days are shown in Figure 27.

	Characteristic Day	Date	Criteria		Justification
			(A)	(B)	
Cayetano 2111	Summer High	10/14/2010	Yes	Yes	Criteria met
	Summer Low	4/4/2010	Yes	No	The load demand profile is significantly lower that the criteria limit. In this case, the PV profile is less significant.
	Winter High	11/8/2010	Yes	Yes	Criteria met
	Winter Low	2/14/2010	Yes	Yes	Criteria met

Table 13. Result of criteria based selection of characteristic days.

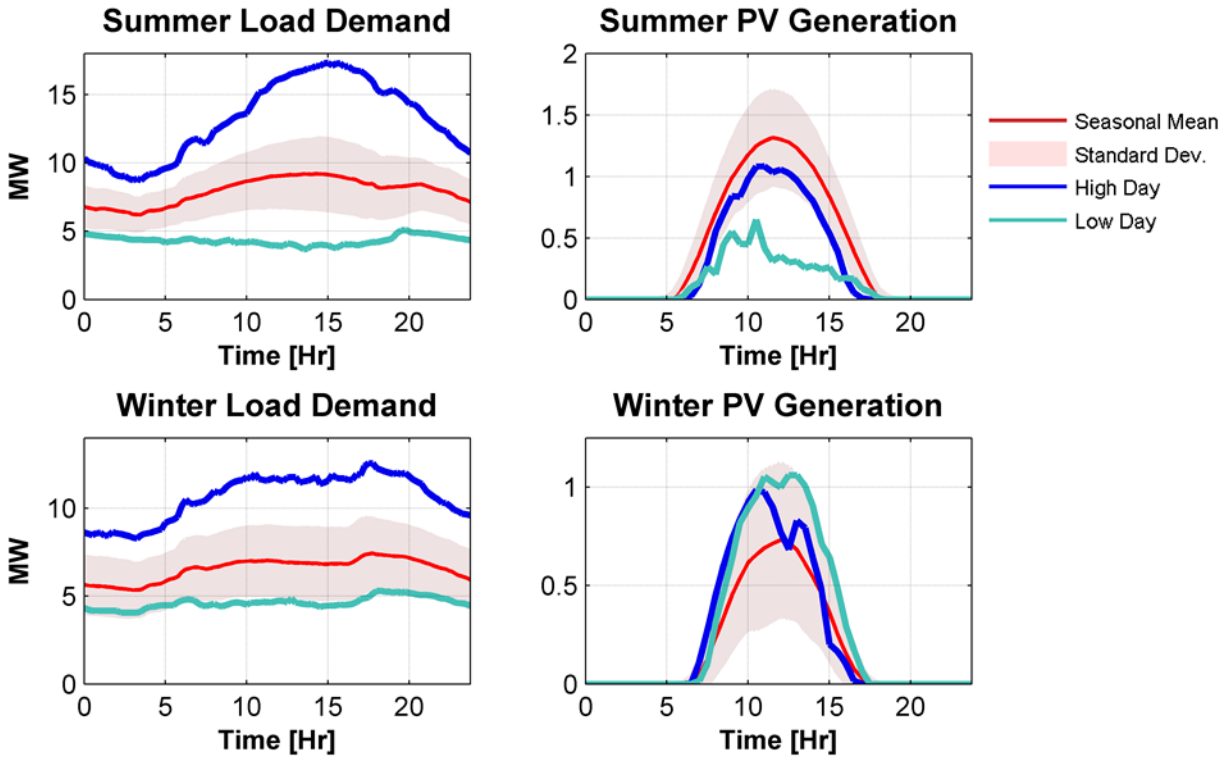

Figure 27. Characteristic days selected for Cayetano 2111 circuit model.

After the three phase balanced model of the circuit is formed and the characteristic days selected, the load demand is calibrated to compensate for the unaccounted line loss in the initial estimate of the circuits load demand, as described Calibration section (G). Once the characteristic day is calibrated, the derived DF is used to correct the initial estimate of the circuit load demand for any simulation, henceforth. The time resolved load demand, estimated PV generation, and DF used in the calibration of each characteristic day are found in Appendix B.

5.1.3.2 Residential Circuit (Cayetano 1102) Three-Phase Balanced Feeder Model

The balanced 3 phase feeder model of the residential circuit (Menlo 1102) comprises of 42 buses: 1 bus representing the sub-station, 1 bus representing the Menlo 1101 feeder, and 40 buses representing the Menlo 1102. The Menlo 1102 is the circuit of interest in this study, but the current draw from the adjacent feeder (Menlo 1102) impacts the tapping behavior of the Load Tap Changing transformer found at the sub-station and is simulated as a lumped load; the real and reactive load demand of the Menlo 1101 is shown in Appendix C. The Menlo 1102 has two operating voltage 12.47kV and 4.16kV: buses 2 through 19 and 32 through 40 operate at 21kV and buses 23 through 24 operate at 4.16kV. Appart from the Load Tap Changing transformer at the sub-station, the circuit also has a 3% boosting transformer, found at bus 14, and step down transformers, found at buses 23 and 34. Bus 34 steps the voltage from 21kV to 4.16 kV, but the generation and the load demand found behind the transformer are lumped and the measurements are taken from the 21kV side of the transformer. Figure 28 is a diagram of the residential (Menlo) circuit model.

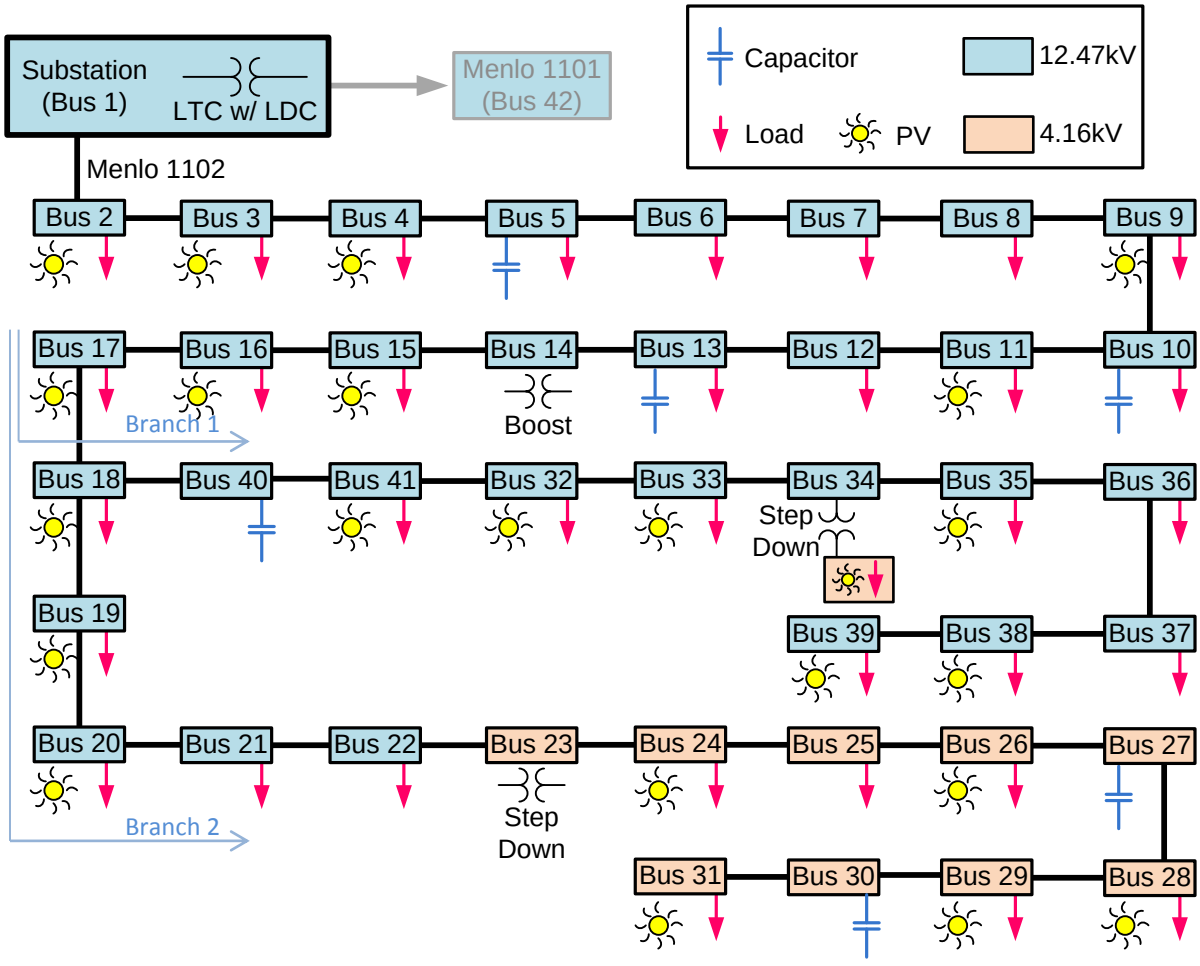

Figure 28. The residential circuit (Menlo 1102) balanced three phase model block diagram.

The model represents the Menlo 1102 feeder's load demand distribution via 40 buses. The distribution value at each bus is derived using the method presented in section E. The 6 capacitors in the circuit are each represented with a bus to maintain their spatial postion within the circuit. The 165 PV installations of the feeder are represented within 23 buses. The PV installations were aggregated the same as the load demand for each bus. The line impedance between each bus is the aggragated series positive sequence resistances and reactances. The values used for each buses line impedance, load demand, capacitor, and PV rating are listed in Table 14.

Bus	Line Length [ft]	Line Resistance [Ω]	Line Reactance [Ω]	Load Demand Distribution	Capacitor Rating [kVAR]	PV Rating [kW]
2	3515	0.0673	0.1232	6.41%	-	12.4
3	630	0.0110	0.0095	5.03%	-	6.5
4	1716	0.0472	0.1335	2.08%	-	10.9
5	1401	0.0389	0.1117	0.18%	600	-
6	177	0.0049	0.0141	2.96%	-	0
7	1905	0.0530	0.1518	0.99%	-	-
8	1955	0.0500	0.1336	3.41%	-	-
9	1910	0.0531	0.1522	2.16%	-	16.3
10	430	0.0120	0.0343	4.49%	900	-
11	617	0.0172	0.0492	12.60%	-	135.7
12	655	0.0182	0.0522	3.41%	-	-
13	1503	0.0327	0.0738	0.02%	600	-
14	307	0.0085	0.0245	-	-	-
15	231	0.0064	0.0184	13.31%	-	312.2
16	4175	0.1161	0.3327	3.32%	-	34.3
17	2696	0.0749	0.2149	6.74%	-	101.9
18	1133	0.0315	0.0903	1.30%	-	10.1
19	718	0.3359	0.0869	0.58%	-	77.6
20	2152	0.9939	0.2604	0.12%	-	20.3
21	2860	1.3385	0.3461	1.30%	-	-
22	3904	1.0567	0.2274	1.88%	-	-
23	515	0.0953	0.0160	-	-	-
24	195	0.0361	0.0091	2.01%	-	69.1
25	1826	0.5263	0.2078	0.91%	-	-
26	692	0.2007	0.0789	1.90%	-	3.8
27	352	0.0347	0.0359	-	300	-
28	461	0.0454	0.0470	0.29%	-	3.8
29	1585	0.5477	0.1819	0.60%	-	2.8
30	405	0.1895	0.0490	-	300	-
31	158	0.0739	0.0191	2.48%	-	13.6
32	1954	0.1332	0.1187	0.74%	-	4.3
33	320	0.0295	0.0305	3.27%	-	94.7
34	1702	0.1785	0.1689	5.07%	-	23.8
35	706	0.0826	0.0727	2.71%	-	49.4
36	3743	0.4379	0.3855	0.00%	-	-
37	5561	0.6459	0.5725	0.34%	-	-
38	3307	0.3869	0.3406	1.23%	-	7.4
39	5320	2.4792	0.6432	2.44%	-	20.4

40	202	0.0056	0.0161	-	900	-
41	970	0.0424	0.0549	3.70%	-	18.6

Table 14. Menlo 1102 model bus configuration.

The Menlo circuit features a Load Tap Changing (LTC) transformer with Load Drop Compensatation (LDC) at the sub-station and various capacitor switching controls at the capacitor installation. The capacitor controls switching present on the circuit include Time-Clock (TC) and Time-Clock with Voltage Override (TC w/ VO). Table 15 includes the list of switching controls found at each bus for two characteristic days evaluated. The detailed control settings for the LTC and capacitor installation are found in Appendix C.

Bus	Equip.	Rating	Summer High	Summer Low
1	LTC	16 MVA	LDC	LDC
5	Cap	0.6 MVAR	On	On
10	Cap	0.9 MVAR	TC w/ VO	TC w/ VO
13	Cap	0.6 MVAR	TC w/ VO	TC w/ VO
27	Cap	0.3 MVAR	Off	Off
30	Cap	0.3 MVAR	TC w/ VO	TC w/ VO
40	Cap	0.9 MVAR	TC w/ VO	TC w/ VO

Table 15. Cayetano 2111 model voltage regulation controls.

As described in section D, the Menlo circuit model is calibrated to seasonal characteristic extreme high and low days. Given the inconsistency of the measured data during the winter season (section A.1), only summer charactereristic days were evaluated. The evaluation of the charactereristic days selected for the Menlo model are described in Table 16 and the characteristic days are shown in Figure 27.

	Characteristic Day	**Date**	**Criteria**		**Reason**
			(A)	**(B)**	
Menlo 1102	Summer High	9/28/2010	Yes	Yes	Criteria met
	Summer Low	7/2/2010	No	Yes	The Menlo circuit load demand it extremely erratic. While the selected is not a standard deviation below, it one of the few profile below the average for the majority day.

Table 16. Result of criteria based selection of characteristic days.

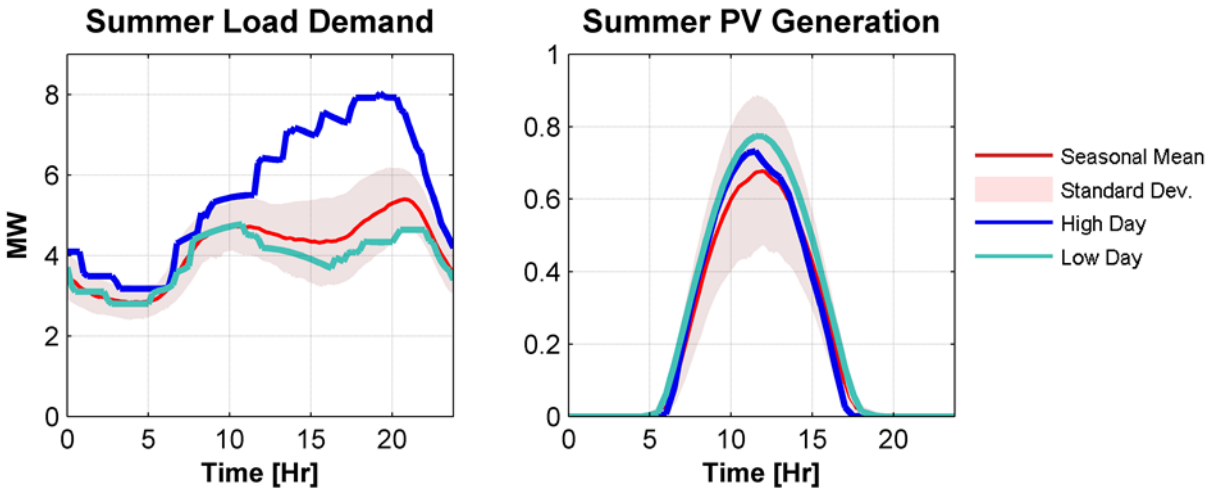

Figure 29. Characteristic days selected for Menlo 1102 circuit model.

After the three phase balanced model of the circuit is formed and the characteristic days selected, the load demand is calibrated to compensate for the unaccounted line loss in the initial estimate of the circuits load demand, as described in section G. Once the characteristic day is calibrated, the derived DF is used to correct the initial estimate of the circuit load demand for any simulation, henceforth. The time resolved load demand, estimated PV generation, and DF used in the calibration of each characteristic day are found in Appendix C.

5.1.3.3 Evaluation Results

In this research, the commercial (Cayetano) and residential (Menlo) circuit models are evaluated at characteristic seasonal extreme days. For each day, the initial load demand is estimated from the sub-station SCADA measurement and distributed throughout the bus in the three phase balanced feeder model for both circuits and then calibrated with a DF to account for line loss. The derived DF are specific to each characteristic day, so it is applied to similar days to evaluate the representative nature of the calibration. The results are then compared to the available sub-station SCADA measurements: this includes sub-station real and reactive power, voltage, and current for the Cayetano and real and reactive power and current for the Menlo. The error is calculated between the simulation results and the SCADA measurements using Normalized Root Mean Square Error (NRMSE), as shown in equation 5-46, to rationalize the error into a single metric.

$$NRMSE = \frac{\sqrt{\sum_{t=1}^{96}\left(x_{SCADA,t} - x_{SIM,t}\right)^2}}{x_{SCADA,max} - x_{SCADA,min}} \qquad \text{5-46}$$

$x_{SCADA,t}$ → *The SCADA measurement at time "t"*
$x_{SIM,t}$ → *The simulation result at time "t"*
$x_{SCADA,max}$ → *The day maximum SCADA measurement*
$x_{SCADA,min}$ → *The day minimum SCADA measurement*

The results of the DF evaluation each characteristic day are shown in Table 17. The NRMSE between the various days is expected to vary given the predictive Load Drop Compensation and capacitor switching controls present in both circuits, but consistency between the alternative days is also expected. Consistency is the expected expectation between the NRMSE for the alternative days.

Circuit	Day	Date	Normalized RMS Error [%]			
			P_{NRMSE}	Q_{NRMSE}	I_{NRMSE}	V_{NRMSE}
Cayetano	Summer High	10/14/2010	3.08E-03%	0.04%	1.15E-06%	1.68E-05%
		10/13/2010	0.13%	9.23%	1.09E-06%	2.28E-05%
		10/15/2010	0.18%	3.62%	1.54E-06%	1.79E-05%
	Summer Low	4/4/2010	3.59E-03%	0.12%	5.13E-06%	3.51E-05%
		4/6/2010	0.14%	9.95%	4.04E-06%	3.85E-05%
		4/7/2010	0.15%	19.72%	5.48E-06%	2.84E-05%
		4/9/2010	0.17%	15.49%	6.7E-06%	5.27E-05%
	Winter High	11/8/2010	1.13E-04	0.01%	1.56E-06%	3.45E-05%
		11/11/2010	0.50%	14.27%	2.74E-06%	1.99E-05%
		11/10/2010	0.52%	11.46%	2.92E-06%	3.01E-05%
		11/16/2010	0.42%	11.32%	2.35E-06%	3.14E-05%
	Winter High	2/14/2010	2.48E-03%	0.09%	5.89E-06%	3.61E-05%
		2/28/2010	0.02%	18.18%	5.88E-06%	2.49E-05%
		1/10/2010	0.06%	3.59%	5.07E-06%	3.09E-05%
		3/13/2010	0.05%	2.80%	3.66E-06%	5.3E-05%
Menlo	Summer High	9/28/2010	3.17E-03%	0.16%	5.72E-06%	-
		9/27/2010	0.13%	1.82%	5.23E-06%	-
		10/12/2010	0.37%	15.15%	5.22E-06%	-
		10/13/2010	0.26%	9.30%	5.76E-06%	-
	Summer Low	7/2/2010	3.75E-03%	0.11%	1.06E-05%	-
		7/31/2010	0.14%	15.61%	9.1E-06%	-
		8/14/2010	0.12%	14.78%	7.95E-06%	-
		8/4/2010	0.09%	0.85%	1.83E-05%	-

Table 17. The Deficit Factor evaluation results for the Cayetano and Menlo characteristic days.

Reflecting upon the evaluation results, NRMSE for sub-station real power, voltage, and current are consistent between the characteristic days. Sub-station reactive power tends to have a larger range of variability give the course nature so switching capacitor controls. Even so, the maximum NRMSE for the sub-station reactive power is 19.72% and is deemed acceptable for this research. Given the results above, the derived DFs for each of the Cayetano and Menlo characteristic days are shown to be an acceptable representation of the circuit at the point of the sub-station measurement.

5.2 Task 3: Quantify PV Integration Limits

Phenomena that limit PV penetration with standard inverters and distribution circuit operation are to be identified for the three scenarios described. The models from Task 1 will be used to parametrically evaluate PV grid impacts in a variety of conditions. The specific parameters for investigation will be developed through the PG&E/APEP partnership, but will likely include the sensitivity of distributed generation (DG) PV array size on integration limit along with temporal/stochastic effects, such as diurnal and cloud cover dynamics, on the distribution system. Guidelines for PV integration limits and

performance tradeoffs will be developed for typical distribution circuits that have neither communication nor advanced inverter topologies.

Following the development of the three phase balanced characteristic day circuit models for a commercial (Cayetano) and a residential (Menlo) circuit, they are used to characterize the effects of High Penetration Photo-Voltaic (High-Pen PV) generation on the circuits. The evaluation focuses on the behavior of the primary feeder in order to understand the impact of High-Pen PV on line-voltage and voltage control equipment, such as Load Tap Changing transformer with Load Drop Compensation and switching capacitors. The results of the evaluation are presented in three parts: 1) the concepts background (section 5.2.1), 2) evaluation results (section 5.2.2), and 3) a summary of the findings (section 5.2.3). The results are presented using the terminology and metrics presented in the conceptual section.

5.2.1 Conceptual Background

To enable a clear and effective discussion, concepts used in the analysis of high penetrations of Photo Voltaic (High-Pen PV) on distribution circuits are presented prior to the results. The concepts discussed in this section are used in the analysis PV generation characteristics, load characteristics, and voltage rise characteristics in radial distribution circuits.

5.2.1.1 Photo-Voltaic Generation Characteristics

PV generation is a variable that is power dependent on the local weather. Typically, the nameplate rating of a PV installation indicates the maximum output of PV generation in standard test conditions. To understand the influence of High-Pen PV on the distribution circuit, the capacity and variability of PV generation must be described. PV Penetration, Region, and Peak are used in this study to describe the influence of High-Pen PV on distribution circuits

$$Nameplate\ PV\ Penetration = \frac{PV\ Nameplate}{Yearly\ Peak\ Load\ Demand} \cdot 100 \qquad \textbf{5-47}$$

In this study, a power ratio is used to describe PV penetration. The percentage of nameplate PV capacity to yearly peak load demand is known as Nameplate PV Penetration, summarized in equation 5-47. Nameplate PV Penetration is commonly used by utilities to describe the amount of installed PV capacity in distribution circuits [12]. Table 18 is the Nameplate Penetration of the Cayetano and Menlo circuits as of 2010. While the Nameplate Penetration contains information about the amount of installed PV capacity relative the circuits peak load demand, it does not reveal information about 1) the variability of solar generation and 2) the coincidence to peak PV generation to peak load demand.

Circuit	PV Nameplate	Peak Load Demand	Penetration
Cayetano 2111	1.873 MW	12 MW	15.6%
Menlo 1102	1.105 MW	9.1 MW	12.1%

Table 18. 2010 PV Penetration of Cayetano and Menlo Circuits.

PV generation is a variable power source that is dependent on the amount of solar irradiance received from the Sun, so the amount of generation could potentially vary from nothing to full capacity depending on weather. Since the Nameplate Penetration does not reveal information about variability, High-Pen PV is evaluated at zero and full capacity to understand the steady-state extremes of PV generation.

Nameplate PV Penetration also does not contain information about the coincidental nature of Peak PV generation and peak load demand. On clear sunny days, peak PV generation occurs approximately midday, while peak load demand occurs in the afternoon for commercial circuits and evening for residential circuits (see section 5.1.1). The Nameplate Penetration metric does not capture this fact, so the entire day is simulated to understand the non-coincidental nature of PV generation the load demand on the distribution circuit.

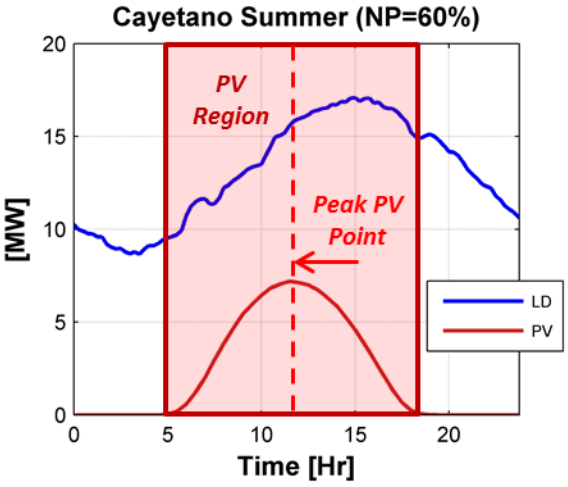

Figure 30. PV Region and Peak PV of a Cayetano Summer Day.

During the day, a PV installation influences line voltage and control equipment when the PV installation is generating power. The period during the day when PV installations are generating power is referred to as the PV Region. Effects on the distribution circuit caused by High-Pen PV will occur in this region. In the PV region, the maximum sensitivity to PV generation will occur during the time of day of maximum generation, referred to as the Peak PV Point in this document. The analysis of full day simulations will focus on the PV region and the Peak PV Point in order to characterize High-Pen PV influence on distribution circuits.

Given the variable and non-coincidental nature of PV, it is important to characterize PV generation with generic metrics to analyze different circuit topologies with High-Pen PV. This study utilizes Nameplate Penetration, PV Region, and the Peak PV Point to analyze a commercial and residential circuit.

5.2.1.2 Load and Generation Distribution

Distribution circuits can vary greatly in both topology and load demand distribution. In this study of High-Pen PV, a commercial and a residential distribution radial circuit are under investigation. To characterize the distribution of the load demand and the generation on the circuits, the Load Center and Generation Center metrics are used.

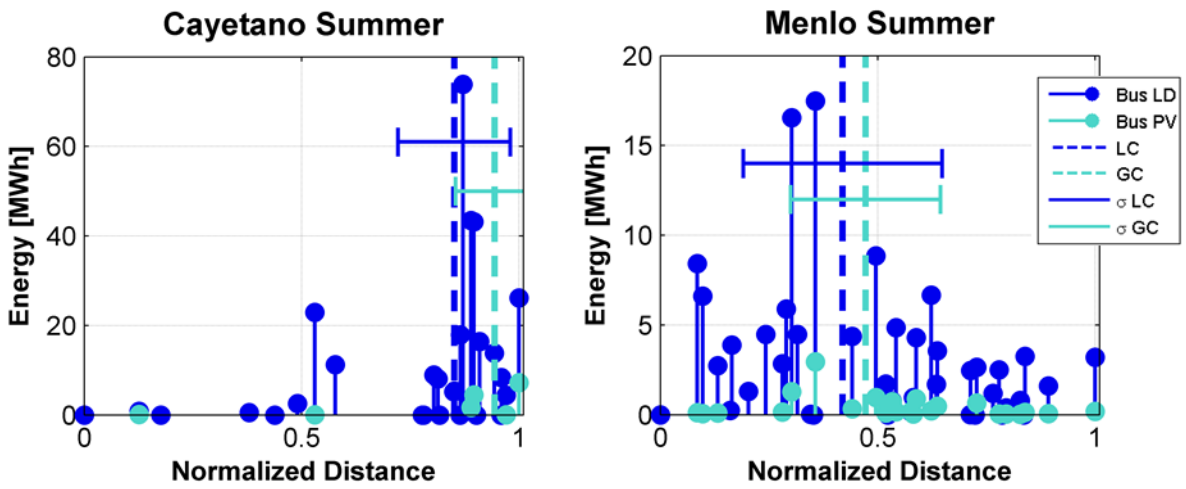

Figure 31. Load and Generation Centers of the Cayetano and Menlo as of 2010.

Figure 31 is the bus load and PV generation distribution of the Cayetano and Menlo circuit versus the normalized distance from the sub-station for a summer day in 2010. Each vertical stem represents the bus energy consumed and/or generated by the bus load and/or generation. The normalized distance represents the length of distribution line between each bus and the sub-station. This length is normalized to the longest stretch of line between a bus and the sub-station on the feeder. Using a normalized distance, the sub-station is 0 and the farthest bus is 1. The dashed vertical lines represent the load center and generation centers on the circuit and the horizontal error bar indicates the standard deviation. The metrics for the load center and generation center are weighted averages of energy-to-distance from the sub-station. 5-48 and 5-49 below are formulation of the Load Center (LC) calculation and the standard deviation of the Load Center (σ_{LC}). Likewise, 5-50 and 5-51 formulate the Generation Center (GC) and the standard deviation (σ_{GC}). The LC and GC metrics are useful to describe the relative location of the load and generation in relation to the sub-station. The LC and GC standard deviation indicate how the load demand and generation are distributed along the line; a small standard deviation value indicates a tight distribution around the load/generation center and a large value indicates a loose distribution.

$$Load\ Center\ (LC) = \frac{\sum_i E_{LD,i} \cdot d_i}{\sum_i E_{LD,i}} \qquad \textbf{5-48}$$

$$\sigma_{LC} = \sqrt{\sum_i \left\{ \frac{E_{LD,i}}{\sum_j E_{LD,j}} \cdot (d_i - LC)^2 \right\}} \qquad \textbf{5-49}$$

$$Generation\ Center\ (GC) = \frac{\sum_i E_{PV,i} \cdot d_i}{\sum_i E_{PV,i}} \qquad \textbf{5-50}$$

$$\sigma_{GC} = \sqrt{\sum_i \left\{ \frac{E_{PV,i}}{\sum_j E_{PV,j}} \cdot (d_i - GC)^2 \right\}} \quad \text{5-51}$$

i , j = 1,2,…, Total Bus Count
$E_{LD,i}$ = Total Day Energy consumed by Bus "i"
$E_{PV,i}$ = Total Day Energy generated by Bus "i"
d_i = Normalized line distance of Bus "i" from sub-station

Applying the Load Center and Generation center metrics to the Cayetano and Menlo provides insight into the location and distribution of the load and PV installations present on both circuits and enable a parametric comparison of the two circuits. From Figure 31 and Table 19, we see that the Cayetano has an LC value of 0.85 and Menlo has an LC value of 0.42. This indicates that the load is located at the end of the circuit for Cayetano and located mid-circuit for the Menlo. The distribution of the load demand about the LC is indicated by the standard deviation; the Cayetano load demand is tightly distributed about the LC (+/- 0.13) while the Menlo is loosely distributed (+/- 0.23). For both the circuits, the GC is located relatively close to the LC, which is expected for roof-top PV installations. Again, the distribution of Cayetano PV tightly clustered about the GC (+/- 0.09), while Menlo PV is loosely distributed (+/- 0.17). This distribution, as indicated by the GC standard deviation, is also expected since Cayetano features only a few large roof-top PV installations in a business park, while Menlo feature many small roof-top PV installations in a residential neighborhood.

Circuit	Season	LC	σ_{LC}	GC	σ_{GC}
Cayetano	Summer	0.85	±0.13	0.94	±0.09
	Winter	0.85	±0.13	0.94	±0.09
Menlo	Summer	0.42	±0.23	0.47	±0.17

Table 19. Cayetano and Menlo Load and Generation Center in 2010.

High-Pen PV spatial influence on distribution circuits is dependent on the distribution of the load demand and PV installations. Using the LC and GC metrics, a parametric description of the distribution of the load and generation is established.

5.2.1.3 Voltage Drop and Rise in Radial Distribution Circuits

During the process of transmitting energy from the sub-station through the distribution circuit and to the customer, energy is lost, resulting in a decrease in line voltage. This decrease in voltage, also known as voltage drop or line drop, is a critical characteristic of radial distribution circuits and is a crucial aspect in how High-Pen PV interacts with the distribution circuit. The monotonic decrease in line voltage as distance increases from the sub-station is a fundamental assumption used by utilities in both the design and regulation of distribution circuits [13]. The following subsections describe the classic theory behind voltage drop, followed by a description of the theory of voltage rise caused by generation located in the circuit.

A. Voltage Drop Approximation

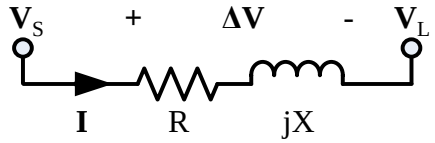

$\mathbf{V}_S = V_S \angle\delta$	→	*Source Voltage*
$\mathbf{V}_L = V_L \angle 0$	→	*Load Voltage*
$\mathbf{\Delta V} = \Delta V \angle\varphi$	→	*Voltage Drop*
R	→	*Line Resistance*
X	→	*Line Reactance*
$\mathbf{I} = I \angle -\theta$	→	*Line Current*

Figure 32. Line to Neutral Line Drop Model.

Figure 32 is a basic model of a single phase of a balanced three phase distribution line. If the phases are balanced, then we can neglect the return impedance [2, Ch. 2.7], therefore it is not shown in Figure 32. In typical radial distribution circuits, power flows from the sub-station ($\mathbf{V_S}$) to the load ($\mathbf{V_L}$), as indicated by the direction of the line current (**I**) magnitude. The voltage drop (**ΔV**) is expressed in two forms in Equation 5-52: 1) Kirchhoff's Law and 2) Ohm's Law. In observation of the phasor diagram of the line drop model (Figure 33), the phase difference between $\mathbf{V_S}$ and $\mathbf{V_L}$ is δ. For short transmission lines, as found in distribution feeders, δ is marginal and may be neglected leading to an approximation of the magnitude of **ΔV**, as shown in Equation 5-53 [5, p. 384]. If δ is small, then this approximation is very accurate [14, pp. 40–41]. Furthermore, if we assume that the line current is inductive (-θ), then the magnitude of **ΔV** can be expressed in terms of the in-phase current (I_R) and out-of-phase current (I_X), as shown in Equation 5-54. The in-phase and out-of-phase currents are the quadrature components of the line current (**I**) and are formulated in Equations 5-55 and 5-56, respectively.

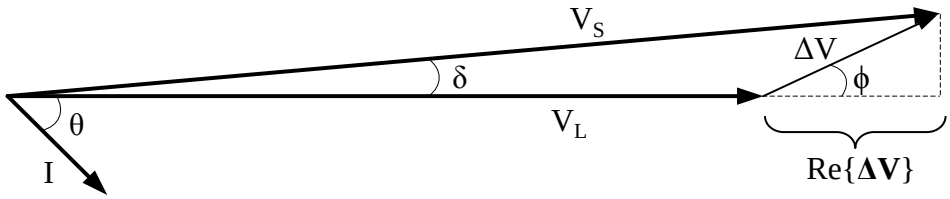

Figure 33. Phasor Diagram of Line Drop Model.

$$\Delta \boldsymbol{V} = \boldsymbol{V_S} - \boldsymbol{V_L} = \boldsymbol{I} \cdot (R + jX) \quad \textbf{5-52}$$

$$\Delta V \approx Re\{\Delta \boldsymbol{V}\} \quad \textbf{5-53}$$

$$\Delta V \approx I_R \cdot R + I_X \cdot X \quad \textbf{5-54}$$

$$I_R = Re\{\boldsymbol{I}\} = I \cdot \cos(\theta) \quad \textbf{5-55}$$

$$I_X = Im\{\boldsymbol{I}\} = I \cdot \sin(\theta) \quad \textbf{5-56}$$

The formulation of line drop (**ΔV)** is presented above in a complicated form. The point to understand is that the line drop is directly proportional to two components: 1) line current and 2) line impedance. If

the line current is high, then the line drop will increase. Alternately, if line impedance is high, then the line drop will increase. It is also important to note that the line drop is approximated in Equation 5-54 using the real (in-phase) and reactive (out-of-phase) components of the line current which are independent of one another. This approximation is very useful in this study of High-Pen PV as PV installations primarily provide real power support by injecting in-phase current. Likewise, switching capacitors influences line voltage by providing reactive power support in the form of out-of-phase current. Using this approximation, we can decouple the influence of High-Pen PV on line voltage from the switching capacitors present on the circuit.

B. Voltage Rise

In the previous section (A), the concept of voltage drop (line drop) was introduced. A classic assumption of radial distribution circuits, without regulation, is that the monotonic decrease of voltage with distance along the feeder increases from the sub-station. For circuits without distributed generation (DG), this assumption is correct since the energy of the circuit is sourced from the sub-station exclusively, resulting in a one directional power flow, referred to as Normal Power Flow (NPF). This one-directional power flow is described as flowing "downstream". When distributed generation is present on the circuit, this assumption is not always true. The energy needed to meet the circuit load demand may come from sources other than the sub-station. In particular situations, energy will flow toward the sub-station, or "upstream", resulting in reverse power flow (RPF). In a reverse power flow condition, the voltage will rise at the DG site to potentially non-standard levels.

This voltage rise phenomenon occurs from multiple factors: 1) DG injects power at the grid voltage (as known as voltage following), 2) the sub-station is a stiff voltage source, and 3) the grid load demand will always exceed the generation capacity of DG. DG, regulated by the IEEE 1547 standard, is not allowed to regulate voltage, so the DG operates in a voltage following mode and can described as a current source in steady-state. A sub-station is the interconnection between the distribution circuit and the transmission system of the grid. Given the transmission system is a low impedance mesh network, with three orders of magnitude greater capacity than an individual load demand of a distribution circuit, it is appropriate to describe the sub-station a stiff voltage source. For example, in California on February 20th, the peak demand was 30074 MW [15] and a combine cycle gas turbine can range to over 300MW and still be considered DG [16]. Therefore, it is correct to say that an individual DG site, such as roof-top PV, will not exceed the grid load demand and will generate at full capacity. In the case of DG in the distribution circuits, excess generation will be exported through the sub-station to the transmission system.

The power generated by DG is injected into the circuit as current at the local bus voltage. The current injected will flow to meet circuit demand, but will follow the path of least impedance. With this notion, we can assume the injected current is consumed by the circuit load demand in the following order: 1) the DG's bus load, 2) down-stream load, and then 3) upstream load. The local bus the DG is connected to will have the lowest impedance between the DG and the load demand and, therefore, the first destination of the power generated by the DG. If the DG produces more generation capacity then the local the load demand, the excess current will flow from the DG's bus potential to a lower potential point on the circuit, as discussed in section 5.2.1.3A. Since DG is not actively regulating its voltage, this lower potential point will be downstream (away from the sub-station) of the DG's bus. As the DG installation is supporting the local and downstream load demand, this support will no longer have to

travel from the sub-station, resulting in the a decrease in line drop to the point of the DG's bus. A decrease in in line drop will result in a voltage increase in the DG's local and downstream buses. However, the adjacent upstream bus of the DG bus is an equal or higher potential than the DG bus until the point of reverse power flow (RPF).

In normal power flow (NPF), the upstream bus voltage ($\mathbf{V_{US}}$) is greater than or equal to the DG bus voltage ($\mathbf{V_{DG}}$). In this case, the line drop ($\mathbf{\Delta V}$) will be positive, as shown in equation 5-57, and, therefore, the line current (I) magnitude will be positive (equation 5-58). Positive line current, in this context, means current is flowing away from the sub-station. In the case of RPF, the line current magnitude is flowing towards the sub-station, resulting in a change in sign. Since the line current is negative, then the line drop is negative; this is only true if $\mathbf{V_{DG}}$ is greater than $\mathbf{V_{US}}$. It is important to note that RPF does not cause a decrease in $\mathbf{V_{US}}$, the sub-station is a stiff voltage source and will maintain $\mathbf{V_{US}}$ to the potential just before the point of RPF. Therefore, RPF caused by the DG will result in an increase of $\mathbf{V_{DG}}$ over the static $\mathbf{V_{US}}$. In summary, NPF results in $\mathbf{V_{US}}$ greater than or equal $\mathbf{V_{DG}}$, while RPF results in $\mathbf{V_{US}}$ less than $\mathbf{V_{DG}}$, as shown in Equation 5-59.

$$\boldsymbol{V_{US} - V_{DG} = \Delta V} \qquad \textbf{5-57}$$

$$\boldsymbol{\Delta V = I \cdot Z_{LN}} \qquad \textbf{5-58}$$

$$\boldsymbol{NPF \rightarrow V_{US} \geq V_{DG}}$$
$$\boldsymbol{RPF \rightarrow V_{US} < V_{DG}} \qquad \textbf{5-59}$$

Reverse power flow occurs because the DG is attempting to operate at full capacity in a grid following mode. In situations when the DG installation is producing even more capacity than the local and downstream load demand combined, DG is forced to push the excess generation upstream towards the sub-station as RPF in order to operate at full capacity. Without RPF, the DG installation will not be able to transmit its excess generation to load demand upstream. DG installations can inhibit its operating voltage and prevent RPF, but are not required to unless the steady-state voltages are beyond standard bounds set by the ANSI C84.1 standard. It is reasonable to assume that the DG will not impede voltage rise cause by RPF in order to operate at full generation capacity unless the bus voltage is going out of standard limits.

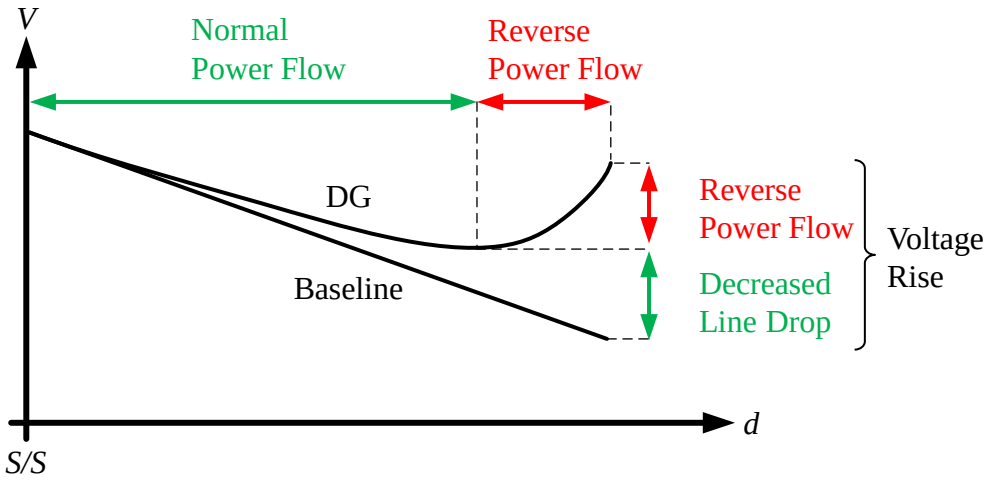

Figure 34. DG Induced Voltage Rise.

Voltage rise, induced by DG, stems from two sources: 1) decreased line drop and 2) reverse power flow (RPF). Voltage rise due to a decrease in line drop does not have the potential to raise voltage past standard limits or even the sub-station voltage, but RPF voltage rise does. The amount of voltage rise experienced during RPF is influenced by factors such as load and generation distribution circuit construction. These factors are discussed in detail in the following section.

A.1 Generation Location Voltage Rise Characteristics

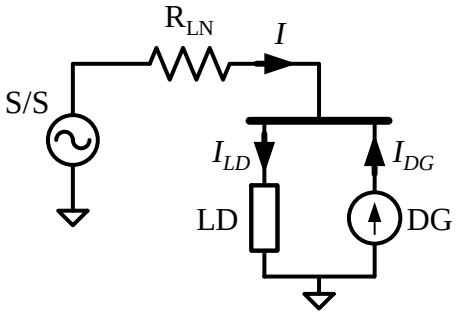

Figure 35. Sub-station to DG bus line drop model.

$$\Delta V = I \cdot R_{S/S} \qquad \textbf{5-60}$$

$$I = I_{LD} - I_{DG} \qquad \textbf{5-61}$$

The amount of DG induce voltage rise is dependent on the location of the generation in relation to the sub-station. Figure 35 and Equation 5-60 form a simple model of the line drop between the sub-station and the DG bus. The resistive impedance ($R_{S/S}$) between the sub-station and DG bus is the cumulative line resistance. Only the resistance is modeled, as it was shown that the voltage drop may be approximated (Equation 5-54) by de-coupling the in-phase and out-of-phase current components in section A. Equation 5-61 is Kirchhoff's Current Law applied at the bus, showing the line (I) current is a composed of the load demand (I_{LD}) and DG current (I_{DG}). Therefore as DG increases, the line current decreases. This is true for any type of spatial generation distribution; what changes is the impedance

between the sub-station and the DG bus. As the distance from the sub-station increases, the cumulative line impedance will also increase. As the line impedance increases, the amount of line drop (ΔV) increases. In comparison of different DG bus locations with the identical generation, DG located closer to the sub-station (Generation Center (GC) → 0) will induce less voltage rise than a DG located farther from the sub-station (GC → 1) simply because of the difference in line impedance.

To clarify the discussion above, an ideal four bus model Figure 36 of a balanced distribution feeder with varying DG penetrations and spatial distributions is presented in order to visualize the characteristics of voltage rise phenomena. The sub-station (S/S) is modeled as a stiff voltage source and is treated as a slack bus, which means that energy requirements that are not met by DG are met by the S/S. At each bus, there is a line impedance, load, and DG; the parameters of these elements are found in Table 20. The line impedance values increases from bus 1 to 4 as is typical of a distribution feeder. Each bus, equally spaced with the same load demand, results in a Load Center (LC) located at between bus 2 and 3 (LC = 0.5). To demonstrate varying levels of DG penetrations and distributions, six DG penetrations and three distributions are used. The PV penetration variations are 0%, 25 %, 50%, 75%, 100%, and 125% and spatial variations are lumped beginning, middle, and end distributions. A beginning distribution has 100% of the feeders DG located on bus 1. Likewise, a middle and end distributions have 100% of the feeders DG located on bus 3 and bus 4, respectively. The Generation Centers of the Beginning, Middle, and End DG distributions are 0.25, 0.75, and 1, respectively.

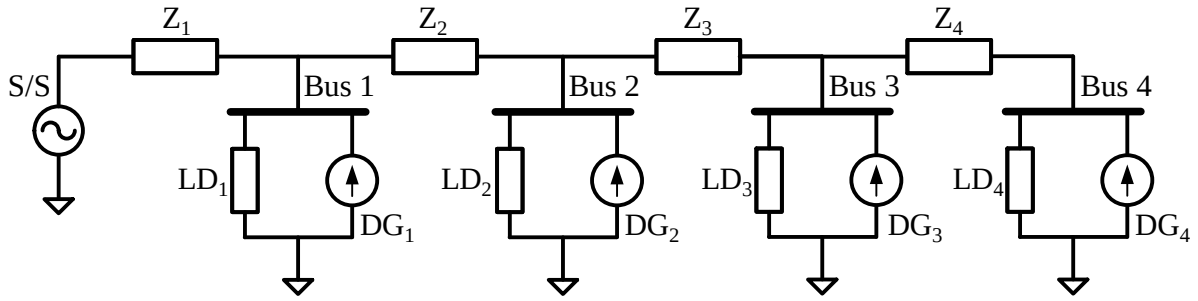

Figure 36. Four Bus Feeder Model.

Bus	Line Impedance (Z) [Ω]	Line Length [ft]	Load Demand (LD) [MW]	Distributed Generation (DG) [% of Penetration]		
				Beginning	Middle	End
1	0.138	1000	2	100%	0%	0%
2	0.184	1000	2	0%	0%	0%
3	0.276	1000	2	0%	100%	0%
4	0.552	1000	2	0%	0%	100%

Table 20. Four Bus Feeder Model Parameters.

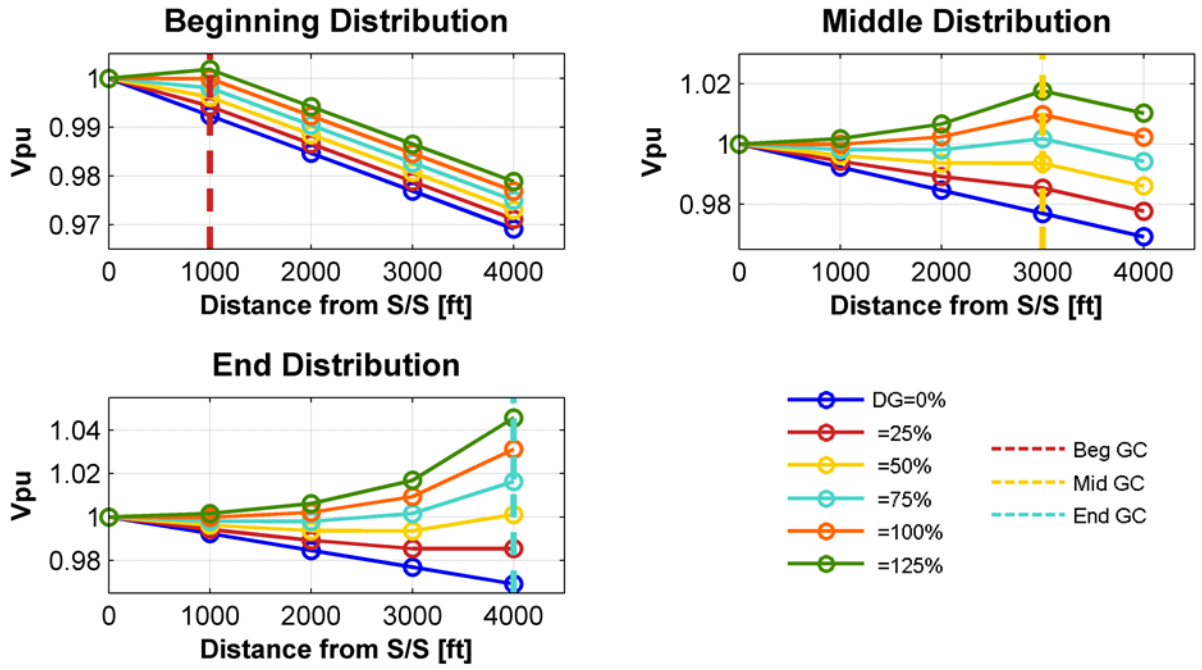

Figure 37. Four Bus Model Bus Voltage vs. Distance.

Figure 37 is the bus voltage profiles for the Beginning, Middle, and Ending distributions with penetration from 0% to 125%. In each distribution scenario plot, the location of the generation is indicated by the Generation Center (GC). By observation, the voltage rise increase rate with penetration is lowest for the Beginning distribution and it is highest for the End distribution. This is as expected as the cumulative resistive line impedance for the Beginning distribution is the lowest and for the End distribution is the highest. Figure 38 and Table 21 reflect these results.

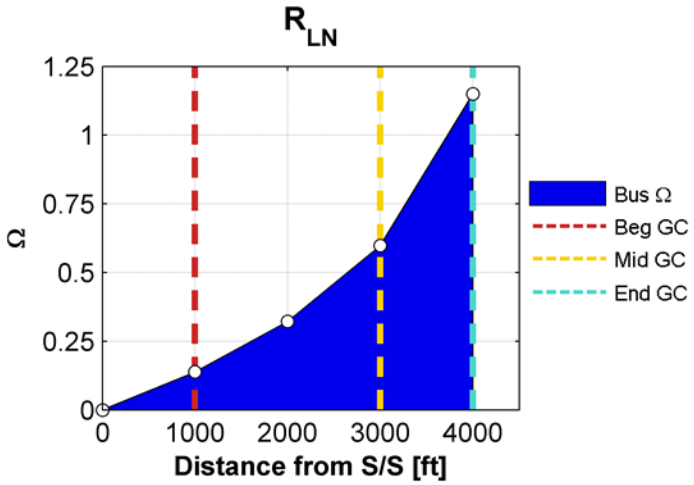

Figure 38. Four Bus Model cumulative line impedance to sub-station.

Distr	Bus	RDG [Ω]	%V Rise per Pen	GC
Beginning	1	0.138	0.008	0.25
Middle	3	0.604	0.033	0.75
End	4	1.15	0.063	1

Table 21. Four Bus Model DG Bus Voltage Rise from Baseline versus Penetration.

In summary, the location of the DG relative to the sub-station impacts the amount of induced voltage rise seen at the DG bus. The voltage rise induced by DG is proportional the cumulative line impedance between the sub-station and the DG bus. Naturally, DG sited farther from the sub-station will have higher cumulative line impedance to the sub-station. Therefore, DG distributions located at the end of a circuit (GC → 1) will induce more voltage rise than distributions located closer the sub-station (GC → 0).

B.1 Reverse Power Flow (RPF) Voltage Rise Characteristics

In RPF situations, the local DG's bus voltage will rise, as described above, but there are factors that exacerbate the voltage rise phenomena. During RPF, the DG bus voltage (V_{DG}) is greater than the upstream bus voltage (V_{US}) by the amount of potential consumed in the line drop (ΔV) between the buses. Therefore, the line drop dictates the amount of voltage rise at V_{DG}. As described in Equation 5-58, ΔV is a product of line current (I) and line impedance (Z_{LN}), therefore, large I or Z_{LN} will result in a large voltage rise of V_{DG} during RPF.

To simplify this discussion, the characteristics of RPF are presented using a DC approximation. As discussed in section A, DG produces in-phase current primarily, so it is fair to only consider real (in-phase) component (real power) in a discussion about RPF induced by DG. Moving forward, the amount of line current (I) flowing upstream is proportional to the amount of excess generation capacity (P_{EC}) available at a given moment, as approximated in Equation 5-62. Excess generation capacity is defined as the generation capacity (P_{DG}) surpassing the DG bus load demand ($P_{LD,DG}$) and downstream ($P_{LD,DS}$) load demand, as shown in Equation 5-63. The DG bus load demand and downstream load demand is compactly referred to as the local DG load demand ($P_{LD,lcl}$), as shown in Equation 5-64. As P_{EC} increases, the DG bus voltage (V_{DG}) also increases, but at a rate significantly slower than P_{EC}. Therefore, P_{EC} is still the dominant factor in the increase of the upstream line current.

$$I = \frac{P_{EC}}{V_{DG}} \qquad 5\text{-}62$$

$$P_{EC} = P_{DG} - P_{LD,lcl} \geq 0 \quad \textbf{5-63}$$

$$P_{LD,lcl} = P_{LD,DG} + P_{LD,DS} \quad \textbf{5-64}$$

I	→	Line current [A]
P_{EC}	→	Excess Generation Capacity [W]
$P_{LD,lcl}$	→	Local load demand included the DG bus and all downstream buses [W]

Excess generation capacity (P_{EC}) causes reverse power flow. The minimum amount of DG penetration required to induce RPF is referred to as the RPF penetration (RPF_{pen}), as shown in Equation 5-65. As DG penetration increases past the RPF penetration, the more P_{EC} is available for RPF. The extent that an RPF flow upstream is dependent on the amount of excess capacity is remaining after flowing through each upstream bus. The amount of excess capacity at each upstream bus ($P_{EC,USj}$) is defined in Equation 5-66. The upstream path from the DG bus to the sub-station is the shortest distribution line path possible. Buses splitting from this direct upstream path are aggregated to the path, forming the upstream buses as referred to in this work. The upstream buses are indexed (j) from the point of view of the DG bus; zero is the DG bus and the sub-station the final index ($j_{S/S}$). As DG penetration increases past the RPF penetration, the amount of P_{EC} will increase and will eventually induce RPF past the DG bus. To define the extent of RPF, the upstream index, such that minimizes the magnitude of $P_{EC,USj}$ and the $P_{EC,USj}$ and is at or below zero, is the estimated end bus of RPF, as defined in Equation 5-67. This is an estimate of the extension of RPF from the DG bus since it does not consider the power consumed by line-loss.

Finally, the line impedance the RPF has to flow through is an important characteristic of voltage rise. This impedance (RPF_R) is defined as the resistance between the DG bus and upstream bus at the RPF_{PT} index, as shown in Equation 5-68. Only the line resistance is accounted for since voltage rise caused by DG can be described using just the resistance, as discussed in the voltage drop estimation section (A).

$$RPF_{PEN} = \frac{P_{LD,lcl}}{P_{LD,PK} \cdot D_{BUS}} \quad \textbf{5-65}$$

$$P_{EC,USj} = P_{EC} - \sum_{i=1}^{j} P_{LD,USi} \quad \textbf{5-66}$$

$$RPF_{PT} = j \ \ such\ that \ \min_{j} \left| P_{EC,USj} \right| \ \ and \ P_{EC,USj} \leq 0 \quad \textbf{5-67}$$

$$RPF_R = \begin{cases} \sum_{i=1}^{j} R_{i-1}, & j > 0 \\ 0, & j = 0 \end{cases} \quad \textbf{5-68}$$

$P_{EC,USj}$	→	Excess Generation Capacity at the j^{th} upstream bus from the DG bus [W]
RPF_{PEN}	→	The DG penetration to induce reverse power flow
RPF_{PT}	→	The upstream index of the farthest upstream bus experiencing reverse power flow from the DG bus.
RPF_{R}	→	The line resistance between the DG bus and upstream bus at the RPF_{PT} index
$j = 0,1,\ldots,j_{S/S}$	→	The index of upstream buses ascending towards the sub-station
$j_{S/S}$	→	The sub-station upstream index
D_{BUS}	→	Percentage of System DG Penetration located at bus.

The position of the DG in relation to the sub-station impacts the amount of local load demand as seen from the DG bus. The closer the DG bus is to the sub-station, the more buses are located downstream resulting in an increase in $P_{LD,lcl}$. Therefore, DG installations located closer to the sub-station will require larger penetrations of DG to produce excess generation capacity; likewise, DG installed at the end of the feeder will require lesser penetrations to achieve excess generation capacity. The average position of DG installations on a feeder can be described utilizing the Generation Center (GC) metrics, as presented in section 5.2.1.2, where GC equal to zero indicated generation at the sub-station and equal to one is at the end of the feeder. Using the GC terminology on a typical distribution feeder, a feeder with a GC close to zero will require greater levels of DG penetration to produce excess capacity than if the feeder's GC is close to one.

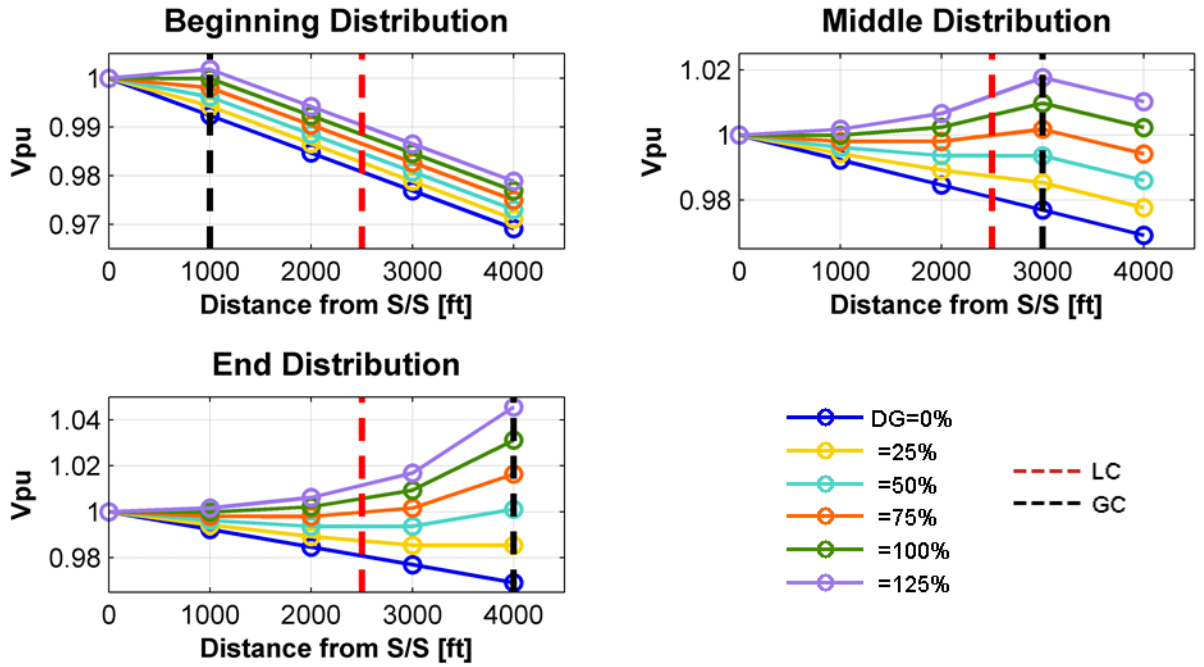

Figure 39. Four Bus Model Bus Voltage vs. Distance.

To enhance the discussion of the characteristics of RPF voltage rise, the four bus model, as presented in section (A.1), is used. Observing the Beginning, Middle, and End DG distributions voltage profiles of the

four bus model, RPF occurs at different penetrations. Table 22 has the RPF penetration, the penetration capacity that satisfies the local and downstream load demand, and the GC for each distribution. The Beginning distribution features the highest RPF penetration levels and the lowest GC, with the Ending distribution having the lowest RPF penetration and the highest GC. Now observing the load demand, again the Beginning distribution features the highest and the Ending distribution the lowest. As described above, RPF only occurs if the DG's capacity surpasses the local load demand, which is composed of the DG's bus and downstream load demand. As a result, the Beginning distribution, with the highest local load demand, requires the higher levels of DG penetration to induce RPF than the Middle and Ending distributions. As described previously, distributions with lower GC have required higher amounts of DG penetration to induce RPF.

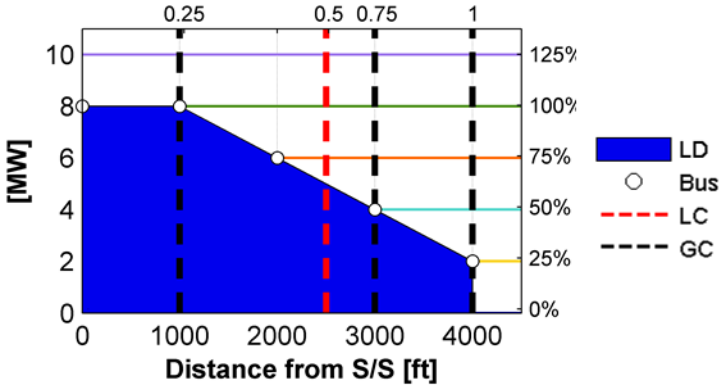

Figure 40. Four Bus Model Cumulative Bus Load Demand.

DG Distr.	RPF Pen	Local LD	GC
Beginning	100%	8MW	0.25
Middle	50%	4MW	0.75
End	25%	2MW	1

Table 22. RPF Penetration Levels for Four Bus Model.

For the Middle and Ending distribution circuits, the simulated penetration went beyond the RPF penetration. At these higher penetrations, it is evident that RPF is induced past the DG bus, to the adjacent upstream bus and beyond, extending the RPF further upstream. The induced RPF upstream will now raise the upstream bus voltages, which in turn raises the DG's bus voltage. The amount of voltage rise seen at the upstream busses is not as significant as the DG's bus voltage rise since the amount of excess capacity inducing RPF is significantly reduced by each ascending upstream buses load demand. In this example, the Ending distribution induces RPF at bus 4 for 50% penetration, buses 3 and 4 for 75%, buses 2, 3, and 4 for 100%, and finally buses 1, 2, 3, and 4 for 125% penetration. As the extension of RPF increases to more upstream buses on the feeder, so DG bus voltage increases further. The same characteristics are also seen for the Middle distribution for penetration higher than 75%. In summary, as penetrations increase past the RPF penetration, RPF will extend from the DG bus to the ascending upstream buses resulting in a further increase in voltage rise at the DG's local bus.

It is important to note that DG generation capacity and load demand can vary dynamically during the day. In the case of a PV installation, the generation capacity will vary from nothing to full nameplate capacity (minus parasitic losses) as it is dependent on the availability of solar irradiance. It is important to note that excess generation capacity is calculated using load demand concurrent with the DG generation. For PV, the maximum possible amount of excess generation will occur at the Peak PV Point (section 5.2.1.1), so a conservative calculation of excess generation should be the ideal PV nameplate rating and load concurrent to the Peak PV Point.

The construction of the distribution line also affects the amount of voltage rise of the DG bus voltage. In a typical feeder radial distribution feeder, the diameter of the distribution cable decreases as distance

increases from the sub-station; this is done typically for economic reasons [5, p. 226]. The radius of the wire is inversely proportional to the resistance of the wire, so a cable half the diameter of another is twice the resistance [1, Ch. 2.3]. In terms of RPF voltage rise, DG installations located at buses with lower line impedance will have less voltage rise in comparison to installations at buses with high upstream line impedance. Given the nature or radial distribution construction, DG situated at the end of circuit will tend to have higher amounts of voltage rise during RPF.

At higher penetrations, The RPF extends past the DG bus and to upstream buses, as previously discussed. In extended RPF scenarios, the upstream buses voltage increase due to RPF which in-turn causes a further increase in the DG bus voltage. The cumulative impedance (RPF_R) of the RPF's range emphasizes the relationship of extended RPF and RPF voltage rise; as RPF extends further upstream, the RPF_R increases resulting in the DG bus voltage increasing. Figure 41 illustrates the cumulative line impedance that the RPF must travel over until the excess generation capacity is consumed (RPF point). As evident in the figure, penetrations beyond the RPF penetration results in extending the RPF point upstream. As a result, as penetration increases past the RPF penetration, the cumulative line impedance to the RPF point increases.

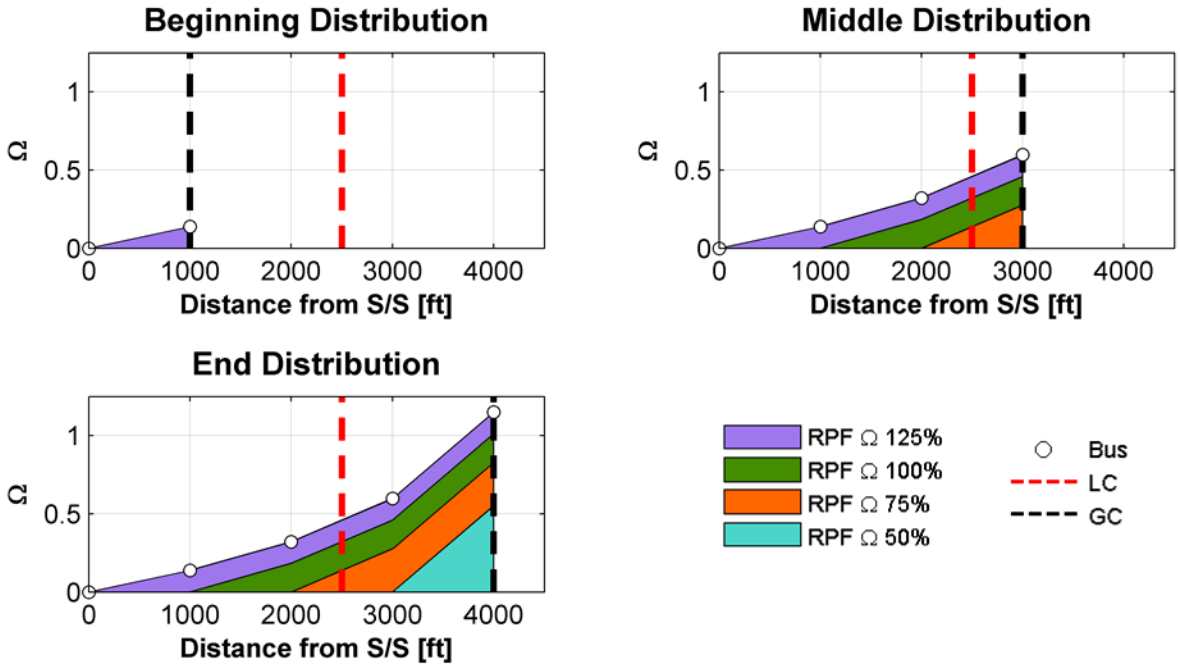

Figure 41. Four Bus Model Upstream Reverse Power Flow Impedance.

This described result is observed in the four bus model. The extension of RPF results in higher voltage rises as seen in the End distribution between 100% and 125% penetration (Figure 41). At the 125% penetration, the voltage rise (from baseline) is 7.7% and with RPF_R equal to 1.15Ω. The 100% penetration has a 6.2% voltage rise with only 1.012Ω to the RPF point; the 125% penetration scenario's RPF_R is 30mΩ greater and the voltage rise from baseline is 1.5% greater than the 100% penetration scenario, confirming the above statement.

The impedance of extended RPF is influenced by the generation distribution. For example, in the four bus models as presented, both the Middle distribution at 100% penetration and the End distribution at 75% DG have 4MW is excess generation capacity. Observing Figure 39 again, the voltage rise from the baseline for the End distribution is 1.4% higher than the voltage rise for the Middle. For the same amount of excess capacity, the End distribution faces 0.828Ω impedance to the RPF point as opposed the 0.46Ω impedance of the Middle distribution. Generation distributions located closer to the end of the feeder tend to have more voltage rise than distributions at the beginning for the same amount of excess capacity.

By observing Figure 39, we can see the line drop between the DG bus and adjacent upstream bus is significant during RPF. As penetration increases, the largest amount of voltage rise occurs between the between the DG bus and upstream bus. Table 23 shows the percentage of voltage rise at the DG bus over the adjacent upstream bus (ΔV_{DG}) as a percentage of total RPF voltage rise: RPF voltage rise is defined as the voltage rise from penetration greater than the RPF penetration. Even in cases of extended RPF, the majority of the voltage rise is at the DG bus. In all RPF situations, the entirety of the excess capacity forced upstream goes through the DG's upstream distribution line ($RPF_{R,0}$) as line current. In extended RPF, only portions of the excess capacity will pass through upstream buses distribution line. Therefore, the line impedance of the DG bus is a point of sensitivity.

Distribution	**Bus**	**R_{DG} [Ω]**	**% of ΔV_{DG} to Total RPF V Rise [%]**						**LC/GC**
			0%	*25%*	*50%*	*75%*	*100%*	*125%*	
Beginning	1	0.138	-	-	-	-	-	100	2
Middle	3	0.276	-	-	-	100	80	61	0.67
End	4	0.552	-	-	100	78	70	63	0.5

Table 23. Four Bus Model DG Bus Voltage Rise Between the DG bus and the Upstream bus versus Penetration.

It is important to note distribution line impedance is composed of a resistive and reactive component, but we are only considering the resistive component. As derived in section A, Equation 5-54 decouples line drop as components of in-phase and out-of-phase current. Since DG is not allowed to regulate voltage per IEEE 1547 and generation of reactive power only takes away from the capacity of the DG unit, DG units can be assumed to generate real power, or in-phase current, exclusively. Therefore, voltage rise caused by DG via in-phase current injection interacting with the resistive component of the line impedance.

Up to this point, the influence of excess generation and line impedance on RPF voltage rise has been discussed, but not the relationship of the load and generation distributions on RPF voltage rise. The four bus model presented thus far has only investigated a single load profile (uniform). Using the load center (LC) and generation center (GC) metrics, as presented in section 5.2.1.2, the average location of the load and generation on the primary feeder can be described. Increase amounts of excess generation and line impedance increases the amount of RPF voltage rise. In extended RPF conditions, both the excess generation and the line impedance are greater. If the DG bus is located closer the majority of the upstream load, the extension of the RPF point decreases, which results in a less RPF voltage rise. Alternatively, the closer the feeder's LC and GC, the less RPF voltage rise the DG bus is exhibit.

A concise way to describe the above discussion is the ratio of load center to generation center, as shown in Figure 42. The closer the load and generation distribution are on the feeder, the closer to LC/GC ratio

is to one. If the generation is at the end of the feeder and the load at the beginning, the LC/GC ratio will approach zero. Inversely, if the generation is at the beginning and the load at the end of the feeder, the LC/GC ratio is very large. In terms of extended RPF, the farther the load distribution is upstream from the generation (LC/GC→0), the higher the voltage rise. If the load distribution is closer to the generation during extended RPF (LC/GC→1), the amount of RPF voltage rise decreases. If the load distribution is located downstream of the generation (LC/GC→∞), the RPF penetration increases and decreases the amount of extended RPF. In summary, a feeder with a low LC/GC is likely have higher RPF voltage rise than a feeder with a higher LC/GC ratio.

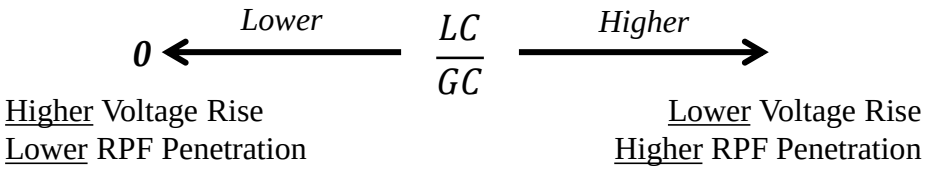

Figure 42. Load Center to Generation Center Ratio.

To illustrate this point, the four bus model is evaluated as before except with a load distribution weighted towards the end of the feeder. Table 24 contains the values used in both the Uniform and the End load distributions and the calculated load center. The load center for the End distribution is 0.91 versus the 0.63 of the Uniform distribution. Figure 43 is the cumulative load demand for the End distribution; the cumulative load demand profile for the Uniform is illustrated in Figure 40. The generation centers and resulting LC/GC ratios for both load distributions is shown in Table 24 and Table 25; in all cases, the LC/GC ratio is greater for the end distribution than the uniform distribution. Accordingly, we should expect to a decrease in RPF voltage rise and an increase in RPF penetration from the uniform to end load distributions.

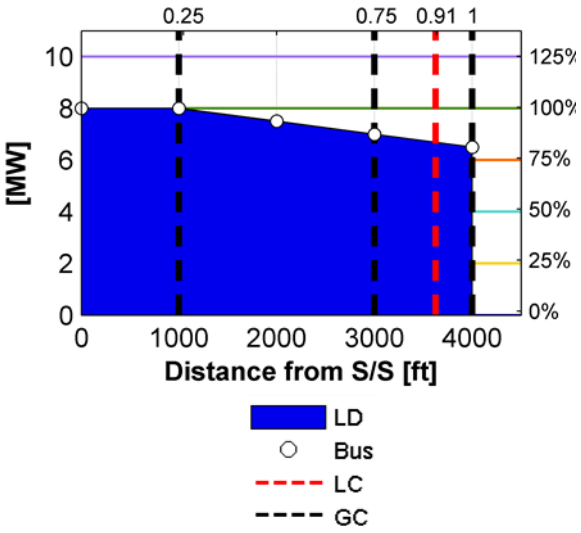

Figure 43. Four Bus Model Cumulative Bus End Distribution Load Demand.

Bus	Load Demand Distribution	
	Uniform	End
1	2 MW	0.5 MW
2	2 MW	0.5 MW
3	2 MW	0.5 MW
4	2 MW	6.5 MW
Load Center	0.63	0.91

Table 24. Four Bus Model Load Distributions.

DG Distribution	GC	GC/LC	
		Uniform	*End*
Beginning	0.25	2.5	3.64
Middle	0.75	0.83	1.21
End	1	0.63	0.91

Table 25. Four Bus Model Generation Center to Load Center Ratio.

Observing Figure 44, we can see the End load distribution incurs a larger line drop than the Uniform load. Also, the net voltage increase between the baseline and 125% penetration is relatively same, but the type of voltage rise is different. The End load features a larger portion of the observed voltage rise attributed to line loss reductions than the Uniform load. Inversely, the End load features less voltage rise due RPF than the Uniform load. This result is echoed in Table 26. The amount of RPF voltage rise is less for the End load than the Uniform load. Also the RPF penetration is higher is the End load than the Uniform load. In summary, the End load distribution with the higher LC/GC ratio demonstrated less RPF voltage drop and higher RPF penetrations.

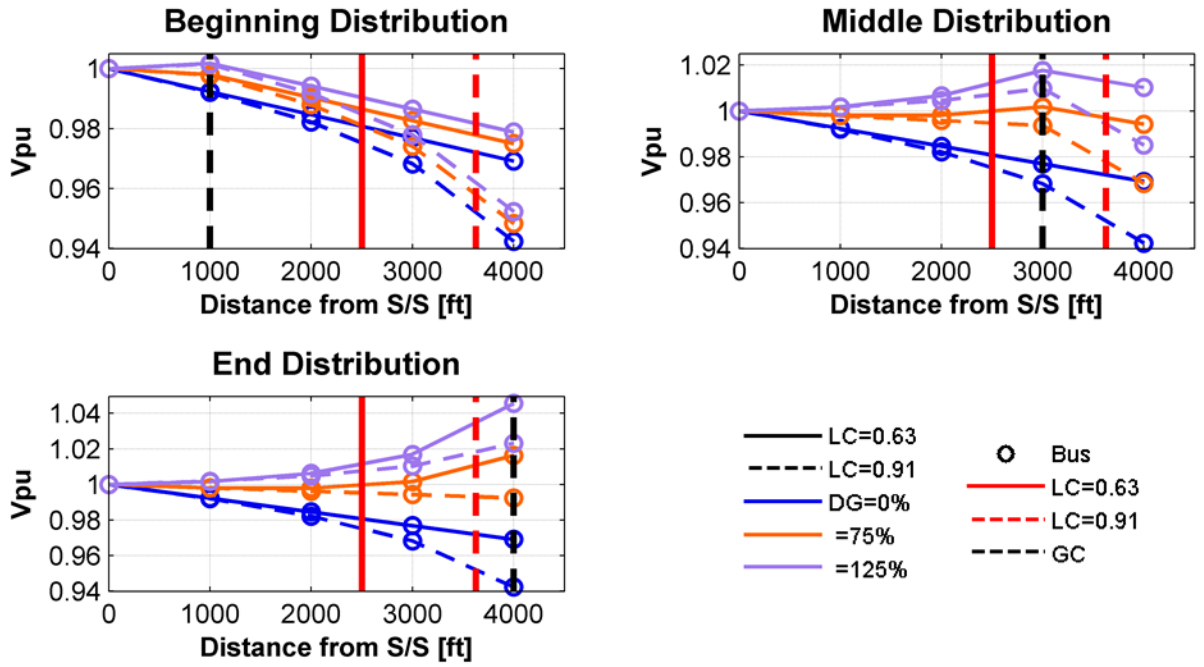

Figure 44. Four Bus Model Bus Voltage versus Distance for Uniform (LC=0.63) and End (LC = 0.91) Load Demand Distributions.

In summary, voltage rise caused by DG is caused by a decrease in line loss and RPF; RPF voltage rise has the potential to increase bus voltages beyond standard limits. As discussed above, RPF voltage rise is aggravated by excess generation and line impedance: increase either and the RPF voltage rise increases. Both excess generation and line impedance is heavily influenced the load distribution and line construction. The end of distribution circuit is prone to excess generation at lower penetrations and has higher line impedances. The relationship of the load and generation distributions on the feeder influence RPF voltage rise and can be described using the LC/GC ratio of the feeder. RPF voltage rise may push voltages above standard bounds, but buses prone to RPF voltage rise can be identified before the problem occurs. By observing characteristics described above, buses with a high RPF voltage rise may be identified and corrective actions taken.

LD Distr	Gen Distr	LC/GC	% RPF Voltage Rise from baseline [%]						RPF Pen
			0%	25%	50%	75%	100%	125%	
Uniform	Beginning	2.5	-	-	-	-	-	0.179	100%
Uniform	Middle	0.83	-	-	-	0.372	0.985	1.77	50%
Uniform	End	0.63	-	-	0.750	1.842	3.316	4.563	0.25%
End	Beginning	3.64	-	-	-	-	-	0.1544	100%
End	Middle	1.21	-	-	-	-	0.198	0.987	87.5%
End	End	0.91	-	-	-	-	0.806	2.32	81.25%

Table 26. Percent RPV Voltage Rise and RPF penetration Comparison between Uniform and End Load Distributions.

C.1 Voltage Rise Siting Score

Distributed Generation (DG) induced voltage rise is composed of two components: line loss reductions and reverse power flow (RPF). The amount of voltage rise due to line loss reductions is described using the series line resistance ($R_{S/S}$) between the sub-station and DG bus, as shown in Generation Location Voltage Rise Characteristics section (A.1). Voltage rise induced by RPF is characterized by analyzing excess generation and line resistance, as described in RPF Voltage Rise Characteristics section (A.1). RPF penetration (RPF_{PEN}) of a bus indicates the penetration point when excess generation occurs. To describe line resistance, the estimated RPF line resistance (RPF_R) and the DG line resistance (RPF_{R0}).

In combination, the four factors above can describe the voltage rise characteristics of a single DG bus. Sub-station line resistance describes the generation amount of voltage rise due to a decrease in line losses, and RPF penetration, RPF series upstream line resistance, and DG bus line resistance describe RPF voltage rise. Since these four parameters may be calculated without an iterative model, the components can be combined to form a scoring metric to rate the DG induced voltage rise potential at each bus in the circuit. The Voltage Rise Siting (VRS) score is such a metric defined in Equation 5-69. Each of the four terms are normalized and weighted equally. The VRS bus score ranges from 0 to 100, and a low VRS bus score is interpreted as bus with marginal voltage rise and a high score as a bus with significant voltage rise as DG penetration increases.

$$VRS_i = 25\left(\frac{100 - RPF_{Pen,i}}{100}\right) + 25\left(\frac{RPF_{R,i}}{RPF_{R,Norm}}\right) + 25\left(\frac{RPF_{R0,i}}{RPF_{R0,Norm}}\right) + 25\left(\frac{R_{S/S,i}}{R_{S/S,Norm}}\right) \quad \textbf{5-69}$$

$RPF_{PEN,i}$	→	Bus "i" RPF penetration [%]
$RPF_{R,i}$	→	Bus "i" RPF upstream resistance [Ω]
$RPF_{R,Norm}$	→	RPF upstream resistance normalization factor [Ω]
$RPF_{R0,i}$	→	Bus "i" DG bus upstream resistance [Ω]
$RPF_{R0,Norm}$	→	DG bus upstream resistance normalization factor [Ω]
$R_{S/S,i}$	→	Bus "i" cumulative series resistance to sub-station [Ω]
$R_{S/S,Norm}$	→	Cumulative series resistance to sub-station normalization factor [Ω]
i = 0,1,…,n	→	Bus index
n	→	Maximum bus index

As stated above, the components of the VRS score may be calculated without the need of an iterative solver as used in the simulation of the three phase balance feeder models. To perform the calculation, the circuit-wide peak real power load demand (P_{PK}), DG bus penetration (PEN), and the circuit load demand distribution (LDAF) is estimated. P_{PK} may be the yearly peak or the peak real power load demand at the peak PV time of day. A high DG penetration should be selected to ensure RPF occurs in the majority of the circuit's buses. The penetration found at the bus under evaluation using PPK and penetration is shown in Equation 5-70. The LDAF may be estimated using customer energy demand or simply estimated. The application of the LDAF to find bus load demand is shown in Equation 5-71, the necessary LDAF properties are shown in 5-72.

$$P_{DG,j} = \frac{PEN}{100} \cdot P_{PK} \quad \textbf{5-70}$$

$$P_{LD,i} = P_{PK} \cdot LDAF \quad \textbf{5-71}$$

$$such\ that \begin{cases} \sum_{i}^{n} LDAF_i = 1 \\ LDAF_i \leq 1 \end{cases} \quad \textbf{5-72}$$

$P_{DG,j}$	→	DG bus "j" generation [W]
PEN	→	Nameplate PV penetration [%]
P_{PK}	→	Cumulative circuit peak load demand [W]
$P_{LD,i}$	→	Bus "i" load demand [W]
$LDAF_i$	→	Bus "i" load demand allocation factor
j	→	DG Bus index
i = 0,1,…,n	→	Bus index
n	→	Maximum bus index

The bus components (RPF_{PEN}, RPF_R, RPF_{R0}, $R_{S/S}$) of the VRS bus score are easily calculated knowing the bus generation and circuit load demand as described above. RPF_{PEN} and RPF_R are calculated using Equations 5-65 and 5-68 as presented in the RPF Voltage Rise Characteristics section (B.1). RPF_{R0} is the evaluations buses line resistance and $R_{S/S}$ is calculated by summing the direct series line resistance between the sub-station and the DG bus.

The normalization factors ($RPF_{R,NORM}$, $RPF_{R,NORM}$, $RPF_{R0,NORM}$) enable direct comparison between different circuit configuration. The normalization factor is the maximum value of the range of a particular component. For example, if various bus RPF_R values equal to 0Ω, 0.3222Ω, 0.598Ω, and 1.15Ω, the normalization factor $RPF_{R,NORM}$ is 1.15 Ω.

Load Distribution	**Bus**	**RPF_{PEN} [%]**	**RPF_R [Ω]**	**RPF_{R0}[Ω]**	**$R_{S/S}$ [Ω]**	***VRS***
Uniform	1	100	0	0.138	0.138	***22.3***
	2	75	0.322	0.184	0.322	***39.6***
	3	50	0.598	0.276	0.598	***57.9***
	4	25	1.15	0.552	1.15	***88.1***
End	1	100	0	0.138	0.138	***22.3***
	2	93.75	0.184	0.184	0.322	***31.9***
	3	87.5	0.46	0.276	0.598	***45.4***
	4	81.25	1.012	0.552	1.15	***71.0***
Normalization Factor		*100*	*1.15*	*0.552*	*1.15*	

Table 27. The Voltage Rise Score (VRS) for the 4 bus uniform and ending load model scenarios. The score was evaluated with a P_{DG} = 8MW (100%) and P_{PK} = 8MW.

Table 27 shows the VRS score for the uniform and end load demand distribution cases and the component values and normalization factors used in the calculation. The VRS score was calculated using a peak load demand of 8MW and 100% penetration. The VRS score evaluates each bus as a point generation source, so the spatial generation scenarios are already taken into account. In both

distributions, the bus score for buses closer the sub-station are lower than buses farther from the sub-station. This is interpreted as buses at beginning of the circuit will have less voltage rise from DG than buses at the end of the circuit, which follows the discussion of the previous two sub-sections. We can also observe that bus 4 for the uniform load demand distribution is a higher score than bus 4 for the end load demand distribution. This is also expected since the amount of local load demand at bus 4 is much higher for the end distribution, as indicated by a higher RPF penetration. This result is interpreted that DG sited at bus 4 in a uniform load distribution will have more voltage rise than at bus 4 in an end load distribution.

The statements made above are supported by observing the simulation results of the 4 bus model for both load demand distribution. The amount of voltage rise from baseline and the component of the voltage rise due to RPF are lower for low VRS scores and higher for high VRS scores. Observing bus 4 of both distributions, the voltage rise from baseline is approximately 1.4% higher for the uniform case than the end case. The respective VRS score is 88.1 and 71 for the uniform and end load distributions.

LD Distr	DG Distr	DG Bus	VR from BL[%]	RPF VR [%]	*VRS*
Uniform	Beginning	1	0.758	0	***22.3***
	Middle	3	4.076	0.985	***57.9***
	End	4	7.644	4.562	***88.1***
End	Beginning	1	0.758	0	***22.3***
	Middle	3	3.357	0.198	***45.4***
	End	4	6.570	0.806	***71.0***

Table 28. Comparison of Voltage Rise Score to Voltage Rise from Baseline and RPF Voltage Rise for the 4 bus scenarios.

In summary, the aspects of voltage rise caused at a DG bus can be scored using Voltage Rise Siting score described in Equation 5-69. DG sited at a bus with a high score will expect more voltage rise that a bus with a lower score, as shown in Table 28. The VRS score takes into account the location of the DG on the circuit relative the sub-station ($R_{S/S}$) and the components of reverse power flow voltage rise (RPF_{PEN}, RPF_R, RPF_{R0}). The VRS score is also normalized to enable so that circuits with different load distribution may be compared. VRS is calculation only requires information of line impedance and load distribution and does not require interactive solver. The VRS score may be used as tool to identify buses at risk of voltage rise.

5.2.1.4 Line Loss

As energy is transmitted through the sub-station to the load, a portion of the energy is lost on the distribution lines as heat. This loss is typically referred as I^2R losses, or line losses. Distributed Generation can reduce line-loss by providing power generation locally to the demand, but spatial variations of the load and generation impact the line-loss savings of DG.

Starting with a DC example (Figure 45), line-loss is simply the real power consumed by the conductor between the source and the load; modeled as a 1Ω resistor in the DC example. The impedance of the conductor is fixed at construction (with slight variations dependent on temperature), so the line current (I) dictates the amount of line-loss. The line current is composed of the load demand (I_{LD}) and local generation (I_{DG}), as shown in Equation 5-81**.** As the amount of DG increases, the line current decreases,

and line-loss decreases until the DG penetration surpasses the reverse power-flow (RPF) penetration. Since the DG directly affects line current, we expect the line-loss to behave as a quadratic function of DG penetration. At the RPF penetration, the DG is completely supplying the load demand at the local and downstream buses. At this point, the line current on the upstream DG bus is approximately zero with no line-loss. In this ideal DC example we expect the minimal amount of line-loss at approximately the RPF penetration: 100% with P_{DG} = 10W. Since the RPF penetration is a metric describing a specific bus, it is not directly applicable to a realistic feeder with distributed load and generation and therefore is not the same as the minimum line-loss penetration.

$$P_{LL} = I^2 R \qquad \text{5-73}$$

$$I = I_{LD} - I_{DG} = \frac{V_S - V_B}{R} \qquad \text{5-74}$$

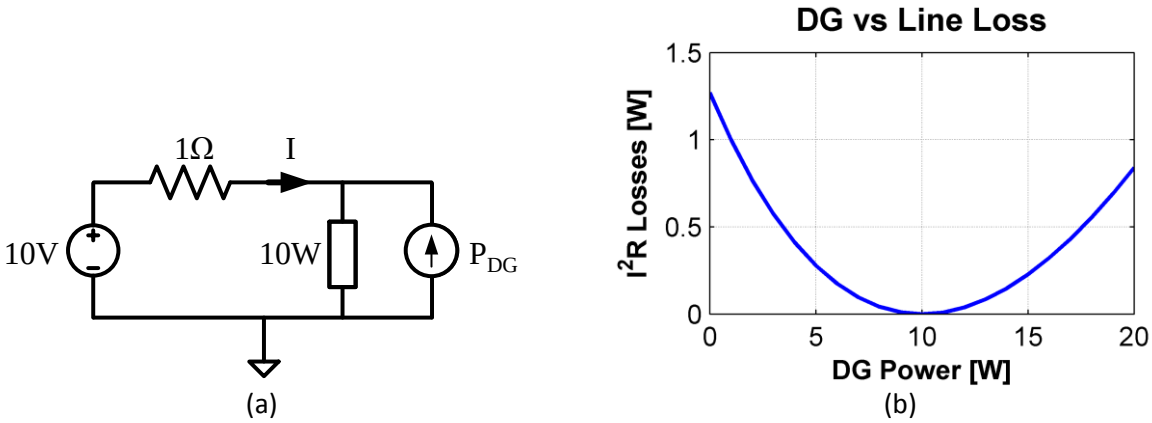

Figure 45. DC Line-loss example: (a) Model, (b) DG Power Generation versus Line Loss.

Although different than the RPF penetration, the minimum line-loss penetration is influenced by RPF. An alternative viewpoint on line-loss is to observe the voltage Equation (Equation 5-74). Assuming the source voltage is fixed (V_S), the amount of line current decreases as the bus voltage rises until the bus voltage rises beyond source voltage during RPF. As discussed in voltage rise section (B), voltage rise due to DG has two components: voltage rise from decreased line-loss and voltage rise from RPF. As DG penetration increases to the RPF penetration, the bus voltage is increases due to decrease in line-losses. As the DG penetration surpasses the RPF penetration, the voltage rise is due to RPF. In terms of the line-loss minimum penetration, DG penetration below the minimum results in line-loss savings due to the decrease in line drop. As DG penetration increases above the minimum penetration, then line-loss increases due to RPF. DG penetrations with less RPF will have less line-loss than penetration with more RPF. While the RPF penetration and minimum line-loss penetration are different metrics, they are an indication of RPF. With and understanding the causes of RPF and the nature of distribution lines, as presented in section B, feeders with generation at the end of the circuit will have lower RPF penetrations than feeders with generation at the beginning. Likewise, we should expect to see a similar result in terms of the minimal line-loss penetration.

$$\boldsymbol{S_{LL}} = \Delta \boldsymbol{V_{LN}} \cdot (\boldsymbol{I})^* \quad \textbf{5-75}$$

$$\Delta \boldsymbol{V_{LN}} = \boldsymbol{Z} \cdot \boldsymbol{I} \quad \textbf{5-76}$$

$$\boldsymbol{I} = I_R - jI_X \quad \textbf{5-77}$$

$$\boldsymbol{S}_{LL} = I^2\boldsymbol{Z} = P_{LL} + jQ_{LL} \quad \textbf{5-78}$$

$$I = \sqrt{I_R^2 + I_X^2} \quad \textbf{5-79}$$

$$\boldsymbol{Z} = R - jX \quad \textbf{5-80}$$

$$P_{LL} = (I_R^2 + I_X^2) \cdot R \quad \textbf{5-81}$$

Line-loss over an AC circuit is very similar to DC circuits, except for an added component. The complex power consumed by AC distribution line in terms in line drop ($\boldsymbol{\Delta V_{LN}}$) and line current ($\boldsymbol{I}$), as shown in equation 5-75. Utilizing Ohm's law (Equation 5-76) and the quadrature definition of line current (Equation 5-77), we arrive at an expression of complex line power in terms of line current magnitude (I) and complex impedance (Z). Line-loss is still attributed the power consumed by the line and turned into heat and therefore the real component (P_{LL}) of the complex line power. Applying the definitions of line current magnitude and complex impedance (Equations 5-79, 5-80) and the real component of the complex line power, we arrive at the final expression of line-loss in AC circuits (Equation 5-81). This AC expression of line-loss is similar to the DC expression except for contribution of the out-of-phase current component (I_X). DG will only directly influence the in-phase current (I_R), so assuming that line-loss is a quadratic function of DG penetration is still valid.

Generation Distribution	GC	σ_{GC}	Bus 1	Bus 2	Bus 3	Bus 4
Beginning	0.25	0	100%	0%	0%	0%
Middle	0.75	0	0%	0%	100%	0%
End	1.0	0	0%	0%	0%	100%
Beg. Distr.	0.3	0.13	91%	5%	3%	1%
Mid. Distr.	0.72	0.15	6%	6%	82%	6%
End Distr. 1	0.96	0.13	1%	3%	5%	91%
End Distr. 2	0.91	0.21	6%	6%	6%	82%
End Distr. 3	0.86	0.23	6%	13%	13%	68%

Table 29. Four Bus Model generation distributions. The generation distributions represent the percentage of the total feeder generation on each bus.

Load Distribution	LC	σ_{LC}	Bus 1	Bus 2	Bus 3	Bus 4
Uniform	0.63	0.3	2MW	2MW	2MW	2MW
End	0.91	0.21	0.5MW	0.5MW	0.5MW	6.5MW

Table 30. Four Bus Model load distribution.

To understand the nature of line-loss on a feeder with varying load and generation distributions, a four bus model, as described in section B, is used. The various load and generation distributions used in this discussion is detailed in Table 29 and Table 30.

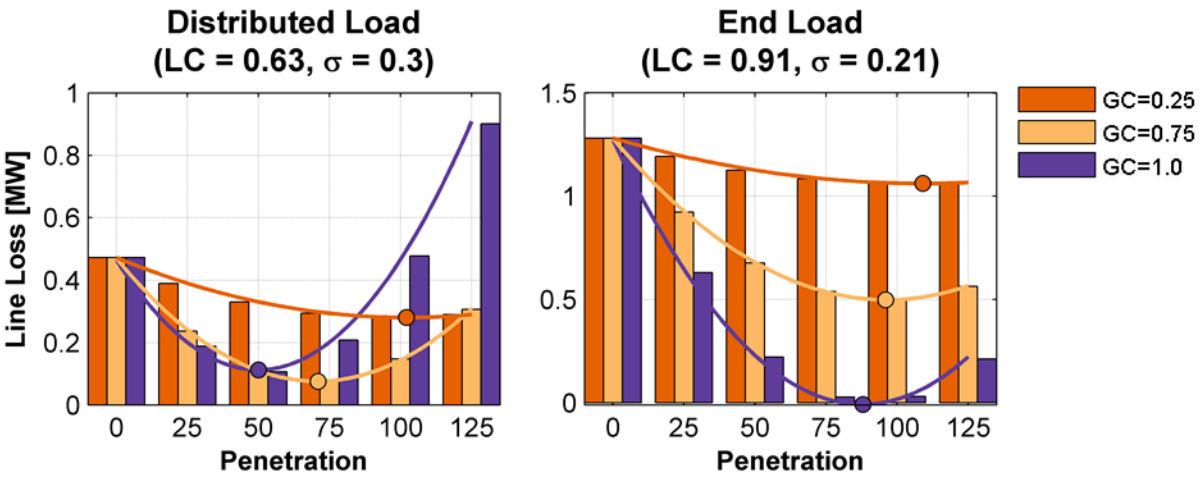

Figure 46. Four Bus Model line-loss versus penetration for a distributed load (left) and an end load (right) distribution.

Observing Figure 46, we see the line-loss results for Beginning, Middle, and End generation distributions for a Uniform load and an End load distribution. The plots show three trends: 1) the line loss behave as a quadratic function of penetration and therefore has a minimum, 2) the numerical order of the minimal line-loss penetrations and 3) the generation distributions do not have equal line-loss minimums.

Given the expression of line loss in Equation 5-81 and since DG penetration directly affects the amount of line current, we expect the calculated line loss to behave as a quadratic function as observed in Figure 46. To estimate the line loss value between the simulated penetrations, an approximation of the line line as a function of penetration is found using a lease squares quadratic fit (Equation 5-68). From this estimate, a minimum line loss penetration is found as shown in Figure 46.

$$LL(pen) = p_1 \cdot pen^2 + p_2 \cdot pen + p_3 \qquad \textbf{5-82}$$

LL → *Line Loss [W]*
pen → *DG penetration [%]*
p_1, p_2, p_3 → *Coefficients of quadratic line loss function*

As previously discussed, the minimum line-loss penetration and the RPF penetration are both indications of RPF. Ending DG distributions will encounter RPF before a Beginning distribution, in terms of DG penetration. Therefore the increasing numerical order of minimum line-loss penetrations is the 1) End, 2) Middle, and 3) Beginning DG distributions for both load distributions is as expected. Using the minimum line-loss penetration as indication of RPF is useful to describing the difference between point and distributed DG distributions, as discussed later.

Also expected is that the different DG distribution yielded different minimum line-loss values. For both load distribution cases, the closer the generation is located to the load, the lower the line-loss ultimate minimum. This statement agrees with our initial assumption that DG can reduce line-loss because it is located closer to the load than the sub-station. This quality can be described using the LC/GC ratio of the load and generation distributions: as LC/GC approaches unity, the closer the generation is to the load, and the lower the line loss minimum. Observing Table 31, the Middle DG distribution achieved the lowest line-loss minimum for the Uniform load distribution, and the End DG distribution did the same for the End load distribution. In both cases, the LC/GC ratios are the closest to unity indicating the relative distance from the load to the generation.

Generation Distribution	**GC**	**Load Distribution (LC)**					
		Uniform Load (0.63)			***End Load (0.91)***		
		LC/GC	*Min Loss Pen [%]*	*Loss [kW]*	*LC/GC*	*Min Loss Pen [%]*	*Loss [kW]*
Beginning	0.25	2.52	103	280	3.64	110	1060
Middle	0.75	0.84	75	80	1.21	97	500
End	1.0	0.63	51	110	0.91	89	0

Table 31. Four Bus Model line-loss results for a uniform load (left) and an end load (right) distribution.

Distribution circuits typically feature a truly distributed load distribution. The last example only used DG sited as point installation and not truly distributed. The term distributed used in this context is referring to the spatial variance about the average (load and generation center); this is described using the standard deviation (σ) of the Load or Generation Center as described in section 5.2.1.2. For a point DG source, σ_{GC} will equal zero. Observing Figure 47, the plot is line-loss results for a uniform load distribution except with distributed ($\sigma_{GC} \neq 0$) Beginning, Middle, and End distributions. The table in Figure 47 is a comparison between the point DG distributions ($\sigma_{GC} = 0$) and distributed DG ($\sigma_{GC} \neq 0$). In all cases, minimum line-loss achieved was lower for the distributed cases than the point cases. For the same penetration, a point DG distribution is more likely to cause RPF than a distributed DG distribution, as indicated by the minimum line-loss penetration being lower in all cases for the point DG than the distributed DG. This infers that distributed DG will feature less RPF than point DG and therefore will feature more line-loss savings. In general, for two DG distributions with a similar GC, a distributed DG profile ($\sigma_{GC} \neq 0$) will have more ultimate line loss savings point DG profile ($\sigma_{GC} = 0$).

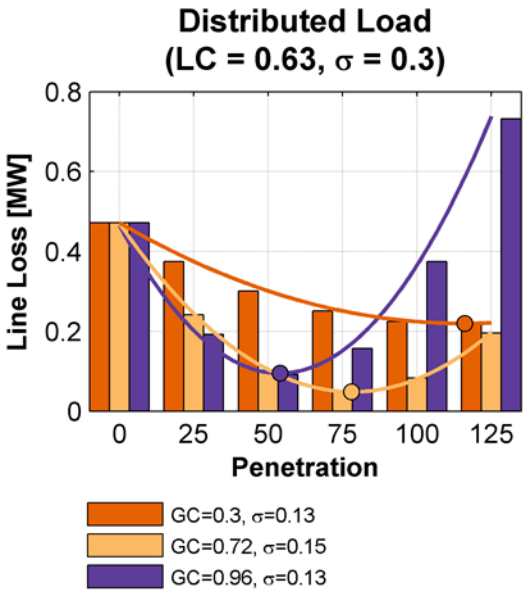

(a)

Generation (GC)	GC	σ_{GC}	Uniform Load		
			LC = 0.63, σ_{LC} = 0. 3		
			LC/GC	*Min Loss Pen [%]*	*Loss [kW]*
Beginning	0.25	0	2.52	13	280
	0.3	0.13	2.1	117	220
Middle	0.75	0	0.84	75	80
	0.72	0.15	0.88	79	40
End	1.0	0	0.63	51	110
	0.96	0.13	0.66	55	100

(b)

Figure 47. Four Bus Model line-loss plot (a) and table (b) for a distributed generation and uniform load distribution.

The common theory is DG in distribution feeders improves system efficiency through the reduction of line-loss. Line-losses will decrease as DG penetration increases until the minimum line-loss penetration; DG penetrations beyond this point will not decrease line-losses. The minimum line-loss penetration related to the reverse power flow (RPF) penetration, therefore the DG distribution will influence the minimum line-loss penetration and a circuit DG penetration beyond the minimum line-loss penetration will feature RPF voltage rise concerns. Feeders with DG distribution located at the beginning of the circuit will feature a higher minimum line-loss penetration than if the feeder had an end DG distribution. Apart from influencing the minimum line-loss penetration, the spatial distribution influences the amount of line-loss savings may be achieved. In general, closer the generation is to the load, the lower the line-losses. This quality is compactly described using the LC/GC ratio of a circuit: circuits with an LC/GC ratio approach unity will have lower line-losses than circuits with an LC/GC ratio diverging from one. Finally, distribution circuits feature a truly distributed load ($\sigma_{LC} \neq 0$), so distributed distributions ($\sigma_{GC} \neq 0$) will have lower line-loss than point distributions ($\sigma_{GC} = 0$). It is correct to say that DG will reduce line-losses in a distribution circuit, but there is an optimal DG penetration to reduce line-losses that is influenced by the spatial distributions of the DG on the circuit.

5.2.2 Results

On objective of this research is to identify the PV penetration limits of a commercial (Cayetano) and a residential (Menlo) circuit. Three phase balanced models of both circuits were created and evaluated at the point of the sub-station against measured data, as presented in Model Development and Evaluation section 5.1.3. Using the calibrated models, the generation varied in capacity and location to understand the effect if High-Pen PV on the 1) the voltage profile of the primary feeder, 2) the voltage regulation

equipment, 3) sub-station power factor, and finally 4) the line loss characteristics. Before the results of the analysis are presented, the evaluation methods and reasoning are presented below.

To evaluate varying levels of PV penetration at steady state, ideal PV generation is used. The penetration metric does not reveal information about aspects that de-rate a PV installation: thermal, shading, mis-match, wire loss, inverter loss, and more de-rate an installation to approximately 76% nameplate capacity [17]. During the development of the baseline model it was important to account the de-rating factors, as detailed in PV Generation Estimation (section 5.1.2.4A), but simulating the rated PV at full nameplate rating is actually a "worst case" scenario for voltage regulation equipment. Therefore in this research, PV generation is simulated at full nameplate capacity at the peak PV time of day. Table 32 is the list of penetrations and the equivalent nameplate capacity used in the evaluation of the Cayetano and Menlo circuits. The Cayetano was evaluated for 0% (baseline), 15%, 30%, 40%, 50%, 60%, 70%, 80%, 90%, and 100%, while the Menlo was evaluated for 0% (baseline), 15%, 30%, 40%, 60%, 80%, and 100%. The Menlo circuit was not evaluated at the same penetrations of the Cayetano circuit due to the length of simulation of the Menlo model. The evaluated range is same and is evaluated at multiple points for both circuits, which provide enough information to observe trends and draw conclusions from the simulation results.

Circuit	**Peak**	**PV Penetration Equivalent [MW]**									
		0%	*15%*	*30%*	*40%*	*50%*	*60%*	*70%*	*80%*	*90%*	*100%*
Cayetano	12MW	0	1.8	3.6	4.8	6	7.2	8.4	9.6	10.8	12
Menlo	9.1MW	0	1.4	2.7	3.6	-	5.5	-	7.3	-	9.1

Table 32. The nameplate equivalent to PV Penetration used in the evaluation of Cayetano and Menlo.

PV generation is a variable power generation source dependent on the availability of solar irradiance at the site. This study is focused on the steady behavior of High-Pen PV on distribution circuits, so ideal generation curve was used to simulate the steady state variability of PV generation. Since day-light hour vary from season to season, an average PV curve was derived and normalized (to the season) using SolarAnywhere data local to the circuit: see section B.1 for more information about SolarAnywhere irradiance data. The normalized PV generation curves used in the evaluation of the Cayetano and Menlo circuits are shown in Figure 48. The range of the PV region and time of day of peak PV for each curve is found in Table 33.

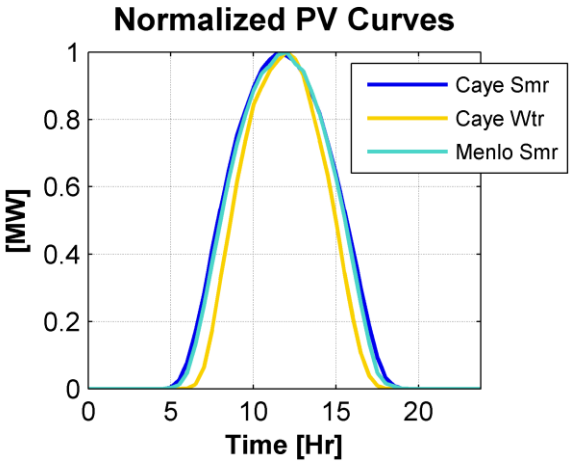

Figure 48. Normalized Seasonal average PV curves use in Cayetano and Menlo evaluation.

Circuit	Season	PV Region	Peak PV
Cayetano	Summer	[4:45 19:15]	11:30
	Winter	[5:45 18:15]	12:00
Menlo	Summer	[4:45 19:15]	12:00

Table 33. Statistics of normalized seasonal average PV.

The spatial influence of High-Pen PV is evaluated using four different generation distributions: radial, beginning, middle and end distributions. The radial distribution is the distribution of the existing PV (as of 2010) of each circuit. The beginning, middle, and end distributions are point generation distributions; all the generation of the circuit is located at a single bus for a point distribution. Table 34 and Table 35 are the generation distributions used in the evaluation of the Cayetano and Menlo.

Bus	Radial	Beginning	Middle	End
3	0.74%	100%	0%	0%
8	0.21%	0%	100%	0%
16	33.10%	0%	0%	0%
23	12.49%	0%	0%	0%
25	0%	0%	0%	0%
27	0.32%	0%	0%	0%
29	53.13%	0%	0%	100%

Table 34. Cayetano generation distribution scenarios.

Bus	Radial	Beginning	Middle	End
2	1.18%	100%	0%	0%
3	0.62%	0%	0%	0%
4	1.04%	0%	0%	0%
6	0%	0%	0%	0%
9	1.55%	0%	0%	0%
11	12.93%	0%	0%	0%
15	29.74%	0%	0%	0%
16	3.27%	0%	100%	0%
17	9.71%	0%	0%	0%
18	0.96%	0%	0%	0%
19	7.39%	0%	0%	0%
20	1.93%	0%	0%	0%
24	6.58%	0%	0%	0%
26	0.36%	0%	0%	0%
28	0.36%	0%	0%	0%
29	0.27%	0%	0%	0%
31	1.30%	0%	0%	100%
32	0.41%	0%	0%	0%
33	9.02%	0%	0%	0%
34	2.27%	0%	0%	0%
35	4.71%	0%	0%	0%
38	0.70%	0%	0%	0%
39	1.94%	0%	0%	0%
41	1.77%	0%	0%	0%

Table 35. Menlo generation distribution scenarios.

The load centers in relation the generation centers of the Radial, Beginning, Middle, and End generation distributions is shown in Figure 49. The Cayetano circuits load distribution is clustered at the end of the circuit resulting in a load center (LC) of 0.85 with a standard deviation (σ_{LC}) of 0.13. On the other hand, the Menlo circuit widely distributed about the center of the circuit resulting in a load center of 0.42 and standard deviation of 0.23. Table 36 summarizes the Cayetano and Menlo circuits load centers and standard deviation the four generation distributions described above.

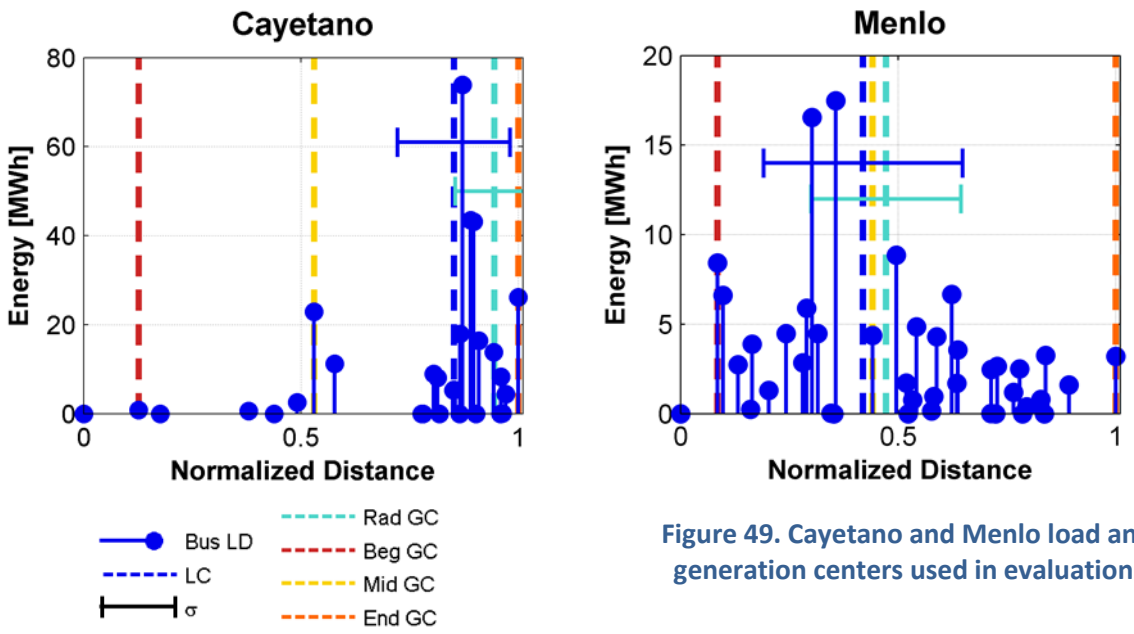

Figure 49. Cayetano and Menlo load and generation centers used in evaluation.

Circuit	LC (σ_{LC})	GC (σ_{GC})			
		Radial	*Beginning*	*Middle*	*End*
Cayetano	0.85 (0.13)	0.94 (0.09)	0.13 (0)	0.53 (0)	1.0 (0)
Menlo	0.42 (0.23)	0.47 (0.17)	0.08 (0)	0.44 (0)	1.0 (0)

Table 36. The load and generation distributions used in the evaluation of Cayetano and Menlo.

To simulate High-Pen PV using the above description of varying penetrations and generation distributions are combined to form multiple simulation scenarios. For each scenario, the PV penetration's equivalent generation capacity is distributed across the circuit's buses as specified by the generation distribution. When done correctly, the sum of all the bus nameplate generation rating will equal the PV penetration's equivalent capacity. The output of the PV generation component models is varied from zero to full capacity using the product of the normalized PV generation curve and the distributed generation rating. The PV curve is selected to match the season of the characteristic day under evaluation; for example, the Cayetano summer High and Low days will use the same PV curve derived for the Cayetano summer season, as shown in Figure 48.

Accounting for all the combinations of penetration and spatial variations for each characteristic day, there are 160 unique model runs for the Cayetano circuit and 54 for the Menlo circuit. Please note that the Cayetano is evaluated for four characteristic days (summer/winter, high/low) while the Menlo is evaluated only over the summer season (summer, high/low), as detailed in Day Selection section (D). Each simulation is processed to calculate the bus real and reactive power, per-unit voltage and phase angle using the complex bus voltage and current simulation output, as detailed in the Post-Processing section (F).

Property	Criteria
Bus voltage	[0.98 to 1.05] per unit
Voltage regulating operating equipment	Change in operation from baseline (0%)
Sub-station power factor	0.97 lagging to 0.99 leading
Line-loss	Observation

Table 37. Evaluation Criteria.

To analyze the results, properties and aspects of the system are evaluated using the criteria presented in Table 37. The properties of interest include bus voltage, operation of voltage regulation equipment, sub-station power factor, and line-loss. The criteria defined for bus voltage is more stringent than the ANSI C84.1 (Range A) requirement which specifies that the service voltage must be within 0.95 to 1.05 per unit. Since this research is simulating the voltage primary feeder of the circuit, the range is shortened to 0.98 to 1.05 per unit to account for at least a 3% drop between the primary feeder and the point of service [18, p. 5] due to line and transformer losses. The voltage regulation equipment of interest includes the sub-station Load Tap Changer (LTC) with Load Drop Compensation (LDC) and switching capacitors in the circuits. Any change from the baseline simulation (0% penetration) is reported in this evaluation. The sub-station power factor is regulated by the California Independent System Operator (CAISO), but the evaluation criterion is derived from PG&E's Guide for Planning Area Distribution reference [19, p. 8]. Finally, line-loss does not have a formal reporting criterion, but is observed in all cases. The results of the evaluation are detailed in proceeding subsections.

5.2.2.1 Results – Voltage

As discussed in the preceding section, the bus voltage for all the Cayetano and Menlo circuit simulation scenarios are evaluated to be with in the 0.98 to 1.05 per unit voltage range. Figure 50 is a summary of the Cayetano maximum and minimum bus voltages during the PV region (plotted as separate signals). Each plot is different distribution with the result for each of the four characteristic days over the range of simulated penetrations (0 to 100%). In all scenarios, the Cayetano circuit did not feature any out-of-standard voltage extremes.

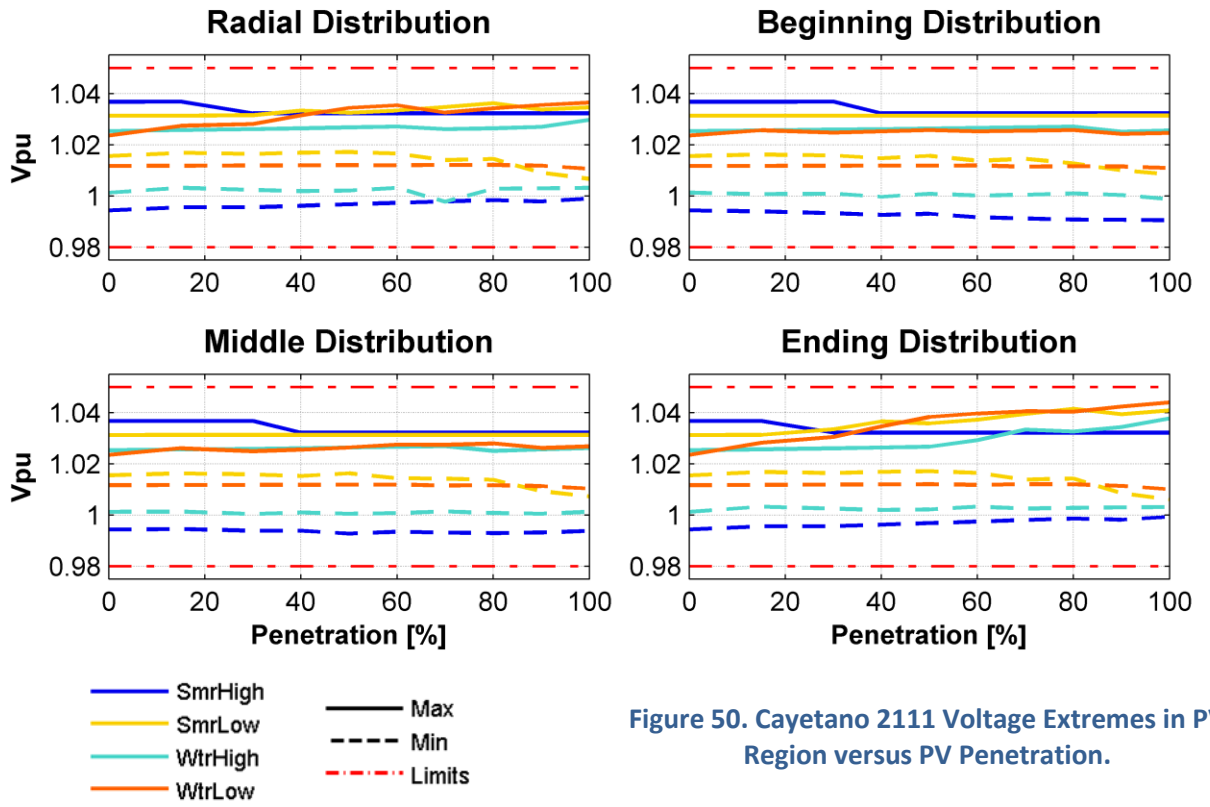

Figure 50. Cayetano 2111 Voltage Extremes in PV Region versus PV Penetration.

Figure 51 is a summary of the scenario results for the Menlo circuit. The formats of the plots are identical to that described above with the exception that the Menlo circuit is only evaluated for two characteristic days. The Menlo End generation distribution scenarios featured non-standard high voltage for both the summer high and low days and for the all penetration greater than the baseline (0%). The Summer High characteristic day also had minimum bus voltages marginally below the low voltage threshold (0.98pu) for all penetrations in the radial, middle, and end generation distribution scenarios. This marginal low voltage condition and did not change from the baseline penetration, so it is concluded that is not caused by High-Pen PV. This is not the case for the Menlo Summer High day with a Beginning generation distribution scenario. The penetrations ranging from 0 to 40% demonstrated a marginal low voltage condition, but penetrations greater than 40% show a steady decline in the bus voltage to 0.948 V_{pu} at 100% penetration.

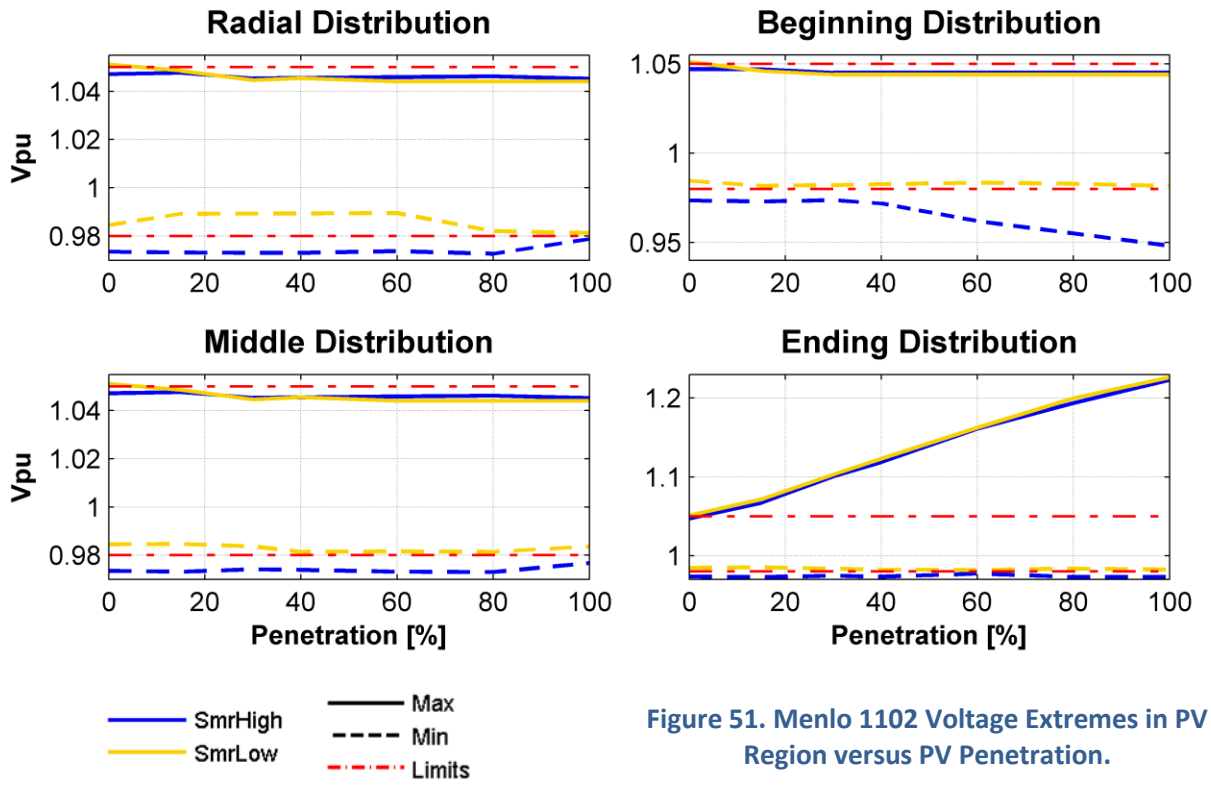

Figure 51. Menlo 1102 Voltage Extremes in PV Region versus PV Penetration.

In Summary, The Cayetano circuit did not feature any out-of-standard voltage conditions in the PV region while the Menlo circuit did. The Menlo circuit with an End generation distribution demonstrated high voltage conditions and the beginning generation distribution showed low voltage conditions. Although the Cayetano did not have any out-of-standard bus voltage, the circuit did demonstrate similar behaviors that led to the non-standard voltage conditions of the Menlo circuit. The preceding section addresses the technical details of the high voltage condition instigated by High-Pen PV as seen on the Menlo circuit in comparison the Cayetano. The low voltage condition observed from the Menlo Beginning generation scenario is actually tightly coupled with the operation of the Load Drop Compensation (LDC) control of the sub-station Load Tap Changer (LTC) and is discussed in depth in the Voltage Control Equipment section (0).

A. Voltage Results - High Voltage

In the results presented in the previous section, only the Menlo Ending generation distribution scenario exhibited out-of-standard high voltage in the PV region. Other distribution scenarios exhibited voltage rise as penetration increased as shown in Figure 52, but did not have the high voltage conditions. High-Pen PV is the cause of the voltage condition since the high voltage condition occurred in the PV region and increased with penetration, but why did the condition only occur for the Menlo Ending distribution scenario?

As discussed in the Voltage Rise section (B), DG bus voltage increases as DG penetration increases by two mechanisms: first as line drop reduction and second reverse power flow (RPF). Voltage rise from

reverse power flow has the potential to raise the voltage out of standard bounds, while voltage rise from line-loss reductions does not (unless the sub-station is operating out of standard bounds, which is not the case here). To understand why the Menlo End distribution struggled with high voltage, we will analyze the characteristic differences between the Menlo End distribution with the Menlo Middle and Cayetano End distributions; two distribution scenarios that exhibit noticeable amounts of voltage rise but remained in standard limits. The analysis below will focus on the voltage rise characteristics exhibited by the three distributions. It is important to note that in all distribution scenarios, the sub-station voltage lowered as a result of increased penetration, but this interaction is due to the Load Drop Compensation controller of the sub-station Load Tap Changing transformer and is discussed in Low Voltage section (B).

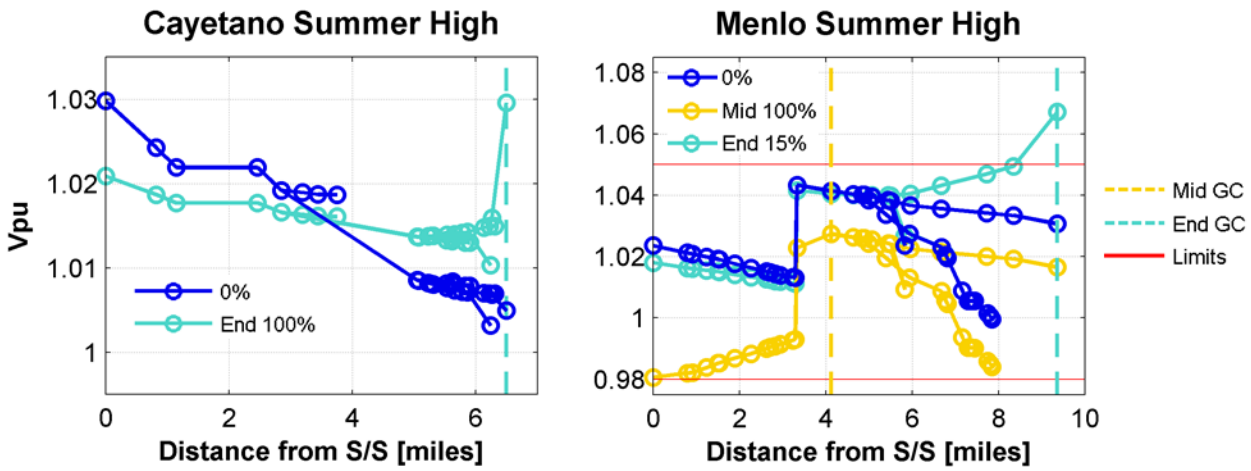

Figure 52. Bus voltage versus distance from sub-station for the Cayetano and Menlo Summer High scenarios at the Peak PV time of day.

Observing Figure 52, we see the bus voltage profile versus distance for the Menlo End distribution at 15% penetration, the Cayetano End at 100%, and the Menlo Middle at 100%. The Menlo End distribution shows a greater amount of voltage rise at 15% penetration than both the Cayetano End and Menlo Middle at 100% penetration. Recalling the discussion in the Generation Location and Voltage Rise Characteristics section (A.1), the cumulative line resistance from the Distributed Generation (DG) location to the sub-station influences the voltage rise per penetration rate. Sites with higher line resistance to the sub-station will have faster voltage rise per penetration rates than a site with a lower line resistance to the sub-station.

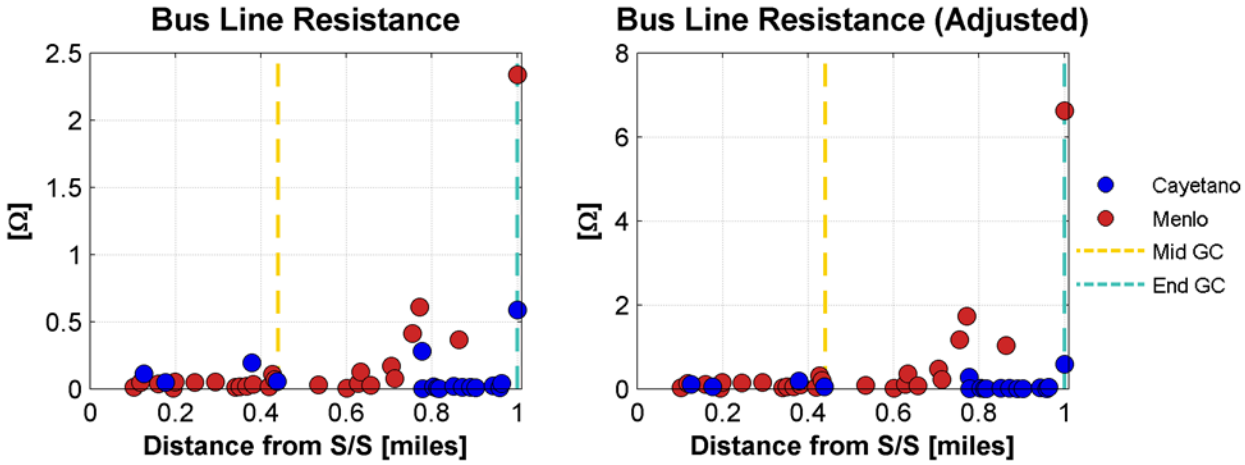

Figure 53. The bus line resistance along the direct path from the sub-station to the generation site versus normalized distance for the Cayetano End, Menlo Middle, and End distribution scenarios.

The left plot in Figure 53 shows the bus line resistances along the direct path the generation sites for the Cayetano End, Menlo Middle, and Menlo End generation distribution scenarios; the Generation Center (GC) for the Menlo Middle is 0.44 and the Cayetano End and Menlo End is 1. For both circuits the primary feeder utilizes heave conductor (low resistance) for the majority of the circuit and thinner conductor (higher resistance) towards the end of the feeder. But the Cayetano and Menlo do not operate at the same voltage, so for the same amount of load demand the Menlo requires more line current and incurs more line drop than the Cayetano. In order to compare the line resistance between the Cayetano and Menlo, we must transform the Menlo circuit's line impedance to its effective 21 kV circuit equivalent.

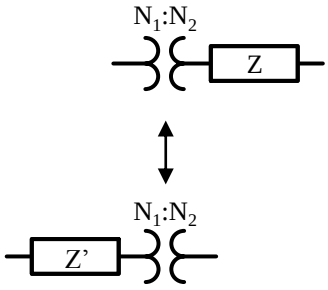

Figure 54. Equivalent Impedances.

$$Z' = \left(\frac{N_1}{N_2}\right)^2 \cdot Z \qquad \textbf{5-83}$$

Using equation 5-83, a line impedance in a 21kV system (Z') is effectively 2.8 $((N_1/N_2)^2)$ times greater than its equivalent (Z) in a 12.47 kV system. Now comparing the effective 21kV line resistance of the Cayetano and Menlo circuit (right plot in Figure 53), we see that the effective line resistance is much higher than the Cayetano simply because of the operating voltage.

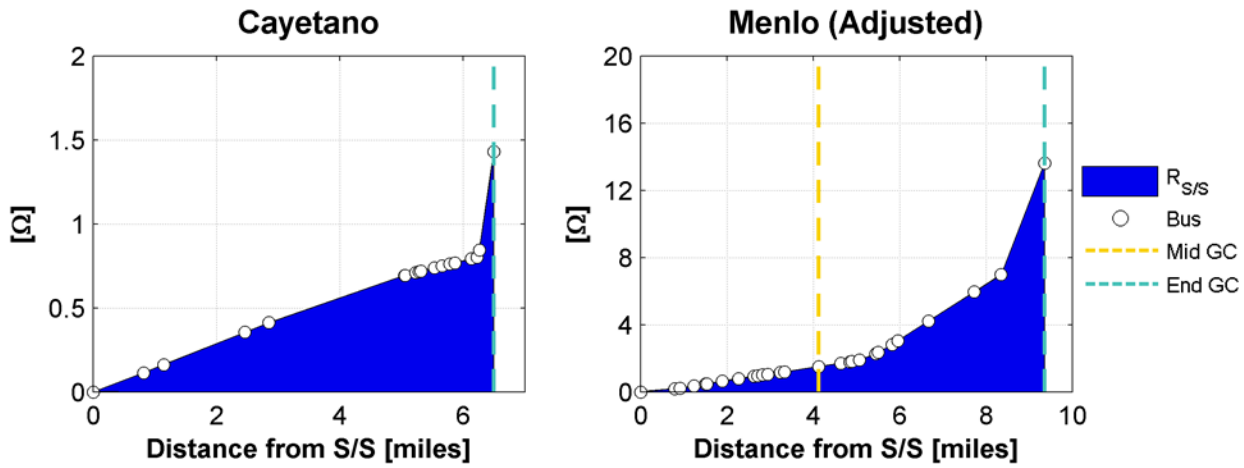

Figure 55. Cumulative bus line resistance to the sub-station ($R_{S/S}$) versus distance from the sub-station for the Cayetano and Menlo circuits. The line resistances shown are for an effective 21kV system.

Now observing the cumulative line resistance to the sub-station ($R_{S/S}$) in Figure 55, we see the Cayetano End with 1.46Ω, Menlo Middle with 1.5Ω, and Menlo End with 13.51Ω (effective impedances on a 21kV system). Given the prior discussion and the $R_{S/S}$, the rate of voltage rise per penetration is expected to be much higher for the Menlo End distribution scenario than the Cayetano End and Menlo Middle distribution scenarios.

Observing the line resistance to the sub-station give a qualitative understanding about voltage rise per penetration increase rate, but it does not shed light on the Reverse Power Flow (RPF) characteristics of a DG site. Voltage rise induced by RPF has the potential to increase bus voltage out of standard bounds, and buses prone to large amounts of RPF voltage rise have two characteristics: large amounts of excess capacity and high RPF resistance, as discussed in Reverse Power Flow Voltage Rise Characteristics section (B.1).

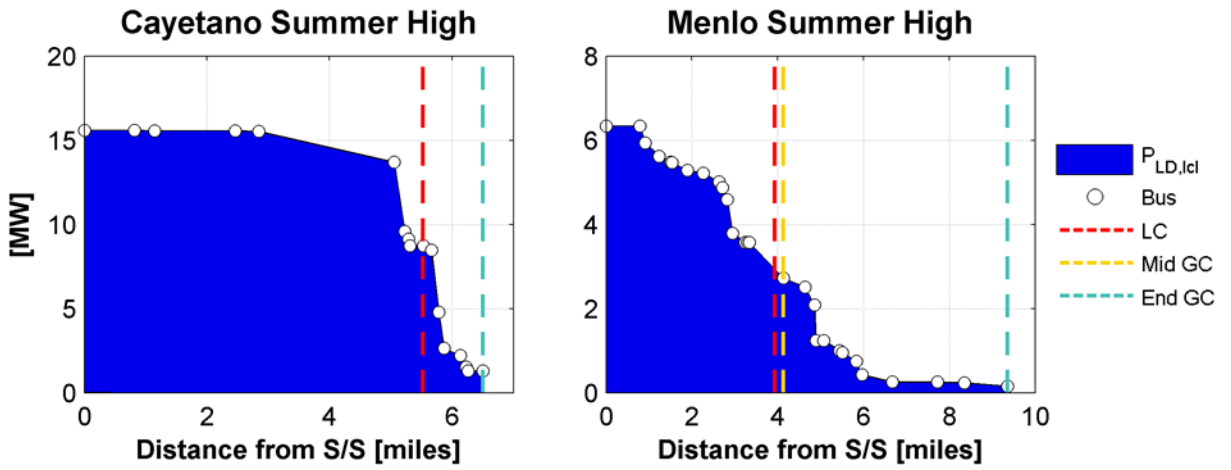

Figure 56. The local (bus and downstream) load demand seen at each bus on the DG buses upstream path for the Cayetano and Menlo Ending generation distribution scenarios.

Excess capacity, as defined in equation 5-63, is the generation capacity that surpasses the local (DG bus and downstream) load demand ($P_{LD,lcl}$). Increased levels of excess capacity results in increased voltage rise due to RPF. Without excess capacity, RPF does not occur. The penetration point at excess generation occurs is referred to as the RPF penetration (RPF_{pen}) and is defined in equation 5-65. Sites with a low RPF penetration will experience more RPF than sites with higher RPF penetrations. The RPF penetration, dependent on the time of day, is calculated at the Peak PV time of day in this study. Figure 56 is the local load demand at each bus on the direct path from the sub-station to the PV site for the Cayetano End, Menlo Middle, and Menlo End distributions.

The local load demand will change dramatically from day to day, resulting in a change in RPF penetration, as shown in Table 38. By observing the results of the table, we see the End distributions have lower RPF penetration than the Middle distribution indicating the End distributions will host more RPF at higher penetrations and as a result more RPF voltage rise.

Circuit	LC/GC	Day	RPF_{pen} [%]
Cayetano End	0.85	Summer High	10.9
		Summer Low	2.7
		Winter High	8
		Winter Low	3.3
Menlo Middle	0.95	Summer High	25.7
		Summer Low	19.6
Menlo End	0.42	Summer High	1.7
		Summer Low	1.1

Table 38. The LC/GC ratio's and RPF penetrations for the characteristic days of the Cayetano End, Menlo Middle, and Menlo End distributions.

In comparing two PV sites, the RPF penetration indicates the amount the excess capacity the site will source at higher penetrations, but does not indicated is the relationship site to the load. The Load Center to Generation Center (LC/GC) ratio, as presented in the RPF Voltage Rise Characteristics section (B.1), provides an indication of both RPF penetration and the spatial relationship. A large LC/GC ratio ($LC/GC \rightarrow \infty$) indicates the Generation Center is located upstream of the Load Center and closer to the sub-station, while a small ratio ($LC/GC \rightarrow 0$) indicates the generation located downstream of the load and towards the end of the circuit. As a result, a site with a large LC/GC ratio will have a higher RPF penetration than a site with a lower LC/GC ratio. Furthermore, sites with a LC/GC ratio approaching one ($LC/GC \approx 1$) indicates a site is collocated with the load distribution. Ratios diverging from unity indicate an increased distance from the GC to the LC. Again referring to Table 38, the Menlo End distribution has the lowest and farthest from one LC/GC ratio of 0.42. From this result, we can differentiate the difference between the Cayetano End and Menlo End distribution. While both distributions exhibit low RPF penetrations, the Cayetano End distribution is located closer the load than the Menlo End distribution.

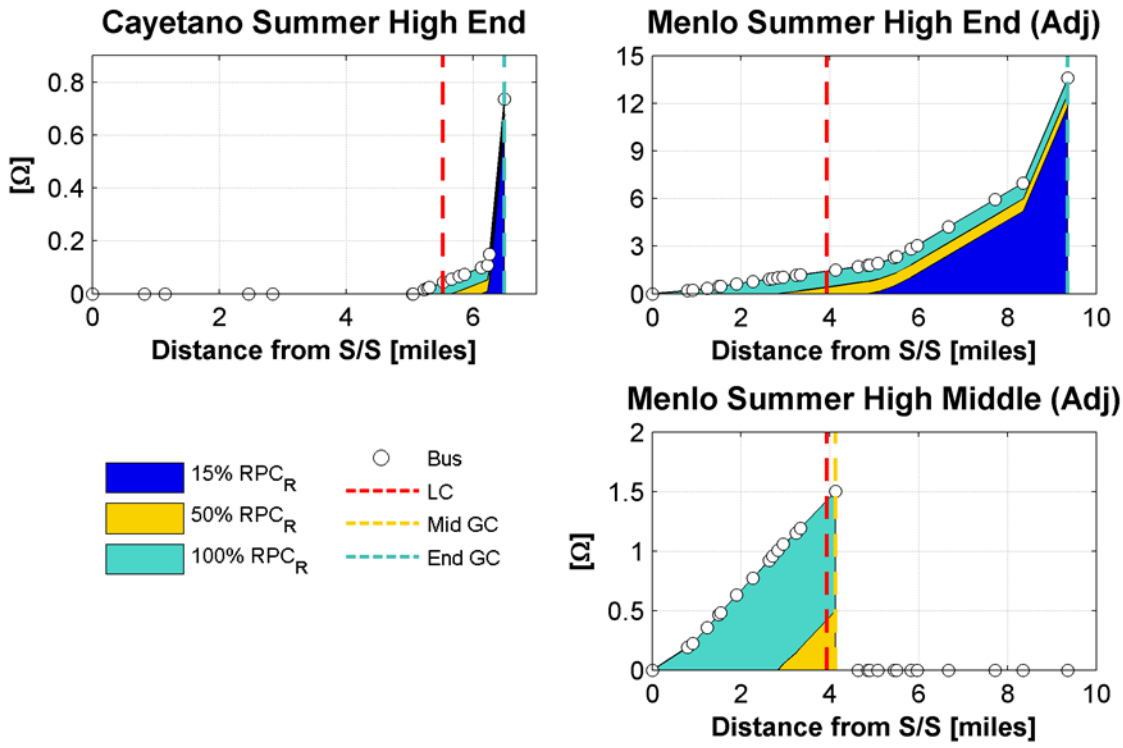

Figure 57. The RPF resistance (RPF_R) at the DG bus and upstream buses for various penetrations for the Cayetano Ending and Menlo Middle and Ending generation distributions.

As excess generation increases, the amount of reverse power flow going upstream of the DG site increases. As stated above as excess generation increases, the DG site's bus voltage rises from RPF voltage rise. The amount of voltage rise is dictated by the upstream line impedance the excess capacity must flow through. The cumulative line resistance the excess capacity flow through is referred to as RPF resistance (RPF_R). The calculation of RPF resistance is defined using equation 5-68 in the RPF Voltage Rise Characteristics section (B.1). As excess capacity increases with a penetration, the induced RPF will flow farther upstream and therefore increasing the amount of RPF resistance. Figure 57 shows the RPF resistance (effective 21kV equivalent) for the Cayetano End, Menlo Middle and End distributions for increasing penetrations. From the plot, the resistive RPF line impedance at 100% penetration for the Cayetano End, Menlo Middle, and Menlo End is 0.74 Ω, 1.5 Ω, and 13.6 Ω; the Menlo End distribution RPF_R is significantly larger than the other distribution and resulting in more voltage rise as the PV site will raises its bus voltage to overcome the RPF_R voltage drop.

Again referring to the LC/GC ratio, we can observe the benefit of downstream generation located close the load center. The Cayetano End and Menlo End scenarios both feature low RPF penetrations, but the RPF_R of the Cayetano End is significantly lower than the Menlo End scenario. Since the GC of the Cayetano End scenario is located close to the load (LC/GC = 0.85), we see the extension of RPF_R as penetration increases less than for the Menlo End scenario (LC/GC = 0.42).

In the evaluation of High-Pen PV in the Cayetano and Menlo circuits, the Cayetano End, Menlo Middle, and Menlo End generation distribution scenarios exhibited significant amounts of DG induced voltage

rise, but only the Menlo End scenario had non-standard high voltages. The analysis above presented the differences between the three situations in terms of cumulative series sub-station resistance ($R_{S/S}$), excess generation, and cumulative reverse power flow (RPF_R). The Menlo End scenarios in cases exhibited higher amounts of $R_{S/S}$, excess generation, and RPF_R, resulting in higher amounts of voltage rise. It was also observed the influence of the location of downstream generation center (GC) to the load center (LC). When the GC is located away from the LC, as in the Menlo End scenario, the excess generation and RPF_R values are greater resulting in higher voltage rise.

In summary, the Menlo End exemplifies the characteristics of DG induced voltage rise. The PV installation was sited at the end of circuit with high sub-station line resistance ($R_{S/S}$), a low RPF penetration, and downstream and away from the Load Center (low LC/GC). As a result, the PV site experienced RPF at low penetration levels resulting in a high RPF line resistance (RPF_R).

The Cayetano End and Menlo Middle PV installation sites did have characteristics of voltage rise, but not all the characteristics and not to the extent of the Menlo End distribution. The Cayetano End scenarios exhibited a high $R_{S/S}$ and a low RPF penetration, but the PV installation was sited close the Load Center. The Menlo Middle scenarios only featured a high $R_{S/S}$. The Cayetano End and Menlo Middle exhibited DG induced voltage rise, but a much lower rate due to the characteristics of the PV installation siting.

By analyzing the components of voltage rise, we can form an understanding on what can be done to improve the system to mitigate voltage rise. Apart from reconfiguring the load distribution on the circuit, lowering the system impedance of a DG site will aid in reducing the amount of DG induced voltage rise. Another approach is to identify locations in the circuit prone to DG induced voltage rise and avoid siting large PV installations in troublesome locations.

B. Voltage Results - Low Voltage

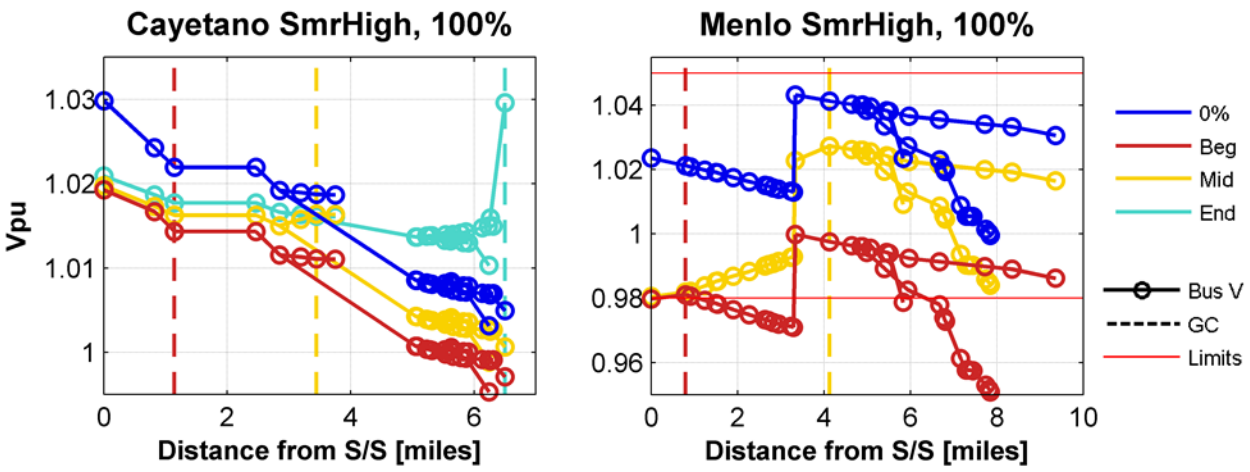

Figure 58. Bus voltage versus distance for various generation distributions at a 100% penetration for both the Cayetano and Menlo summer high scenarios.

An out-of-standard low voltage condition was identified for the Menlo Summer High Beginning distribution scenario for penetrations greater than 40% in Figure 51. The low voltage condition is

caused by the interaction of the High-Pen PV with the sub-station Load Tap Changer (LTC) with Load Drop Compensation (LDC) controller. As PV penetration, the LTC taps down and lowers the voltage. This observation is present in all the scenarios simulated for the Cayetano and Menlo circuits. Observing Figure 58, at 100% penetration the sub-station voltage is lower due to the LTC w/ LDC than the baseline (0%) sub-station voltage for all distribution scenarios, but some generation distribution scenarios are at a higher risk of an out-of-standard low voltage condition than others. Below, potential low voltage conditions caused by High-Pen PV are discussed through understanding the relationship of the operation of the sub-station LTC w/ LDC and the generation's location from the sub-station and the load demand. Then the observed isolated low voltage condition is discussed using Menlo circuit's system impedance.

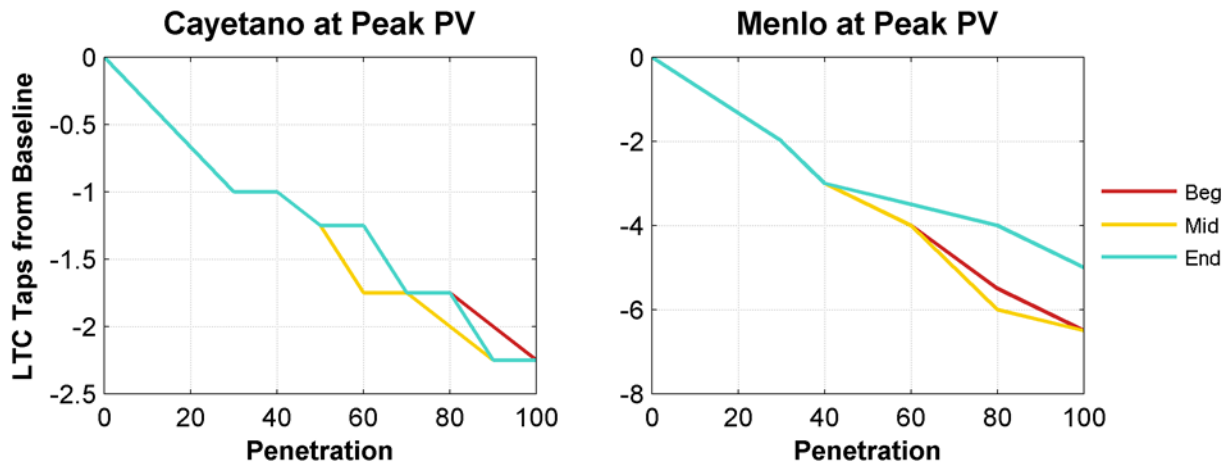

Figure 59. The average LTC tap position difference from baseline (0%) at Peak PV time of day for the Cayetano and Menlo.

As stated above, the low voltage condition is caused by the interaction of High-Pen PV with the LDC controller. Observing Figure 59, the LDC controller operates the LTC at a lower tap position than the baseline (0%) at PV penetration increases. The effect is maximized at the Peak PV time of day. The explanation of this observation is easily understood by observing the how the LDC controller operates.

Figure 60 is a model of an LTC with a LDC controller. The basic operating principle of the LDC controller is to maintain voltage at the load center (V_{LC}) as constant by adjusting the sub-station voltage up and down: more line drop equates to a higher sub-station operating voltage. To approximate the line drop between the sub-station and V_{LC}, the LDC uses a measurement of line current at the sub-station. Line drop is calculated using an estimate of the line impedance (R and X) between the sub-station and the load center. Line current is proportional to line drop: high current equates to more line drop than low current. The LTC is a mechanical device and the current changes very dynamically during day, so the LDC controller operates as a dead-band controller. Using the current measurement, an ideal operating voltage (V_{LC} plus the line drop) is found, but the LDC will not initiate the LTC to change tap position unless the measured voltage is outside the bandwidth (BW) of the ideal voltage. The LDC dead-band controller is described by equation 5-84.

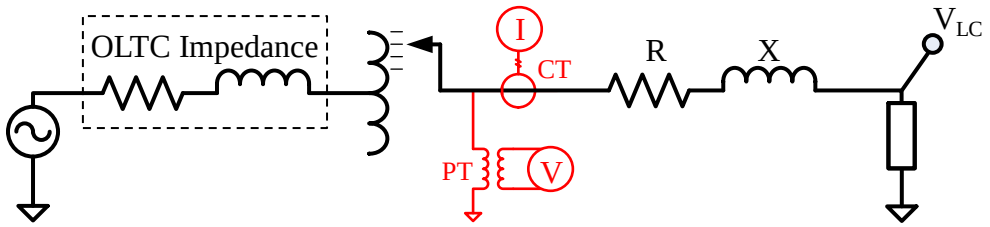

Figure 60. Load Tap Changer Transformer with Load Drop Compensation Model

$$\begin{cases} \frac{V}{PT} > V_{LC} + \frac{I}{CT}(R + jX) + \frac{BW}{2} & \rightarrow \quad Increase\ Tap \\ \frac{V}{PT} < V_{LC} + \frac{I}{CT}(R + jX) - \frac{BW}{2} & \rightarrow \quad Decrease\ Tap \\ otherwise & \rightarrow \quad Do\ Nothing \end{cases} \qquad \textbf{5-84}$$

Please see the detailed discussion of the LTC w/ LDC in section A *for a detailed description of LDC control variables*

$$I = I_{LD} - I_{PV} \qquad \textbf{5-85}$$

High-Pen PV influences the LDC controller through the sub-station current measurement (I/CT). As shown in equation 5-85, the sub-station line current (I) is a combination of the load demand current (I_{LD}) minus PV generation current (I_{PV}). Therefore as PV penetration increases, the sub-station line current decreases. As a result, the operating voltage band is lowered and the tap position is likely to decrease. Figure 61 is example of this behavior over the course of the day for the Menlo Beginning distribution scenario. As penetration increases, the sub-station current decreases, resulting in the LDC tapping the LTC down. This effect is maximized at the Peak PV time of day. In summary, as penetration increases, the LDC controller lowers the sub-station voltage via tapping position of the LTC.

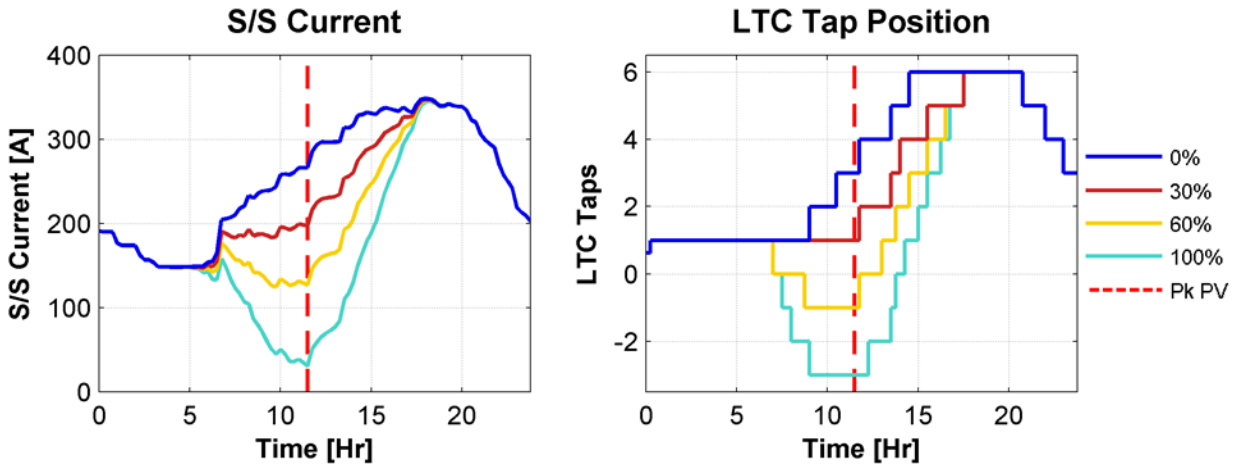

Figure 61. Measured sub-station current and LTC tap position versus time for a Menlo Beginning distribution scenario.

As the LDC lowers the sub-station voltage, the bus voltage at the end of the feeder is also lowered. Voltage rise induced by High-Pen PV could support the end bus voltage to prevent a low voltage condition, but is dependence on the location of the generation in terms of the sub-station and load. As discussed in the Generation Location Voltage Rise Characteristics section (5.2.1.3B.B.1), generation locations with higher cumulative line resistive impedance to the sub-station have more voltage rise than locations with lower resistive line impedance to the sub-station. Observing Table 39, we see for both the Cayetano and Menlo circuits, the distributions from lowest to highest line-impedance ($R_{S/S}$) values to the sub-station are the Beginning, Middle, and End distributions. Therefore, we expect the voltage rise to be greater for the End distribution than the Middle distribution and so on. The generation's location relative load demand is also an important factor in understanding the amount of DG induced voltage rise to expect.

Circuit	**PV distr.**	**$R_{S/S}$ [Ω]**	**LC/GC**	**RPF Penetration (%)**			
				Summer High	*Summer Low*	*Winter High*	*Winter Low*
Cayetano	Beginning	0.16	6.5	129	23.7	95.8	39.3
	Middle	0.48	1.6	14.2	3.6	10.5	4.3
	Ending	1.42	0.85	10.9	2.7	8	3.3
Menlo	Beginning	0.07	5.25	59.8	45.7	-	-
	Middle	0.52	0.95	25.7	19.6	-	-
	Ending	4.8	0.42	1.7	1.1	-	-

Table 39. The LC/GC ratio and RPF penetration for all Cayetano and Menlo simulation scenarios.

In the Reverse Power Flow Voltage Rise section (A.1), this relationship is described using the LC/GC ratio and a DG buses RPF penetration. DG buses with a lower LC/GC ratio expect to see a lower RPF penetration than buses with a higher LC/GC ratio. A bus with a lower RPF penetration will have more voltage rise than a bus with a higher RPF penetration. Observing Table 39, we can see for all the Cayetano's and Menlo's characteristic days, the rank of the distributions with the highest LC/GC ration and RPF penetrations is the Beginning, than Middle, and finally Ending distribution. Again, we expect the voltage rise to be greater for the End distribution than the Middle distribution and so on. In

observation of the relationship of DG location to both the sub-station and load demand, we see that the Beginning distribution will have the least amount of induced voltage rise followed by the Middle distribution and then the End distribution. Therefore, as the LDC is lowering the system voltage we expect the Beginning distributions to be more at risk to an out-of-standard low voltage condition than End distributions due to a lack of DG induced voltage rise.

In Figure 62, the bus voltage with and without LDC controller is illustrated for a Summer High day at 100% penetration for the Cayetano and Menlo circuits. Observing the bus voltage profiles with the LDC contribution removed, we can see the amount of voltage rise at the end of the bus from largest to smallest is the 1) End distribution, than 2) the Middle, and finally 3) the Beginning distribution. Now observing the voltage profiles with the LDC contribution, we see a lower bus voltage profile in all generation scenarios. Potential low voltage condition are at a higher risk is the LDC voltage decrease is greater than the amount of voltage rise induced by High-Pen PV. This potential condition is evident for the Cayetano Beginning and Middle distribution scenarios in comparison to the baseline, but the Menlo Beginning distribution condition is only actual low voltage condition in the example below.

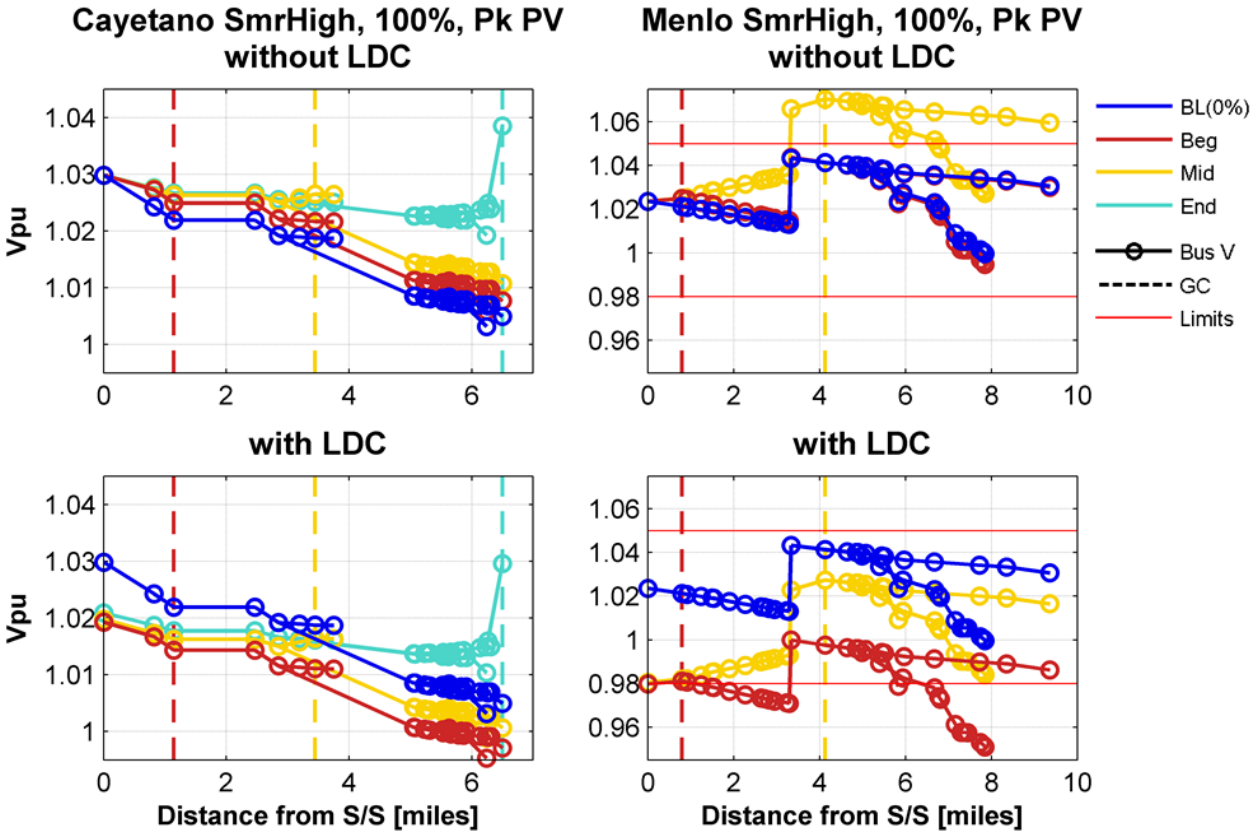

Figure 62. Bus voltage (at Peak PV) versus distance with and without the tapping caused by LDC control for the Cayetano and Menlo Summer High 100% scenario.

Figure 63 is the voltage differenc from the baseline of the lowest bus voltage over the range of simulated PV penetrations with and without the LDC. Distributions with and LC/GC ratio greater than 1 (LC/GC > 1) trend to decrease in the bus voltage from the base line as penetrations increase.

Distribution scenarios with an LC/GC ratio less than or equal to 1 (LC/GC ≤ 1) do not decrease in bus voltage. Using the LC/GC ratio, LTC w/ LDC could potentially cause a low voltage condition at elevated PV penetrations if the LC/GC > 1.

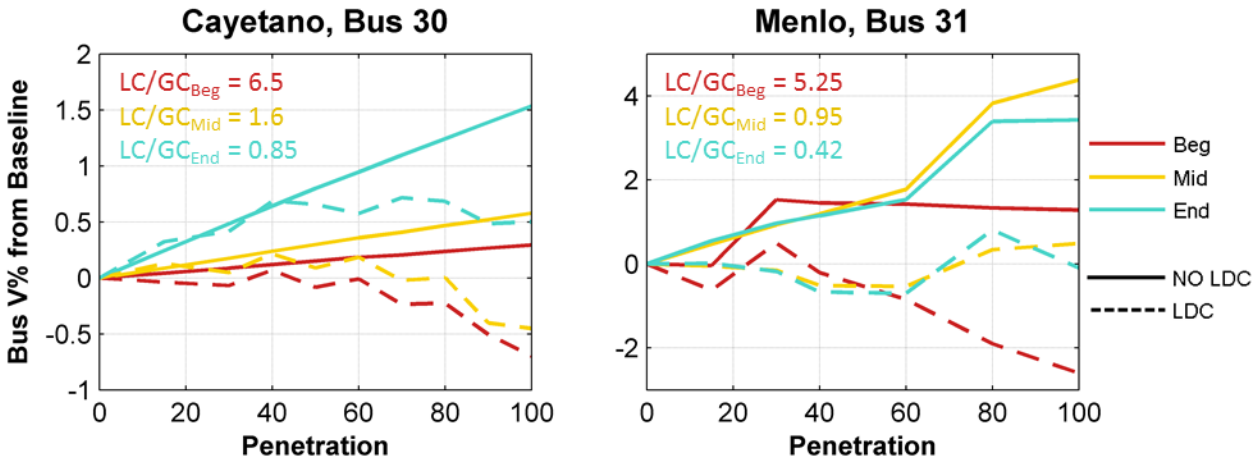

Figure 63. The percentage voltage change from baseline (0%) versus time for the lowest voltage bus for the Cayetano and Menlo circuits.

Up to this point, the point of discussion has focused on influence of High-Pen PV on the LDC controller causing a decrease in system voltage, but not on the specific scenarios with low voltage conditions. As detailed above, the LDC controller lowers the sub-station LTC tap lowering the system voltage, but only the Menlo Beginning distribution scenario experienced low voltage. Figure 64 is the bus line impedance to the sub-stataion for both branches of the Menlo circuit. The lowest voltage bus (bus 31) indicated by a vertical red dashed line in the figure. As discussed in Residential Circuit (Menlo) section (5.1.1.2), the Menlo circuit services a 4.16kV section via a 12kV to 4.16kV step-down transformer. A load operating in a lower voltage system will draw proportionally higher amounts of current and thusly will incur more line drop. The equivalent impedance of the 4.16kV section in a 12kV base increases the impedance by a factor of nine. Even without the sub-station LTC w/ LDC lowering the voltage, this section of line already experienced a signficant amount of volage drop. This low voltage condition in this section could be solved by 1) changing the effective line impedance by modifying the operating voltage from 4.16kV to 12kV; 2) install a Voltage Regulator to maintain the voltage independent of the sub-station; or 3) modify the LDC controller to simply not tap down for this scenario.

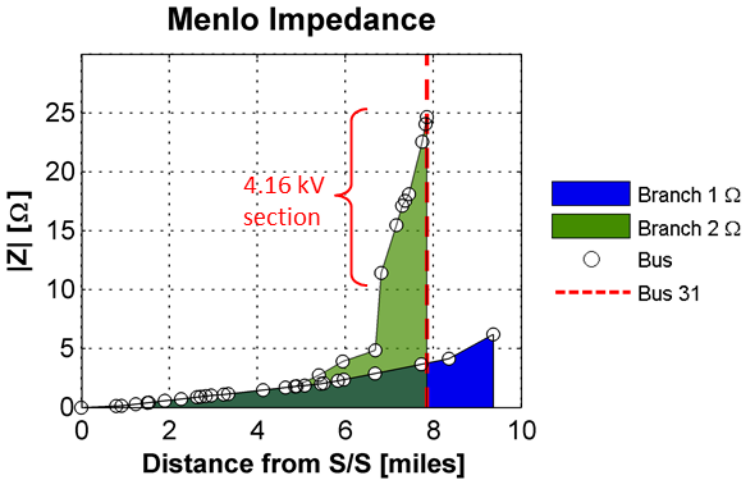

Figure 64. The cumulative impedance magnitude of the Menlo circuit. Bus 31 is the end bus of the branch that experienced low voltage condition for Menlo Beginning distributions scenarios.

In summary, distributions with an LTC w/ LDC and a generation center upstream of the load center (LC/GC > 1) have the potential of a low voltage condition at elevated levels of PV penetration. This is the case of the Menlo Beginning distribution with penetrations greater than 40%, but the high line impedance section at the end of the circuit aggravated the situation. From the scenario observations, the LTC w/ LDC interaction with High-Pen PV is a potential low voltage concern when LC/GC is greater than one (LC/GC > 1), but not when LC /GC is less than or equal to one (LC/GC ≤ 1). Low voltage conditions caused by High-Pen PV are easily remedied via adjusting the line impedance, a Voltage Regulator, or modifying the LDC controls.

5.2.2.2 Voltage control equipment

The voltage control (regulation) equipment found on the Cayetano and Menlo circuits include switched capacitor banks and the Load Tap Changing transformer with Load Drop Compensation (LTC w/ LDC) control. The observed effects from varying penetration and spatial distribution of High-Pen PV on voltage control equipment found in the Cayetano and Menlo circuits are presented for 1) switching capacitors and 2) the LTC w/ LDC.

A. Voltage Control Equipment Results - Capacitor

The types of controls featured in the Cayetano and Menlo circuits include Time-Clock (TC), Temperature (Temp), TC with Voltage Override (VO), and Temp with VO, as shown in Table 40 and Table 41. The TC and Temp switching controls do not use feedback influenced by High-Pen PV, but VO switching controls do. VO controls operated with a high voltage threshold and low voltage threshold; if the voltage goes above the high voltage threshold the VO control switches the capacitor off and if the voltage goes below the low voltage threshold, the VO controls switches the bank on. As described above, High-Pen PV influences voltage in two ways: a high voltage condition from Distributed Generation induced voltage rise and low voltage condition caused by the LDC.

Bus	NP [MVAR]	Smr High	Smr Low	Wtr High	Wtr Low
4	1.8	Temp	Temp	Off	Off
10	1.2	Temp	Temp	Off	Off
15	1.2	Temp	Temp	Temp	Temp
20	1.2	TC w/ VO	TC w/ VO	TC w/ VO	TC w/ VO
21	1.2	TC w/ VO	TC w/ VO	TC w/ VO	TC w/ VO
22	1.2	TC	TC	TC	TC
30	1.8	Temp w/ VO	Temp w/ VO	Off	Off

Table 40. Cayetano Capacitor Controls.

Bus	NP [MVAR]	Smr High	Smr Low
5	0.6	On	On
10	0.9	TC w/ VO	TC w/ VO
13	0.6	TC w/ VO	TC w/ VO
27	0.3	Off	Off
30	0.3	TC w/ VO	TC w/ VO
40	0.9	TC w/ VO	TC w/ VO

Table 41. Menlo Capacitor Controls.

Table 42 is the average of the total capacitor switching event differential from the baseline (0%) in the PV region for all the characteristic days. A switching event in this context is when the capacitor switches from either on to off or off to on. The Cayetano featured only a marginal change from baseline for Beginning 100% and Radial 70%. The Menlo averaged a switching event differential for penetration greater than 15% for the Beginning distribution and for penetration greater than 40% for the Middle and End distributions.

Circuit	Distr.	Average Capacitor Switching Events Difference From Baseline									
		0%	*15%*	*30%*	*40%*	*50%*	*60%*	*70%*	*80%*	*90%*	*100%*
Cayetano	Beginning	0	0	0	0	0	0	0	0	0	0.5
	Middle	0	0	0	0	0	0	0	0	0	0
	End	0	0	0	0	0	0	0	0	0	0
	Radial	0	0	0	0	0	0	0.25	0	0	0
Menlo	Beginning	0	1	1	1	-	1	-	1	-	1
	Middle	0	0	0	1	-	1	-	1	-	1
	End	0	0	0	1	-	1	-	1	-	1
	Radial	0	0	0	0	-	0	-	0	-	0

Table 42. Average characteristic day capacitor switching event difference from baseline (0%) in PV region.

The capacitor switching profile changed on the Cayetano on two specific instances. The first instance was the capacitor bank at bus 20 during the Cayetano Summer Low day for a Beginning distribution and 100% penetration scenario. The bus 20 capacitor features Time-Clock with Voltage Override controls and the event was a low voltage event that occurred from 12:00 to 13:00. The second instance was occurred during the Cayetano Winter High with a Radial distribution at 70% penetration scenario for the bus 21 capacitor. The bus 21 capacitor has TC with VO controls as well, but the TC controls setting are set to turn on the bank at night and off during the day. In the baseline case, the bank would not turn off however in the morning due to the VO controls holding the bank on. The capacitor bank voltage was not greater than the low voltage threshold plus overhead. In this particular instance, the voltage did increase beyond the low voltage plus overhead threshold resulting in the bank switching off. These instances only occurred under very specific circumstances and did not demonstrate a noticeable trend as penetration increases.

The capacitor switching profile for the Menlo circuit did consistently change as penetration increased, but only for the bus 30 capacitor installation. The bus 30 capacitor featured TC with VO control and is situated at the end of the Menlo circuit in the 4.16kV section of line. Observing Figure 65, we can see that the bus 30 capacitor bank switching on during the PV region for longer periods of time as penetration increased. As noted above, the bus 30 capacitor bank is located in the 4.16kV section of line, resulting in high line impedance and significant voltage drop. As discussed in the Low Voltage results section (B) above, as penetration increases, the Load Tap Changer with Load Drop Compensation (LTC w/ LDC) at the sub-station would tap down resulting in low voltages for 4.16kV section of the circuit. The bus 30 capacitor bank would respond accordingly by banking on during these low voltage condition. As a result, as penetration increases the bus 30 capacitor switch on, but in response to the low voltage sceneario created by the operation of the LTC w/ LDC.

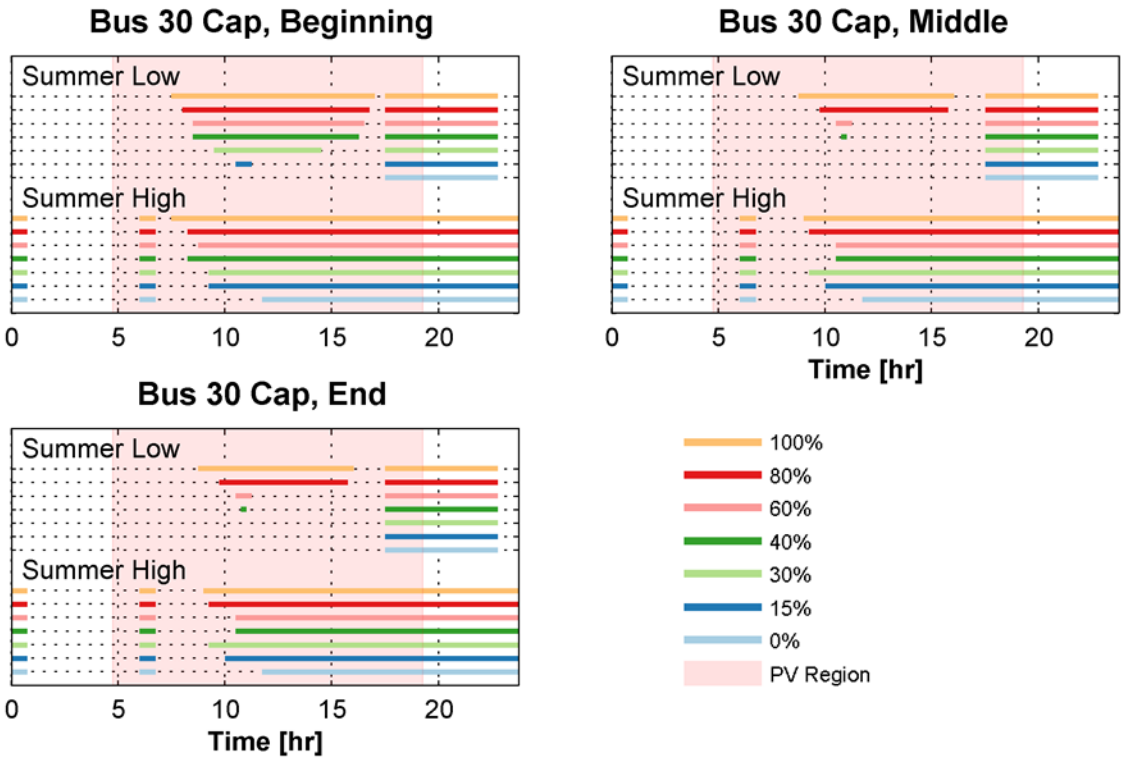

Figure 65. Menlo Bus 30 Time-Clock with Voltage Override control On/Off state.

In summary, the Cayetano and Menlo only experienced a marginal increase in capacitor switching during the PV region as penetration increased. The Cayetano experienced only two instances when the capacitor operation profile changed, but did not show a specific trend as PV penetration increased. The Menlo circuit featured a capacitor bank at the end of the feeder that did bank on for long periods of time during the PV region as penetration increased, but because of the operation of the sub-station LTC w/ LDC. Of the capacitor control observed, only the Voltage Override (VO) controls are influenced by High-Pen PV since the feedback is voltage. Time-Clock and Temperature based controls do utilize feedback (time and temperature) that is directly influenced by PV generation and therefore will not change as PV penetration increases. This study only observed the capacitor switching using an ideal steady-state PV profile and does not speak to scenarios with highly variable solar profiles.

B. Voltage Control Equipment Results - Sub-station Load Tap Changer with Load Drop Compensation (LTC w/ LDC)

Observing Figure 59 in the Low Voltage results section (B), the sub-station Load Tap Changer with Load Drop Compensation (LTC w/ LDC) tends to tap down at Peak PV generation. As penetration increased, the amount of down tapping from baseline would increase. This result was observed for all the spatial generation distributions with marginal differences. Given that the LTC w/ LDC tends to tap down at Peak PV as penetration increases, does this imply that total number of tap position changes during the day would also increase?

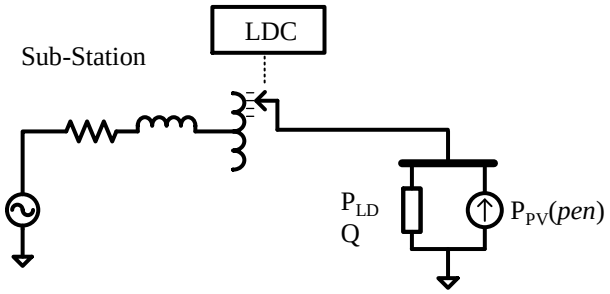

Figure 66. LTC w/ LDC Tap Evaluation Model Diagram.

Parameter	Cayetano	Menlo
Voltage (kV_{L-L}]	21	12.47
Nameplate [MVA]	27	16
Impedace [Ω%]	j0.09	j0.08
Regulation [%]	±10	±10
Steps	32	32
V_{LC} [V_{120}]	122	117
R [Ω]	4	1.875
X [Ω]	0	0
Band [V_{120}]	±1	±1.4
CT ratio	1300:1	800:5
PT ratio	100:1	60:1

Table 43. Cayetano and Menlo settings for LTC w/ LDC Tap Evaluation Model.

To evaluate this question, a simplified circuit model, shown in Figure 66, of the Cayetano and Menlo was created to evaluate the LTC w/ LDC for the entire year and not just on the characteristic days. The inputs of the model includes the time resolved circuit load demand (P_{LD}), the sub-station reactive power measurement (Q), and the PV generation (P_{PV}). The total capacity changes as a function of penetration (pen). The settings the LDC controller for the Cayetano and Menlo circuits is shown in Table 43.

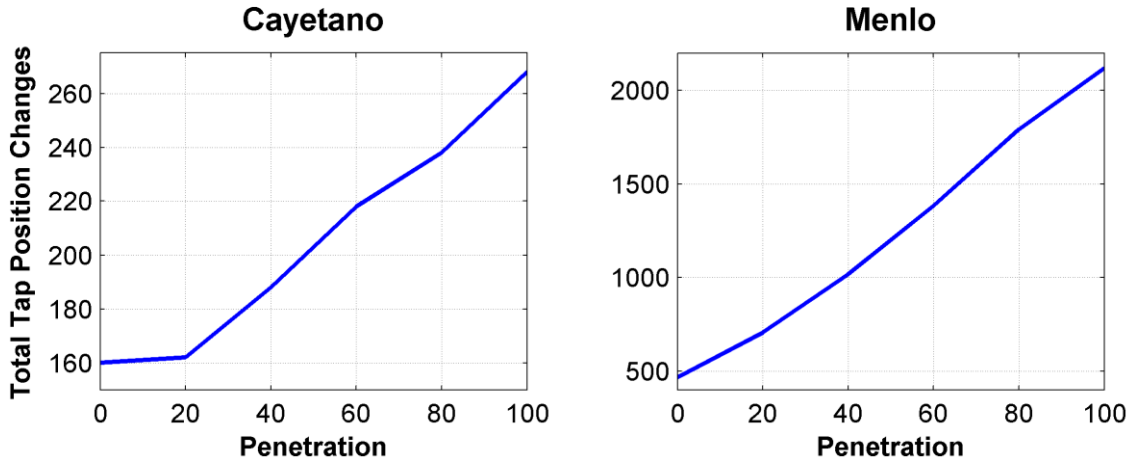

Figure 67. Total yearly tap position changes for the Cayetano and Menlo circuits versus penetration.

Observing Figure 67, both the Cayetano and Menlo approximately increase linearly with penetration. The LTC yearly tap increase per penetration rate is 0.1 taps/pen for 0% to 20% and then 1.3 taps/pen between 20% to 100%. The low rate of increases between 0% and 20% is because PV penetration has not increases to a point to cause the LDC to tap down from its current position. An example is shown with the Cayetano Summer High day in Figure 68 and Table 44; the total daily tap changes did not increase until penetration 60% and greater in this example. For the Menlo circuit taps changes increased at an approximate rate of 16.54 taps/pen over the entire domain of penetrations.

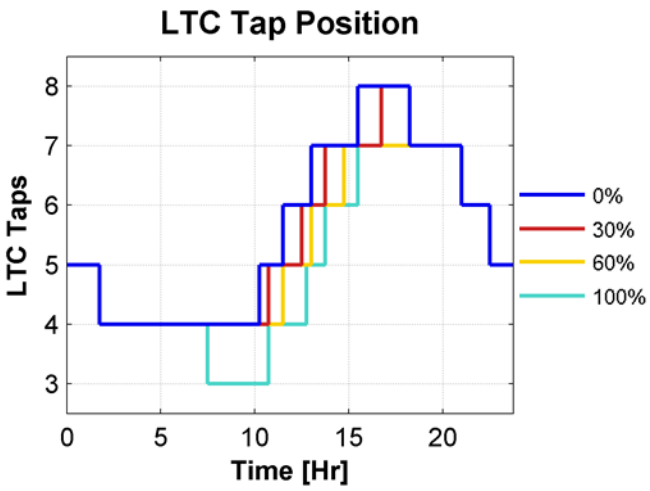

Figure 68. Cayetano Summer High LTC tap position versus time.

Penetration	Total Taps
0%	8
30%	8
60%	10
100%	12

Table 44. Total tap changes during the Cayetano Summer High day.

It is important to note why the total number of LTC tap position changes is greater for the Menlo than the Cayetano. The LDC controller of the LTC derives the ideal operating voltage via local current measurement at the sub-station, so characteristics affecting the amount and range of sub-station current will affect the LDC controller. The Cayetano operates at 21kV while the Menlo operates at 12.47kV, so the current draw through the sub-station is greater for the Menlo than the Cayetano for the same amount of load demand. To compound this issue, the LDC current transformer (CT) ratio is greater for the Cayetano than the Menlo. As a result, the measured current (I_m) the LDC reads is greater for the Menlo than the Cayetano for the same amount of current, as shown with equation 5-86. Between the operation voltage and the CT ratio selection, the Menlo is expected to feature more tap position changes than the Cayetano, as observed in Figure 67.

$$I_m = \frac{I}{CT} \qquad 5\text{-}86$$

In summary, increased PV penetration resulted in an increase in total yearly tap changes for the Cayetano and Menlo circuits. Due to the operation settings of the LDC controller, the Menlo circuit experienced a faster increase in total taps over the year than Cayetano circuit.

5.2.2.3 Sub-Station Power Factor

The sub-station real (P) and reactive (Q) power is a net of the circuit load demand and generation, as shown in equations 5-87 and 5-88. In the Cayetano and Menlo circuits, the only form of generation includes PV (P_{PV}) and switched capacitor banks (Q_{CAP}). The power factor (PF) is a ratio that indicates amount real power to total power, as defined in equation 5-89. The sub-station power factor, in California, is regulated by at the high-side of the transformer to be 0.99 leading ($Q < 0$) to 0.97 lagging ($Q > 0$) by the California Independent System Operator (CAISO), and executed by PG&E for the Cayetano and Menlo circuits [19, p. 8]. Please note that the power factor equation does not differentiate between lagging and leading, so in this research a leading power is negative ($Q < 0 \rightarrow PF < 0$) and lagging

is a positive power factor ((Q > 0 → PF > 0). Using this context, the terminology "decreasing power factor" means the absolute value of the power factor is decreasing (|PF| → 0).

$$P = P_{LD} + P_{Loss} - P_{PV} \quad \text{5-87}$$

$$Q = Q_{LD} + Q_{Loss} - Q_{CAP} \quad \text{5-88}$$

$$PF = \begin{cases} \dfrac{|P|}{\sqrt{P^2 + Q^2}}, & Q \geq 0 \ \ Lagging \\ \dfrac{-|P|}{\sqrt{P^2 + Q^2}}, & Q < 0 \ \ Leading \end{cases} \quad \text{5-89}$$

As discussed before, PV installation primarily generate real power due to IEEE 1547 standard prohibiting distributed generation from regulating its bus voltage and therefore de-incentivizing a DG installation to operate below unity power factor. As PV penetration increases, the net amount of sub-station power will decrease: this effect is maximized at the Peak PV time of day. Since the High-Pen PV is providing real power support but not reactive power, we should expect to see the sub-station power factor decrease with penetration. An example is illustrated in Figure 69 for the Menlo Summer Low baseline (0%) and 60% penetration scenarios. As the penetration increases, the sub-station real power profile changes dramatically, while the reactive power profile marginally changes. The result is a decrease in the power factor in the PV region with the effect maximized at the Peak PV time of day (12:00pm).

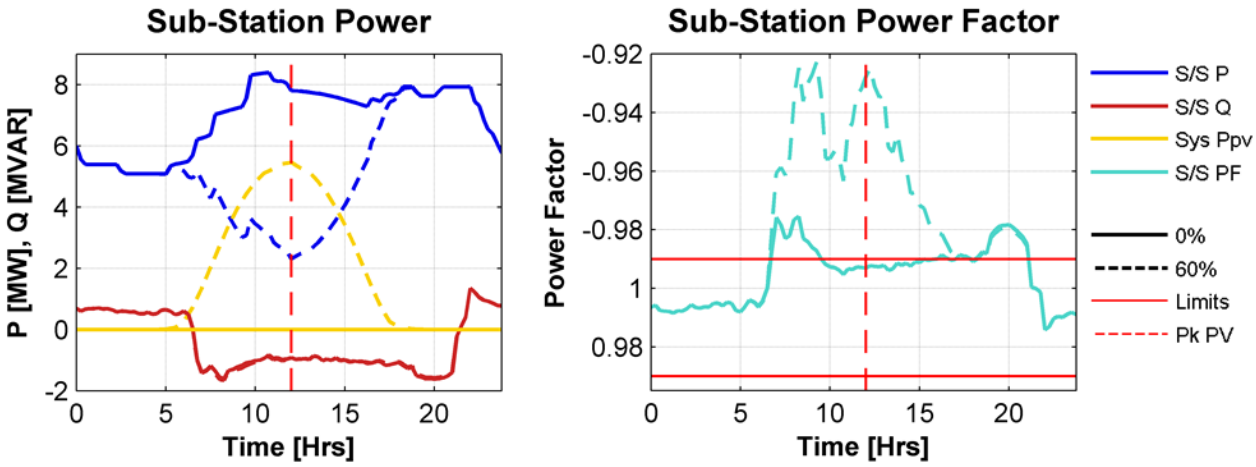

Figure 69. The net sub-station real and reactive power and total system PV generation versus time (left) and sub-station power factor versus time for a Menlo Summer Low day.

Figure 70 is the power factor at the Peak PV time of day for the Cayetano and Menlo for penetrations ranging from 0% to 100%. From observing the plot, we can see the sub-station power factor for characteristic High days change by a marginal amount, but the characteristic low days decrease to a minimum point then increases back to unity.

By observing the difference between a High and Low day load demand, we can understand the power factor profiles are different. A characteristic High day is an above (seasonal) average load demand day while a Low day is a below (seasonal) average day, as discussed in the Day Selection section (D). Therefore a characteristic High day has a larger load demand (P_{LD}) profile than a characteristic Low day. For a given amount PV generation (P_{PV}), the High day will have a greater net sub-station power (P) than the Low day. As a result, the power factor is greater for a High day than a Low day for the same amount of generation present.

The characteristic Low days is shown to have minimum penetration point. This minimum point is approximately the penetration where the circuit is beginning to export power through the sub-station via reverse power flow. In terms of equation 5-89, the net power at the sub-station is negative ($P < 0$). Penetrations past this minimum will increase the magnitude of the sub-station power ($|P|$), which in-turn increase the power factor back towards unity. The characteristic High days will also show this behavior, but higher penetration given the larger load demand.

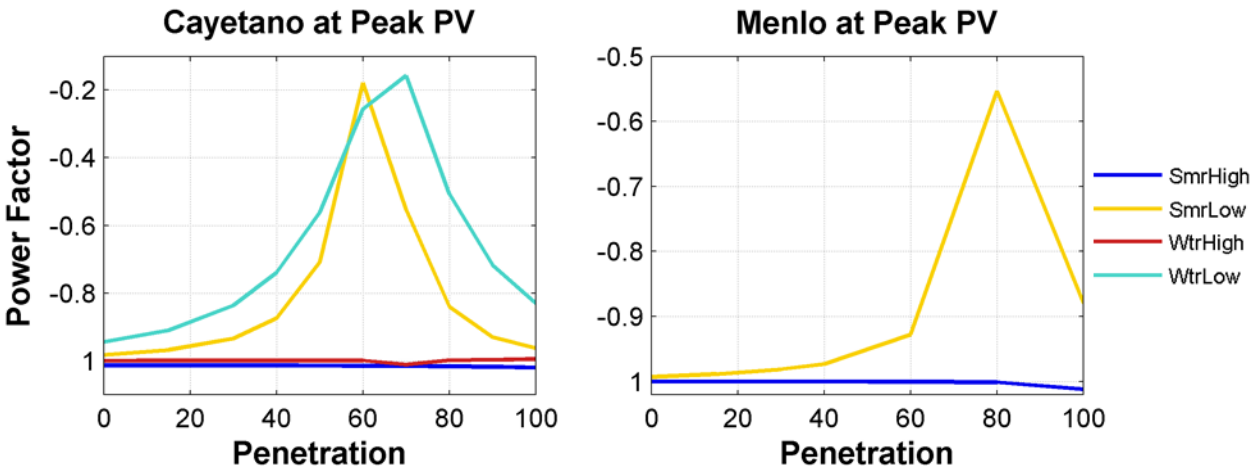

Figure 70. The sub-station power factor at the Peak PV time of day versus penetration for the Cayetano and Menlo Radial scenarios.

In the PV region, any non-unity power factor is aggravated by increased penetrations of PV. Reactive power support is effectively provided by very large switched capacitor banks. The decrease in power factor is not a concern from a transmission standpoint, but may indicate that unneeded reactive support is switching on during characteristic Low days. Switching controls that do not rely on system feedback of voltage, power, or power factor will likely switch regardless of circuit's needs. Time based controls are an example of such controls. Figure 71 is the real and reactive power and power factor profile of a Cayetano Summer Low day at 0% and 30% penetrations. At approximately 6:45am, a Time-Clock control switching capacitor banks on even though the sub-station power is already at unity. At 30% penetration, the power factor at Peak PV decreased from a leading 0.98 to a leading 0.92. Using a switching control that sensed the current state of the system would avoid needless switching event.

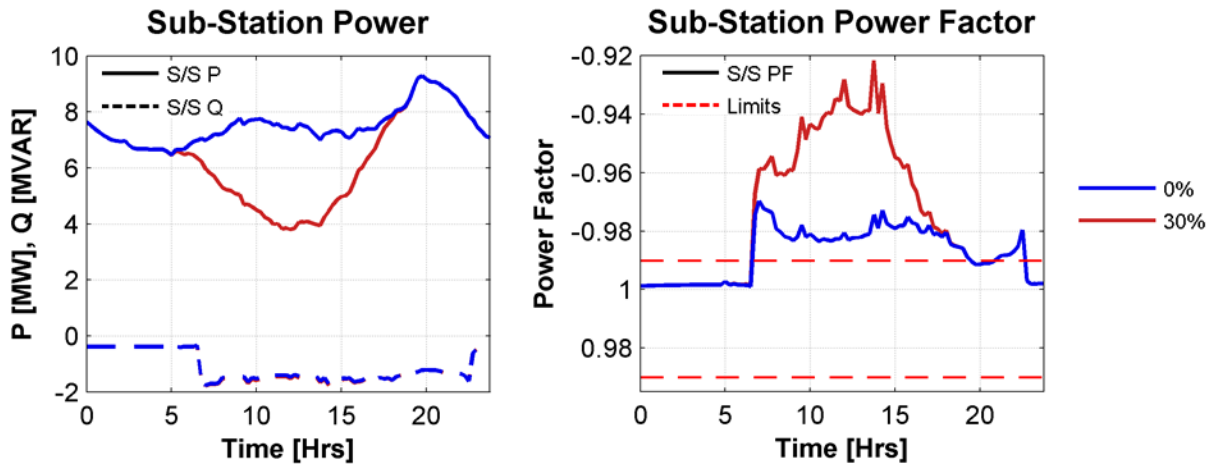

Figure 71. The net sub-station real and reactive power versus time (left) and sub-station power factor versus time for a Cayetano Summer Low day.

In typical distribution circuits, the sub-station power factor is preferred operate at unity power factor to decrease line-losses and release line capacity [1, Ch. 2.3] with the assumption normal power flow. With High-Pen PV, an expectation of unity at the sub-station will be difficult. On characteristic Low days, the power factor will decrease during normal operation ($P > 0$) as penetration increases. The power factor will continue to decrease until the point of export ($P < 0$), at which the power factor will now increase towards unity as penetration increases. For High load demand days, the effect is marginal. Unnecessary capacitor switching on characteristic Low load demand days will further decrease power factor in the PV region as well and may consider exchanging a switching control that responds to the circuits, such as VAR switching controls. In all, the decrease in power factor cause by High-Pen PV does not appear to be a critical issue apart that the power factor is beyond the regulated bounds (0.97 lagging to 0.99 leading) set by CAISO. For circuits with High-Pen PV, these power factor restrictions may be an unnecessary road block to increased PV penetration.

5.2.2.4 System Loss

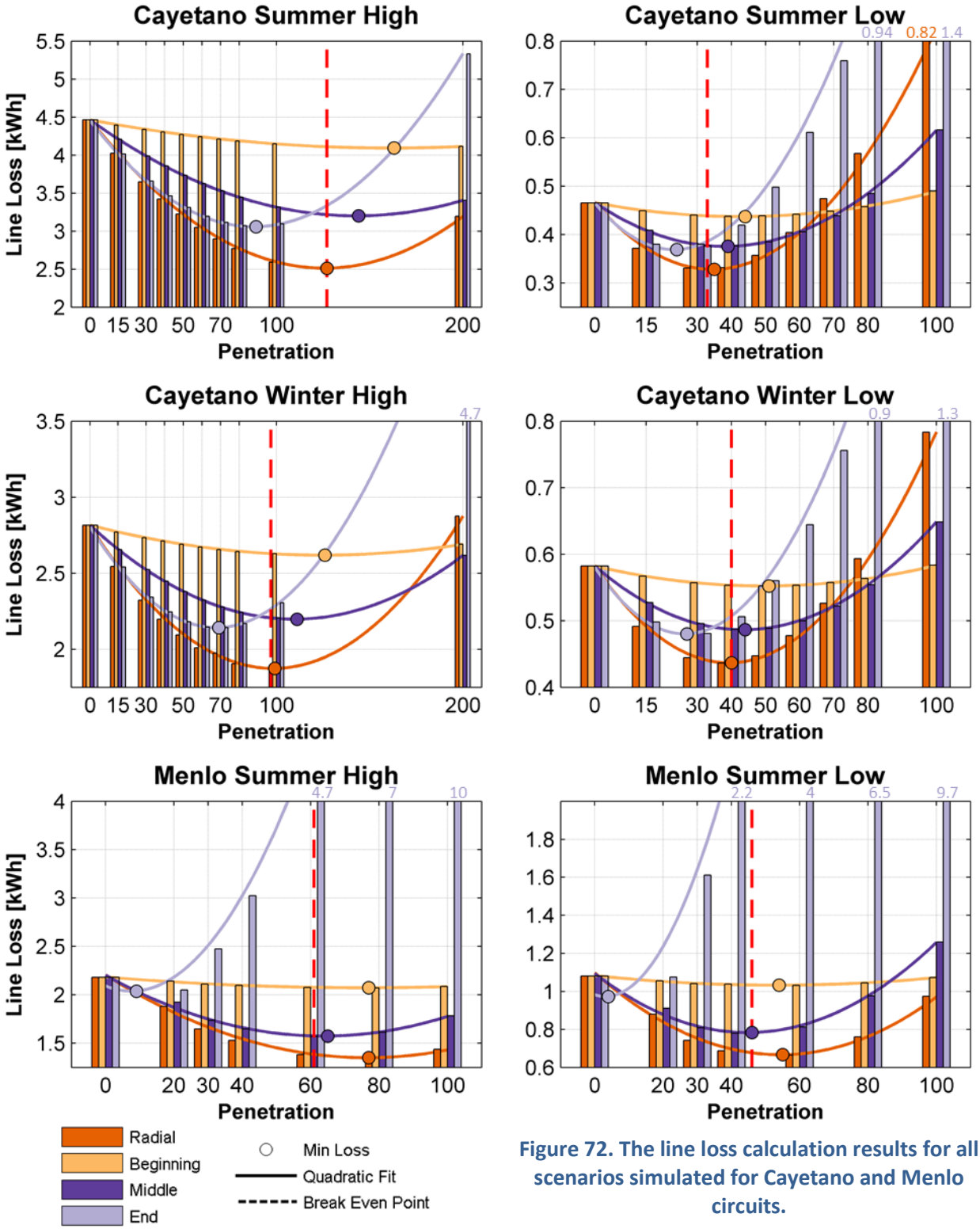

Figure 72. The line loss calculation results for all scenarios simulated for Cayetano and Menlo circuits.

Using the line loss analysis methodology presented in the Line Loss section (5.2.1.4), the total line loss energy was calculate for all the simulated scenarios for the Cayetano and Menlo circuits, as shown in Figure 72. As discussed in the line loss analysis introduction, we expect the line loss to behave as quadratic function of PV penetration, as observed above. Using the simulation results for each characteristic day and generation distribution scenario, the line loss, as a function of penetration, is estimated using a quadratic fit (in a least squares sense). The estimated line loss is plotted as line in Figure 72. From the estimated line loss function, a minimum penetration is identified. This minimum penetration is referred to as the minimum loss penetration.

From the line loss analysis discussion (section 5.2.1.4), we expect to observe the following: 1) the minimum loss penetration and 2) the line loss at the minimum penetration will vary dependent on 1) the relationship of the load and generation distribution and 2) the energy of the load demand. These expectations of the line loss results presented in Figure 72 are evaluated in the proceeding analysis.

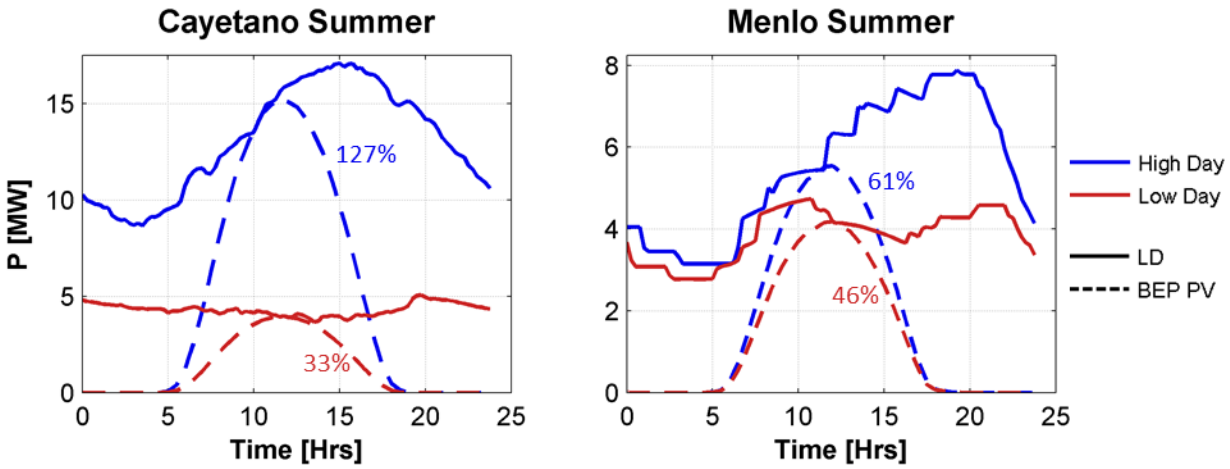

Figure 73. Break-Even Point penetration estimates for Cayetano and Menlo Summer days.

Above, the process of deriving the minimum loss penetration is through approximating the line loss function using simulation results of multiple penetration scenarios. An alternative way to estimate the minimum loss penetration is by finding the PV penetration (using an ideal PV curve) that meets the system load demand for a single point of time during the day. This penetration is referred to as the Break-Even Point (BEP) in this analysis. Figure 73 illustrates the BEP calculated for the Cayetano and Menlo Summer High and Low days. Observing Table 45, we can see that as LC/GC approaches one (LC/GC → 1), the BEP error from the minimum loss penetration decreases. Of all the Cayetano days, the Radial distribution has the closest LC/GC ratio to one (0.9) with the lowest BEP error of 6% from the minimum line loss penetration. Likewise, the Menlo Middle distributions had the closest LC/GC ratios to unity (0.95) and the lowest BEP error of 6.5% from the minimum loss penetration. Therefore, for circuits with generation centers co-located with the load centers (LC/GC ≈ 1), the BEP is a viable estimate of the minimum loss penetration.

Day	LC (σ_{LC})	BEP [%]	Day LD [MWhr]	Distr	GC (σ_{GC})	LC/GC	RPF pen [%]	Min Loss Pen [%]	Line Loss [MWhr]
Cayetano Summer High	0.85 (0.13)	127	313	Beg	0.13 (0)	6.5	129	163	4.1
				Mid	0.53 (0)	1.6	14.2	144	3.2
				End	1.0 (0)	0.85	10.9	89	3.1
				Rad	0.94 (0.09)	0.9	20.9	127	2.5
Cayetano Summer Low	0.85 (0.13)	33	103	Beg	0.13 (0)	6.5	23.7	44	0.44
				Mid	0.53 (0)	1.6	3.6	39	0.38
				End	1.0 (0)	0.85	2.7	24	0.37
				Rad	0.94 (0.09)	0.9	5.1	35	0.33
Cayetano Winter High	0.85 (0.13)	97	254	Beg	0.13 (0)	6.5	95.8	126	2.6
				Mid	0.53 (0)	1.6	10.5	111	2.2
				End	1.0 (0)	0.85	8	69	2.1
				Rad	0.94 (0.09)	0.9	15.2	99	1.9
Cayetano Winter Low	0.85 (0.13)	40	111	Beg	0.13 (0)	6.5	39.3	51	0.55
				Mid	0.53 (0)	1.6	4.3	44	0.49
				End	1.0 (0)	0.85	3.3	27	0.48
				Rad	0.94 (0.09)	0.9	6.1	40	0.44
Menlo Summer High	0.42 (0.23)	61	229	Beg	0.08 (0)	5.25	59.8	77	2.1
				Mid	0.44 (0)	0.95	25.7	65	1.6
				End	1.0 (0)	0.42	1.7	9	2
				Rad	0.47 (0.17)	0.89	131.8	77	1.35
Menlo Summer Low	0.42 (0.23)	46	165	Beg	0.08 (0)	5.25	45.7	55	1
				Mid	0.44 (0)	0.95	19.6	46	0.78
				End	1.0 (0)	0.42	1.1	4	0.97
				Rad	0.47 (0.17)	0.89	86.5	55	0.67

Table 45. Tabulated load, generation, and line loss characteristics for Cayetano and Menlo characteristic day and generation distribution scenarios.

As observed in Figure 72, a minimum loss penetration exists, but why? As discussed in the Line Loss section (5.2.1.4), the minimum loss penetration is related to reverse power flow (RPF). As the PV penetration increases towards the minimum loss penetration, the line loss decreases due the voltage rise from line drop reduction. As penetration increases past the minimum loss penetration, the line losses increase due the RPF induced voltage rise. Observing Table 45, the RPF penetration is less than the minimum loss penetration for all scenarios. Recalling the definition, RPF penetration is the penetration point at which the DG sites local and downstream load demand is met with PV generation capacity; any penetration beyond the RPF penetration will induce RPF. RPF penetration calculated in Table 45 is for the largest DG site in the distribution scenario at the Peak PV time of day. By the minimum loss penetration being significantly greater than the RPF penetration indicates that a significant amount of RPF is occurring at the minimum loss penetration. Therefore, RPF is the dominant cause of voltage rise for penetrations larger than the minimum loss penetration and the cause of increased line losses.

Also observed in in Figure 72, the ascending order of the point generation distributions minimum loss penetration is 1) End, 2) Middle, and then 3) Beginning. This is observed in all the characteristics days, but why. The reason is the relationship between the load and generation distributions, which is described using the LC/GC ratio. As noted before, RPF penetration is related to the minimum loss penetration. From RPF Voltage Rise Characteristics section (B.1), as LC/GC ratio tends to zeros (LC/GC →

0), the RPF penetration decreases; likewise, as LC/GC grows large (LC/GC → ∞), the RPF penetration increases. The minimum loss penetration indicates the point where RPF becomes dominant, so it is expected that circuits with a large RPF penetration will have a larger minimum loss penetration. Therefore, Circuits with a smaller LC/GC ratio tend to have generation located at the end of the circuit and a lower minimum loss penetration, while circuits with a larger LC/GC ratio tend to have generation at the beginning of the circuit and a higher minimum loss penetration. Observing Table 45, we can see that the ascending rank of the point generation distributions LC/GC ratio is 1) End, 2) Middle, and then 3) Beginning; the same as observed for the minimum loss penetration. In short, circuits with a large LC/GC ratio will have a higher minimum loss penetration than circuits with a LC/GC ratio.

In terms of overall lowest line loss at the minimum loss penetration, generation distributions with a GC closer the LC (LC/GC → 1) featured lower line losses at the minimum loss penetration than distributions with generation located away from the load. Again observing Table 45 for the point generation profiles ($\sigma_{GC} = 0$), both the Cayetano End (LC/GC = 0.85) and Menlo Middle (LC/GC = 0.95) distributions achieved the lowest line loss at the minimum loss penetration and both are sited the closest to the LC in their respective circuits. This confirms the common sense notion that generation located closer to the load will achieve less line losses that generation located farther from the load.

Currently, only point generation distributions ($\sigma_{GC} = 0$) have been addressed, but how does the above discussion change when the generation is distributed ($\sigma_{GC} > 0$), but not point generation? In comparison of a distributed and point generations with similar GC, there are two differences: 1) the minimum loss penetration is greater for distributed generation and 2) the line loss is lower at the minimum penetration for distributed generation. The Radial distributions scenarios are truly distributed generation profiles. Given the generation is distributed over multiple buses; it is expected that RPF penetration of the largest DG site is higher than point distributions with a similar GC. This is observed in Table 45 when comparing the RPF penetration of the Cayetano Radial (GC = 0.94) scenarios to the Cayetano End (GC = 1) scenarios; in all cases, the RPF penetration is greater for the Radial distribution. This is also true when comparing the Menlo Radial (0.47) scenarios to the Menlo Middle (0.44) scenarios; the Radial distribution has a greater RPF penetration. Since the RPF penetration is greater, the minimum loss penetration is also greater, which is confirmed in Table 45. The Radial distributions also had the lowest overall line loss at the minimum loss penetration for both the Cayetano and Menlo, as shown in Table 45. This is an expected result given the discussion of the distributed versus point generation profiles in the Line Loss section (5.2.1.4).

$$LL_E(LD_E) = m \cdot \left(LD_E - LD_{E,LOW}\right) + LL_{E,LOW} \quad \textbf{5-90}$$

$$m = \frac{LL_{E,HIGH} - LL_{E,LOW}}{LD_{E,HIGH} - LD_{E,LOW}} \quad \textbf{5-91}$$

LL_E → Interpolated line loss of a typical day [Whr]
LD_E → The total load demand energy for a typical day [Whr]
$LL_{E,HIGH}$ → Line loss energy of a characteristic High day [Whr]
$LD_{E,HIGH}$ → Load demand energy of a characteristic High day [Whr]
$LL_{E,LOW}$ → Line loss energy of a characteristic High day [Whr]
$LD_{E,LOW}$ → Load demand energy of a characteristic Low day [Whr]

The final observation to make is the difference between character High and Low days. For a High day, the minimum loss penetration and overall line loss are greater than the simulated Low day, as shown in Table 45. This is an expected result since High days have greater load demand resulting more current in the distribution lines.

The above analysis focuses on the calculation of line loss for particular characteristic days, but this analysis may be expanded to provide a result considering the load demand for the entire year. Since the characteristic High and Low days were selected as statistically extreme days, it can assumed that days with an average load demand profile will incur line loss less than the High day, but more than the Low day. By using daily load demand energy, the line loss results of Figure 72 and Table 45 is interpolated for the entire year for both the Cayetano and Menlo using equations 5-90 and 5-91. The line loss results are interpolated for each distribution and penetration combination as a function of the load demand energy. The interpolated results are summed with its' respective distribution and penetration for the entire year. Then a line loss function is estimated using a quadratic fit. Finally, yearly minimum loss penetration, representing the entire year, is derived. The results of the described analysis are shown in Table 46. The yearly minimum loss penetration indicates the penetration that minimizes lines losses for the entire year, but the minimum loss penetrations of the High and Low days provide a better indication of RPF.

Circuit	**Year Min Loss Penetration (%)**			
	Beginning	*Middle*	*End*	*Radial*
Cayetano	71	66	41	61
Menlo	55	47	4	56

Table 46. Year Min Loss Penetration estimate for Cayetano and Menlo circuits via interpolation.

In summary, we observed from the simulated scenarios for the Cayetano and Menlo circuits that line loss behaves as quadratic function of penetration and therefore a minimum loss penetration exists. If the Load Center (LC) and Generation Center (GC) of the circuit are co-located, then this minimum loss penetration may be approximated using the Break-Even Point (BEP). As PV penetration increases towards the minimum loss penetration, then line loss will decrease as primary result of line drop reductions. As PV penetration increases past the minimum loss penetration, the line loss will increases from the line loss at the minimum loss penetration. This increase is attributed to dominant influence of reverse power flow.

The minimum loss penetration is also observed to be influenced by the relationship of load and generation distributions. Generation located upstream of the LC towards the sub-station ($LC/GC \rightarrow \infty$) will have a larger minimum loss penetration than generation located downstream of the LC at the end of circuit ($LC/GC \rightarrow 0$). Generation distribution profiles in proximity of the circuit load ($LC/GC \approx 1$) will have lower line loss at the minimum loss penetration than generation located farther away upstream ($LC/GC \rightarrow \infty$) or downstream ($LC/GC \rightarrow 0$). Distributed generation profiles ($\sigma_{GC} > 0$) are also observed to have higher minimum loss penetration and lower line loss at the minimum penetration than point distributions ($\sigma_{GC} = 0$) with similar Generation Centers.

Finally, using the line loss calculated for extreme characteristic days and the daily load demand energy, a yearly minimum loss penetration may be calculated for the entire circuit. The yearly minimum loss penetration takes into consideration the variety of load demand energy levels for the entire year to understand the potential line loss savings of a circuit's fixed PV penetration.

5.2.3 Summary

Identifying the operation limitations and characteristics of a commercial (Cayetano) and a residential (Menlo) circuit with High-Pen PV is the primary objective of this research. Each circuit was evaluated using a three phase balanced feeder model developed and calibrated using circuit description and measurement information. High-Pen PV was evaluated by varying PV generation on the circuit in penetration and distribution to evaluate 1) the primary feeder voltage profile, 2) the operation of voltage regulation equipment, 3) sub-station power factor, and 4) system line losses. The detailed results the evaluation on the Cayetano and Menlo circuits are detailed in the previous sections. Below is a concise summary of the results.

Primary feeder voltage profile evaluation.

3. The majority of the simulation scenarios did not feature out of standard voltage at the primary feeder as penetrations increased with the exception of the Menlo End and Menlo Beginning generation distribution scenarios.
4. The Menlo End distribution scenarios demonstrated out-of-standard high voltages induced by PV generation for all evaluated PV penetrations. Other scenarios (Cayetano End and Menlo Middle) demonstrated similar voltage rise behavior, but without non-standard voltages. The Menlo End generation scenarios produced high voltages due to high line impedance and high levels of excess generation capacity; both characteristic of sites located at the end of a feeder away from the Load Center.
5. The Menlo Beginning distribution scenarios demonstrated out-of-standard low voltage condition for evaluated penetrations greater than 40%. It was shown that as penetration increases, the sub-station Load Drop Compensation control would lower the sub-station voltage via tapping. Other generation distributions (LC/GC > 1) demonstrated similar behavior, but did not experience out-of-standard voltages. The Menlo Beginning scenarios featured a high impedance section of line at the end of the feeder resulting in a significant voltage drop. As the sub-station LDC lowered the voltage, the section would drop below standard voltage levels.
6. The out-of-standard voltages issue may be remedied by addressing circuit impedance, bus siting evaluation, and the application of voltage regulation equipment.

Voltage Regulation Equipment evaluation.

5. Based on the observation of the simulated penetration and distribution scenarios of the Cayetano and Menlo circuits, the High-Pen PV had a marginal impact on capacitor switching. Only two of the 160 simulated Cayetano circuit scenarios showed a change in capacitor switching in the PV region. The Menlo circuit featured a capacitors installation with Voltage Override switching controls that would switch on with increased PV generations, but in response to the sub-station Load Tap Changing transformer dropping the circuit voltage with PV generation. Of the controls evaluated, only Voltage-Override switching controls are impacted by PV generation.
6. As discussed in the Low Voltage section, PV generation in the circuit causes the sub-station LTC with LDC control to lower the circuit voltage via tapping. The LDC operation was simulated for the entire year, and both the Cayetano and Menlo circuits show increases in yearly tap position changes increase with penetration.

Sub-station power factor evaluation.

1. It was observed in both the Cayetano and Menlo simulation scenarios that sub-station power factor decreases (leading or lagging) as PV penetration increases. This is attributed to the lack of reactive power support provided by PV generation.
2. The sub-station power factor marginally decreased for characteristic High days, but significantly decreased for characteristic Low days.
3. Unnecessary capacitor switching for reactive power or voltage regulation by Time-Clock switching controls aggravated the decrease in sub-station power factor. Capacitor switching controls that utilize system feedback could prevent the unnecessary capacitor switching aggravating the sub-station power factor.

Circuit line loss evaluation.

1. Increased PV penetration reduces system line loss until PV generation induced reverse power flow becomes dominant. This optimum PV penetration is referred to as the minimum loss penetration. The Break Even Point (BEP) is a method to estimate the minimum loss penetration. The error of the estimation is reduced as the circuit LC/GC ration approaches one (LC/GC → 1).
2. Circuits with a larger LC/GC ration will have a higher minimum loss penetration than circuits with a lower LC/GC ratio. The Beginning generation distribution scenarios typically have a larger LC/GC ratio than an End generation scenario.
3. Circuits with LC/GC close to one (LC/GC ≈ 1) will achieved lower line losses at the minimum loss PV penetration than circuits with LC/GC ratio away from one. Radial generation distributions scenarios typically have a LC/GC ratio approximately equal to one.
4. For a circuit with distributed load demand ($\sigma_{LC} > 0$), distributed PV generation ($\sigma_{GC} > 0$) will have a higher minimum loss penetration achieve lower line losses at the minimum loss penetration than point PV generation ($\sigma_{GC}=0$). The Radial generation distribution scenarios are examples of distributed PV and Beginning, Middle, and End generation distribution scenarios are example so point PV generation.
5. The minimum loss penetration is significantly higher for a characteristic High than a characteristic Low day. Using the total load demand energy and interpolation, a minimum loss penetration for the entire may be estimated.

High-Pen PV has a steady-state impact on distributions circuits. This analysis focused on High-Pen PV's influence on voltage, regulation equipment, line loss, and more on the primary feeder. The majority of the results indicated a marginal impact of High-Pen PV, but there are examples of negative impacts on voltage and regulation equipment. The analysis presented above identified these negative influences and decomposed the condition into metrics to clearly identify the root cause of the issue.

5.3 Task 4: Advanced Inverter Controls

5.3.1 Inverter-Based Generation

The grid-tied DC-AC inverter converts a DC power source into an AC grid synchronized source by the pulse width modulation of one or more high frequency switches and is a core component in the

integration of PV into the grid. A current controller modulates the duty cycle of the active switches to synchronize the inverter output with the grid, control power output, and stabilize the operation of the inverter while low-pass filters reduce output ripple. Ancillary control components provide other functions such as maximum power point tracking and anti-islanding shutoff.

DC-AC inverters are highly dynamic nonlinear devices, and as is the case with any new technology, the incorporation of such inverters into the existing grid infrastructure may produce both beneficial and adverse effects. To understand these effects, accurate inverter models are required. Due to the differences between traditional power generators and DC-AC inverters modeling techniques that approximate DC-AC inverters as traditional AC generators do not hold, especially under transient conditions.

Several major differences between DC-AC inverters and traditional power sources include:

1. *Faults / Anti-Islanding:* With traditional power generation, sources contribute fault currents limited only by the device and equivalent line impedances until protective devices such as fuses or circuit breakers open. Rotating generators also carry significant physical inertia, increasing available fault energy. DC-AC inverters utilize current mode feedback in their operation which provides inherent current limiting, and the electrical inertia provided by capacitor storage is much less. Additionally, IEEE 1547.1 compliance require provisions for a complete halt of any power generation in the case of an islanding situation. Electrical islands occur when the utility grid is de-energized, but local sources continue to provide power. These differences abruptly change the fault current and large-signal characteristics of the existing grid.

2. *Dynamic Response:* Due to the switching nature of DC-AC inverters, coupled with their high frequency of operation (> 10KHz typical), such devices are nonlinear and highly dynamic. Unlike power sources which utilize large rotating machines, DC-AC inverters have very little or no electrical inertia, and are more sensitive to line and load transients.

3. *Controller Differences:* DC-AC inverters utilize different control mechanisms than traditional generators. Prime movers driving synchronous generators are typically controlled via droop controllers, whereas inverters utilize voltage following or current mode control. Ancillary controls such as maximum power point tracking in the case of PV adds further controller complexity to inverters.

4. *High Variability:* Renewable energy sources are dependent on environmental conditions thus are highly variable. Unlike fuel powered plants, renewable energy operators have very little control over generation availability. In the case of excessive power generation, curtailment methods may be used to avoid voltage swells. However, very little can be done in the situation where energy demand exceeds supply without an energy storage mechanism, and voltage sags may occur as consequence.

5.3.1.1 Reactive Power

In AC circuits, reactive power is required to produce the electric and magnetic fields found in reactive elements such as inductors and capacitors. In addition to real power required to produce work, reactive power flows into the system during the first half of the AC cycle to generate electric and magnetic fields.

As these fields collapse during the second half cycle, this energy is returned to the source, resulting in a net zero energy transfer. In power systems analysis, reactive power is expressed in units of volt-amps reactive (VAR). In single phase AC systems, the total instantaneous power may be expressed as:

$$S = VI = V_m \sin(\omega t) I_m \sin(\omega t - \emptyset) \qquad \textbf{5-92}$$

Where S is apparent power, V_m is the voltage amplitude, I_m is the current amplitude, ω is the fundamental frequency, and $\emptyset$ is the phase angle between voltage and current. This expression may be rewritten to directly express real and reactive power components as shown in 5-93 with the first and second terms representing real and reactive power, respectively.

$$S = V_m I_m \cos(\emptyset)(1 - \cos 2\omega t) - V_m I_m \sin(\emptyset) \sin(2\omega t) \qquad \textbf{5-93}$$

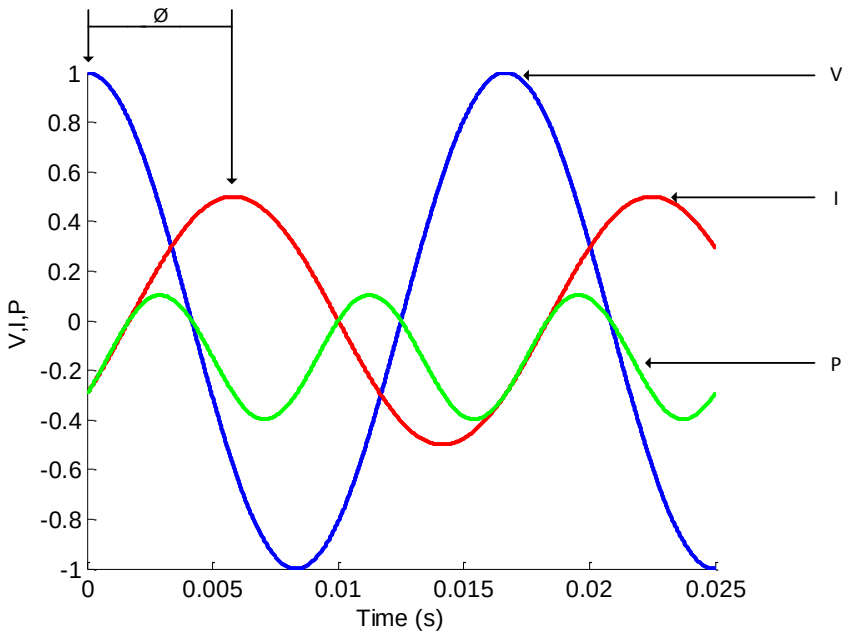

Figure 74. Example voltage, current, and apparent power waveforms.

In steady-state analysis, average real power and reactive power may be expressed as:

$$P = {I_{rms}}^2 R = \frac{V_{rms}}{R} \quad \text{5-94}$$

$$Q = {I_{rms}}^2 X = \frac{V_{rms}}{X} \quad \text{5-95}$$

Where P is real power in watts, Q is reactive power in volt-amps reactive (VAR), R is resistance in ohms, and X is reactance in ohms.

Additionally, the power factor (PF) of a system is described by the ratio of real to apparent power. Apparent Power (VA) is the geometric sum of real power and reactive power.

$$P.F. = \frac{P}{S} = S\cos(\emptyset), \;\; S = \sqrt{P^2 + Q^2} \quad \text{5-96}$$

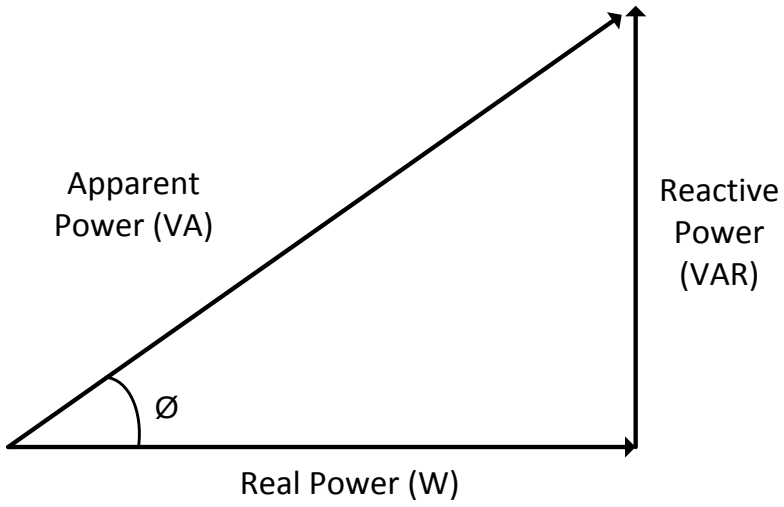

Figure 75. Power triangle.

In general, inductive elements consume reactive power and capacitive elements produce reactive power. Standard nomenclature denotes reactive power consumption as a positive quantity, and reactive power generation as a negative quantity. Typical reactive power loads include AC induction motors and line impedances. Typical reactive power producers include synchronous generators and capacitors.

Load	Power Factor
Florescent Lighting	0.90
Industrial Motor	0.85
Heat pump / Air conditioner	0.83
Washer	0.65

Table 47. Typical electrical loads and associated power factors.

Reactive power, while necessary in AC circuits containing inductance and/or capacitance, has undesirable characteristics:

1. *Reactive power consumes line capacity:* The presence of reactive power flow increases the amplitude of the AC current required to transmit a given amount of real power across a transmission line. This results in greater ampacity requirements, which necessitates thicker and more expensive transmission conductors and supporting structures such as pylons and conduit. As a result, many utilities place minimum power factor limits on their industrial customers and install capacitors to generate VAR in close proximity to reactive power loads to reduce transmission.

2. *Decreased transmission efficiency:* While reactive power itself results in zero net energy consumption, the flow of reactive power across resistive elements such as a transmission line resistance results in real I^2R losses. In AC transmission systems, the requirement of transmitting reactive power results in increased line currents, increasing real transmission losses.

3. *Reduced voltage regulation:* Voltage drop across a transmission line is a function of the line current and line impedance. Increased line currents due to the transmission of reactive power results in greater voltage drops. Additionally, inductance from the transmission line itself increases line impedance, further reducing the receiving end voltage. Utilities often install boosting transformers or capacitors to raise the receiving end voltage to acceptable levels and shunt reactors to lower line voltage in light loading conditions.

5.3.1.2 Volt/VAR Correction

Utilities install capacitors to provide reactive power near loads to mitigate low voltage/power factor issues. Traditional capacitor banks have fixed ratings, and are either permanently connected or fully switched in or out throughout the day depending on load conditions. Similarly, shunt reactors are installed to address excessive voltage rises during light loading conditions attributed by the Ferranti effect, and also only provide full on / full off control. Recently, power electronics based FACTS devices such as static synchronous compensators (STATCOM) and static variable compensators (SVC) have been implemented provide variable reactive power to support the stability of grid voltage. While effective, the application of these devices at the distribution level is not common, due to high costs. However, with the increased penetration of DG, it is becoming increasingly feasible to incorporate variable volt/VAR support into inverters to implement these features at the distribution level.

5.3.1.3 Active Volt/VAR Regulation

Inverters are based on the same power electronics technology as STATCOMs and SVCs, and retain many of the same topological features. The flexibility, fast response, and physical proximity to loads make inverters ideal for providing reactive power support. It is possible to configure inverters to utilize spare capacity to provide reactive power. This is especially effective in situations where inverters are outputting minimal real power, such as in shaded and nighttime conditions in PV systems. The benefits provided by volt/VAR regulation are two-fold:

1. *Local VAR Support:* By introducing an artificial phase shift into the inverter current output, a grid tied inverter may be operated at any arbitrary power factor, up to the VA limits of the inverter. By providing VAR at the location of reactive power loads, local VAR support alleviates the negative consequences of reactive power transmission as discussed in the previous section. This may be achieved with no reduction in real power output, provided that only spare inverter capacity is utilized to provide reactive power.

2. *Local Line Voltage Regulation.* Line voltages decrease as power production falls or load demand increases. A common and abrupt occurrence of this is due to sudden changes in insolation, such as panel shading due to clouds, animals, or other sources of obstruction. To mitigate this, it is possible to produce reactive power when real power production is unavailable to regulate the voltage levels at site of installation. In the case of shaded conditions, the majority of inverter capacity may be devoted to reactive power generation. It is important to note that distributed generation voltage regulation is not currently allowed by the IEEE 1547 standard. However, the IEEE 1547.8 group is working propose the removal of this limitation.

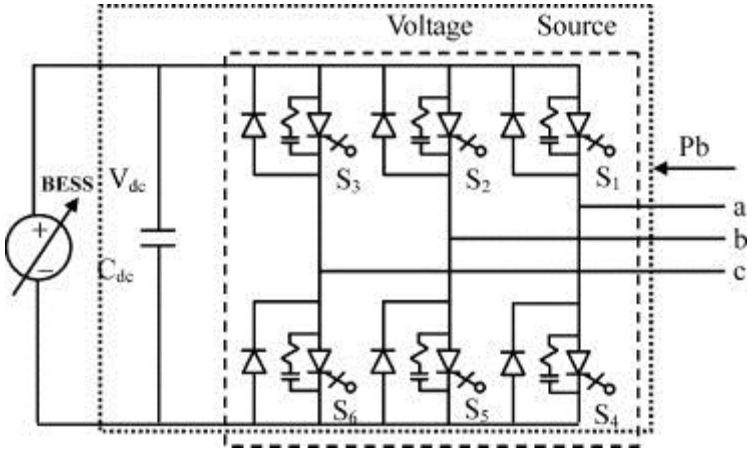

(a)

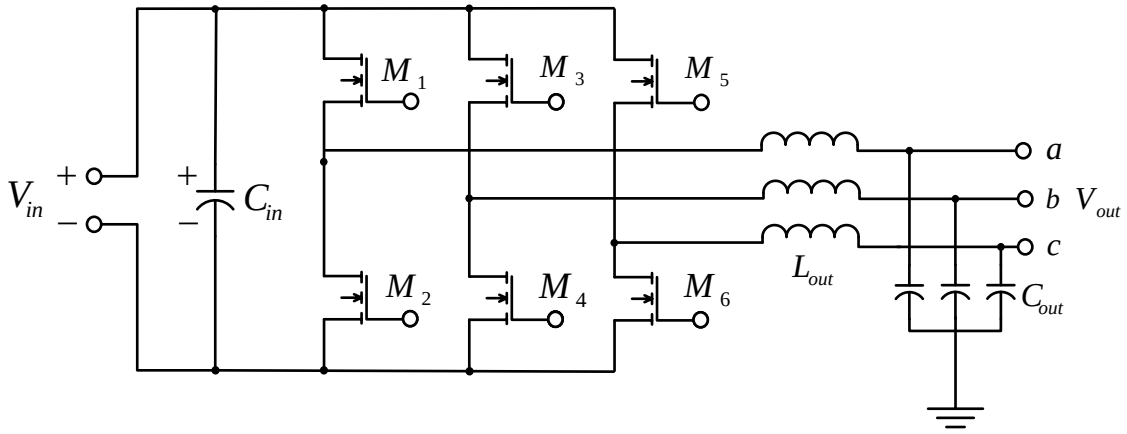

(b)

Figure 76. (a) STATCOM schematic. (b) Three phase inverter schematic.

5.3.2 Approach

5.3.2.1 Inverter Model

To accurately model inverter behavior, two inverter models, of a single phase low power inverter and a three phase medium power inverter, were developed in the Mathwork's SimPowerSystems software environment. This approach allows for transient level and stability analysis not available through steady state modeling methods. Parameters were chosen to emulate the characteristics of commercially available inverters. The inverter block diagram is Figure 77. It is composed of four components; the phase-locked loop, controller, power electronics block, output filter, and the anti-islanding block. Advanced inverter controls such as volt/VAR regulation and active power filtering are implemented as an addition to the existing inverter structure. The SimPowerSystems development environment was chosen as it allows for waveform level analysis, integration of the inverter model into a power system model, and control algorithm development capabilities. Detailed description of inverter components follows:

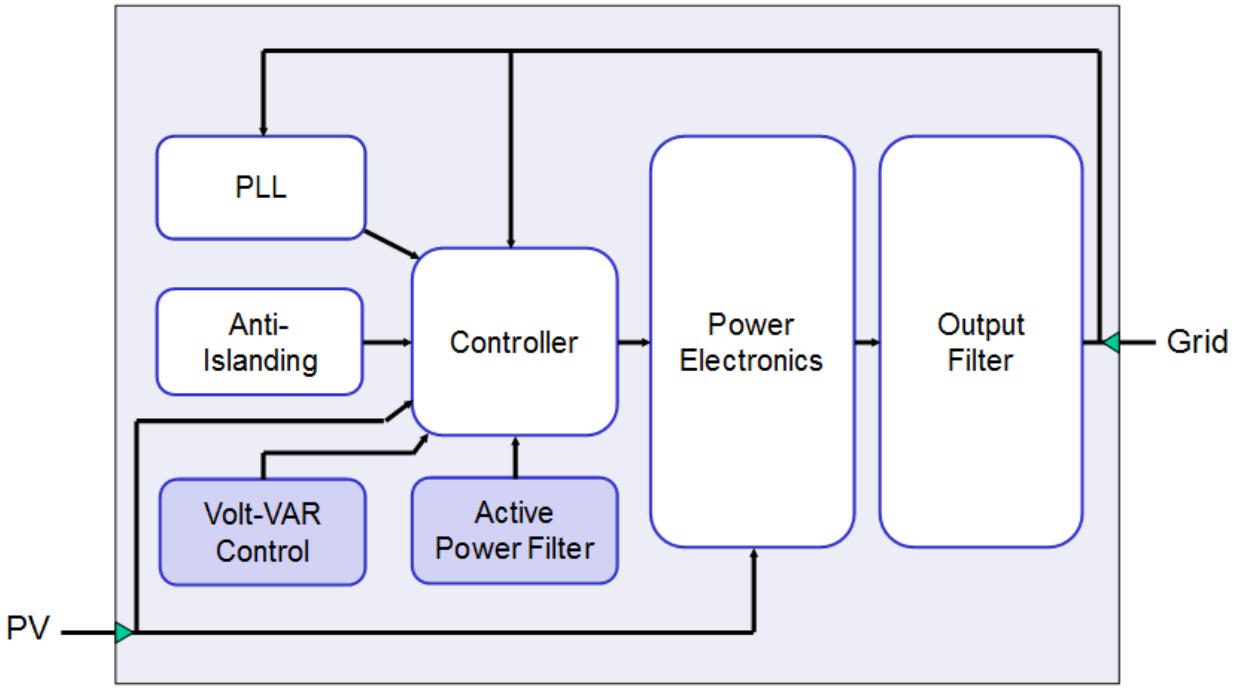

Figure 77. System components overview.

A. Anti-Islanding

Electrical islands occur when a distributed generation source continues to power a circuit when utility generation is offline. Unintentional islands may be dangerous to utility personnel operating under the false pretense of a de-energized circuit, or may cause devices such as reclosers and other inverters to behave erratically. For these reasons, distributed generation resources are required disconnect from the grid when an island condition is detected as per IEEE 1547.1. There are multiple methods for island detection, such as Sandia voltage shift, impedance sensing, harmonic detection. Passive methods of under/over voltage and under/over frequency at setpoints of 132/106 V and 60.5/59.3 Hz, respectively, are utilized in this study. Upon detection of an abnormal operating condition, the inverter model disconnects itself from the grid.

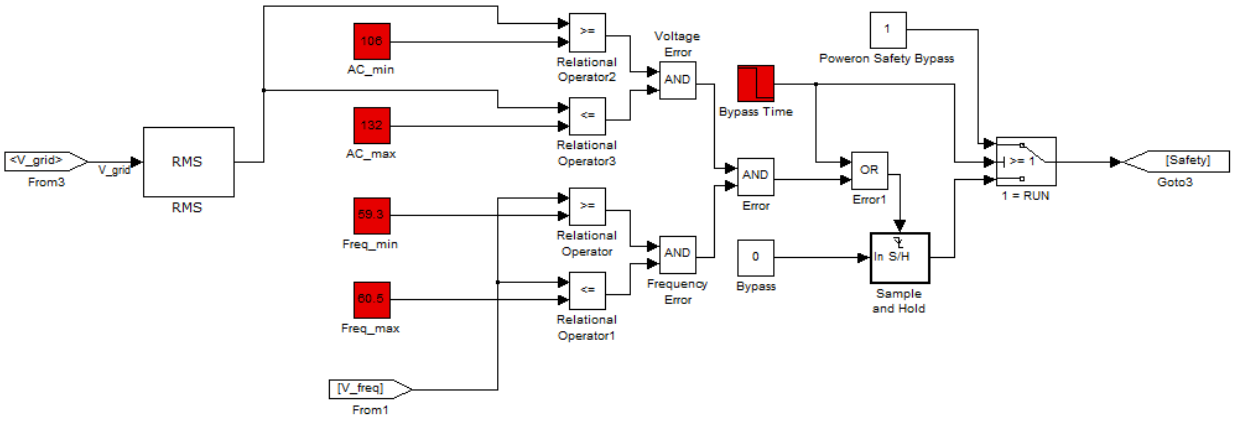

Figure 78. Anti-islanding mechanism. Line voltage is compared against voltage and frequency limits.

B. Phase-Locked Loop

Grid tied inverters must synchronize current output with the grid voltage. This functionality is provided by the phase-locked loop (PLL). The PLL itself consists of a voltage controlled oscillator, PID controller, and phase detector configured in a feedback loop (Figure 79). In the PLL synchronization subsystem, a normalized 60Hz grid voltage is fed into the discrete phase-locked loop block with controller gains of $G_p = 180$, $G_i = 3200$, $G_d = 1$ which outputs the measured phase angle. The phase angle is then fed into a sinusoidal function block to produce a synchronized reference signal. In single phase systems, by reconstructing the reference sinusoidal signal from the phase measurement as opposed to synthesizing it directly, it is possible to inject an artificial phase offset in order to produce reactive power at the inverter output. In three phase systems, reactive power control is an inherent component of the *ab*/DQ transform controller.

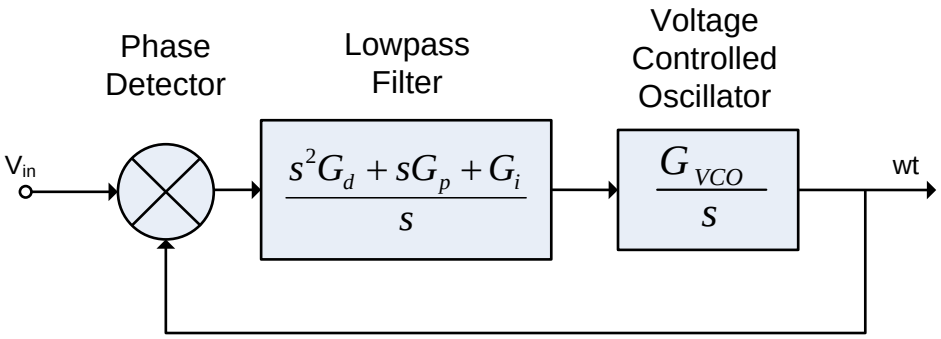

Figure 79. Phase-locked loop components.

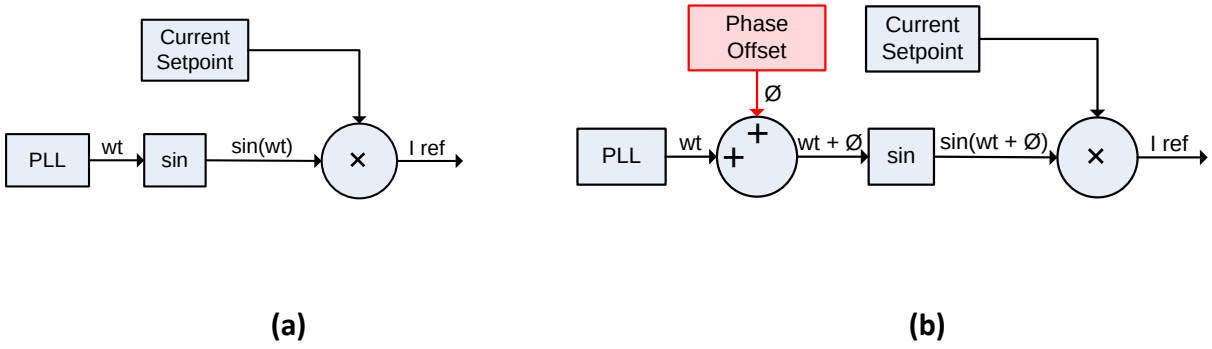

Figure 80. Phase-locked loop reference signal generation. a) Sinusoidal signal reconstruction. b) Reconstruction with artificial phase delay.

C. Power Stage

The power stage provides DC-AC inversion through the high frequency switching of insulated gate bipolar transistors (IGBTs) or metal-oxide semiconductor field effect transistors (MOSFETs). By rapidly alternating the switching pattern of the active switches, voltage inversion and sinusoidal waveform shaping is achieved. The power stage in the simulated model consists of a full bridge topology operating at a switching frequency of 16 kHz powered by a 400V DC source for the single phase system, and 800V DC for the three phase system. A small 0.25 ohm series resistance is inserted to facilitate model convergence. To reduce output ripple, the output of the inverter is fed into a LC filter with a cutoff frequency of 1.7 kHz (L = 2mH , C = 4µF). In the simulated model, the H-bridge block utilizing idealized IGBT devices with an ON-resistance of 0.01 ohms provided by SimPowerSystems was utilized. Firing sequence control is provided by a pulse-width modulation (PWM) block in SimPowerSystems. An input signal V_d, where $-1 < V_d < 1$, is accepted by the PWM block which transforms it into the appropriate firing pulses to achieve a voltage gain of V_d/V_{dc} at the output of the power stage. Full transients are retained in the modeling approach allowing analysis of switching frequency transients.

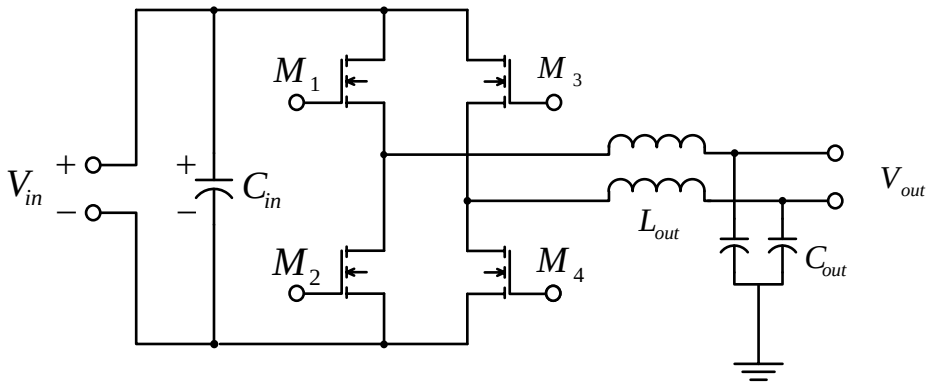

Figure 81. Single phase inverter.

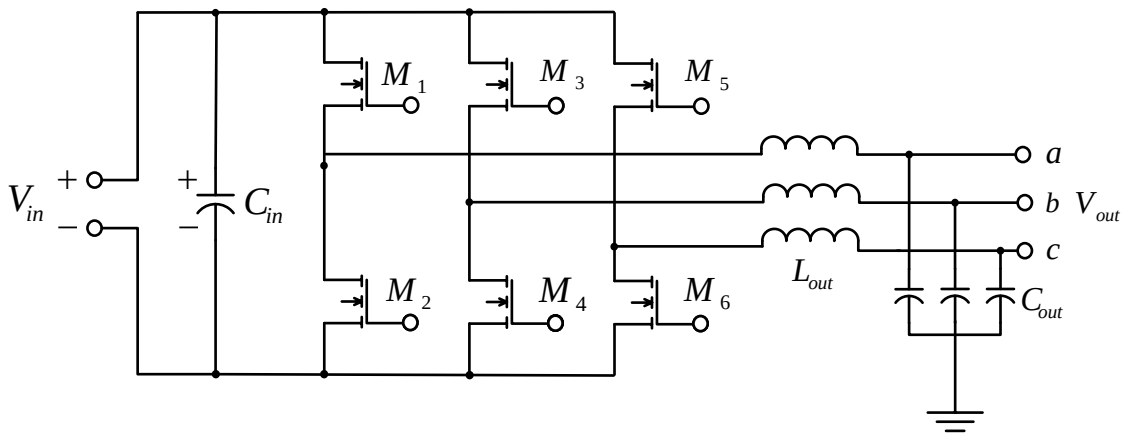

Figure 82. Three phase inverter.

D. Controller

In the grid-connected mode, the inverter operates as a grid synchronized current source. To achieve synchronization, the reference signal from the phase-locked loop is tracked by the output power stage. The controller block is introduced to ensure that the output current of the power stage accurately tracks the reference signal. There are numerous controllers utilized in commercial inverters. To create a simulated model representative of field deployed devices, two of the most popular controllers for single phase inverters, the proportional-integral (PI) controller and the proportional-resonant (PR) controller, are modeled in this study. In three phase systems, the alpha-beta / direct-quadrature (*acb*/DQ0) transform controller is often utilized and is modeled.

D.1. Single Phase vs. Three Phase Controllers

Single and three phase inverters share many of the same anti-islanding and phase-locked loop components. However, due to the topological differences in the power and filter stage, single and three phase inverters differ greatly in their controller scheme. As only one orthogonal output element is available for measurement in single phase inverters, these devices utilize single-input, single-output (SISO) type controllers. Additionally, these inverters must rely on the completion of an entire sinusoidal cycle to yield RMS measurements which greatly increases the response time of single phase inverters and necessitates complex calculations to measure real and reactive power. Three phase systems, with three orthogonal measurements (a,b,c voltages or currents), may utilize multiple-input, multiple-output (MIMO) techniques such as the *ab*/DQ transform. Due to the ability to instantaneously measure RMS values in three phase circuits three phase controllers may react instantaneously to changes in input or load. In this study, two of the most common controllers for single phase systems, the proportional integral and proportional resonant, and the *ab*/DQ controller for three phase systems are investigated.

transform controller is often utilized and is modeled.

D.2. Proportional-Integral Controller

The proportional-integral-derivative controller combines a proportional, integrator, and differentiator feedback loop to achieve tracking. The PID controller is a widely used device; in industry, over 80% of controllers are of this type. In inverters, the differentiator is often omitted to reduce the amplification of high frequency noise due to device switching, resulting in a proportional-integral (PI) controller. The transfer function of the PI controller is expressed by:

$$T(s) = \frac{k_p s + k_i}{s} \qquad \text{5-97}$$

As the proportional-integral controller alone cannot track a sinusoidal reference signal with zero steady state error, a grid voltage feed-forward path is introduced. While this modification reduces steady state error, it does introduce the possibility of distorting output current if the grid voltage is distorted. Additionally, the introduction of a feed-forward path may push the controller beyond its stability limits. In the simulated model, conservative gains of $K_p = 0.05$ and $k_I = 0.75$, where K_p and K_I are proportional and integral gains respectively, with a plant gain of 400 were selected. The bode plots of the closed loop system are presented in Figure 83.

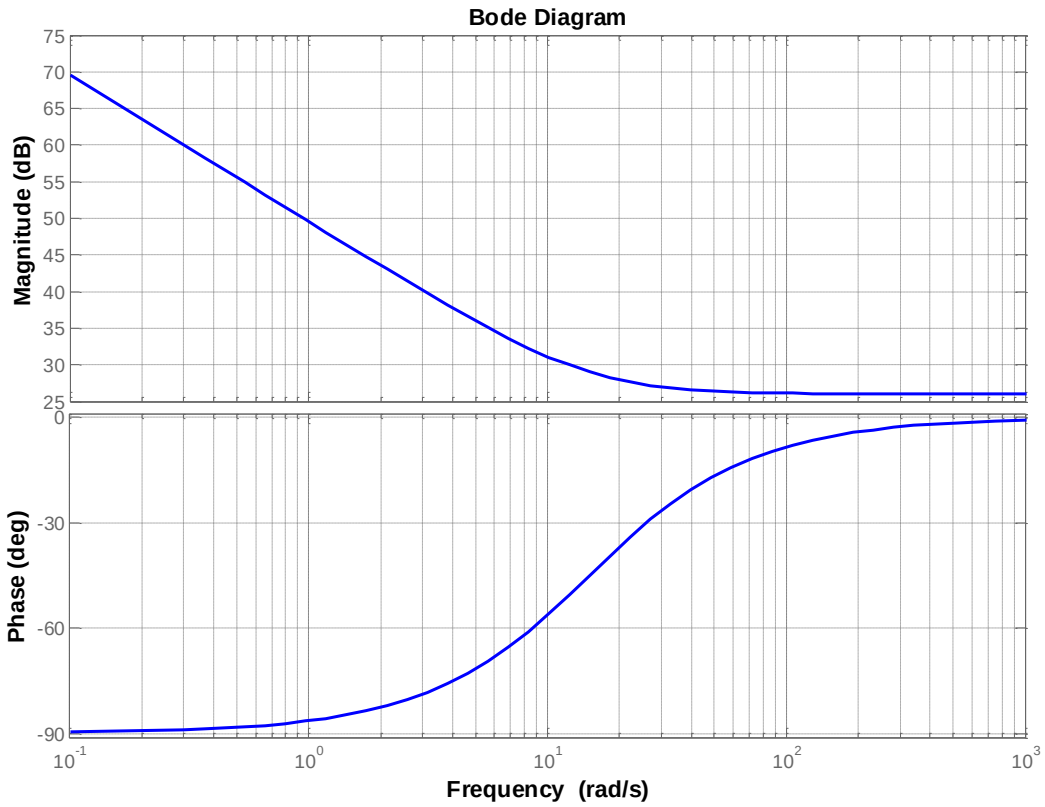

Figure 83. PI controller Bode diagram.

D.3. Proportional-Resonant Controller

The basic operating principal of the proportional-resonant controller is to introduce a large gain at a specific frequency, typically the grid frequency, to achieve tracking. With a sufficiently large gain, steady state error may be reduced to acceptable levels without the need of a feedforward path, and the resonant nature of this controller attenuates harmonic distortion. In practice, this operates as a high gain AC integrator. The transfer function of the PR controller is:

$$T(s) = k_p + \frac{2k_i \omega s}{s^2 + 2\omega s + \omega^2} \qquad \text{5-98}$$

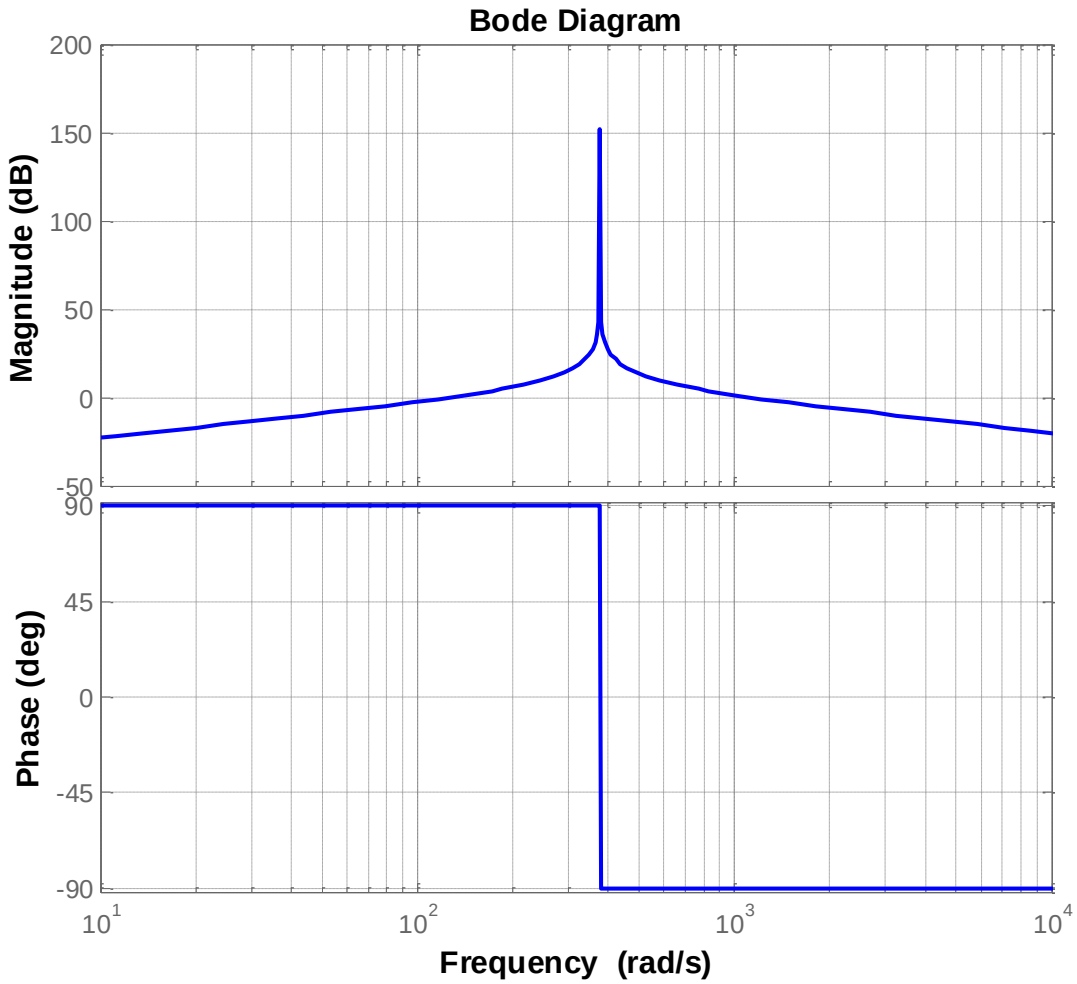

Figure 84. PR controller Bode diagram.

The proportional resonant controller eliminates the steady state tracking error and feedforward requirement of the PI controller, and provides improved performance when combined with high order output filters such as the LCL filter. However, the implementation and control effort is more sophisticated, and the controller itself performs poorly when not operated at its designed resonant frequency. The PR controller in this study was designed to operate at a resonant frequency of 60Hz with a maximum gain of 152dB (39810717.0553). The same output filter was used in both the PI and PR controller models.

D.4. abc/DQ0 Controller

In three phase inverters, the *abc*/DQ0 transform is a method to convert AC three phase components into two DC direct (I_d) and quadrature (I_q) quantities, with the direct and quadrature components proportional to real and reactive power output, respectively. In balanced three phase systems this greatly simplifies controller design as once in the DC domain, standard PID controllers can be utilized to

track the I_d and I_q to desired setpoints. These DC quantities are then transformed back into the *abc* domain via a DQ0/*abc* transform to provide reference signals to the power stage. In the three phase system, an output filter with L = 2mH and C = 4µF was used.

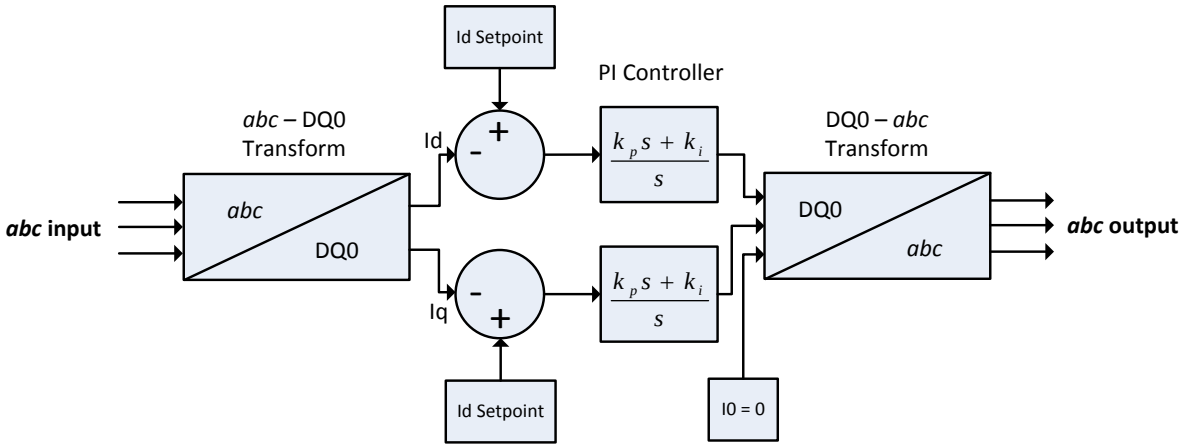

Figure 85. Three phase *abc*/DQ0 controller.

$$T = \begin{bmatrix} \cos(wt) & \cos(wt - \frac{2\pi}{3}) & \cos(wt + \frac{2\pi}{3}) \\ -\sin(wt) & -\sin(wt - \frac{2\pi}{3}) & -\sin(wt + \frac{2\pi}{3}) \\ \frac{\sqrt{2}}{2} & \frac{\sqrt{2}}{2} & \frac{\sqrt{2}}{2} \end{bmatrix} \quad \text{5-99}$$

Equation 5-100: The abc – DQ0 matrix transform. $I_{DQ0} = I_{abc}*T$. The inverse of this matrix provides the DQ0 – abc transform.

E. Power Flow Controller

In the single phase inverter model, the real and reactive power outputs are controlled by a user defined current amplitude and phase. It is more practical to directly accept real and reactive power set points by implementing a power flow controller. The inputs to the power follow controller are real and reactive power values which are then transformed into current amplitude and phase values utilized by the PI/PR controller via the following equations:

$$|I_{ref}| = \frac{\sqrt{(P_{ref})^2 - (Q_{ref})^2}}{V_{line}} \qquad \text{5-101}$$

$$\emptyset_{ref} = \tan^{-1}\left(\frac{Q_{ref}}{P_{ref}}\right) \qquad \text{5-102}$$

Where P_{ref} is the desired real power output, Q_{ref} is the desired reactive power output, V_{line} is the RMS line voltage, and I_{ref} and $\emptyset_{ref}$ are the calculated current magnitude and phase offset values used to construct the reference signal to be sent to the controller block. This is implemented in the MATLAB model as shown in Figure 86. A feedback loop is introduced to achieve real and reactive power output tracking.

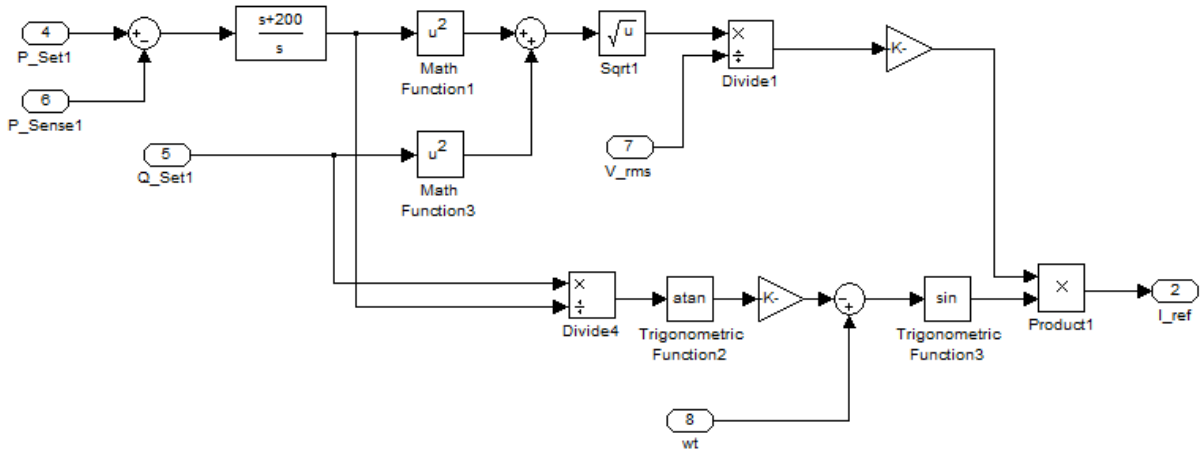

Figure 86. Power flow controller.

To achieve closed loop output power tracking, real power input is sensed by measuring the average power inputted by the DC source. As the DC-AC inverter is a theoretically lossless device, any input power, less losses, is transferred into the output. This avoids the complicated computation of deriving real and reactive power RMS measurements from the sinusoidal output current and voltage waveforms. The input power is obtained by measuring and = multiplying the DC input voltage and DC input current. A 120Hz notch filter and low-pass filter are applied to remove harmonics and high frequency noise. This measured value is then used to create a feedback loop to track real power output. A PI controller is included in the power feedback loop to improve tracking.

Reactive power is injected into the output by adding a phase offset into the output of the reconstructed sinusoidal reference waveform. To calculate the necessary phase offset to generate a certain amount of reactive power, the power flow equations 5-101 and 5-102 were utilized. The reactive power controller built upon a feedforward control path and relies on the tracking action of the real power controller to maintain a regulated output.

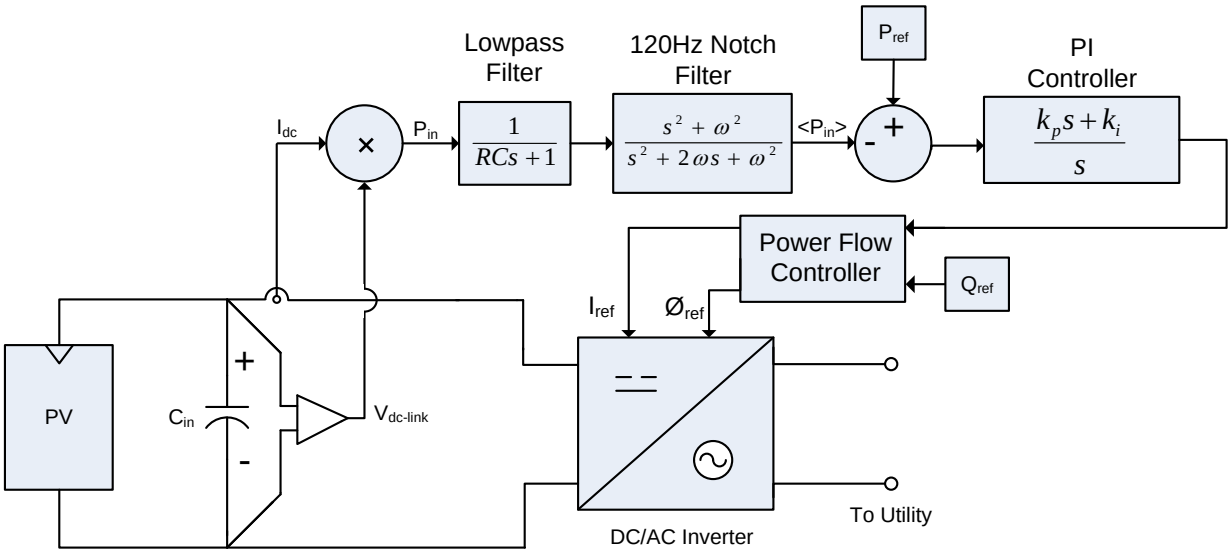

Figure 87. Real power tracking feedback loop.

In three phase systems real and reactive power components of both the input and output do not pulsate and may be calculated instantaneously throughout the entire AC cycle. As such, these measurements may be directly used to close the output power feedback loop; it is only required to filter switching harmonic disturbances which is achieved via a low pass filter. Similar to the single phase inverter where tracked real and reactive power values are utilized to generate I_{ref} and $Ø_{ref}$ to the PI/PR controllers, the tracked real and reactive power components in the three phase model are used to generate I_d and I_q setpoints for the abc/DQ0 controller.

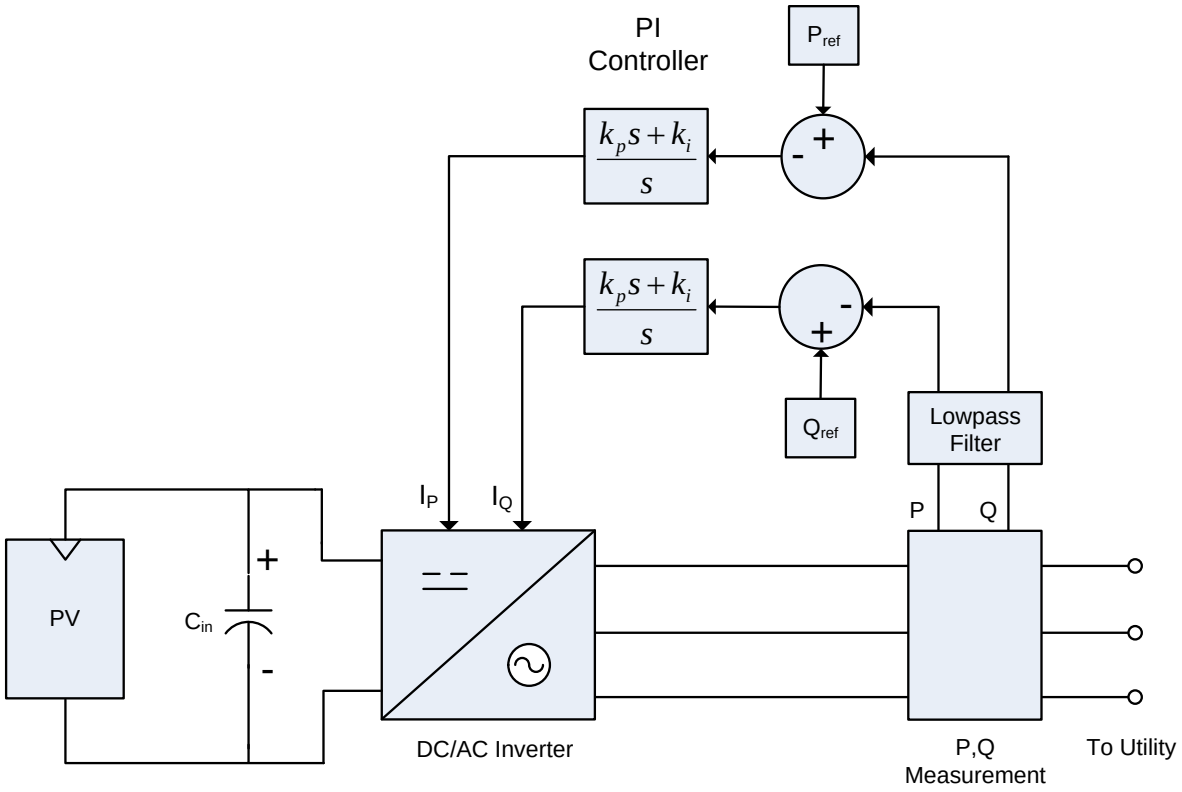

Figure 88. Real and reactive power tracking feedback loops.

The following show several simulation results to step changes in real and reactive power setpoints. The inverter model is connected to a 120Vrms, 60Hz ideal voltage source through an impedance of Z = 0.02 + j0.05 ohms, and a local load of 5kW, 5kVAR. To test real power response, single phase inverters with PI and PR controllers were adjusted to output 1kW, 0kVAR. At t = 0.4s, the setpoint is changed to 4kW, 0kVAR. The simulated inverter output results show zero steady state error tracking after the transition with minimal overshoot and disturbance to reactive power output. At t = 1.0s, the real power setpoint is adjusted to its original 1kW value. In the three phase system, real power is adjusted from 1kW to 40kW. Figure 89 shows simulated results.

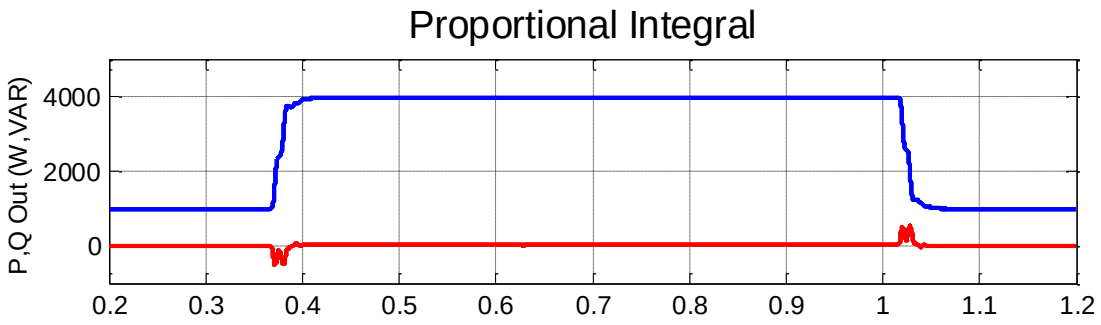

(a)

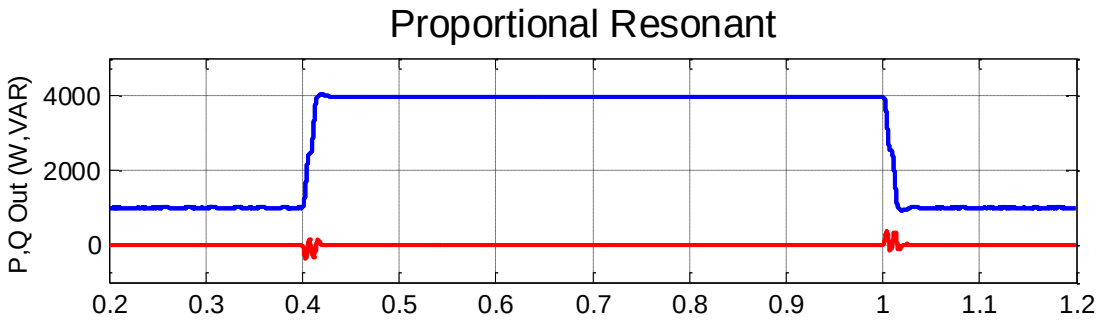

(b)

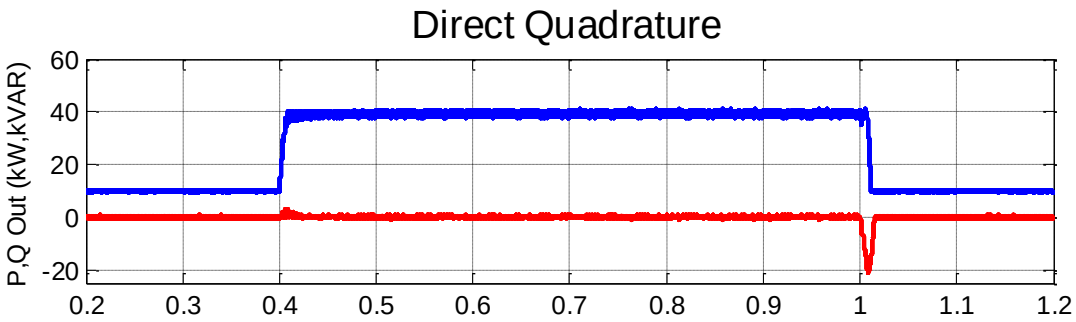

(c)

Figure 89. Inverter reponse to a step change in real power setpoint. a) PI Controller. b) PR controller. c) DQ controller.

To test reactive power response, inverter setpoints were adjusted to output 4kW, 0kVAR. At t = 0.4s, the reactive power setpoint is changed to 2kVAR while the real power setpoint is maintained at 0kW. The simulated results show less than 5% steady state error tracking after the transition with minimal overshoot and disturbance to real power output. At t = 1.0s, the reactive power setpoint is adjusted to its original 0kW value. In the three phase system, real power is adjusted from 0kVAR to 20kVAR. Figure 90 show simulated results.

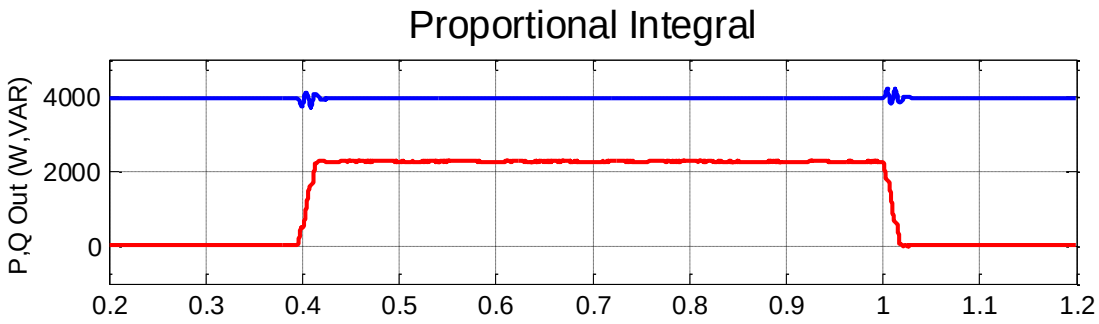

(a)

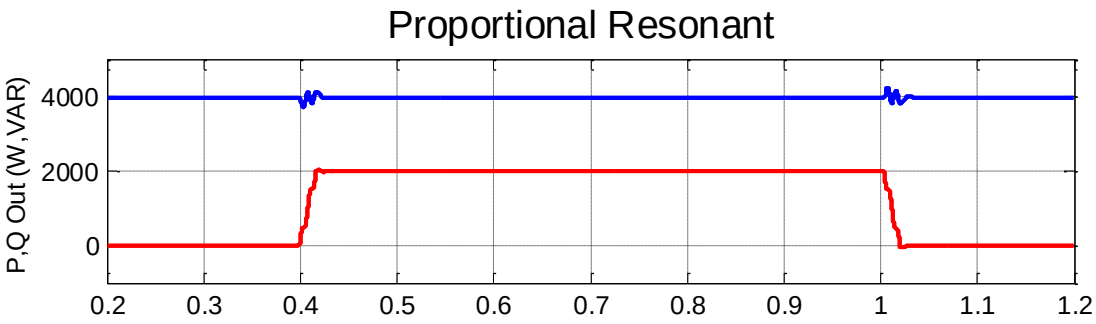

(b)

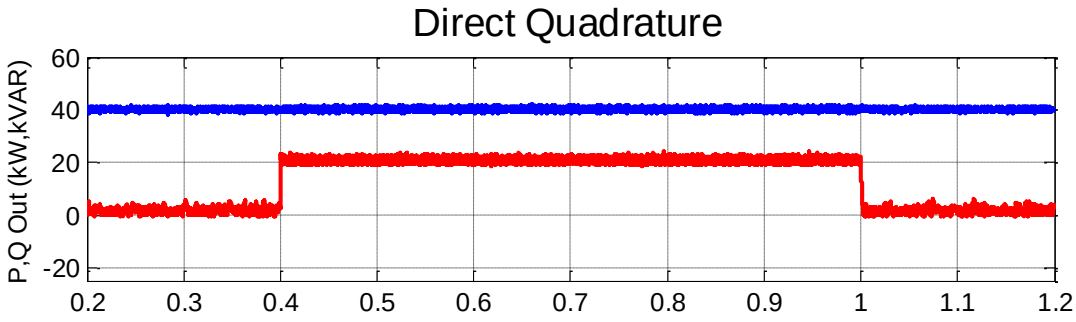

(c)

Figure 90. Inverter reponse to a step change in reactive power setpoint. a) PI Controller. b) PR controller. c) DQ controller.

5.3.2.2 Advanced Inverter Model

In addition to real power production, the value of inverter coupled DG may be enhanced by incorporating ancillary functions. An advanced inverter feature investigated in this research is volt/VAR control, in which an inverter actively regulates local line voltage by producing or consuming reactive power, essentially providing STATCOM functionality. While STATCOMs have traditionally been large, centralized installations, the increasing prevalence of DG systems and their associated inverters have opened new prospects for incorporating distributed STATCOM into the grid. In the future, individual DE systems may be allowed to regulate voltage, allowing utilities to reduce their investment in power factor and voltage correction devices.

To implement volt/VAR, the RMS line voltage, instead of reactive power output, is measured at the point of common coupling and used to close the feedback loop that provides the setpoint of the reactive power input to the power flow controller. In this configuration, the inverter will attempt utilize spare capacity to produce reactive power, up to the output limits of the inverter, to maintain the local line

voltage. A PI controller is included in the feedback loop to improve tracking. In this manner, volt/VAR regulation is achieved without major modifications to the existing inverter control structure, and no modifications to the physical construction of the inverter itself. Figure 91 and Figure 92 show the implementation of volt/VAR for single and three phase systems.

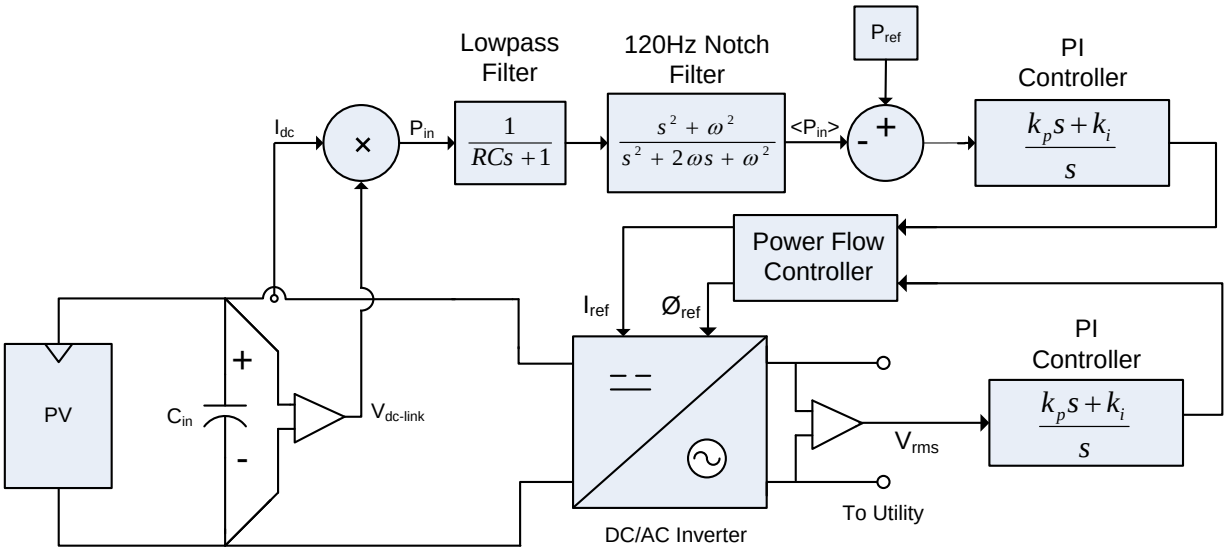

Figure 91. Volt/VAR feedback tracking loop for single phase inverters.

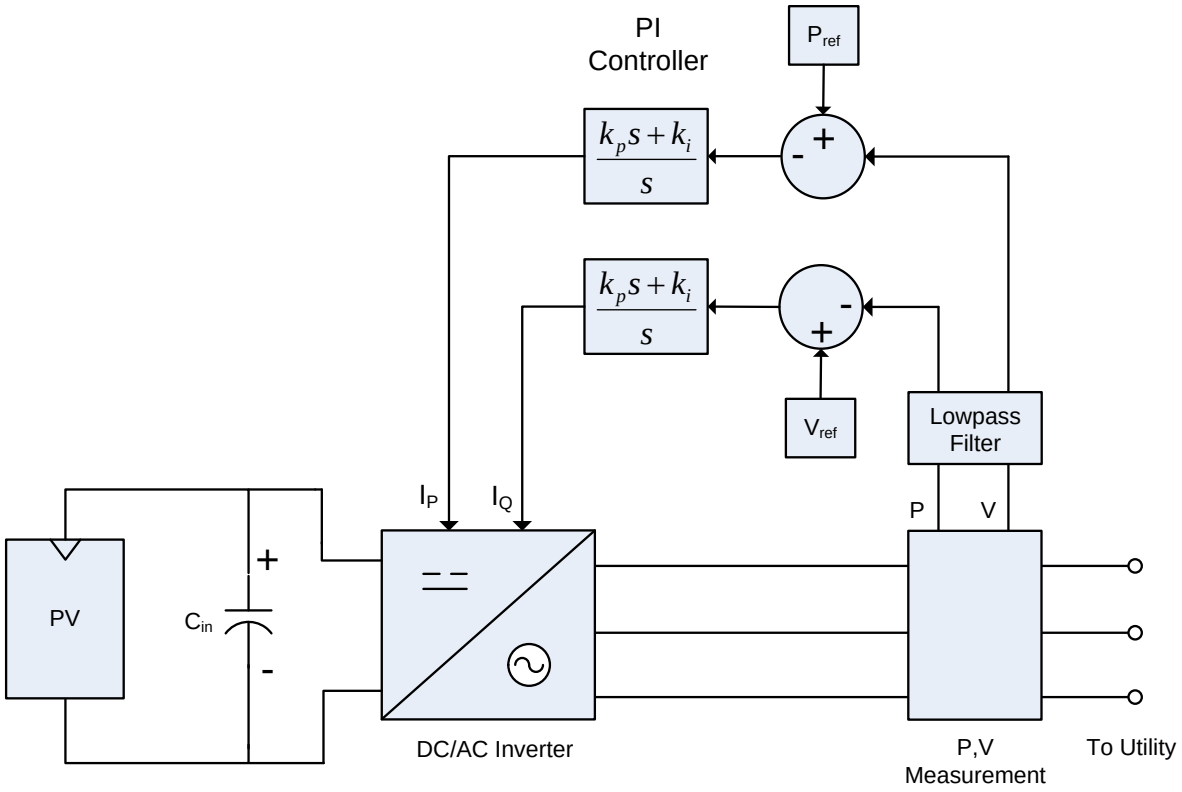

Figure 92. Volt/VAR feedback tracking loop for three phase inverter.

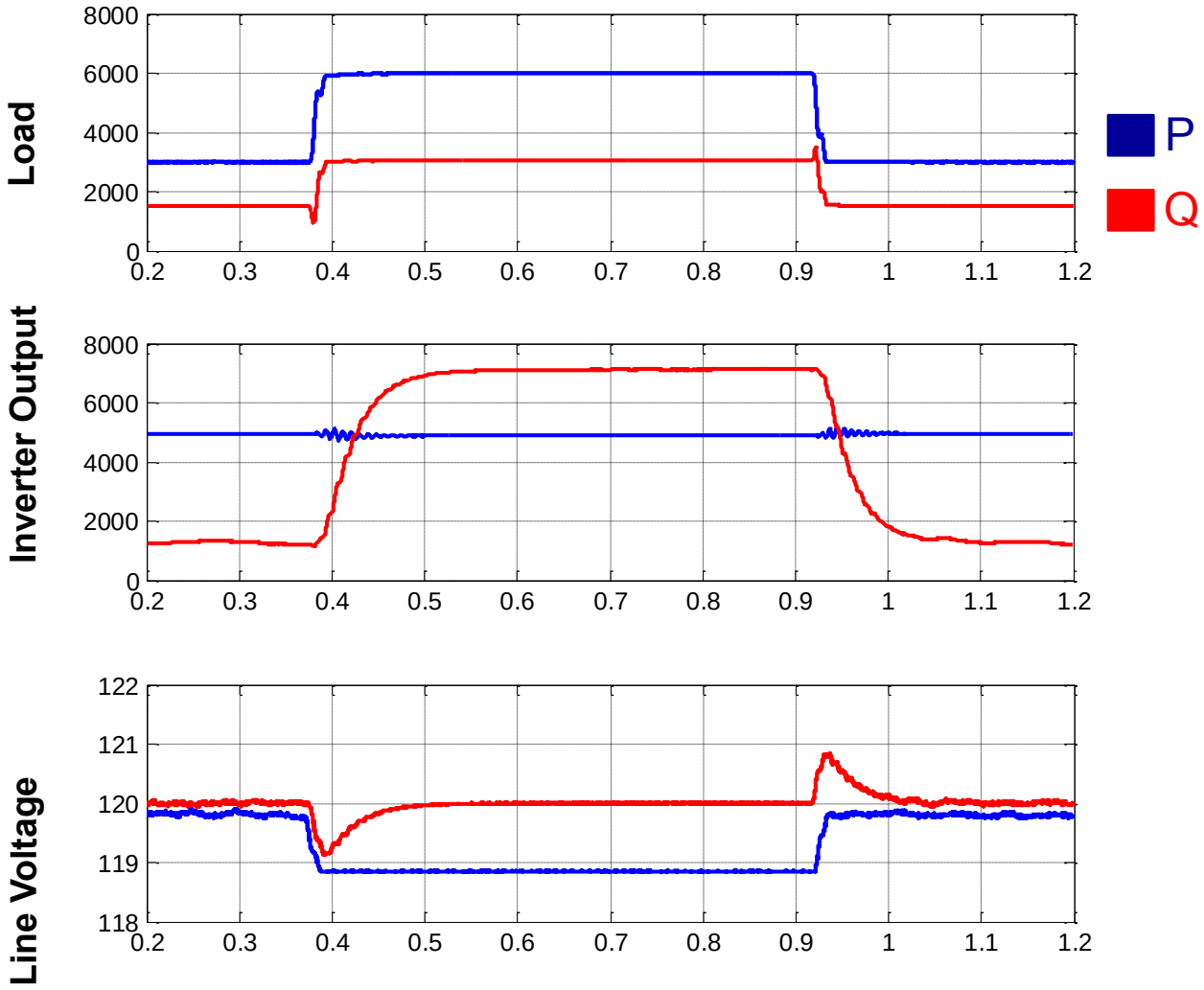

Figure 93. Single Phase Volt/VAR Control Response to a Load Transient.

5.3.2.3 Circuit Data

Inverter coupled distributed energy resources are a key component in the development of Smart Grid implementation. In addition to providing energy, the value of these resources may be enhanced by developing advanced control functionalities previously discussed. However, to ensure a successful transition, these devices must be coordinated with the existing infrastructure and other DE devices.

Real world circuit data provide by Pacific Gas and Electric Company (PGE) were used to study the impact of high penetration inverters with advanced inverter controls. Two circuits that contain utility connected PV have been selected for study; to obtain a wide range of circuit characteristics the circuits were selected to be representative of a commercial feeder with highly concentrated distribution of PV and a residential circuit with a widely dispersed allocation of PV.

Both the Cayatano and Menlo circuits utilize a radial topology with lateral circuits branching off of a main feeder line. Within the lateral circuits, many of the busses are both physically and electrically similar resulting in negligible differences in inverter steady state and transient behavior. To reduce redundant calculations and limit simulations to a manageable quantity, the circuits were reduced using centroid load lumping. Cayatano was reduced from 237 busses to 29, and Menlo from 827 busses to 41.

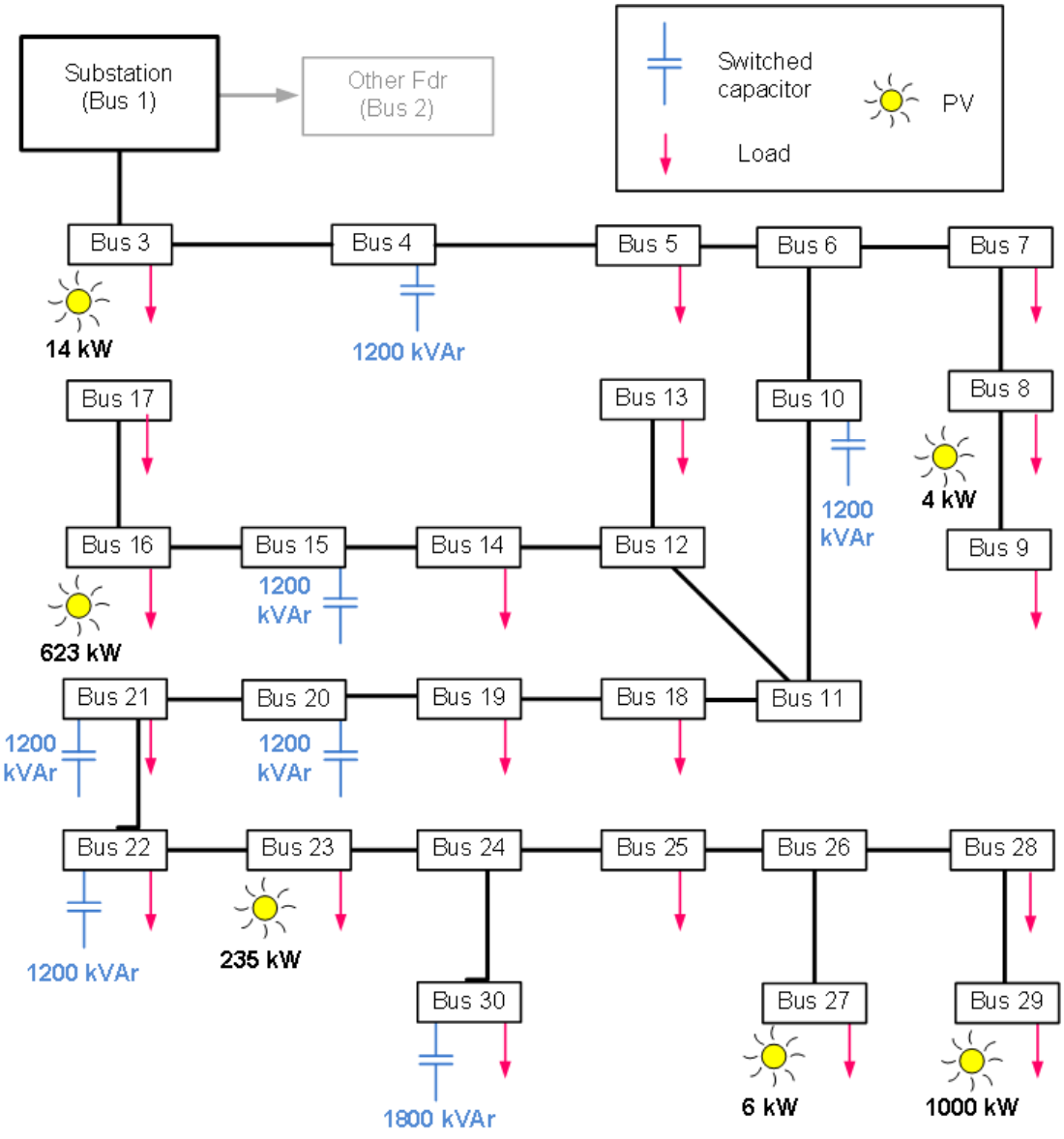

Figure 94. Reduced Cayatano circuit.

Node	Length to Substation (feet)	Resistance to Substation (omhs)	Reactance to Substation (ohms)
1	0	0	0
2	-	-	-
3	1094	0.0190356	0.01641
4	1578.856429	0.027472102	0.023683
5	3459.553059	0.060196223	0.051893
6	5280.154806	0.091874694	0.079202
7	6305.865169	0.109722054	0.094588
8	6841.25593	0.119037853	0.102619
9	7143.09613	0.124289873	0.107146
10	11785.42572	0.205066407	0.176781
11	12023.07366	0.209201482	0.180346
12	12170.57928	0.211768079	0.182559
13	12350.86392	0.214905032	0.185263
14	338.7166042	0.005893669	0.005081
15	777.1360799	0.013522168	0.011657
16	908.2521848	0.015803588	0.013624
17	1050.294632	0.018275127	0.015754
18	12304.42697	0.214097029	0.184566
19	12595.34082	0.21915893	0.18893
20	12944.98377	0.225242718	0.194175
21	13468.0824	0.234344634	0.202021
22	13995.2784	0.243517844	0.209929
23	14690.46692	0.255614124	0.220357
24	14985.47815	0.26074732	0.224782
25	16276.15231	0.28320505	0.244142
26	16355.36829	0.284583408	0.245331
27	16524.72659	0.287530243	0.247871
28	16498.77653	0.287078712	0.247482
29	16639.45318	0.289526485	0.249592

Table 48. Reduced Cayatano circuit bus to substation impedances.

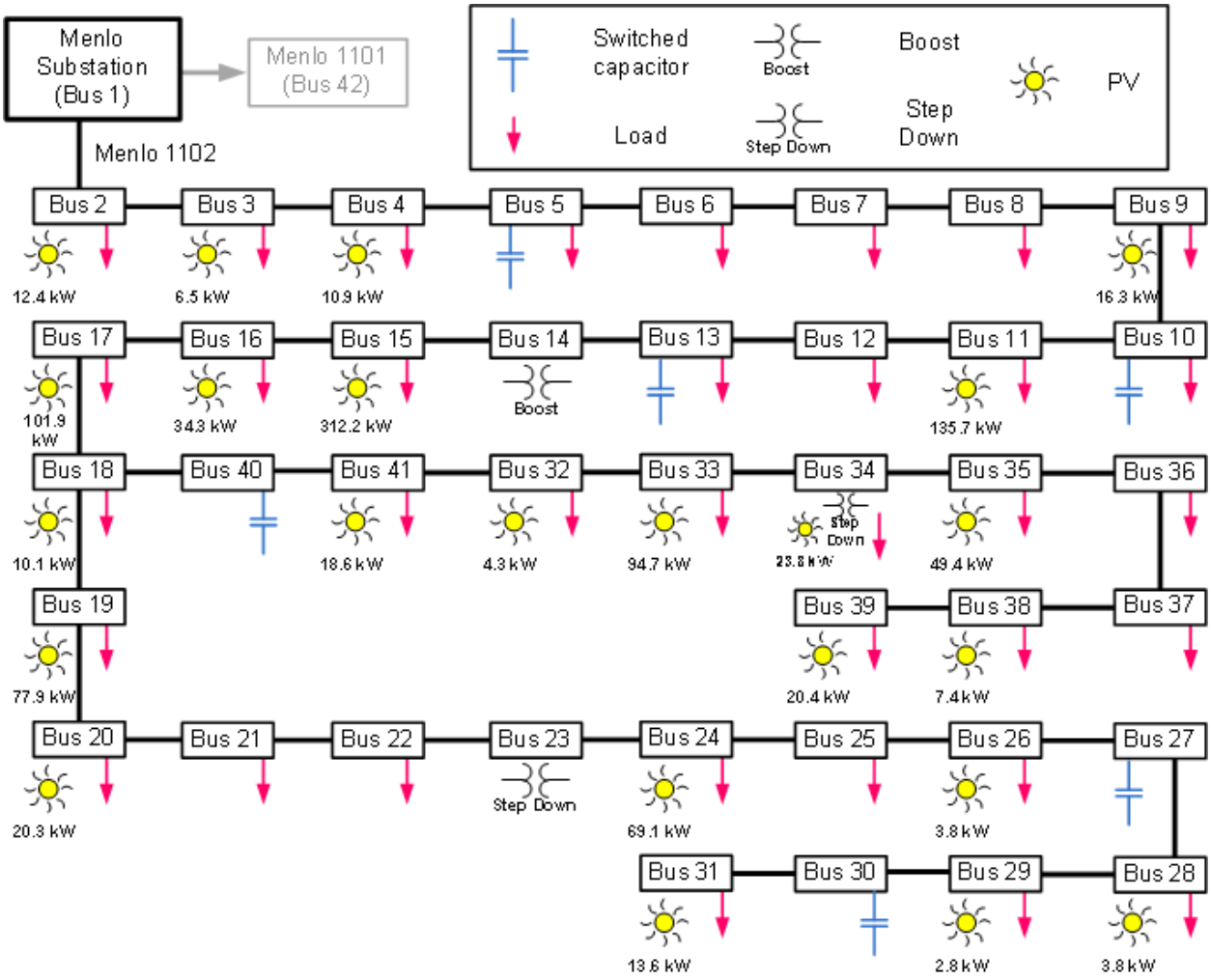

Figure 95. Reduced Menlo circuit.

Node	Length to Substation (feet)	Resistance to Substation (ohms)	Reactance to Substation (ohms)
1	0	0	0
2	2367	0.0411858	0.035505
3	3496.029289	0.06083091	0.052440439
4	4471.550209	0.077804974	0.067073253
5	6313.650628	0.109857521	0.094704759
6	7620.947699	0.13260449	0.114314215
7	8784.640167	0.152852739	0.131769603
8	9443.240586	0.164312386	0.141648609
9	10666.35565	0.185594588	0.159995335
10	13632.53347	0.237206082	0.204488002

11	15524.15272	0.270120257	0.232862291
12	16504.62552	0.287180484	0.247569383
13	17267.21548	0.300449549	0.259008232
14	17920.86402	0.311823034	0.26881296
15	18658.69456	0.324661285	0.279880418
16	19158.83473	0.333363724	0.287382521
17	19644.11925	0.341807675	0.294661789
18	20119.5	0.3500793	0.3017925
19	21614.96862	0.376100454	0.324224529
20	22347.84728	0.388852543	0.335217709
21	23258.99372	0.404706491	0.348884906
22	23848.26778	0.414959859	0.357724017
23	26259.83473	0.456921124	0.393897521
24	30394.6569	0.52886703	0.455919854
25	35445.57741	0.616753047	0.531683661
26	38050.26778	0.662074659	0.570754017
27	39273.38285	0.683356862	0.589100743
28	44165.8431	0.76848567	0.662487646
29	45423.62134	0.790371011	0.68135432
30	46201.06695	0.803898565	0.693016004
31	48464.07741	0.843274947	0.726961161
32	34600.98349	0.602057113	0.519014752
33	38725.22301	0.67381888	0.580878345
34	49925.70675	0.868707298	0.748885601
35	61513.95548	1.070342825	0.922709332
36	72945.24672	1.269247293	1.094178701
37	81279.68656	1.414266546	1.219195298
38	84989.3743	1.478815113	1.274840614
39	89378.40177	1.555184191	1.340676027
40	20119.5	0.3500793	0.3017925
41	23002.19082	0.40023812	0.345032862

Table 49. Reduced Menlo circuit bus to substation impedances.

5.3.3 Results

5.3.3.1 Multi-Inverter Stability

Grid-tied inverters utilize standalone control systems that may detrimentally interact with other local inverters. To study the local level interactions between multiple single phase inverter units, a multi-inverter node model was constructed. The node consists of three single phase inverters representing residential PV installations, and RL loads representing loads. The node is designed to be typical of a residential installation where several residences are serviced by a common utility transformer.

Inverters and loads within each node are connected to each other with an impedance of Z = 0.01 + j0.005 ohms and then to the grid through a common step-up transformer (Z = 5%) as depicted in Figure 96. As the coupling between inverters within the node is much stronger than that between nodes, inverter interactions remain localized at low PV penetrations.

A three phase node model was also developed for studies of higher capacity installations. This node consists of three inverters connected in a radial configuration to a common bus through individual transformers (Z=5%) and tie-in impedances of Z = 0.01 + j0.005 ohms as depicted in Figure 97.

To investigate multi-inverter stability, test nodes are placed at each of the major busses in the Menlo and Cayatano reduced model circuits with each inverter connected to a constant local load of 5kW, 2.5kVAR. After the inverters have reached a stable steady-state operating condition an additional switched load of 5kW, 2.5kVAR at each inverter is switched in. The generation capacities are varied until instabilities are observed and maximum generation to load ratios are recorded for each bus.

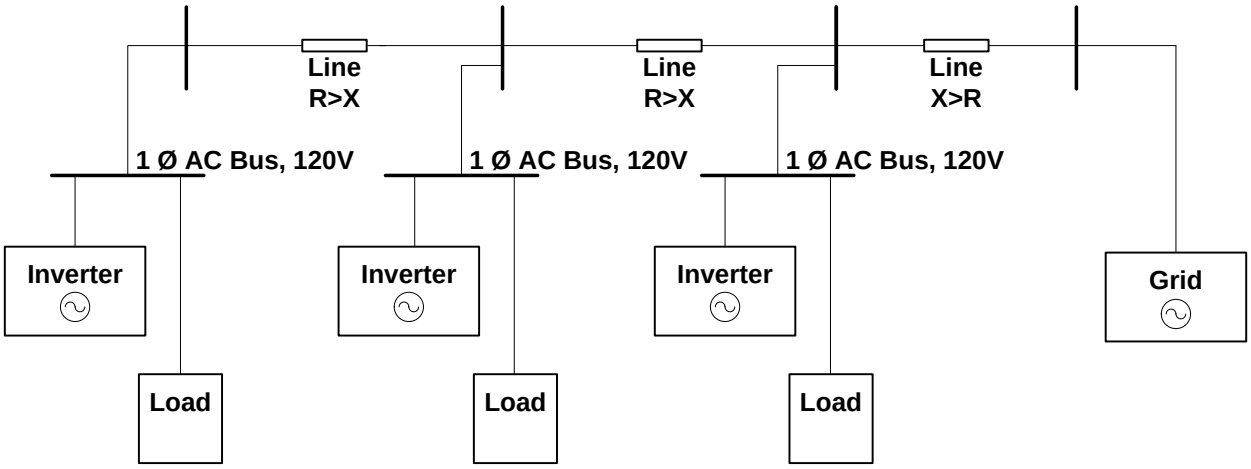

Figure 96. Single phase multi-inverter node.

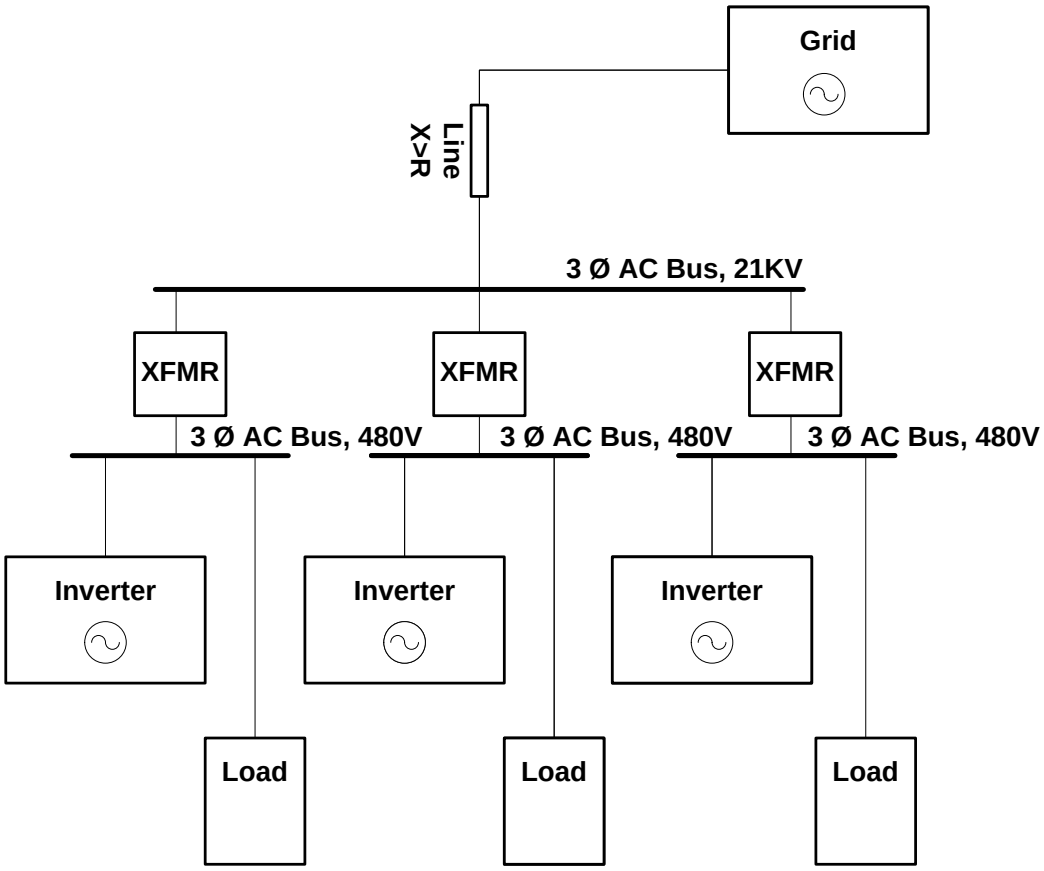

Figure 97. Three phase multi-inverter node.

Simulated results indicate a possibility of multi-inverter failure in the presence of a combination of a high node to substation impedance and high generation to local load in volt/VAR control enabled inverters.

Node	Length to Substation (feet)	Resistance to Substation (ohms)	Reactance to Substation (ohms)	Max Gen/Load Ratio
1	0	0	0	-
2	2367	0.0411858	0.035505	34.8165
3	3496.029289	0.0608309	0.052440439	10.25198536
4	4471.550209	0.077805	0.067073253	9.764224896
5	6313.650628	0.1098575	0.094704759	8.843174686
6	7620.947699	0.1326045	0.114314215	8.189526151
7	8784.640167	0.1528527	0.131769603	7.607679917
8	9443.240586	0.1643124	0.141648609	7.278379707

9	10666.35565	0.1855946	0.159995335	6.666822175
10	13632.53347	0.2372061	0.204488002	5.183733265
11	15524.15272	0.2701203	0.232862291	4.23792364
12	16504.62552	0.2871805	0.247569383	3.74768724
13	17267.21548	0.3004495	0.259008232	3.36639226
14	17920.86402	0.311823	0.26881296	3.03956799
15	18658.69456	0.3246613	0.279880418	2.67065272
16	19158.83473	0.3333637	0.287382521	2.420582635
17	19644.11925	0.3418077	0.294661789	2.177940375
18	20119.5	0.3500793	0.3017925	1.94025
19	21614.96862	0.3761005	0.324224529	1.19251569
20	22347.84728	0.3888525	0.335217709	0.82607636
21	23258.99372	0.4047065	0.348884906	0.37050314
22	23848.26778	0.4149599	0.357724017	0.07586611
23	26259.83473	0.4569211	0.393897521	0
24	30394.6569	0.528867	0.455919854	0
25	35445.57741	0.616753	0.531683661	0
26	38050.26778	0.6620747	0.570754017	0
27	39273.38285	0.6833569	0.589100743	0
28	44165.8431	0.7684857	0.662487646	0
29	45423.62134	0.790371	0.68135432	0
30	46201.06695	0.8038986	0.693016004	0
31	48464.07741	0.8432749	0.726961161	0
32	34600.98349	0.6020571	0.519014752	0
33	38725.22301	0.6738189	0.580878345	0
34	49925.70675	0.8687073	0.748885601	0
35	61513.95548	1.0703428	0.922709332	0
36	72945.24672	1.2692473	1.094178701	0
37	81279.68656	1.4142665	1.219195298	0
38	84989.3743	1.4788151	1.274840614	0
39	89378.40177	1.5551842	1.340676027	0
40	20119.5	0.3500793	0.3017925	1.94025
41	23002.19082	0.4002381	0.345032862	0.49890459

Table 50. Menlo Maximum Generation to Load Ratios Before Multi-Inverter Instability.

Node	Length to Substation (feet)	Resistance to Substation (omhs)	Reactance to Substation (ohms)	Max Gen/Load Ratio
1	0	0	0	0
2	-	-	-	-
3	1094	0.019036	0.01641	23.906
4	1578.856	0.027472	0.023683	23.42114
5	3459.553	0.060196	0.051893	21.54045
6	5280.155	0.091875	0.079202	19.71985
7	6305.865	0.109722	0.094588	18.69413
8	6841.256	0.119038	0.102619	18.15874
9	7143.096	0.12429	0.107146	17.8569
10	11785.43	0.205066	0.176781	13.21457
11	12023.07	0.209201	0.180346	12.97693
12	12170.58	0.211768	0.182559	12.82942
13	12350.86	0.214905	0.185263	12.64914
14	338.7166	0.005894	0.005081	24.66128
15	777.1361	0.013522	0.011657	24.22286
16	908.2522	0.015804	0.013624	24.09175
17	1050.295	0.018275	0.015754	23.94971
18	12304.43	0.214097	0.184566	12.69557
19	12595.34	0.219159	0.18893	12.40466
20	12944.98	0.225243	0.194175	12.05502
21	13468.08	0.234345	0.202021	11.53192
22	13995.28	0.243518	0.209929	11.00472
23	14690.47	0.255614	0.220357	10.30953
24	14985.48	0.260747	0.224782	10.01452
25	16276.15	0.283205	0.244142	8.723848
26	16355.37	0.284583	0.245331	8.644632
27	16524.73	0.28753	0.247871	8.475273
28	16498.78	0.287079	0.247482	8.501223
29	16639.45	0.289526	0.249592	8.360547

Table 51. Cayetano Maximum Generation to Load Ratios Before Multi-Inverter Instability.

5.3.3.2 Transient Analysis

Due to continually changing environmental and electrical variables an inverter must cope with disturbances to both PV and line conditions. Examples include sudden shading due to cloud cover or animals and the connection of heavy electrical loads. With standard inverters operating at unity power factor, both of these disturbances result in sharp changes in line voltage. While it is possible to utilize inverter capacity to immediately produce reactive power in an attempt to regulate line voltage, control

systems cannot react immediately and voltage disturbances may occur, especially if the inverter control system is not appropriately tuned to current grid conditions.

A. Input Disturbance Response

A single 5kW single phase or 40kW three phase inverter is placed at each of the major nodes in the Menlo and Cayatano reduced model circuit. Line load conditions are held constant while PV input power is adjusted from 100% to 25% to simulate a loss of PV production by modulating the real power setpoint. Unity power factor and volt/VAR control enabled inverters are simulated and the magnitude and duration of the resulting line voltage transient is observed. In all cases, the level of transient observed with volt/VAR control is less than with traditional controls.

Node	Length to Substation (feet)	Resistance to Substation (ohms)	Reactance to Substation (ohms)	Voltage Regulation (Traditional)	Maximum Transient (volt/VAR)
1	0	0	0	-	-
2	2367	0.0411858	0.035505	0.006203255	0.000639731
3	3496.029289	0.0608309	0.052440439	0.007538901	0.000944875
4	4471.550209	0.077805	0.067073253	0.008526083	0.00120853
5	6313.650628	0.1098575	0.094704759	0.010131198	0.001706396
6	7620.947699	0.1326045	0.114314215	0.011130765	0.00205972
7	8784.640167	0.1528527	0.131769603	0.011950402	0.002374233
8	9443.240586	0.1643124	0.141648609	0.012390278	0.002552233
9	10666.35565	0.1855946	0.159995335	0.013168265	0.002882806
10	13632.53347	0.2372061	0.204488002	0.014887056	0.003684477
11	15524.15272	0.2701203	0.232862291	0.015886363	0.004195727
12	16504.62552	0.2871805	0.247569383	0.016380357	0.00446072
13	17267.21548	0.3004495	0.259008232	0.016754508	0.004666826
14	17920.86402	0.311823	0.26881296	0.017068682	0.004843488
15	18658.69456	0.3246613	0.279880418	0.017416511	0.005042902
16	19158.83473	0.3333637	0.287382521	0.017648389	0.005178076
17	19644.11925	0.3418077	0.294661789	0.017870504	0.005309234
18	20119.5	0.3500793	0.3017925	0.018085442	0.005437716
19	21614.96862	0.3761005	0.324224529	0.018745534	0.005841897
20	22347.84728	0.3888525	0.335217709	0.019060679	0.006039973
21	23258.99372	0.4047065	0.348884906	0.01944536	0.006286229
22	23848.26778	0.4149599	0.357724017	0.019690146	0.006445493
23	26259.83473	0.4569211	0.393897521	0.020661722	0.00709727
24	30394.6569	0.528867	0.455919854	0.02222896	0.008214792
25	35445.57741	0.616753	0.531683661	0.024004991	0.009579909
26	38050.26778	0.6620747	0.570754017	0.024871351	0.010283881
27	39273.38285	0.6833569	0.589100743	0.025267931	0.010614453

28	44165.8431	0.7684857	0.662487646	0.026795619	0.011936743
29	45423.62134	0.790371	0.68135432	0.02717449	0.012276684
30	46201.06695	0.8038986	0.693016004	0.027406055	0.012486805
31	48464.07741	0.8432749	0.726961161	0.02806923	0.01309843
32	34600.98349	0.6020571	0.519014752	0.023717273	0.009351639
33	38725.22301	0.6738189	0.580878345	0.025090972	0.010466301
34	49925.70675	0.8687073	0.748885601	0.028489356	0.013493466
35	61513.95548	1.0703428	0.922709332	0.031623312	0.016625433
36	72945.24672	1.2692473	1.094178701	0.034436501	0.019714978
37	81279.68656	1.4142665	1.219195298	0.036350596	0.021967535
38	84989.3743	1.4788151	1.274840614	0.03717088	0.022970156
39	89378.40177	1.5551842	1.340676027	0.038118589	0.024156382
40	20119.5	0.3500793	0.3017925	0.018085442	0.005437716
41	23002.19082	0.4002381	0.345032862	0.019337714	0.006216823

Table 52. Menlo volt/VAR Control Transient Simulation Results. Generation / Load = 10.

Node	Length to Substation (feet)	Resistance to Substation (omhs)	Reactance to Substation (ohms)	Voltage Regulation (Traditional)	Maximum Transient (volt/VAR)
1	0	0	0	0	0
2	-	-	-	-	-
3	1094	0.019036	0.01641	0.004217	0.000563
4	1578.856	0.027472	0.023683	0.005066	0.000812
5	3459.553	0.060196	0.051893	0.007499	0.00178
6	5280.155	0.091875	0.079202	0.009265	0.002717
7	6305.865	0.109722	0.094588	0.010125	0.003245
8	6841.256	0.119038	0.102619	0.010546	0.00352
9	7143.096	0.12429	0.107146	0.010776	0.003676
10	11785.43	0.205066	0.176781	0.013842	0.006065
11	12023.07	0.209201	0.180346	0.013981	0.006187
12	12170.58	0.211768	0.182559	0.014066	0.006263
13	12350.86	0.214905	0.185263	0.01417	0.006356
14	338.7166	0.005894	0.005081	0.002347	0.000174
15	777.1361	0.013522	0.011657	0.003554	0.0004
16	908.2522	0.015804	0.013624	0.003843	0.000467
17	1050.295	0.018275	0.015754	0.004132	0.00054

18	12304.43	0.214097	0.184566	0.014143	0.006332
19	12595.34	0.219159	0.18893	0.01431	0.006482
20	12944.98	0.225243	0.194175	0.014507	0.006661
21	13468.08	0.234345	0.202021	0.014797	0.006931
22	13995.28	0.243518	0.209929	0.015084	0.007202
23	14690.47	0.255614	0.220357	0.015454	0.00756
24	14985.48	0.260747	0.224782	0.015608	0.007711
25	16276.15	0.283205	0.244142	0.016267	0.008376
26	16355.37	0.284583	0.245331	0.016306	0.008416
27	16524.73	0.28753	0.247871	0.01639	0.008504
28	16498.78	0.287079	0.247482	0.016377	0.00849
29	16639.45	0.289526	0.249592	0.016447	0.008563

Table 53. Cayetano volt/VAR Control Transient Simulation Results. Generation / Load = 10.

B. Line Disturbance Response

An inverter operating at a full output power of 5kW (40kW for three phase systems) is placed at each major node with no locally attached load. A load of 0kW 5kW, 2.5kVAR (50kW, 25kVAR for three phase systems) is switched into the circuit and the resulting line voltage transient is observed. The simulation is re-run with the inverters operating at 0kW to simulate nighttime conditions. Both unity power factor and volt/VAR enabled inverters are simulated. In all cases, the level of transient observed with volt/VAR control is less than with traditional control.

C. Capacitor Switching

The switching of large voltage regulation equipment such as line capacitors, shunt reactors, or on-load tap changers inject large transients into the grid that may interfere with the operation of nearby inverters. The Menlo reduced circuit features switched correction capacitors at nodes 5, 10, 13, 27, 30, and 40 while the Cayatano circuit contains these at 4, 10, 15, 21, 20, 22, and 30. Capacitors at these nodes are switched in and out of the circuit while the waveform level transient response of three phase inverters is observed. No detrimental interactions between volt/VAR control enabled inverters and traditional hard-switched voltage correction devices was observed.

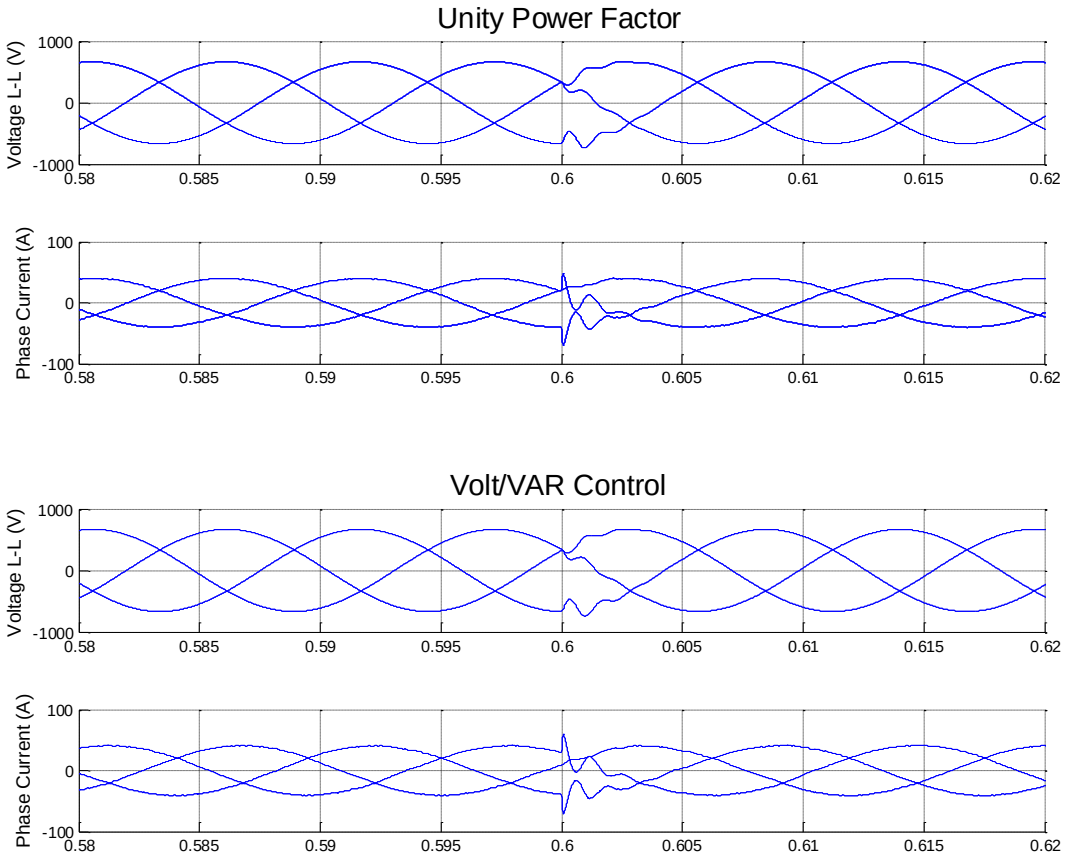

Figure 98. Inverter response to capacitor switching. A 1200kVAR capacitor bank is switched in at T = 0.6s.

5.4 Task 5: Integrated Distribution Grid Control

The voltage spatial behavior and power quality of a distribution system depends on load characteristics, generation dynamics, and installed equipment along the circuit. As will be identified in Task 2, certain PV installation scenarios may not be manageable without external communication to other locations on the distribution circuit/ substation. Integrated distribution grid control will be evaluated in this task to determine the extent and complexity needed to address these PV installation cases. The goal is to develop a simple integrated distribution grid control strategy that utilizes communication between available monitoring points (i.e. smart meters and substation) and actuators (PV inverters) to increase PV integration flexibility. PG&E will provide insights into components that can be practically controllable (i.e., transformers, capacitors) in addition to PV inverters. Since each substation autotransformer typically feeds multiple circuits, the voltage cannot be manipulated independently for each circuit and will require communication among adjacent circuits. On the other hand, it may be possible to manipulate circuit capacitors as long as the whole circuit remains within operating requirements.

Developed control strategies will be tuned and evaluated through implementation in developed grid system models for each of the three scenarios.

5.4.1 Steady State Results to T3 Fixes

In the previous section, a commercial circuit (Cayetano) and a residential circuit (Menlo) were analyzed for varying levels of penetration and spatial distribution of PV. The results of the analysis revealed that High-Pen PV does have an influence in the operation of the circuit and in some cases a negative influence. Certain distributions of PV generation led to non-standard high and low voltages. High-Pen PV was also shown to interact the sub-stations Load Tap Changing transformer and power factor in all cases.

This section focuses on progressive steps to overcome these negative influences on voltage and equipment on the primary feeder. Below steps are proposed to potentially correct the observed deficiencies of the Cayetano and Menlo circuits. For each step proposed, an example of the method is applied and then analyzed to the original case. The goal is to show improvement of the deficiency towards normal operation standards, but the example presented may not push the system back to acceptable operation conditions.

5.4.1.1 High Voltage

In the High Voltage Results section (5.2.2.1A), the Menlo End generation distribution scenario demonstrated out-of-standard high voltage conditions for all penetrations. The analysis of the high voltage conditions revealed the cause is due to the construction and location of the generation in the circuit. With the generation sited at the end of the circuit, the DG bus (bus 39) is prone to high line impedance and excess generation capacity leading to a reverse power-flow conditions. The first approach to enable higher penetrations of PV at bus 39 is to re-conductor the line with thicker (low impedance) conductor. The second approach is to us the Voltage Rise Siting score criteria to evaluate sites suitable for high penetration of PV on the Menlo circuit. The approaches are detailed below. The execution of the proposed steps below do not fully corrects the high voltage issue, but would if carried out further.

A. Line Re-Conductor

As described in RPF Voltage Rise characteristics section (B.1), the upstream line resistance in which RPF excess capacity flows through is a critical component in the amount of voltage rise seen at the DG bus. Higher RPF line resistance equates to more RPF induced voltage rise. It was also identified the importance of the line resistance of the DG bus. All excess capacity current flowing upstream will travel the DG bus line section and incur the largest voltage drop. The approach in this section to correct the out-standard high voltages, as seen for the Menlo End generation distribution scenarios, is by re-conductoring the DG bus (bus 39) with thicker, low impedance conductor. The Menlo End point generation is sited on bus 39, which is located at the end of the first feeder branch, as shown in Figure 99.

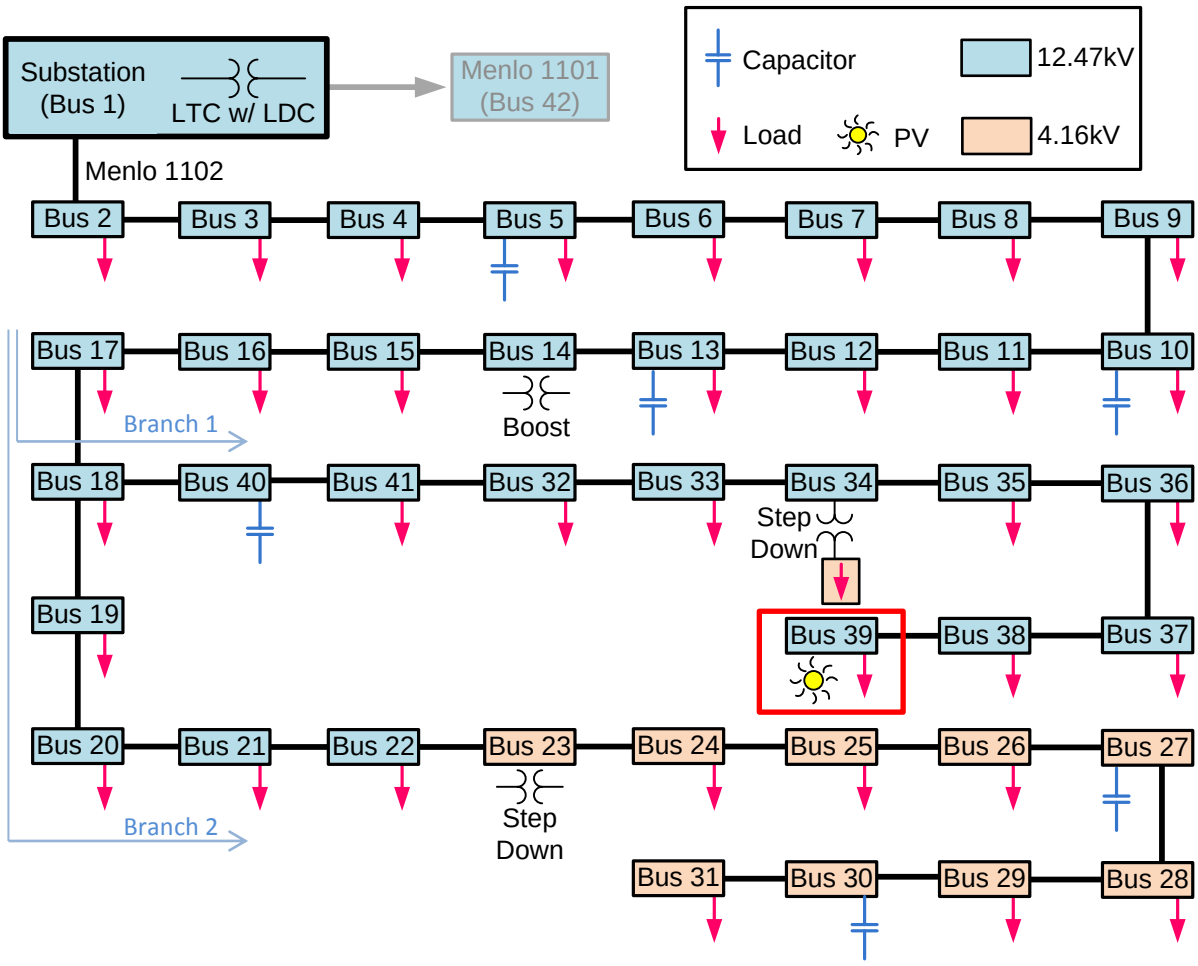

Figure 99. The Menlo circuit block diagram.

Originally, bus 39 was conductored primarily with #4 Aluminum Conductor Steel Reinforced (ACSR). #4 Aluminum ACSR is a stranded conductor with approximately 0.25 inch diameter with a positive sequence line resistance of 0.468 Ω/1000ft. The bus was re-conductored to match bus 38 with 1/0 stranded copper. 1/0 stranded copper is approximately 0.37 inches in diameter with a positive sequence line resistance of 0.117 Ω/1000ft. The line length of bus 39 is 5320 feet, so the line resistance changes from 2.5 Ω to 0.62 Ω after re-conductoring. As a result, bus 39's sub-station resistance ($R_{S/S}$) and the DG bus line resistance ($RPF_{R,0}$) is significantly lower, as shown in Table 54 and Figure 100. Therefore we expect less DG induced voltage rise than the original scenario.

Scenario	Bus 39 $RPF_{R,0}$ [Ω]
Original	2.5
Re-conductored	0.62

Table 54. Before and after bus 39 is re-conductored.

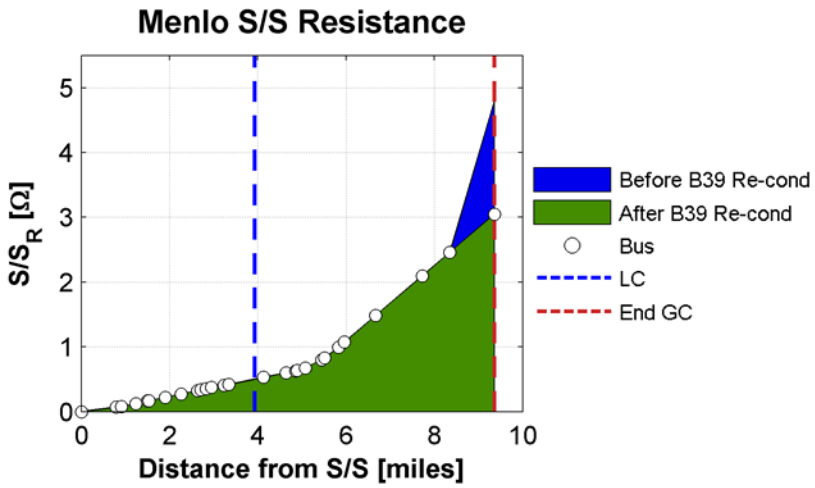

Figure 100. The cumulative Menlo branch 1 sub-station resistance ($R_{S/S}$) before and after the re-conductoring of bus 39.

The simulation results of the re-conductored Menlo End scenarios are shown in Figure 101. The re-conductored scenarios exhibit lower maximum voltages in the PV region as penetration increased, but the voltages still out-of-standard high voltages. At 100% penetration, the re-conductored scenario reduces the amount of voltage rise by 7% from the original case. In this example re-conductoring did not solve the high voltage problem, but did demonstrate improvement of the high voltage condition and is a viable solution for a site that has a marginally high voltage problem.

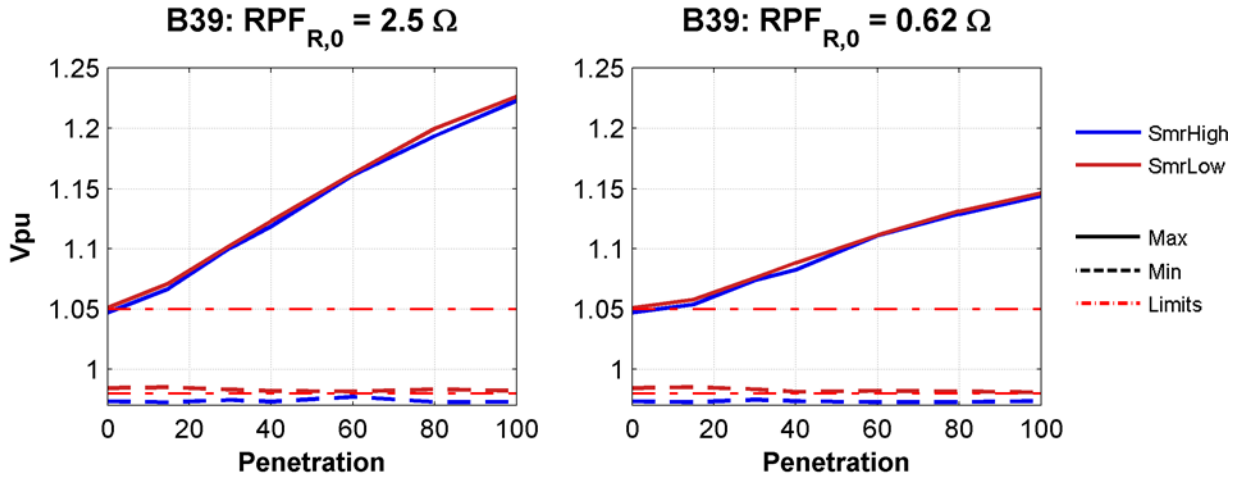

Figure 101. The Menlo End distribution maximum and minimum bus voltage in the PV region versus penetration before and after bus 39 reconductoring.

B. Siting

In the analysis presented in the High Voltage Results section (5.2.2.1A), the Distributed Generation (DG) induced voltage rise siting characteristics where individually analyzed to describe the high voltage condition of the Menlo End generation distribution scenario. An alternative approach to analyzing the

isolated characteristics of DG induced voltage rise is to use the Voltage Rise Siting (VRS) scoring criteria as presented in section (5.2.1.3B.C.1). The VRS score takes into consideration the load distribution, line impedance, and reverse power flow (RPF) factors and forms a qualitative score to enable a comparison between buses of circuits. A bus with a higher VRS score is interpreted to have more DG induced voltage rise than a bus with a lower VRS score. Contrary to the approach presented the previous section (re-conductoring), this approach presented below is a preventative measure to avoid high voltage situations utilizing VRS to identify buses prone to DG induced high voltage.

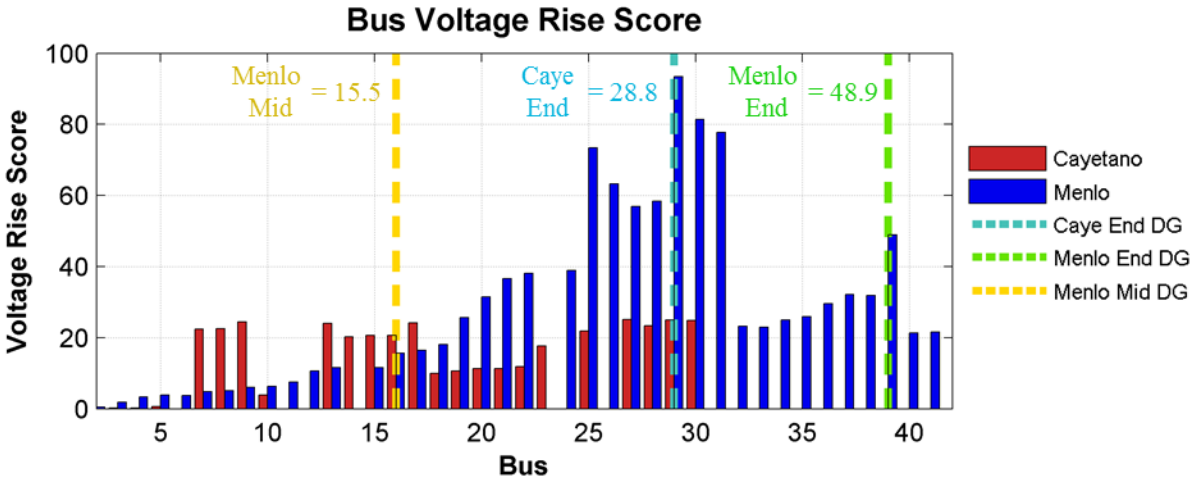

Figure 102. The bus voltage rise score calculated for equivalent Cayetano and Menlo circuits. The score was calculated with for an effective voltage is 21kV and a peak load of 12MW at 50% DG penetration.

For example, a comparison between the Cayetano End, Menlo Middle, and Menlo End scenarios may be shown using VRS. The calculated VRS score comparing the Cayetano and Menlo circuits is shown in Figure 102. To enable a comparison between the circuits, the line impedance was calculated at an effective impedance of 21 kV, the peak load was 12MW with a 50% DG penetration, and the score was normalized using the maximum component values between both circuits. The Cayetano End point generation is sited on Bus 29, the Menlo Middle on Bus 16, and the Menlo End on bus 39. By observation of Figure 102, we can see the Menlo bus 39 VRS score is much higher than the Cayetano bus 29 and Menlo bus 16. This indicates the voltage rise is significantly higher as PV penetration increases at the Menlo bus 39 than the Cayetano bus 29 and Menlo bus 16. This conclusion is supported by the results and analysis presented in the High Voltage Results section (5.2.2.1A). By observing the VRS score, high penetration of point generation should not be sited at Menlo bus 39 since it is prone to DG induced voltage rise.

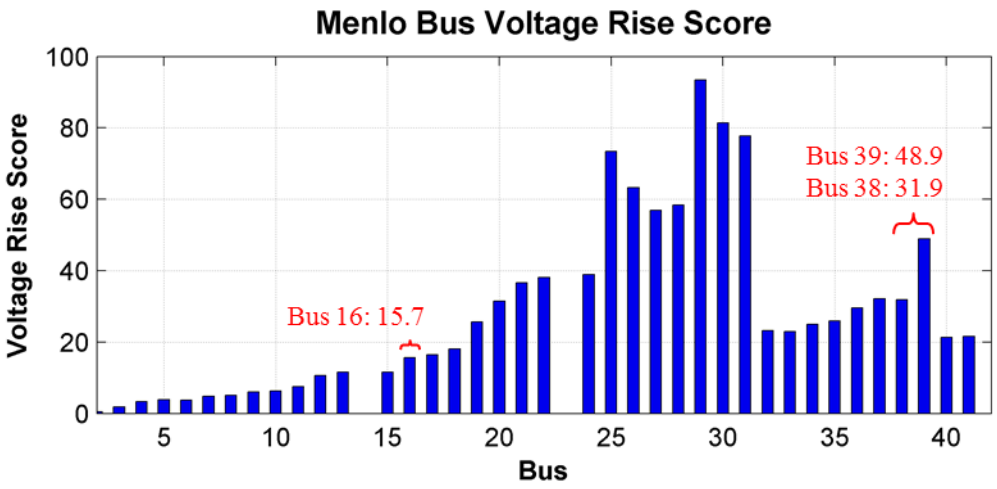

Figure 103. Menlo Bus Voltage Rise Score. The score was calculated with for an effective voltage is 12.47kV and a peak load of 9.1MW at 50% DG penetration.

Applying the VRS score to the Menlo circuit exclusively, we will evaluate buses 16, 38, and 39. Observing Figure 103, the VRS score for the Menlo circuit is calculated using an effective impedance of 12.47kV, 9.1 MW peak load demand with 50% penetration, and normalized to the Menlo circuits maximum VRS component values. The respective scores for bus 16, 38, and 39 is 15.7, 31.9, and 48.9. The component values and normalization factors used in the VRS calculation are shown in Table 55. From the VRS score, we can identify bus 39 to have the highest amount of DG induced voltage rise and bus 16 the lowest. Given the disparity of the scores, we can also expect to see a significant difference in the amount of voltage rise seen at each bus.

Bus	**RPF_{PEN} [%]**	**RPF_{R} [Ω]**	**RPF_{R0} [Ω]**	**$R_{S/S}$ [Ω]**	***VRS***
16	42.9	0.11	0.11	0.53	15.7
38	3.7	2.04	0.36	2.46	31.9
39	2.4	4.38	2.34	4.80	48.9
Normalization Factor	100	19.03	4.43	19.45	

Table 55. Voltage Rise Score components for the Menlo Buses 16, 38, and 39.

To evaluate the claim above, a point PV installation was evaluate at bus 16 (Menlo Middle), bus 38, and bus 39 (Menlo End) for PV penetrations ranging from 0 to 100. The maximum and minimum voltages in the PV region versus penetration are shown in Figure 104. Bus 39 demonstrates the highest amount of DG induced voltage rise followed by bus 38 and then bus 16, as expected. Bus 38's peak voltage in the PV region is 11% lower than Bus 39 and Bus 16 is 18% lower. It should also be observed that DG sited at bus 38 would enable penetrations up to 15%: an improvement over bus 39 (0%).

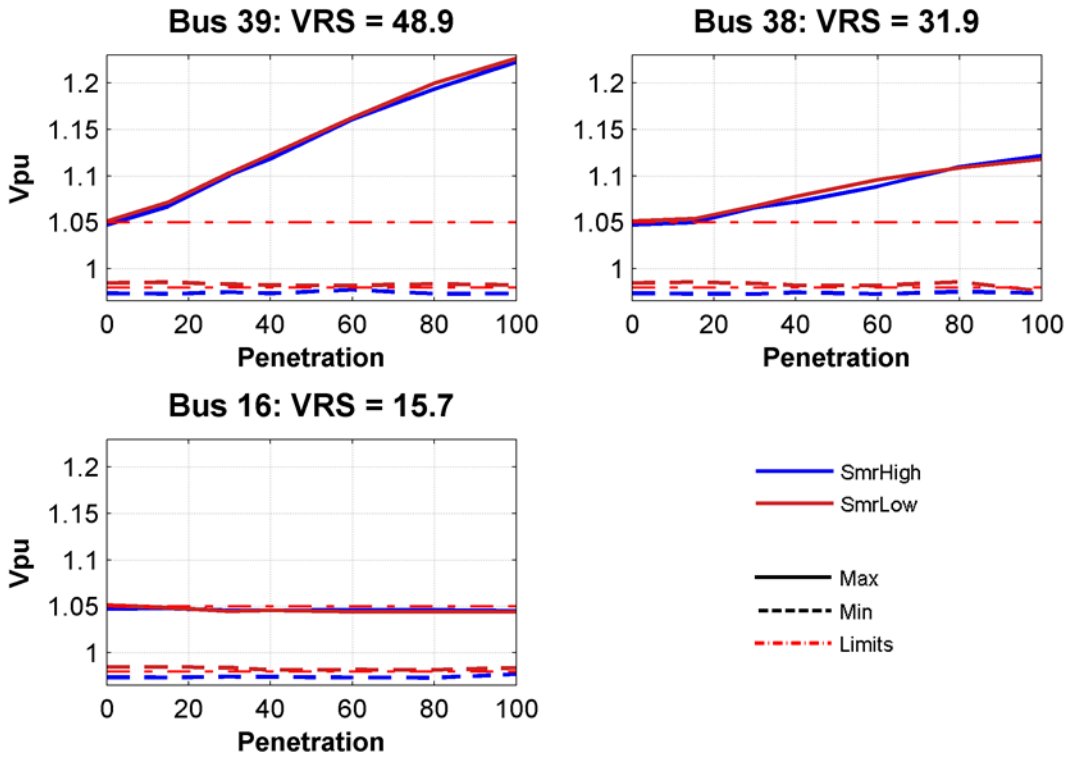

Figure 104. The bus voltage extremes in the PV region for the Menlo with point generation at Bus 39, Bus 38, and Bus 16.

Given the confirmation of the VRS score above, siting high penetrations of DG at buses with a large VRS score, such as bus 38 and 39, could invoke out-of-standard high voltage conditions. The evaluation above demonstrated that bus 38 with a VRS score of 31.9 would produce out-of-standard voltages at PV penetration higher than 15%, which is an improvement to bus 39 with a VRS score of 48.9. The VRS scoring criteria can be a useful tool to form a qualitative to understand the portions of the circuit prone to DG induced voltage rise. Utilizing the tool, buses may be immediately removed from consideration for siting of high penetrations of DG; a step that would have prevented DG being sited at bus 39 in the Menlo End scenario. This approach is a preventative measure that could be used to encourage portions of the circuit resilient to DG induced voltage rise and discourage portion prone to voltage rise.

5.4.1.2 Low Voltage

As discussed in Low Voltage Results section (B), the Menlo Beginning scenario experienced a low voltage condition for penetration greater than 40%. The cause of the low voltage conditions is due to two factors: 1) the Load Tap Changer (LTC) with Load Drop Compensation (LDC) sub-station transformer lowering the system voltage as penetration increases, and 2) the high effective line impedance in the 4.16kV section at the end of Menlo's second branch. Three approaches to remedy the low voltage condition to enable higher penetrations of PV are presented below. The first is to raise the operation voltage from 4.16kV to 12.47kV at the end of Menlo's second branch. The second approach is to place a line regulator at bus 23 to regulate the 4.16kV section independently from the sub-station voltage

regulation. The final approach is to modify the LDC controls to prevent down tapping caused by PV generation.

A. Raise System Voltage

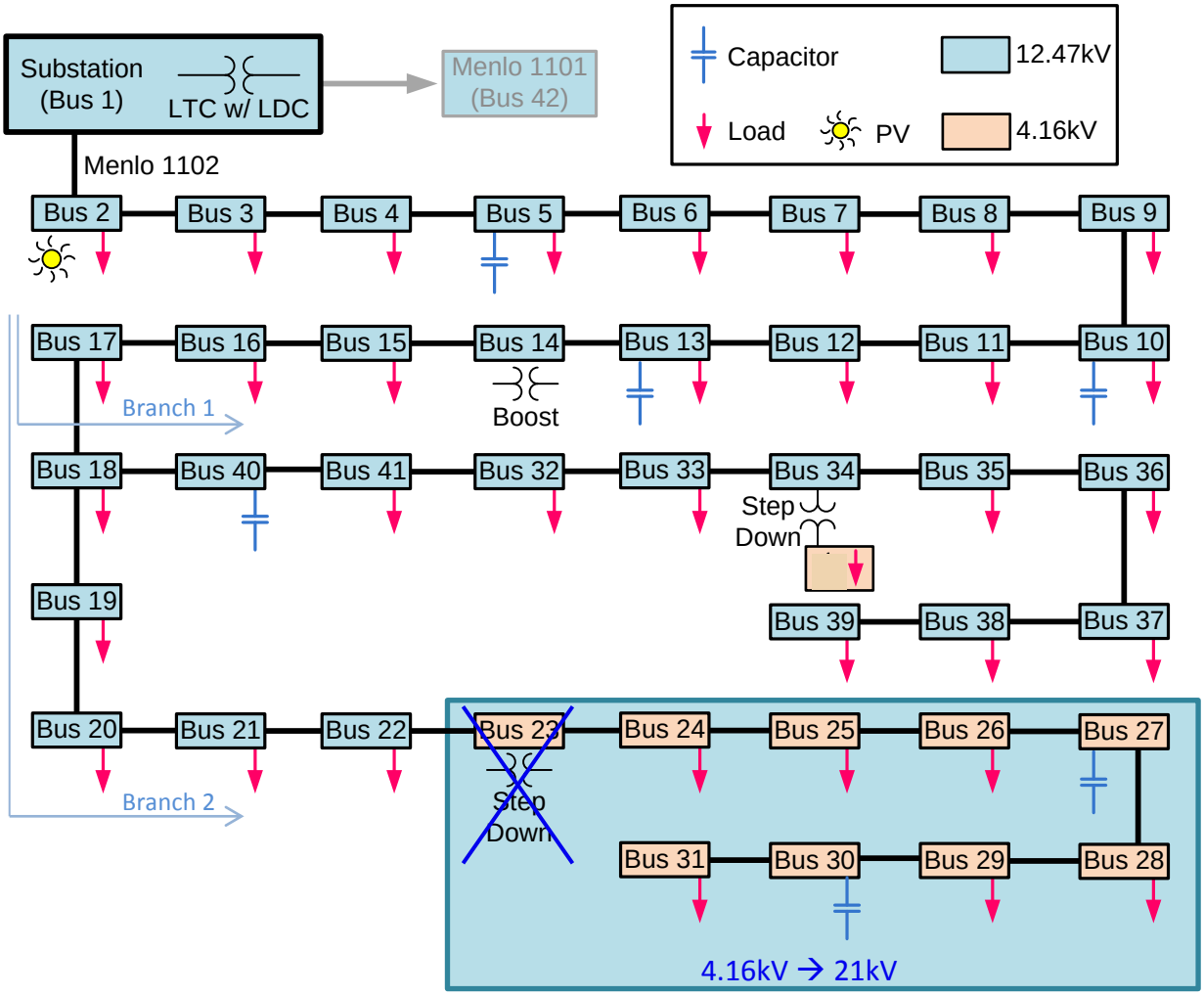

Figure 105. The Menlo circuit block diagram displaying the system voltage modification of the 4.16kV section at the end of the second branch.

In this section, the approach to remedy the low voltage condition is to lower the effective line impedance at the end of Menlo's second branch. Observing Figure 105, the operating voltage of buses 24 through 31 was changed from 4.16kV to 12.47kV. As result, the step down transformer found at bus 23 is no longer needed and removed.

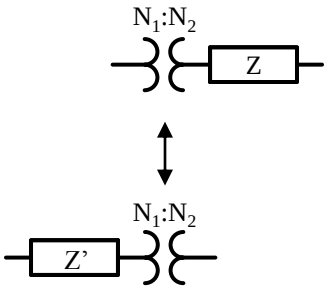

Figure 106. Equivalent Impedances.

$$Z'_{12.47kV} = \left(\frac{N_1}{N_2}\right)^2 \cdot Z_{4.16kV} \qquad \text{5-103}$$

As discussed in the Voltage Drop Approximation section (A), line drop is a function of line current and line impedance. By raising the system voltage, the amount of line current will decrease for the same amount of load demand; this results in less line drop. Given that line current changes dynamically during the day while line impedance remains constant, a discussion about the raising the system voltage using line impedance is less ambiguous than a discussion using line current. In terms of effective line impedance, the 4.16kV section line impedance ($Z_{4.16kV}$) is approximately nine times greater than the line impedance in an equivalent 12.47kV ($Z_{12.47kV}$), as shown in equation 5-103. Therefore, by raising the operation voltage of a 4.16kV section, the effective line impedance is reduced by a factor of nine. Also, by raising the system voltage, the impedance of the 12.47 to 4.16 (delta to wye grounded) step-down transformer is removed. Observing Figure 107, we see the cumulative sub-station line impedance ($Z_{S/S}$) for the Menlo's second branch before and after the 4.16kV section was raised to 12.47kV. By raising the system voltage, the cumulative sub-station line impedance is lowered from 24.6Ω to 6.6Ω. By lowering the line impedance, we are therefore lowering the amount of line drop seen at the end section of branch 2.

Scenario	Bus 31 $Z_{S/S}$ [Ω]
4.16kV	24.6
12.47kV	6.6

Table 56. Sub-station line impedance before and after the system voltage modification.

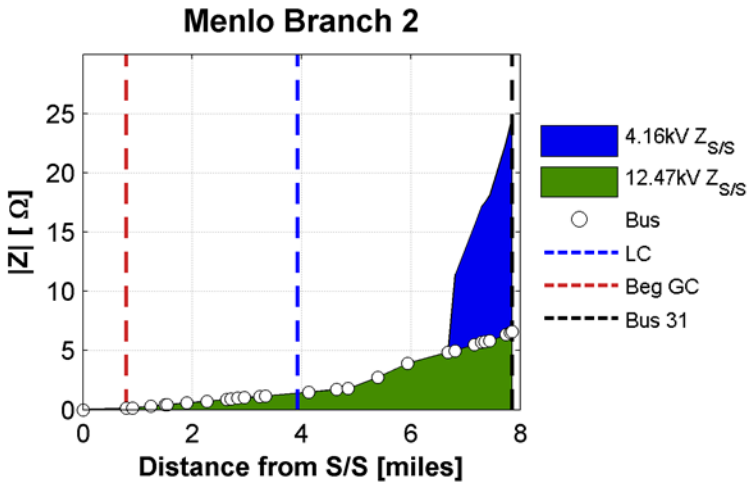

Figure 107. The cumulative line impedance of branch 2 of the Menlo circuit before and after the 4.16kV section was changed to 12.47kV.

Figure 108 contains the maximum and minimum bus voltages in the PV region for the Menlo Beginning generation distribution scenarios. At 100% penetration, the Summer High day improved from an out-of-standard 0.9481V_{pu} in the 4.16kV scenario to 0.9715V_{pu} in the 12.47kV scenario, as shown in Table 57.

The minimum bus voltages are marginally below the 0.98Vpu threshold and not considered a low voltage condition.

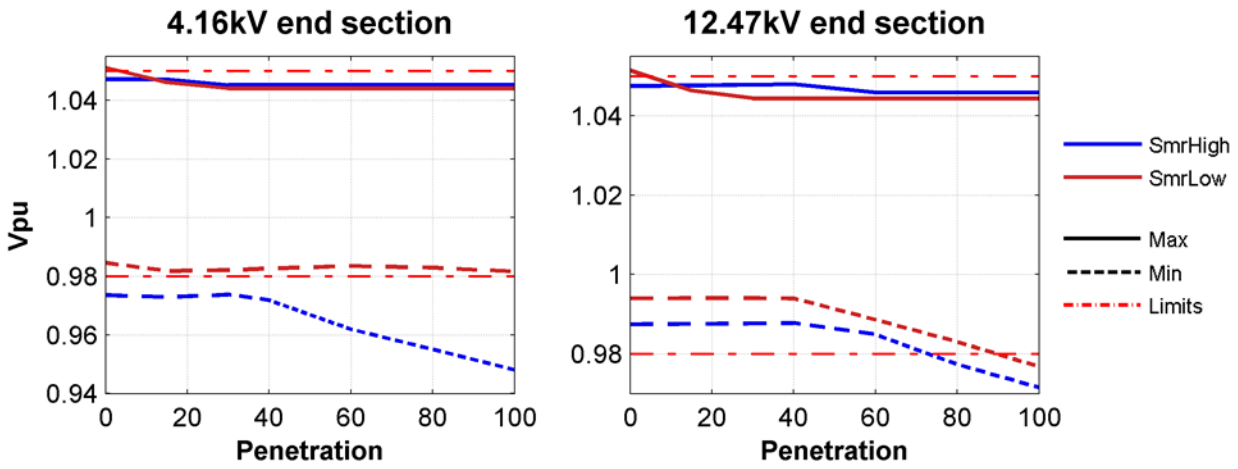

Figure 108. The bus voltage extremes in the PV region for the Menlo Beginning scenario with the Branch 2 end section as 4.16kV end 12.47kV.

Scenario	Characteristic Day	Minimum Bus Voltage in PV region [per unit]	
		0%	*100%*
4.16kV	Summer High	0.9735	0.9481
	Summer Low	0.9845	0.9817
12.47kV	Summer High	0.9874	0.9715
	Summer Low	0.994	0.9771

Table 57. The bus voltage minimum in the PV region for the Menlo Beginning scenario at 0% and 100% with the Branch 2 end section as 4.16kV end 12.47kV.

In the 12.47kV scenario, we see the voltage begin to decrease with penetration at 40% for the Summer Low day and at 60% for the Summer High day due to the LTC w/ LDC operation. In the 4.16kV scenario, we only see this behavior for the Summer High day beginning a 40% penetration, but not the Summer Low day. As discussed in Voltage Control Equipment: Capacitors section (A), the bus 30 capacitor bank with Time-Clock and Voltage Override controls switched on during the day due to a local low voltage condition at the bus (4.16kV scenario). The duration the capacitor remained on increased as penetration increased. The on-line bus 30 capacitor bank would raise the voltage in the 4.16kV section and assisted in voltage regulation, especially in the Summer Low day case. For the 12.47kV scenario, the bus 30 capacitor controls did not sense a low voltage condition and remained off for all penetration past the baseline (0%), as seen in Figure 109.

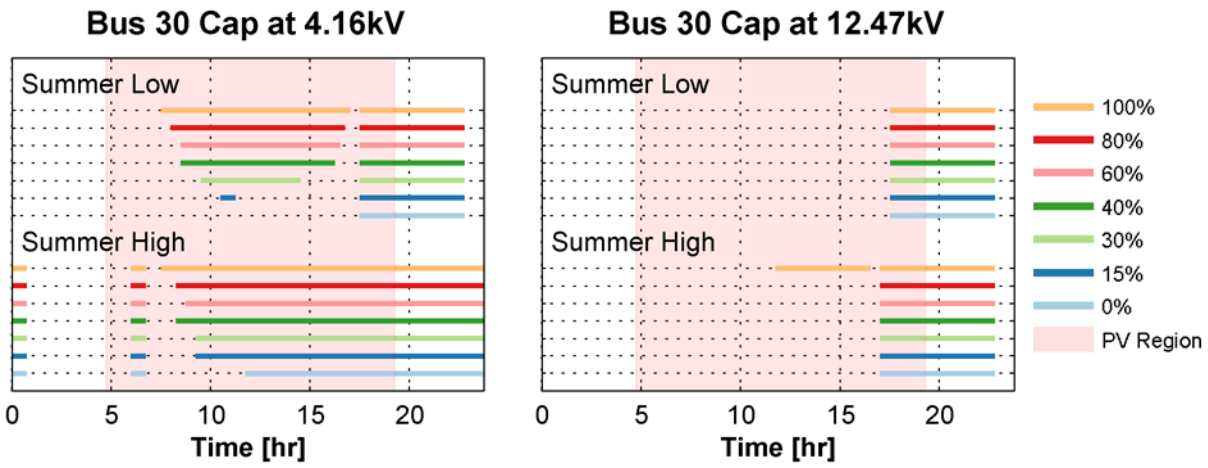

Figure 109. The Menlo Beginning scenario Bus 30 Time-Clock with Voltage Override switching controls switch profile before and after the 4.16kV section was changed to 12.47kV.

In summary, the LTC w/ LDC is again observed to be the cause of the decreasing minimum voltage as penetration increases in the Menlo Beginning scenarios. By raising the operation voltage from 4.16kV to 12.47kV at the end of branch 2, the line drop seen at buses 23 through 31 decreased resulting with the bus voltage remaining in regulation. The solution addresses the high impedance found at the end of the Menlo circuit, and extends the PV penetration from 40% to 100%. The solution presented is response to the specific construction the Menlo circuit.

B. Line Regulator

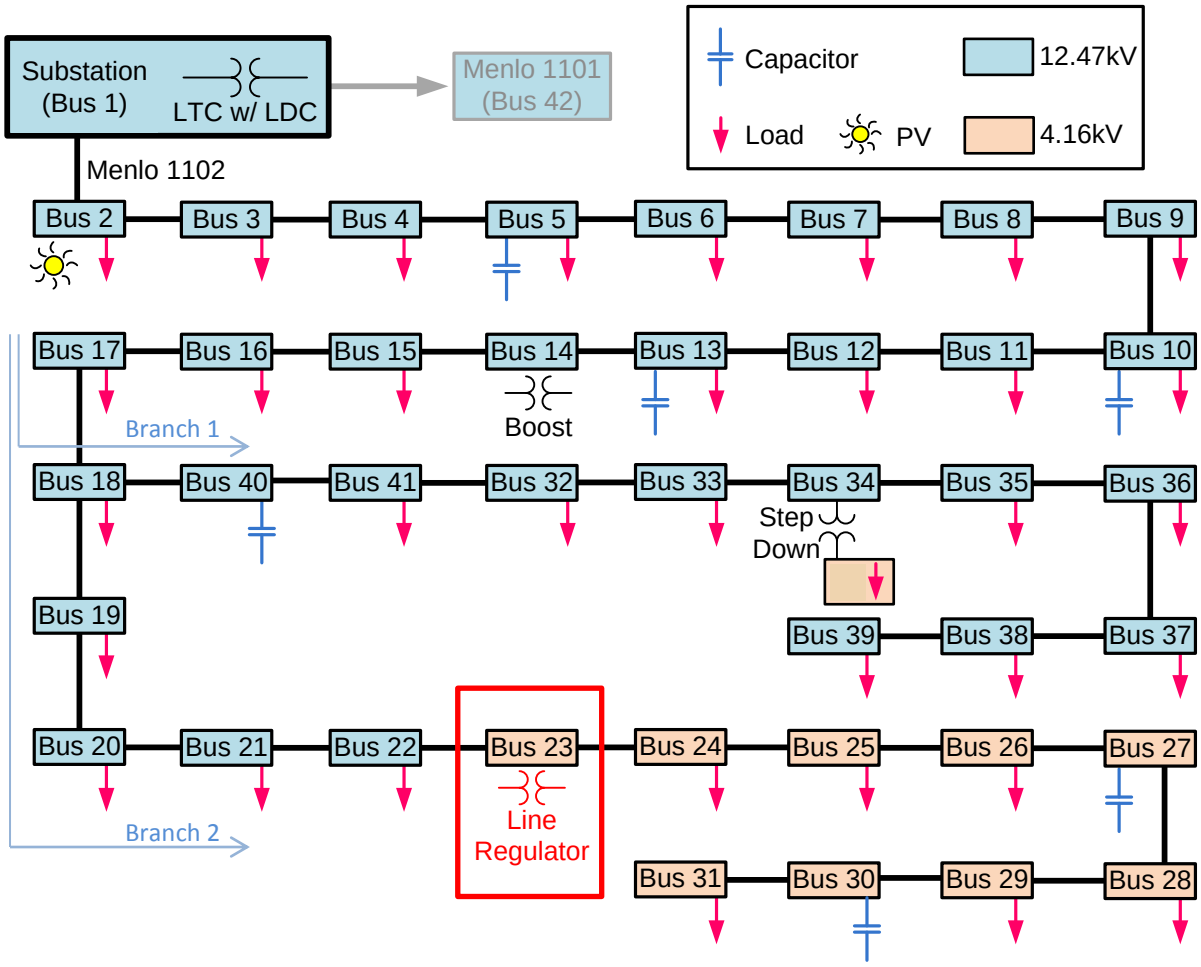

Figure 110. Menlo Beginning generation distribution scenario with Line Regulator.

In this section, a Line Regulator (Figure 110) is used to correct the low voltage condition experienced in the Menlo circuit's 4.16kV section at the end of the second branch. Instead of a fixed step-down transformer at bus 23, a line regulator utilizing Load Drop Compensation (LDC) is used. The settings for the LDC of the line regulator were empirically derived and presented in Table 58.

Parameter	Menlo
Voltage (kV_{L-L}]	12.47:4.16
Nameplate [MVA]	1
Impedance [Ω%]	j0.05
Regulation [%]	±10
Steps	32
V_{LC} [V_{120}]	121
R [Ω]	4
X [Ω]	3
Band [V_{120}]	±1.4
CT ratio	100:1
PT ratio	20:1

Table 58. Line Regulator Load Drop Compensation settings.

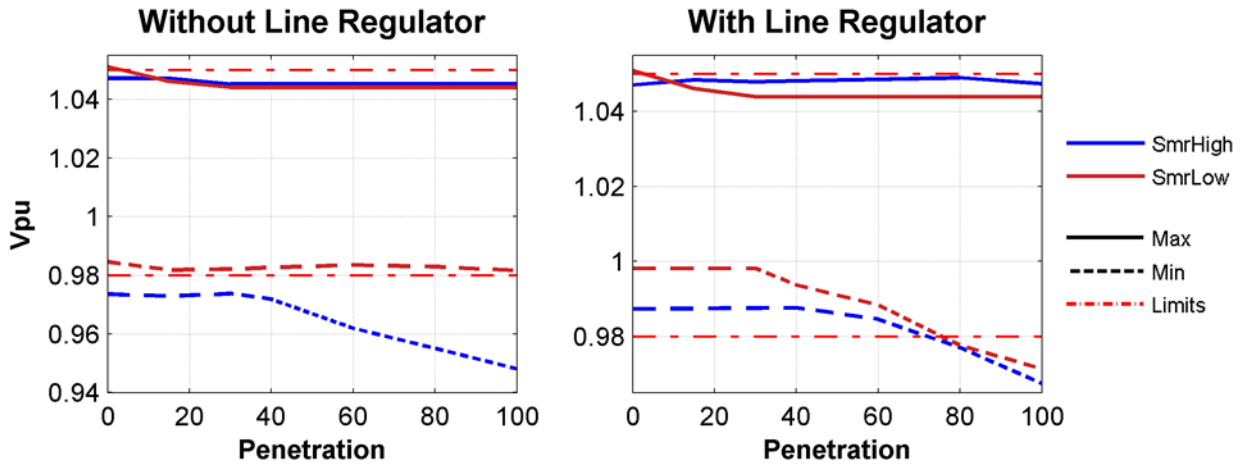

Figure 111. The bus voltage extremes in the PV region for the Menlo Beginning scenario with and without a Line Regulator.

Figure 111 contains the maximum and minimum bus voltages in the PV region for the Menlo Beginning distribution scenarios. At 100% penetration, the Summer High day improved from an out-of-standard 0.9481V_{pu} in the original scenario to 0.9674V_{pu} with the use of a Line Regulator, as shown in Table 59. While this is an improvement in regulation, it is still considered an out-of-standard low voltage condition for the Line Regulator at 100% penetration, but the Line Regulator did enable higher penetrations of PV. The minimum bus voltage for original Menlo Beginning Summer High scenario decreased past 0.97V_{pu} (marginal low voltage) at an approximately 40% penetration and the scenario with a Line Regulator decreased past 0.97V_{pu} at approximately 90% penetration.

Scenario	Characteristic Day	Minimum Bus Voltage in PV region [per unit]	
		0%	*100%*
No Line Regulator	Summer High	0.9735	0.9481
	Summer Low	0.9845	0.9817
Line Regulator	Summer High	0.9873	0.9674
	Summer Low	0.9981	0.9718

Table 59. The bus voltage minimum in the PV region for the Menlo Beginning scenario at 0% and 100% with and without a Line Regulator regulating end section of Menlo's second feeder branch.

The low voltage condition for the Menlo Beginning Line Regulator scenario for penetrations greater than 90% did not occur in the buses located in the 4.16kV section, but in bus 14 which is upstream of the Line Regulator (bus 23). Observing Figure 112, we see the bus voltage range during a Summer High day with and without a Line Regulator. The regulation of the 4.16kV section ranged from 1.0274V_{pu} to 0.9487V_{pu} without the Line Regulator and 1.047V_{pu} to 1.003V_{pu} with the Line Regulator. However, bus 14's minimum voltage decreased from 0.971V_{pu} to 0.9671V_{pu}. As a Line Regulator increases the secondary windings voltage to maintain regulation, the current draw increases on the primary side of the Line Regulator. As a result, the line drop increases for buses upstream of the Line Regulator, resulting in lower voltages as seen with bus 14.

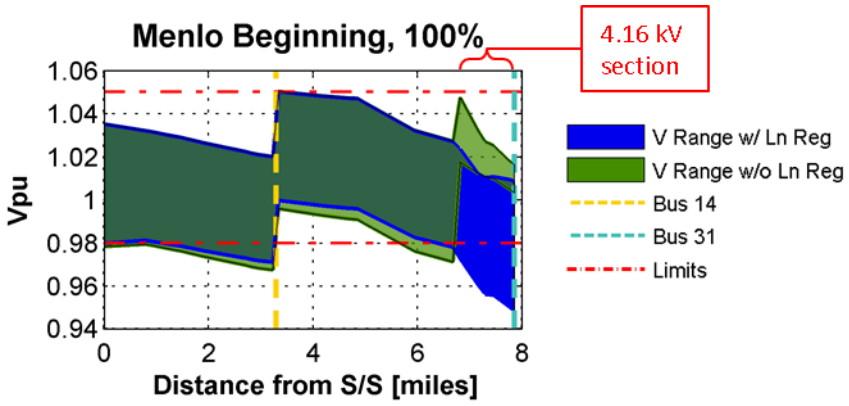

Figure 112. The branch 2 bus voltage extremes for the Menlo Beginning Summer High day scenario at 100% penetration with and without a Line Regulator.

In summary, the Line Regulator increased the penetration at which the low voltage condition occurred from 40% to 90%. This solution to the low voltage condition observed for the Menlo Beginning generation distribution scenario did extend the PV penetration limits, but is tailored the specific construction of the Menlo circuit.

C. LDC PV Current Compensation

Up to this point, the approach to correct low voltage conditions experienced by the Menlo Beginning generation distribution scenarios are specific to the Menlo circuit construction. As detailed in the Results - Low Voltage section (B), the combination of 1) the sub-station LTC w/ LDC decreases the sub-

station voltage as PV generation increases and 2) the lack of voltage rise support provided by PV generation located upstream of the load results in a possible low voltage condition at the end of the feeder. Instead of correcting the voltage regulation at the end of the feeder, this approach modifies the LTC w/ LDC tapping behavior to prevent down tapping caused by PV generation.

$$I_{m,comp} \approx \frac{I_{LD} - I_{PV} + I_{PVest}}{CT}, \quad I_{PV} \approx I_{PVest} \qquad \textbf{5-104}$$

$$I_{PVest} = \frac{P_{PVest}}{3PT \cdot V_m} \qquad \textbf{5-105}$$

$I_{m,comp}$ → Compensated sub-station current measurement [A]
I_{LD} → Circuit-wide load demand current [A]
I_{PV} → Circuit-wide PV generation current [A]
I_{PVest} → Estimated circuit-wide PV generation current [A]
P_{PVest} → Estimated circuit-wide PV generation power [W]
V_m=V/PT → Sub-station line-to-neutral voltage measurement [V]
CT → Current transformer ratio
PT → Potential transformer ratio

High-Pen PV interacts with LDC controls via the local current measurement at the sub-station. As generation increases, the net measured current decreases given the load demand does not change as penetration increases. As the local current measurement decreases, LDC lowers the operating voltage resulting in the LTC tapping down, as shown with equations 5-84 and 5-85. With knowledge of the installed generation in the circuit, the distributed generation current (I_{PV}) contribution in the local sub-station measurement ($I_{m,comp}$) may be approximately compensated by adding an estimation of the PV generation current (I_{PVest}), as shown in equation 5-104. The DG current estimation is calculated using a time resolved estimate of the total DG power generation (P_{PV}) in the circuit and a local sub-station voltage measurement (V_m). PV generation may be estimated using solar irradiance as done in the calibration of the Cayetano and Menlo characteristic day models using SolarAnywhere irradiance estimates. The above description is referred to as LDC Current Compensation.

Circuit	PV Distr.	LC/GC
Cayetano	Beginning	6.5
	Middle	1.6
	End	0.85
	Radial	0.9
Menlo	Beginning	5.25
	Middle	0.95
	End	0.42
	Radial	0.89

Table 60. The LC/GC ratios of Cayetano and Menlo distribution scenarios.

As observed in the Results - Low Voltage section (B), the LDC interaction with High-Pen PV may potentially create a low voltage condition when the generation is located upstream of the load: the LC/GC ratio is greater than one. For circuits with this generation and load distribution topology, LDC Current Compensation is appropriate to use since it will prevent the LDC from down tapping with PV generation. Of the simulated scenarios in the research, the Cayetano Beginning, Middle, and Menlo Beginning generation distributions scenarios meet the above LC/GC ratio criteria (LC/GC > 1), as shown in Table 60.

Figure 115 is the summary of the results from the Cayetano Beginning, Middle, and Menlo Beginning simulations using LDC Current Compensation. The goal of LDC Current Compensation is to de-couple PV generations influence from the operation of the LDC controller to prevent unnecessary down tapping behavior for circuits with a Generation Center upstream of the Load Center (LC/GC > 1). Therefore the operation of the LDC Current Compensation has two expectations: 1) the LDC operation only marginally changes from baseline operation with increased penetration and 2) the maximum and minimum voltages will change only marginally with penetration given the lack of voltage rise support from generation located close the sub-station.

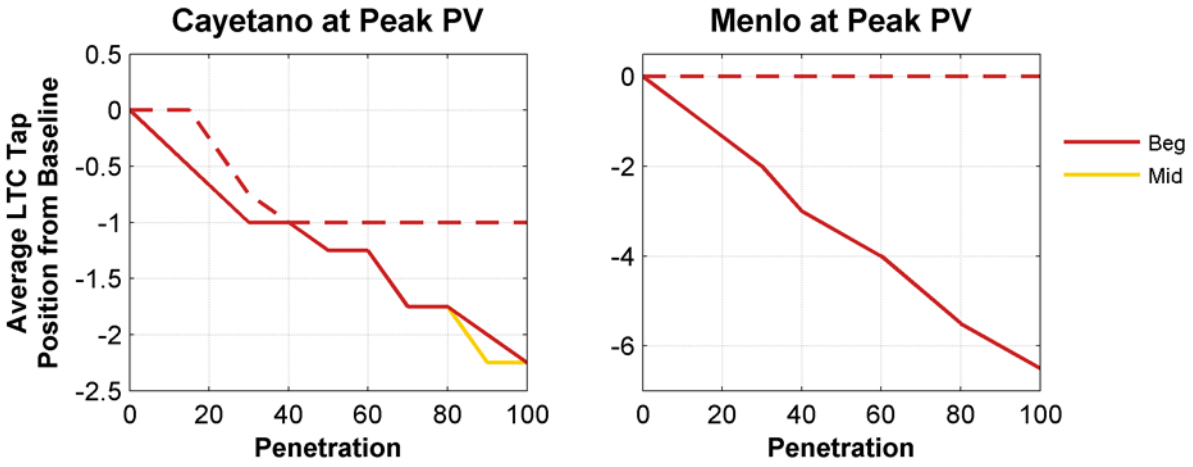

Figure 113. The difference in tap position from baseline at Peak PV time of day for the Cayetano and Menlo circuits.

Observing the average tap position change from baseline operation as penetration increases (Figure 113), both the Cayetano and Menlo with LDC Current Compensation show less down tapping at Peak PV. The Menlo circuit with LDC Current Compensation performed as expected with no change from the baseline operation, but the Cayetano did exhibit a marginal change. Observing Figure 114, we see the Cayetano Beginning Summer High day operation of the LDC control band and LTC tapping for baseline (0%) and 100% penetration with and without LDC Current Compensation. The operation of the 100% penetration without LDC compensation exhibits a definite change in the LTC tapping profile from the baseline case. However, the scenario with LDC Current Compensation has a tapping profile similar in shape to the baseline, only slightly shifted in the PV region. The slight change in the voltage profile is caused by the Beginning generation distribution, but the PV generation did not cause the LDC controller to tap the LTC down. Therefore the Cayetano with LDC Current Compensation's change from baseline operation is not due to down tapping caused by PV generation, but a slight delay in the timing caused by Beginning PV generations effect on sub-station voltage.

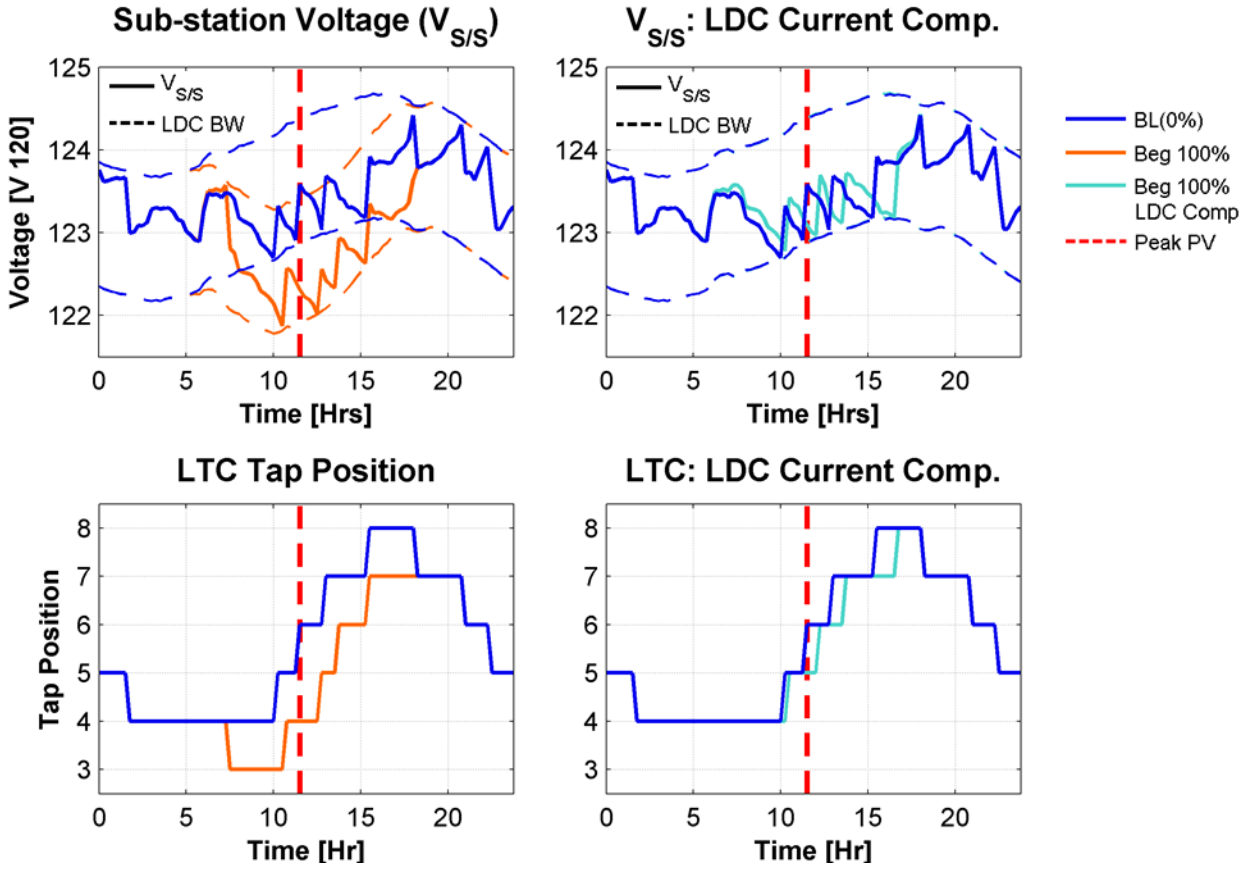

Figure 114. The sub-station voltage and tap position for Cayetano Summer High Beginning scenarios with and without LDC compensation in comparison with baseline operation.

Figure 115 illustrates the bus voltage maximum and minimum values in the PV region for the Cayetano Beginning, Middle, and Menlo Beginning scenarios with and without LDC Current Compensation. Without LDC Current Compensation, the scenarios are within standard voltage bounds with the exception of the low voltage condition exhibited by the Menlo Beginning Summer High day for

penetration greater than 40%. With current compensation, we see the maximum and minimum bus voltage ranges within standard voltage bounds and change only marginally with penetration. The low voltage condition exhibited by the Menlo Beginning Summer High day is now only marginally below the $0.98V_{pu}$ and not considered a low voltage condition. This result is in-line with the expectation for only a marginal change in voltage regulation extremes as penetration increases for circuits with a GC upstream of the LC (LC/GC > 1) coupled with an LTC w/ LDC featuring current compensation.

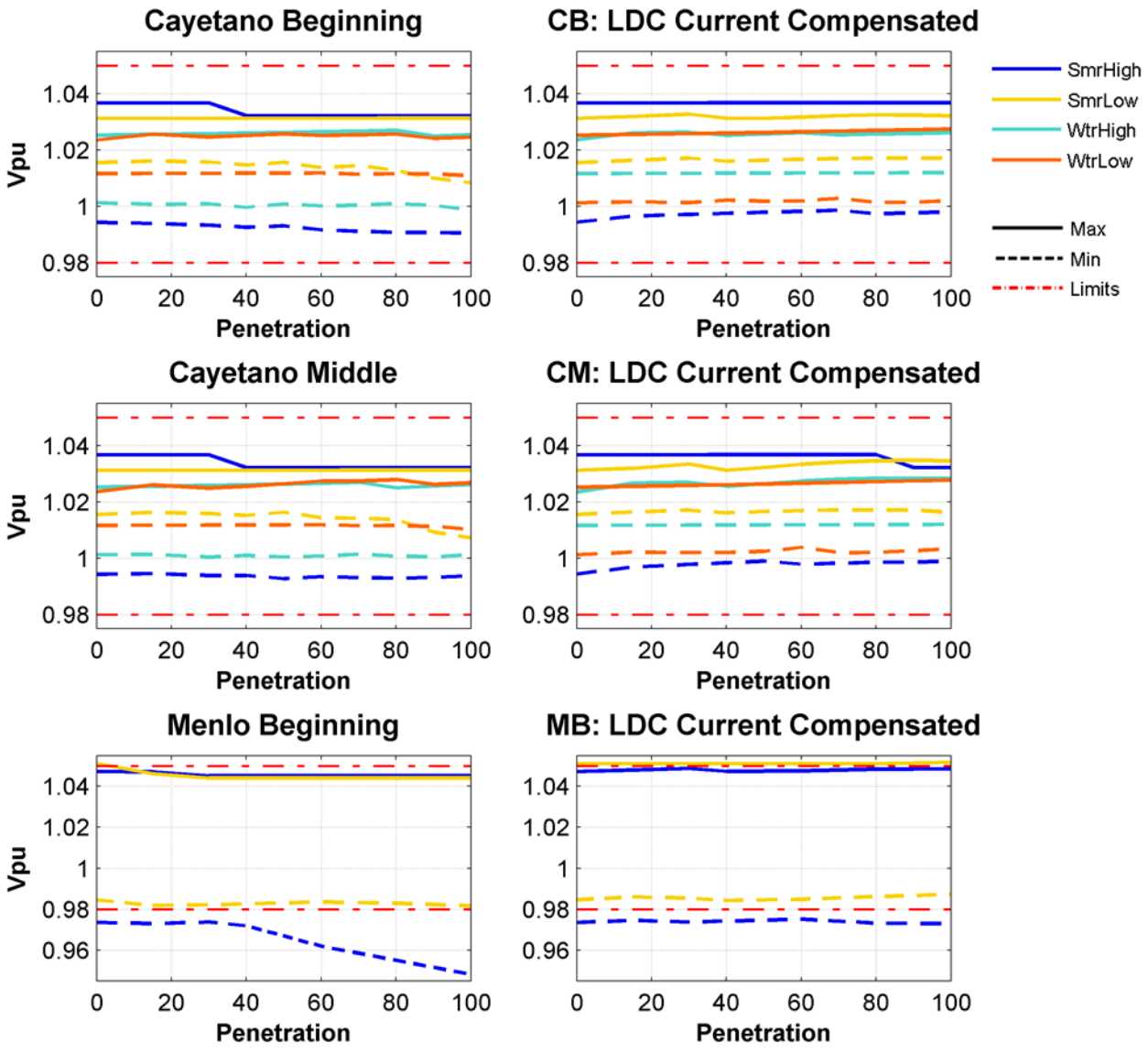

Figure 115. The bus voltage extremes in the PV region versus penetration with and without LDC Current Compensation for Cayetano and Menlo characteristic days with LC/GC > 1.

As presented in Voltage Control Equipment Results – Sub-station LTC w/ LDC section (B), the number of tap operations will increase as penetration increases in the Menlo and Cayetano circuits. Since the purpose of the LDC Current Compensation is to decouple the High-Pen PV from the operation of LTC w/

LDC, a potential benefit is the prevention of increased tap position operations as PV penetration increases. Since taps did not increases in the during the simulation the Cayetano Beginning, Middle, and Menlo Beginning scenarios with LDC Current Compensation, a projection of the yearly number of taps is shown in Figure 116. Observing Figure 116, the LDC Current Compensation enables a 40% reduction of total tap changes for the Cayetano circuit, and 78% reduction for the Menlo circuit.

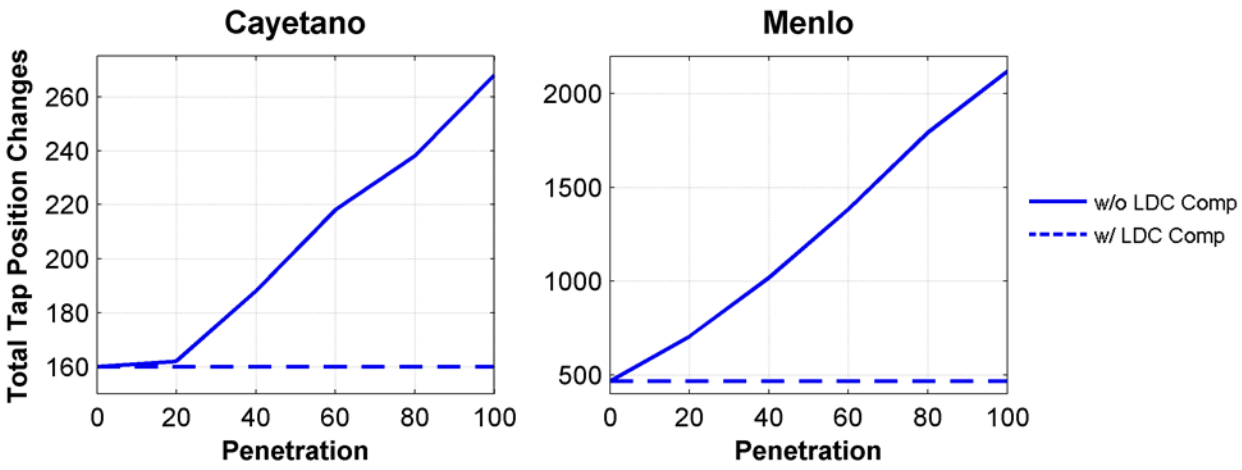

Figure 116. Projected benefit of LDC Current Compensation on total yearly taps for the Cayetano and Menlo scenarios with LC/GC > 1.

When applied to circuits with LC/GC ratio greater than one, LDC Current Compensation is shown to be effective at decoupling PV generation from causing LTC w/ LDC down tapping behavior as PV generation increases during the day. As a result, LDC Current Compensation when applied to the Menlo Beginning scenario corrected the before mentioned low voltage condition by preventing unnecessary LTC tap operations. The above analysis did not evaluate the estimation error tolerance of the presented method, but is left for further analysis in future work.

5.4.1.3 Power Factor Sensitivity

In the Sub-station Power Factor Results section (5.2.2.3), it was observed that as PV penetration increases the sub-station power factor decreases until the point of reverse power flow (at the sub-station). Furthermore, the sub-station power factor of characteristic Low days was observed to be more sensitive to the decrease in power factor as PV penetration increased. The decrease in sub-station power factor was only a marginal impact for characteristic High days. The effect of unnecessary reactive power support provided by Time-Clock controls resulting in exacerbating the decrease in power factor was also observed for both the Cayetano and Menlo circuits. While the operation of the Time-Clock switching controls did not impact the voltage regulation of the circuit, the controls did result in a non-standard sub-station power factor even for the baseline penetration, as shown for a Cayetano Summer Low day in Figure 117.

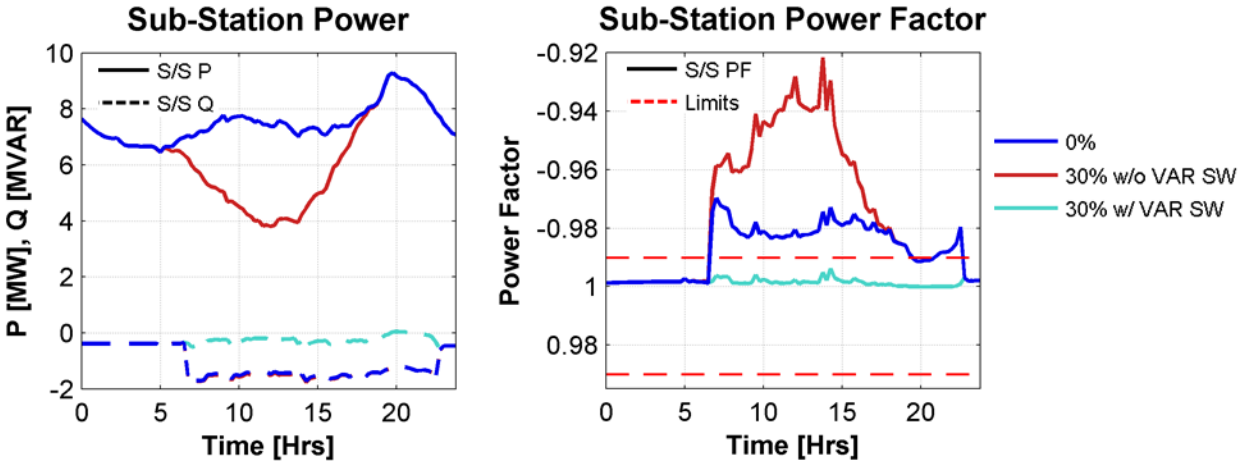

Figure 117. Cayetano Summer Low sub-station power and power factor profiles versus time with and with-out VAR capacitor switching controls.

Instead of Time-Clock (or Temperature) based switching controls that do not utilize feedback directly measured from the circuit, VAR switching controls were introduced instead. Since PV generation currently does not provide reactive power support, VAR based capacitor switching can provide reactive power support based on the measured circuits reactive load demand. For characteristic low days, the reactive power demand is much lower than on for characteristic high days. Via direct measurement, the switching profile of VAR based capacitor switching will switch when reactive power support is needed to maintain approximately unity power factor at the substation. Therefore, we should expect the decrease in power factor to be less for a circuit utilizing VAR based switching instead of Time-Clock or Temperature based switching.

All Time-Clock and Temperature (Time-Clock estimated) controls were replaced with VAR switching controls without change to the nameplate capacity. The bus controls and VAR switching settings are shown in Table 61, Table 62, Table 63, and Table 64. The calculations of high and low switching thresholds are detailed in VAR Control section (C.1.1). The hold-out time of the VAR switching controls are used to coordinate the various capacitor banks such that the capacitor banks located at the end of the feeder respond first.

Bus	NP [MVAR]	Smr High	Smr Low	Wtr High	Wtr Low
4	1.8	VAR	VAR	Off	Off
10	1.2	VAR	VAR	Off	Off
15	1.2	VAR	VAR	VAR	VAR
20	1.2	VAR w/ VO	VAR w/ VO	VAR w/ VO	VAR w/ VO
21	1.2	VAR w/ VO	VAR w/ VO	VAR w/ VO	VAR w/ VO
22	1.2	VAR	VAR	VAR	VAR
30	1.8	VAR w/ VO	VAR w/ VO	Off	Off

Table 61. Cayetano Capacitor Controls.

Bus	NP [MVAR]	Smr High	Smr Low
5	0.6	On	On
10	0.9	VAR w/ VO	VAR w/ VO
13	0.6	VAR w/ VO	VAR w/ VO
27	0.3	Off	Off
30	0.3	VAR w/ VO	VAR w/ VO
40	0.9	VAR w/ VO	VAR w/ VO

Table 62. Menlo Capacitor Controls.

Bus	NP [MVAR]	Control	VAR Thr [kVAR]			Voltage Thr [V_{120}]			
			High (On)	*Low (Off)*	*Hold out [min]*	*Low (On)*	*High (Off)*	*Mgn*	*Over-ride [min]*
4	1.8	VAR	1200	-1050	3.5	-	-	-	-
10	1.2	VAR	800	-700	3	-	-	-	-
15	1.2	VAR	800	-700	2.5	-	-	-	-
20	1.2	VAR w/ VO	800	-700	2	121	126	2.5	60
21	1.2	VAR w/ VO	800	-700	1.5	118	124	2. 5	60
22	1.2	VAR	800	-700	1	-	-	-	-
30	1.8	VAR w/ VO	1200	-1050	0.5	-	-	-	-

Table 63. Cayetano VAR switching capacitor settings.

Bus	NP [MVAR]	Control	VAR Thr [^oF]			Voltage Thr [V_{120}]			
			High (On)	*Low (Off)*	*Hold out [min]*	*Low (On)*	*High (Off)*	*Mgn*	*Over-ride [min]*
10	0.9	VAR w/ VO	600	-525	0.5	117.5	127	3	1
13	0.6	VAR w/ VO	400	-350	1	118.25	127	3.5	2
30	0.3	VAR w/ VO	200	175	2	117	126	4.5	3
40	0.9	VAR w/ VO	600	-525	1.5	121	127	2.25	3

Table 64. Menlo VAR switching capacitor settings.

The results of the Cayetano and Menlo circuit scenarios utilizing VAR switching capacitor controls is shown in Figure 118. The characteristic high days did not show a change from scenarios without VAR switching controls, but sub-station power factor of the characteristic low days decreased from the original circuit scenarios. However, the power factor did decrease as penetration increased up until reverse power flow occurred at the sub-station as observed before.

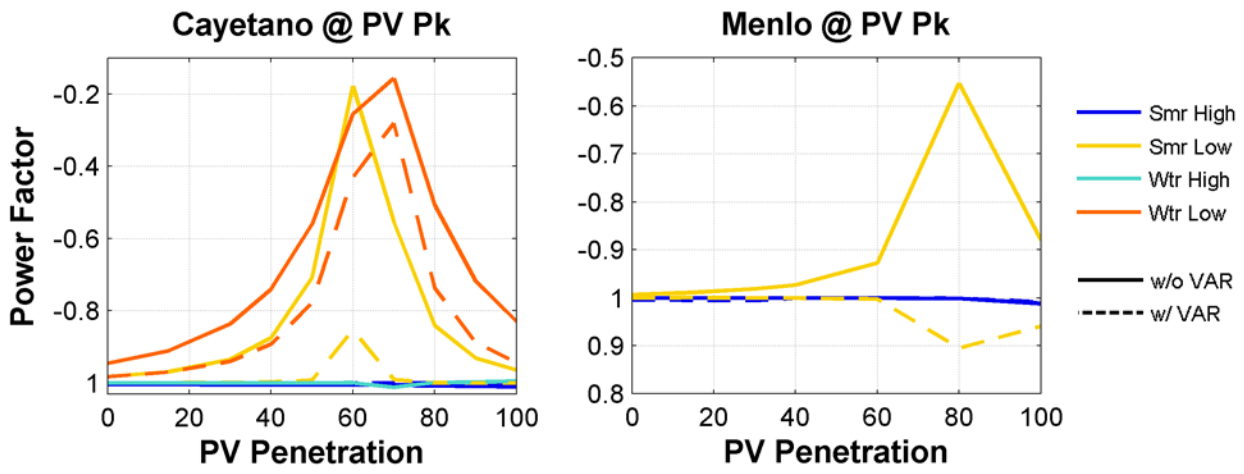

Figure 118. The sub-station power factor versus penetration for the Cayetano and Menlo circuits with and without VAR capacitor switching controls. (Note: PF < 1 → Lagging, PF > 1 → Leading).

As VAR switching controls proved to assist in slowing the decrease rate of sub-station power factor with PV penetration for characteristic low days, but at what cost of total switching operations? Table 65 is the total number of capacitor switching events the Cayetano and Menlo characteristic days at baseline penetration (0%). The scenarios utilizing VAR capacitor controls had an increase in total number switching operations for the Cayetano and Menlo Summer High days than the original capacitor switching portfolio. Conversely, the VAR control scenarios had less than equal to the number of switching operation to the original for all the characteristic low days and the Cayetano Winter High day. Typically, the number of characteristic high days are very few in number, so we can assume that total number of VAR switching events is less than or equal to the original total number of capacitor switching events.

Circuit	**Day**	**Total Capacitor switching events at Baseline penetration**	
		Original Cap Ctrl	*VAR Cap Ctrl*
Cayetano	Summer High	2	8
	Summer Low	2	0
	Winter High	4	0
	Winter Low	2	0
Menlo	Summer High	9	12
	Summer Low	8	8

Table 65. Total Capacitor switching events.

In summary, the observed condition of sub-station power factor decreasing to the out-standard limits was not corrected using VAR switching control. However, VAR switching control did slow the rate in power factor decreased as penetration increased (until reverse power flow at the sub-station) as compared to the original capacitor switching portfolio with Time-Clock control.

5.4.1.4 Summary

Presented above are progressive steps to correct the non-standard high voltages, low voltages, and power factor conditions observed at elevated PV penetrations in evaluation of a commercial and

residential results section (5.2.2). Below, the results of the applications of progressive steps is summarized.

The Menlo End generation distribution suffered from out-of-standard high voltage conditions during the PV region for elevated PV penetrations. The approach taken to remedy the high voltage conditions include 1) re-conductoring to lower the DG sites line impedance and 2) siting the DG bus as a preventive measure. The results of the approach are as follows.

1. Re-conductoring bus 39 from a high impedance #4 ASCR to a lower impedance 1/0 stranded copper distribution line resulted in a 7% decreases in peak voltage in the PV region at 100% penetration. The example did not enable more penetrations, but would if the Menlo circuit was re-conductoring beyond bus 39 to lower impedance conductor.
2. The Voltage Rise Siting score is a qualitative metric useful to identify buses prone to distributed generation (DG) induced voltage rise. Using the Menlo circuit VRS score, the generation at bus 39 (VRS = 48.9) in comparison to bus 38 (VRS = 31.9) showed an 11% improvement at 100% penetration. By re-siting the PV to a bus with a lower VRS score, PV penetrations up to 15% were enabled. Using the VRS score as a tool would be useful to identify and prevent siting high penetrations of PV at portions of the circuit prone to DG induced voltage rise.

The Menlo Beginning generation distribution scenario was observed to have non-standard low voltages in the PV region for penetration greater than 40%. The low voltage occurred on a low voltage (4.16kV) section of the Menlo circuit. To address the voltage issue three approaches were proposed: 1) raising the system voltage of the 4.16kV section, 2) apply a line regulator to the 4.16kV section, 3) modify the LDC controls to prevent down tapping. The results of the approach are as follows.

4. By raising the system voltage to 4.16kV to 12.47kV for the low voltage prone section, the low voltage condition was improved from 40% to 90% penetration. By raising the system voltage, the high impedance delta-wye step-down transformer could be removed and the effective line impedance of the section was reduced by a factor of 9.
5. The fixed step-down transformer was replaced for a Line Regulator. The Line Regulator utilized Load Drop Compensation (LDC) control, and improved the low voltage condition from 40% to 90% penetration.
6. The LDC controls of the Load Tap Changing (LTC) transformer were modified using LDC Current Compensation controls. The current compensation controls prevented the LDC to lower the system voltage due the PV generation. The application of the LDC Current Compensation control on the Menlo Beginning scenario enabled PV penetration for 40% to 100%.
7. The LDC Current Compensation controls was shown to be applicable to circuits with a LC/GC ration greater than one (LC/GC > 1), which is characteristic of circuits with generation located at the beginning of the circuit. When applied to qualified circuits (Cayetano Beginning and Middle, Menlo Beginning) for an entire year, a benefit of 40% reduction of total tap changes for the Cayetano circuit, and 78% reduction for the Menlo circuit.

It was observed that as PV penetration increases, the sub-station power decreases until the point of reverse power flow at the sub-station. It was also identified that characteristic low days are particularly sensitive to this phenomena and aggravated further by needless switching of Time-Clock capacitor switching controls. This low power factor condition was identified in both the Cayetano and Menlo circuits. To improve this condition, VAR switching controls replaced Time-Clock controls, but with mixed

results. The VAR switching controls did improve the power factor, but the power factor still reduced beyond standard levels at elevated PV penetrations. This power factor condition does not affect the operation of the circuit, but is outside of standards.

5.5 Task 6: Practical Feasibility and Outreach

Maintaining practical viability of the developed control strategies is critical for the project, and will be addressed through constant communication between the utility industry (PG&E), an academic institution (UCI), and oversight by a policy/ regulatory commission (CPUC). All three of these sectors must be aligned for widespread PV implementation and deployment. The practical feasibility of controls developed at APEP will be evaluated throughout the project directly by PG&E and through periodic progress reports with the CPUC. The final project task is to specifically quantify the feasibility of the control strategy and implementation method by evaluating hardware, communication, computational modifications, and other necessary upgrades. The required basic hardware components, engineering expertise, and design layouts will be assessed to provide general insight into the cost of a potential upgrade.

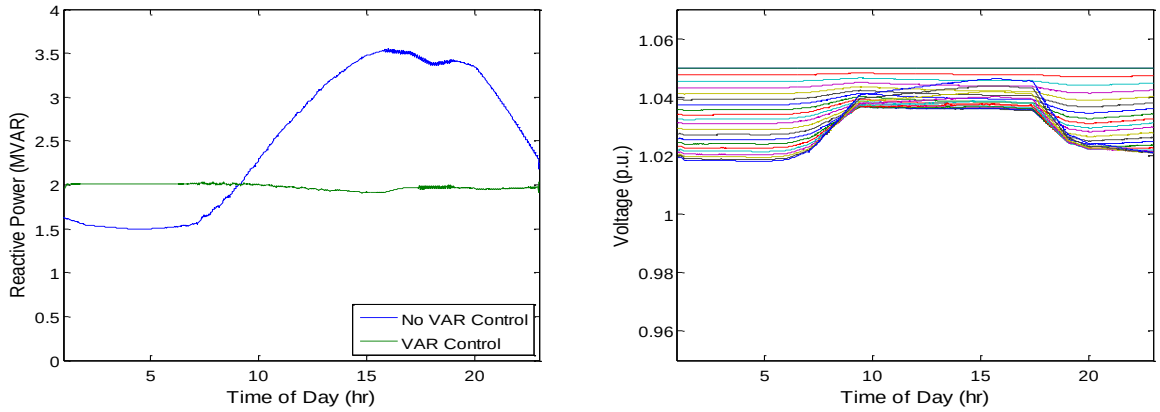

Figure 5: Left: Comparison of reactive power provided by the substation with and without reactive power (VAR) control; Right: Voltage profile utilizing local power curtailment and reactive power control.

Developed control strategies may require changes in standards including IEEE 1547 and UL 1741. The extent to which each control strategy can be implemented with existing standards is to be clearly identified. Further, the simulation results may provide insights and data that can guide and justify the development of new standards. Along with the potential benefits and sensitivity from the simulations, the practical feasibility of the developed control strategy will be quantified.

6. Conclusions

Identifying the operation limitations and characteristics of a commercial (Cayetano) and a residential (Menlo) circuit with High-Pen PV is the primary objective of this research. Each circuit was evaluated

using a three phase balanced feeder model developed and calibrated using circuit description and measurement information. High-Pen PV was evaluated by varying PV generation on the circuit in penetration and distribution to evaluate 1) the primary feeder voltage profile, 2) the operation of voltage regulation equipment, 3) sub-station power factor, and 4) system line losses. The detailed results the evaluation on the Cayetano and Menlo circuits are detailed in the previous sections. The following is a concise summary of the major findings.

Primary feeder voltage profile evaluation.

1. The majority of the simulation scenarios did not feature out of standard voltage at the primary feeder as penetrations increased with the exception of the Menlo End and Menlo Beginning generation distribution scenarios.
2. The Menlo End distribution scenarios demonstrated out-of-standard high voltages induced by PV generation for all evaluated PV penetrations. Other scenarios (Cayetano End and Menlo Middle) demonstrated similar voltage rise behavior, but without non-standard voltages. The Menlo End generation scenarios produced high voltages due to high line impedance and high levels of excess generation capacity; both characteristic of sites located at the end of a feeder away from the Load Center.
3. The Menlo Beginning distribution scenarios demonstrated out-of-standard low voltage condition for evaluated penetrations greater than 40%. It was shown that as penetration increases, the sub-station Load Drop Compensation control would lower the sub-station voltage via tapping. Other generation distributions (LC/GC > 1) demonstrated similar behavior, but did not experience out-of-standard voltages. The Menlo Beginning scenarios featured a high impedance section of line at the end of the feeder resulting in a significant voltage drop. As the sub-station LDC lowered the voltage, the section would drop below standard voltage levels.
4. The out-of-standard voltage issue may be remedied by addressing circuit impedance, bus siting evaluation, and the application of voltage regulation equipment.

Voltage Regulation Equipment evaluation.

1. Based on the observation of the simulated penetration and distribution scenarios of the Cayetano and Menlo circuits, the High-Pen PV had a marginal impact on capacitor switching. Only two of the 160 simulated Cayetano circuit scenarios showed a change in capacitor switching in the PV region. The Menlo circuit featured a capacitor installation with Voltage Override switching controls that would switch on with increased PV generations, but in response to the sub-station Load Tap Changing transformer dropping the circuit voltage with PV generation. Of the controls evaluated, only Voltage-Override switching controls are impacted by PV generation.
2. As discussed in the Low Voltage section, PV generation in the circuit causes the sub-station LTC with LDC control to lower the circuit voltage via tapping. The LDC operation was simulated for the entire year, and both the Cayetano and Menlo circuits show increases in yearly tap position changes with PV penetration.

Sub-station power factor evaluation.

1. It was observed in both the Cayetano and Menlo simulation scenarios that sub-station power factor decreases (leading or lagging) as PV penetration increases. This is attributed to the lack of reactive power support from PV generation.
2. The sub-station power factor marginally decreased for characteristic High days, but significantly decreased for characteristic Low days.
3. Unnecessary capacitor switching for reactive power or voltage regulation by Time-Clock switching controls aggravated the decrease in sub-station power factor. Capacitor switching controls that utilize system feedback could prevent the unnecessary capacitor switching aggravating the sub-station power factor.

Circuit line loss evaluation.

1. Increased PV penetration reduces system line loss until PV generation induced reverse power flow becomes dominant. This optimum PV penetration is referred to as the minimum loss penetration. The Break Even Point (BEP) is a method to estimate the minimum loss penetration. The error of the estimation is reduced as the circuit LC/GC ratio approaches one (LC/GC $\rightarrow$ 1).
2. Circuits with a larger LC/GC ratio will have a higher minimum loss penetration than circuits with a lower LC/GC ratio. The Beginning generation distribution scenarios typically have a larger LC/GC ratio than an End generation scenario.
3. Circuits with LC/GC close to one (LC/GC $\approx$ 1) will achieve lower line losses at the minimum loss PV penetration than circuits with LC/GC ratio further from one. Radial generation distribution scenarios typically have a LC/GC ratio approximately equal to one.
4. For a circuit with distributed load demand ($\sigma_{LC} > 0$), distributed PV generation ($\sigma_{GC} > 0$) will have a higher minimum loss penetration achieve lower line losses at the minimum loss penetration than point PV generation ($\sigma_{GC}=0$). The Radial generation distribution scenarios are examples of distributed PV; and the Beginning, Middle, and End generation distribution scenarios are examples of point PV generation.
5. The minimum loss penetration is significantly higher for a characteristic High than a characteristic Low day. Using the total load demand energy and interpolation, a minimum loss penetration for the entire may be estimated.

High-Pen PV has a steady-state impact on distributions circuits. This analysis focused on High-Pen PV's influence on voltage, regulation equipment, line loss, and more on the primary feeder. The majority of the results indicated a marginal impact of High-Pen PV, but there are examples of negative impacts on voltage and regulation equipment. The analysis presented above identified these negative influences and decomposed the condition into metrics to clearly identify the root cause of the issue.

1. Re-conductoring bus 39 from a high impedance #4 ASCR to a lower impedance 1/0 stranded copper distribution line resulted in a 7% decreases in peak voltage in the PV region at 100% penetration. The example did not enable more penetrations, but would if the Menlo circuit was re-conductoring beyond bus 39 to lower impedance conductor.
2. The Voltage Rise Siting score is a qualitative metric useful to identify buses prone to distributed generation (DG) induced voltage rise. Using the Menlo circuit VRS score, the generation at bus 39 (VRS = 48.9) in comparison to bus 38 (VRS = 31.9) showed an 11% improvement at 100% penetration. By re-siting the PV to a bus with a lower VRS score, PV penetrations up to 15%

were enabled. Using the VRS score as a tool would be useful to identify and prevent siting high penetrations of PV at portions of the circuit prone to DG induced voltage rise.

The Menlo Beginning generation distribution scenario was observed to have non-standard low voltages in the PV region for penetrations greater than 40%. The low voltage occurred on a low voltage (4.16kV) section of the Menlo circuit. To address the voltage issue three approaches were proposed: 1) raising the system voltage of the 4.16kV section, 2) apply a line regulator to the 4.16kV section, 3) modify the LDC controls to prevent down tapping. The results of the approach are as follows.

1. By raising the system voltage from 4.16kV to 12.47kV for the low voltage prone section, the low voltage condition was improved from 40% to 90% penetration. By raising the system voltage, the high impedance delta-wye step-down transformer could be removed and the effective line impedance of the section was reduced by a factor of 9.
2. The fixed step-down transformer was replaced for a Line Regulator. The Line Regulator utilized Load Drop Compensation (LDC) control, and improved the low voltage condition from 40% to 90% penetration.
3. The LDC controls of the Load Tap Changing (LTC) transformer were modified using LDC Current Compensation controls. The current compensation controls prevented the LDC to lower the system voltage due the PV generation. The application of the LDC Current Compensation control on the Menlo Beginning scenario enabled PV penetration for 40% to 100%.
4. The LDC Current Compensation controls was shown to be applicable to circuits with a LC/GC ration greater than one (LC/GC > 1), which is characteristic of circuits with generation located at the beginning of the circuit. When applied to qualified circuits (Cayetano Beginning and Middle, Menlo Beginning) for an entire year, benefits of 40% reduction of total tap changes for the Cayetano circuit and 78% reduction for the Menlo circuit were observed.

It was shown that as PV penetration increases, the sub-station power decreases until the point of reverse power flow at the sub-station. It was also identified that characteristic low days are particularly sensitive to this phenomena and aggravated further by needless switching of Time-Clock capacitor switching controls. This low power factor condition was identified in both the Cayetano and Menlo circuits. To improve this condition, VAR switching controls replaced Time-Clock controls, but with mixed results. The VAR switching controls did improve the power factor, but the power factor still reduced beyond standard levels at elevated PV penetrations. This power factor condition does not affect the operation of the circuit, but is outside of standards.

7. Public Benefits to California

The proposed progressively smarter distribution system will improve the economics of solar PV implementation by (1) reducing the need for costly ad hoc load flow studies to determine whether the PV installation creates unacceptable circuit conditions, (2) increasing the value of PV installations by enabling ancillary services such as active power filtering and controlled reactive power support, and (3) improving circuit efficiency and equipment lifetime as a result of those services. Some relevant distribution system equipment upgrades, such as the smart metering infrastructure, are already in progress in the major California utilities. In addition, the smart circuit PV strategy developed in this research focuses on a staged implementation with progressive benefits to minimize the early cost while maximizing future circuit performance. A progressively smarter distribution system directly benefits California by encouraging a high penetration of solar PV electricity while improving customer power

quality and circuit efficiency. The current distribution circuit infrastructure can neither support a high penetration of PV nor fully utilize ancillary features in a way that benefits the customer, utility, and society.

Understanding PV integration limits and a progressively smarter distribution system is invaluable for utilities to support the increased penetration of solar installations in California. PV penetration limits of the current distribution system are not well known and the current distribution system cannot support high levels of solar distributed generation penetration. The project demonstrates how advanced inverters and communication along monitored points along distribution circuits can be used to increase PV interconnection limits progressively.

Advanced inverter and communication strategies are investigated by evaluating the integration of PV systems on both primary and secondary distribution systems to maximize value to end users as well as the utility. The project provides insights into modeling methodologies and limits to PV penetration, as well as progressive actions that can be taken to enable wide-scale deployment of solar distributed generation technologies.

The project will likely both reduce the installed price of solar electric systems and enable increased numbers of installed solar electric system. By establishing PV integration limits and a progressively smarter distribution system, the utility will have both an understanding of the phenomena limiting PV integration and a reliable solution to avoid possible adverse conditions. This reduces the need for costly custom engineering analysis and modeling. Further, the project provides insight into a progressively smarter distribution system, such that the distribution system can be advanced as PV penetration increases.

The research presented in this report contributes to understanding PV integration limits and developing progressively smarter distribution systems that will be required to enable flexible integration of PV installations in California. Before the proposed technology and concepts are to be deployed, it is essential to systematically evaluate tradeoffs, sensitivities and concepts of PV integration. The net results of this research are (1) the development of strategies to accommodate an increased penetration of renewable resources, (2) the identification of the pathways to facilitate an efficient and more rapid deployment of renewables than will otherwise occur, and (3) a paradigm shift in the understanding of the challenges and needs on both the utility and academic research cornerstones associated with an enhanced deployment of renewables in the State of California.

8. Acknowledgements

This program was (1) funded by, and an integral part of, the California Public Utilities Commission (CPUC) California Solar Initiative (CSI) Research, Development, and Demonstration (RD&D) program under CPUC/Itron Grant # 47904, and (2) managed by Itron, Inc. Any opinions, findings, and conclusions or recommendations expressed in this material are those of the author(s) and do not necessarily reflect the views of the CPUC, ltron, Inc. or the CSI RD&D Program. The authors wish to acknowledge the outstanding contributions of our partner, Pacific Gas & Electric (PG&E), and the three special PG&E contributors to the conduct of this study: Matt Heling, John Carruthers, and Dan Pearson. The three were instrumental in the implementation and overall success of the study, and we were honored to have experienced and benefitted by their collegial and supportive engagement. We are indebted as well to Jonathan Wanjiru, the Itron project manager, who provided key guidance throughout the project.

9. References

[1] T. A. Short, *Electric Power Distribution Handbook*. Boco Raton, FL: CRC, 2004.

[2] J. Glover, M. Sarma, and T. Overbye, *Power System Analysis and Design*, 4th ed. Ontario, Canada: Thomson Learning, 2008.

[3] "S&C IntelliCAP PLUS Automatic Capacitor Control: Operating Instructions." S&C Electric Company, 2009.

[4] "IEEE Standard for Interconnecting Distributed Resources With Electric Power Systems," *IEEE Std 1547-2003*, 2003. .

[5] T. Gonen, *Electric Power Distribution System Engineering*, 1st ed. New York: McGraw-Hill Book Co., 1986.

[6] "SolarAnywhere," *Clean Power Institute*. [Online]. Available: https://solaranywhere.com/Public/About.aspx. [Accessed: 26-Apr-2013].

[7] R. Perez, P. Ineichen, K. Moore, M. Kmiecik, C. Chain, R. George, and F. Vignola, "A new operational model for satellite-derived irradiances: description and validation," *Sol. Energy*, vol. 73, no. 5, pp. 307–317, Nov. 2002.

[8] J. Stein, R. Perez, and A. Parkins, "Validation of PV Performance Models Using Satellite-Based Irradiance Measurements: A Case Study," presented at the ASES Annual Conference, Phoenix, AZ, 2010.

[9] National Climatic Data Center, "Quality Controlled Local Climatological Data (QCLCD)," *NOAA*. [Online]. Available: http://www.ncdc.noaa.gov/land-based-station-data/quality-controlled-local-climatological-data-qclcd. [Accessed: 26-Apr-2013].

[10] M. Heling, "Assessment of the Zero-Emission Vehicle, Shared-Use Station Car (ZEV-SUSC) Mobility Concept with a Focus on energy and Enviromental Sustainability," Master of Science, University of California Irvine, 2008.

[11] A. Luque and S. Hegedus, Eds., *Handbook of Photovoltaic Science and Engineering*. John Wiley & Sons Ltd, 2003.

[12] Pacific Gas and Electric Company, "Electric Rule No. 21: Generating Facility Interconnections." Pacific Gas and Electric Company, 2011.

[13] R. A. Walling, R. Saint, R. C. Dugan, J. Burke, and L. A. Kojovic, "Summary of Distributed Resources Impact on Power Delivery Systems," *Power Deliv. Ieee Trans.*, vol. 23, no. 3, pp. 1636–1644, 2008.

[14] W. H. Kersting, *Distribution System Modeling and Analysis*. CRC Press LLC, 2002.

[15] "Supply and Demand," *California ISO*. [Online]. Available: http://www.caiso.com/Pages/TodaysOutlook.aspx#SupplyandDemand. [Accessed: 20-Feb-2013].

[16] T. Ackermann, G. Andersson, and L. Söder, "Distributed generation: a definition," *Electr. Power Syst. Res.*, vol. 57, no. 3, pp. 195–204, Apr. 2001.

[17] "PV Watts - How to Change Parameters," *NREL*, 26-Apr-2013. [Online]. Available: http://www.nrel.gov/rredc/pvwatts/changing_parameters.html.

[18] GE Corporate Research and Development, "DG Power Quality, Protection and Reliabiliyt Case Studies Report," National Renewable Energy Laboratory, NREL/SR-560-34635, Aug. 2003.

[19] "Guide for Planning Area Distribution Facilities." Pacific Gas and Electric Company, 15-Sep-2009.

10. Appendices

10.1 Appendix A: Sub-Station Supervisory Control and Data Acquisition (SCADA) Measurement Evaluation for Cayetano and Menlo Circuits

To conduct the evaluation of PV penetrations limitations, PG&E provided sub-stations measurements from their Supervisory Control and Data Acquisition (SCADA) system for both the Cayetano 2111 and the Menlo 1102 feeders. The data set collected in 15 minute intervals for an entire year (2010); the signals measured are listed in Table 6. The Cayetano 2111 and Menlo 1102 feeders did not have do not have identical measurement quantities; voltage measurements where not recorded for the Menlo feeder. To verify the consistency of the collected data, apparent power was calculated using real and reactive power (S_{PQ}) and then with voltage and current (S_{VI}). If the data is consistent, then error between S_{PQ} and S_{VI} should be marginal. A day with a daily average of the error between S_{PQ} and S_{VI} greater than 10% is considered inconsistent and will be removed from the data set.

Feeder	Real Power (P)	Reactive Power (Q)	Line-to-Neutral Voltage			Line Current		
			Phase A ($V_{LN,A}$)	Phase B ($V_{LN,B}$)	Phase C ($V_{LN,C}$)	Phase A (I_A)	Phase B (I_A)	Phase C (I_A)
Cayetano 2111	Yes	Yes	Yes	Yes	Yes	Yes	Yes	Yes
Menlo 1102	Yes	Yes	No	No	No	Yes	Yes	Yes

Table 66. Recorded Measurements at Feeder Sub-Station.

For the Cayetano 2111 feeder, real power, reactive power, line to neutral voltage (120V base), and current was recorded in 15 minute intervals. 10-1 was used to convert the recorded 120-base voltage data to an estimated distribution line-to-neutral voltage base of 12.47kV. 10-2 and 10-3 are used to calculate S_{PQ} and S_{VI} from real power (P), reactive power (Q), phase current (I), and the converted line-to-neutral voltage (V_{LN}). The error between the measurements is calculated using 10-4 and the daily error average with 10-5; the data was sampled in 15 minute intervals, which equates to 96 samples per day.

$$V_{LN} = V_{LN,120base} \cdot \left(\frac{12470[V]}{120[V]}\right) \quad \textbf{10-1}$$

$$S_{PQ} = \sqrt{P^2 + Q^2} \quad \textbf{10-2}$$

$$S_{VI} = \left(V_{LN,A}\right)(I_A) + \left(V_{LN,B}\right)(I_B) + \left(V_{LN,C}\right)(I_C) \quad \textbf{10-3}$$

$$E = 100 \cdot \left|\frac{S_{PQ} - S_{VI}}{S_{PQ}}\right| \quad \textbf{10-4}$$

$$E_{Dy\ Avg} = \frac{\sum_i^{96} E_i}{96} \quad \textbf{10-5}$$

The data set for the Menlo 1102 circuit consisted of real power, reactive power, and phase current, but not line-to-neutral voltages. An estimated line-to-line voltage (12.47 kV) was used in place; 12.47kV is low-voltage rating of the Menlo 1102 sub-station transformer and therefore selected. 10-6, 10-7, and 10-8 are used to calculate S_{VI} instead of equations 10-1 and 10-3 as used for the Cayetano 2111. Apart from the calculation of S_{vi}, the rest of the process is same as was used for the Cayetano 2111.

$$V_{LN,est} = \frac{12470}{\sqrt{3}} \quad \textbf{10-6}$$

$$I_{avg} = \frac{I_A + I_B + I_C}{3} \quad \textbf{10-7}$$

$$S_{VI} = 3(V_{LN,est})(I_{avg}) \quad \textbf{10-8}$$

Table 6 contains the results of the average day error calculation for the Cayetano 2111 selected characteristic days. The error average is consistently in the neighborhood of 4.1%; the consistent error is most likely due to the selection of base voltage of 12.47kV. The error average for all the characteristic days is below the 10% threshold and therefore deemed valid for use.

Date	Characteristic Day	Error Average	Valid?
10/13/2010	Summer High	3.89	Yes
10/14/2010	Summer High	3.92	Yes
10/15/2010	Summer High	3.95	Yes
4/4/2010	Summer Low	4.41	Yes
4/6/2010	Summer Low	4.16	Yes
4/7/2010	Summer Low	4.31	Yes
4/9/2010	Summer Low	4.31	Yes
11/8/2010	Winter High	3.92	Yes
11/10/2010	Winter High	3.85	Yes
11/11/2010	Winter High	3.89	Yes
11/16/2010	Winter High	4.00	Yes
11/30/2010	Winter High	4.05	Yes
1/10/2010	Winter Low	4.16	Yes
2/14/2010	Winter Low	4.36	Yes
2/28/2010	Winter Low	4.82	Yes
3/13/2010	Winter Low	4.50	Yes

Table 67. Cayetano 2111 Characteristic Days.

For the Menlo 1102 circuit, not all of the characteristic days contained valid data. Table 67 contains the results of the error average calculations for selected characteristic days of the Menlo 1102 feeder. The summer high/low days and winter high days selected resulted in acceptable error averages. The exception are the winter high days 11/28 and 11/30 which had error averages of 10.77% and 10.18%. Upon further review, the days where deemed acceptable for the use in analysis. All winter low days considered had unacceptable error averages and therefore not used in analysis. Only models for

summer high, summer low, and winter high characteristics days where calibrated for the Menlo 1102 using the feeder data.

Date	Characteristic Day	Error Average	Valid?
9/27/2010	Summer High	5.62	Yes
9/28/2010	Summer High	6.22	Yes
10/12/2010	Summer High	5.98	Yes
10/13/2010	Summer High	6.36	Yes
7/2/2010	Summer Low	3.63	Yes
7/31/2010	Summer Low	5.57	Yes
8/4/2010	Summer Low	7.57	Yes
8/14/2010	Summer Low	4.44	Yes
3/13/2010	Winter High	3.87	Yes
11/24/2010	Winter High	7.18	Yes
11/28/2010	Winter High	10.77	Acceptable
11/30/2010	Winter High	10.18	Acceptable
1/2/2010	Winter Low	44.71	No
11/5/2010	Winter Low	54.99	No
11/6/2010	Winter Low	58.63	No
11/7/2010	Winter Low	47.12	No
12/12/2010	Winter Low	44.03	No
12/13/2010	Winter Low	82.24	No
12/19/2010	Winter Low	80.10	No
12/20/2010	Winter Low	93.31	No
12/25/2010	Winter Low	55.76	No
12/28/2010	Winter Low	73.32	No

Table 68. Menlo 1102 Characteristic Days.

The winter low days did not have acceptable error averages, indicating an inconsistency in the data recorded. The error averages ranged from 44.03% to 93.31%; a significant increase in comparison to other characteristic days. On further analysis of the data, the error stems from the real power measurement and is not isolated to the months of January, November, and December. For example, Figure 119 show two different days (4/24 and 4/29) with similar current and reactive power profiles, but very different real power profiles upon inspection. The weather for both days was sunny with high and low temperature of 71ºF/46 ºF and 60ºF /48ºF respectively. For the 4/24 day, the apparent power (S_{PQ}) profiled derived from the real and reactive power approximately follows the apparent power (S_{VI}) derived from the current; as a result, the error average is approximately 5%. For the 4/29, S_{PQ} does not follow with the S_{VI} curve resulting in error average of 54%. Given the consistency of the weather, reactive power and current profiles between the days, it appears the issue is in the measured real power. The source and reason for the error is unknown at this time and would require a further investigation. For this research, identification and exclusion of days with inconsistent data is sufficient.

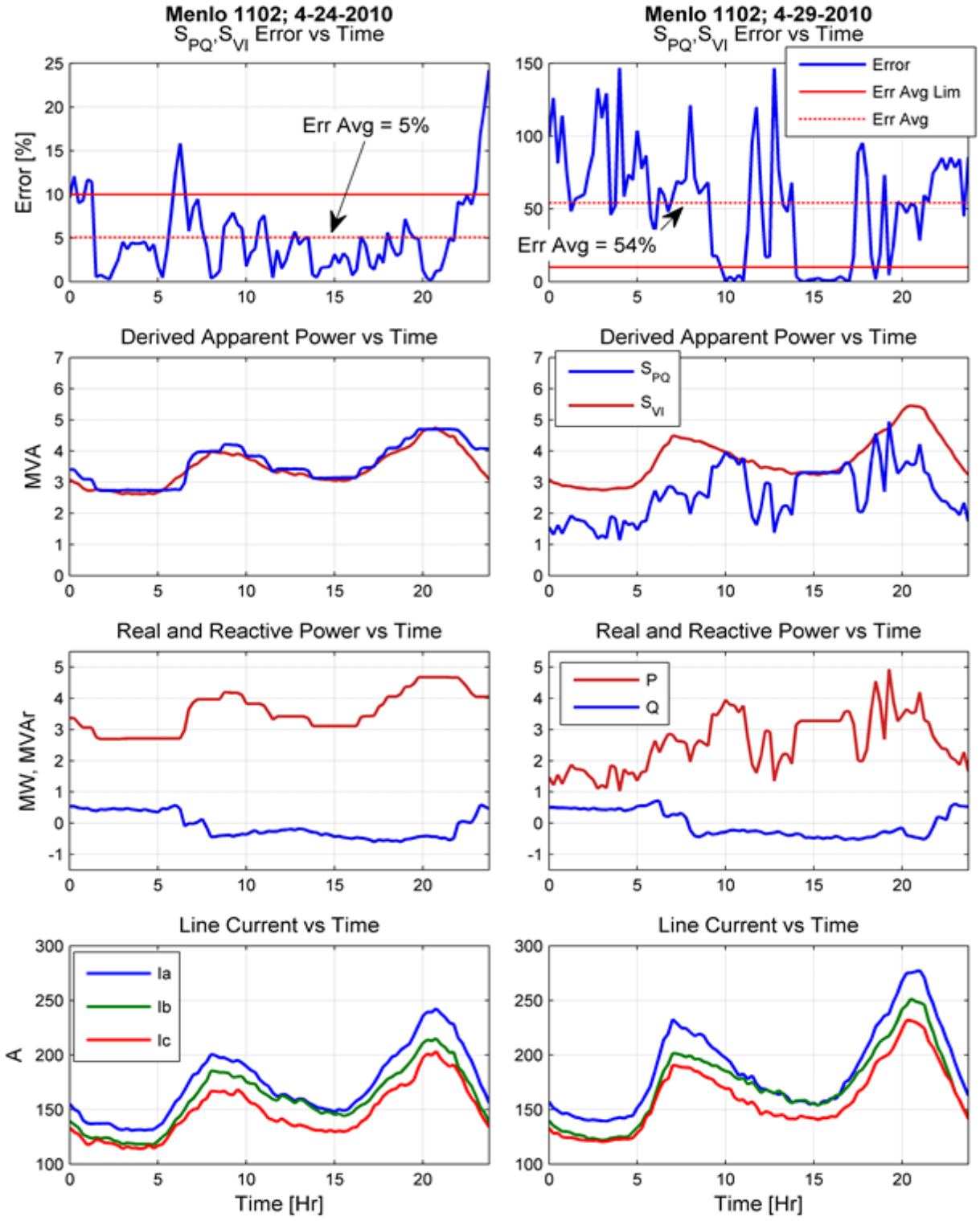

Figure 119. Menlo 1102 data validation example for 4/24/2010 and 4/29/2010.

10.2 Appendix B: Commercial (Cayetano 2111) Model Settings

Time	Summer High Day (10-14-10)					
	Cayetano 2111				Cayetano 2109	
	Real Load Demand (P_{LD}) [MW}	Real Deficit Factor (DF_P)	Reactive Load Demand (Q_{LD}) [MVAR]	Reactive Deficit Factor (DF_Q)	Real Load Demand (P) [MW]	Reactive Load Demand (P) [MW]
12:00 AM	10.333	0.992228	2.418	0.96192	3.061	-0.385
12:15 AM	10.057	0.992405	2.901	0.967852	2.97	-0.491
12:30 AM	9.975	0.992466	2.923	0.969281	2.865	-0.527
12:45 AM	9.838	0.992574	2.88	0.971319	2.765	-0.527
1:00 AM	9.831	0.992583	2.848	0.971478	2.664	-0.527
1:15 AM	9.662	0.992707	2.881	0.973883	2.61	-0.527
1:30 AM	9.665	0.992709	2.845	0.97392	2.558	-0.527
1:45 AM	9.256	0.992948	2.655	0.968133	2.558	-0.527
2:00 AM	9.091	0.993075	2.644	0.970584	2.558	-0.527
2:15 AM	9.007	0.993149	2.437	0.972001	2.556	-0.527
2:30 AM	9.029	0.993132	2.448	0.971669	2.453	-0.527
2:45 AM	8.826	0.993289	2.354	0.97505	2.453	-0.527
3:00 AM	8.74	0.993348	1.963	0.977468	2.453	-0.527
3:15 AM	8.843	0.993267	1.899	0.97559	2.453	-0.527
3:30 AM	8.711	0.993369	1.945	0.97808	2.453	-0.527
3:45 AM	8.985	0.99316	1.91	0.972715	2.453	-0.527
4:00 AM	9.177	0.993015	1.89	0.968755	2.453	-0.527
4:15 AM	9.176	0.993021	2.019	0.968969	2.478	-0.527
4:30 AM	9.289	0.992939	2.237	0.967166	2.558	-0.527
4:45 AM	9.491	0.992785	2.27	0.963632	2.558	-0.527
5:00 AM	9.594	0.992695	2.589	0.962795	2.558	-0.527
5:15 AM	9.682	0.99262	2.702	0.961709	2.592	-0.527
5:30 AM	9.776	0.992534	2.853	0.960669	2.735	-0.527
5:45 AM	10.019	0.992346	2.87	0.957116	2.769	-0.527
6:00 AM	10.823	0.991733	3.06	0.972221	2.92	-0.527
6:15 AM	11.32823	0.991386	2.894	0.96799	3.04	-0.914
6:30 AM	11.57947	0.991232	3.017	0.964442	3.298	-1.029
6:45 AM	11.728	0.991204	2.974	0.962864	3.349	-1.029
7:00 AM	11.73554	0.991288	3.079	0.963404	3.437	-1.029
7:15 AM	11.45877	0.991638	2.938	0.97009	3.361	-1.029
7:30 AM	11.45	0.991792	2.969	0.971651	3.349	-1.029
7:45 AM	11.77551	0.99177	3.111	0.967984	3.349	-1.029
8:00 AM	12.34102	0.991554	3.651	0.960211	3.338	-1.029
8:15 AM	12.48487	0.991565	3.732	0.959231	3.247	-1.029
8:30 AM	12.71771	0.991509	3.773	0.957043	3.244	-1.029
8:45 AM	12.88247	0.991492	3.838	0.955728	3.27	-1.029
9:00 AM	13.09822	0.991424	4.036	0.953722	3.337	-1.029
9:15 AM	13.33035	0.991216	4.26	0.950144	3.381	-0.946
9:30 AM	13.45949	0.991103	4.34	0.948366	3.349	-0.923
9:45 AM	13.52633	0.991152	4.463	0.948561	3.457	-0.923
10:00 AM	13.61718	0.991177	4.6	0.948254	3.455	-0.883

Time	Summer High Day (10-14-10)					
	Cayetano 2111				Cayetano 2109	
	Real Load Demand (P_{LD}) [MW}	Real Deficit Factor (DF_P)	Reactive Load Demand (Q_{LD}) [MVAR]	Reactive Deficit Factor (DF_Q)	Real Load Demand (P) [MW]	Reactive Load Demand (P) [MW]
10:15 AM	14.12326	0.990943	4.821	0.953118	3.455	-0.818
10:30 AM	14.61133	0.990593	5.138	0.947956	3.551	-0.818
10:45 AM	15.13448	0.990168	5.273	0.941661	3.867	-0.762
11:00 AM	15.19163	0.990115	5.314	0.940814	3.881	-0.712
11:15 AM	15.35009	0.989881	5.623	0.939099	3.988	-0.712
11:30 AM	15.75354	0.989472	5.864	0.934756	4.104	-0.712
11:45 AM	16.00377	0.989393	6.006	0.941056	4.137	-0.712
12:00 PM	16.115	0.989306	6.081	0.939993	4.351	-0.712
12:15 PM	16.21412	0.989186	6.141	0.938469	4.405	-0.635
12:30 PM	16.33324	0.989029	6.25	0.936353	4.517	-0.458
12:45 PM	16.53327	0.988738	6.462	0.932655	4.673	-0.093
1:00 PM	16.59229	0.988598	6.542	0.930735	4.774	0.166
1:15 PM	16.68667	0.988579	6.588	0.937272	4.922	0.176
1:30 PM	16.72805	0.988459	6.626	0.936199	5.01	0.216
1:45 PM	16.90994	0.988179	6.789	0.932935	5.157	0.484
2:00 PM	16.90084	0.988127	6.743	0.932091	5.332	0.58
2:15 PM	17.08069	0.987796	6.966	0.929821	5.354	0.58
2:30 PM	17.06654	0.987695	6.948	0.929118	5.6	0.58
2:45 PM	17.27897	0.98741	7.01	0.926405	5.713	0.58
3:00 PM	17.2974	0.987281	7.002	0.92489	5.937	0.723
3:15 PM	17.11606	0.987291	6.972	0.925332	6.137	0.844
3:30 PM	17.25471	0.987029	7.033	0.922964	6.299	0.897
3:45 PM	17.29487	0.986927	7.13	0.928789	6.557	0.977
4:00 PM	17.01502	0.986973	7.053	0.930239	6.577	1.002
4:15 PM	17.07602	0.986827	7.045	0.928933	6.677	1.003
4:30 PM	16.80102	0.986934	7.002	0.930598	6.787	1.108
4:45 PM	16.72634	0.98697	6.93	0.930703	6.983	1.169
5:00 PM	16.71166	0.987006	6.767	0.930623	6.922	1.108
5:15 PM	16.52183	0.98719	6.628	0.932366	6.954	1.108
5:30 PM	16.242	0.98743	6.506	0.934972	6.985	1.145
5:45 PM	15.973	0.987685	6.357	0.937901	6.873	1.108
6:00 PM	15.377	0.98832	5.749	0.944522	6.789	1.039
6:15 PM	15.12	0.988445	5.475	0.9381	6.792	1.002
6:30 PM	15.075	0.988491	5.428	0.938555	6.82	1.002
6:45 PM	15.205	0.988417	5.327	0.936775	6.901	1.002
7:00 PM	15.3	0.988345	5.332	0.935689	7.04	0.978
7:15 PM	15.153	0.988481	5.213	0.937081	7.216	1.002
7:30 PM	14.924	0.988667	5.153	0.93986	7.039	1.002
7:45 PM	14.649	0.988902	5.037	0.943283	6.941	0.983
8:00 PM	14.324	0.989179	4.912	0.947807	6.772	0.897
8:15 PM	14.3	0.989214	4.832	0.948166	6.555	0.897
8:30 PM	14.1	0.989384	4.73	0.95079	6.367	0.897
8:45 PM	13.754	0.989674	4.65	0.956696	6.167	0.66
9:00 PM	13.344	0.989891	4.584	0.952827	5.958	0.334
9:15 PM	13.088	0.990102	4.407	0.955353	5.762	0.496

Time	Summer High Day (10-14-10)					
	Cayetano 2111				Cayetano 2109	
	Real Load Demand (P_{LD}) [MW}	Real Deficit Factor (DF_P)	Reactive Load Demand (Q_{LD}) [MVAR]	Reactive Deficit Factor (DF_Q)	Real Load Demand (P) [MW]	Reactive Load Demand (P) [MW]
9:30 PM	12.847	0.990276	4.291	0.956265	5.51	0.9
9:45 PM	12.567	0.990519	4.073	0.96094	5.198	0.818
10:00 PM	12.426	0.990652	3.831	0.964071	4.912	0.739
10:15 PM	12.321	0.990748	3.537	0.966781	4.628	0.712
10:30 PM	11.891	0.990969	3.157	0.960324	4.37	0.627
10:45 PM	11.68	0.991084	3.112	0.937462	4.113	0.606
11:00 PM	11.337	0.991323	3.323	0.945305	3.861	0.431
11:15 PM	11.155	0.991487	3.228	0.948282	3.663	0.272
11:30 PM	10.967	0.991653	3.129	0.951294	3.463	0.14
11:45 PM	10.693	0.991878	3.014	0.954985	3.294	0.123

Table 69. Commercial (Cayetano) model Summer High day (10-14-10) time resolved load demand.

Time	Summer Low Day (4-4-10)					
	Cayetano 2111				Cayetano 2109	
	Real Load Demand (P_{LD}) [MW}	Real Deficit Factor (DF_P)	Reactive Load Demand (Q_{LD}) [MVAR]	Reactive Deficit Factor (DF_Q)	Real Load Demand (P) [MW]	Reactive Load Demand (P) [MW]
12:00 AM	4.817	0.996295	0.738	0.941753	2.822	-1.134
12:15 AM	4.747	0.996349	0.738	0.943434	2.757	-1.134
12:30 AM	4.725	0.996368	0.738	0.943979	2.654	-1.134
12:45 AM	4.688	0.996397	0.738	0.944866	2.564	-1.134
1:00 AM	4.651	0.996426	0.738	0.945736	2.505	-1.134
1:15 AM	4.603	0.996462	0.738	0.946848	2.456	-1.134
1:30 AM	4.59	0.996473	0.738	0.947157	2.4	-1.134
1:45 AM	4.558	0.996497	0.738	0.947881	2.4	-1.134
2:00 AM	4.536	0.996513	0.738	0.948376	2.4	-1.134
2:15 AM	4.556	0.996498	0.738	0.947926	2.4	-1.134
2:30 AM	4.469	0.996564	0.738	0.949881	2.337	-1.134
2:45 AM	4.404	0.996614	0.738	0.951321	2.295	-1.134
3:00 AM	4.378	0.996633	0.738	0.951885	2.295	-1.134
3:15 AM	4.377	0.996634	0.738	0.951906	2.295	-1.134
3:30 AM	4.38	0.996632	0.738	0.951841	2.295	-1.134
3:45 AM	4.352	0.996652	0.738	0.952445	2.295	-1.134
4:00 AM	4.359	0.996647	0.738	0.952294	2.295	-1.134
4:15 AM	4.36	0.996646	0.738	0.952273	2.295	-1.134
4:30 AM	4.359	0.996647	0.738	0.952294	2.295	-1.134
4:45 AM	4.317	0.996679	0.736	0.953082	2.265	-1.134
5:00 AM	4.15	0.996796	0.646	0.950414	2.305	-1.134
5:15 AM	4.246	0.996688	0.738	0.954102	2.4	-1.134
5:30 AM	4.246	0.996699	0.71	0.952446	2.4	-1.134
5:45 AM	4.25931	0.996702	0.738	0.954124	2.4	-1.134
6:00 AM	4.369621	0.996642	0.738	0.952058	2.427	-1.134
6:15 AM	4.41606	0.996672	0.738	0.951912	2.505	-1.134

Time	Summer Low Day (4-4-10)					
	Cayetano 2111				Cayetano 2109	
	Real Load Demand (P_{LD}) [MW}	Real Deficit Factor (DF_P)	Reactive Load Demand (Q_{LD}) [MVAR]	Reactive Deficit Factor (DF_Q)	Real Load Demand (P) [MW]	Reactive Load Demand (P) [MW]
6:30 AM	4.453499	0.996703	0.738	0.951888	2.521	-1.084
6:45 AM	4.426858	0.996786	0.772	0.877805	2.611	-1.081
7:00 AM	4.288217	0.996901	0.667	0.829362	2.689	-1.094
7:15 AM	4.24944	0.997011	0.612	0.813263	2.82	-0.985
7:30 AM	4.301663	0.997076	0.612	0.813583	2.89	-0.99
7:45 AM	4.204732	0.997101	0.629	0.818371	2.982	-0.983
8:00 AM	4.108802	0.997103	0.632	0.806542	3.108	-0.791
8:15 AM	4.159905	0.997254	0.612	0.802041	3.186	-0.765
8:30 AM	4.288008	0.997353	0.637	0.807479	3.235	-0.765
8:45 AM	4.302785	0.997416	0.633	0.807343	3.3	-0.765
9:00 AM	4.389562	0.997421	0.621	0.800826	3.375	-0.74
9:15 AM	4.110106	0.997548	0.612	0.806229	3.425	-0.738
9:30 AM	4.21665	0.997425	0.641	0.82242	3.458	-0.957
9:45 AM	4.19317	0.997414	0.612	0.80279	3.515	-0.77
10:00 AM	4.15069	0.997443	0.612	0.807031	3.575	-0.816
10:15 AM	4.263662	0.997514	0.637	0.8116	3.475	-0.791
10:30 AM	4.180634	0.997717	0.668	0.821765	3.47	-0.754
10:45 AM	4.177635	0.997546	0.622	0.807072	3.455	-0.738
11:00 AM	4.060635	0.997469	0.664	0.816062	3.455	-0.738
11:15 AM	4.029405	0.99741	0.664	0.814461	3.544	-0.738
11:30 AM	3.946175	0.99739	0.664	0.815855	3.488	-0.738
11:45 AM	3.984377	0.997393	0.664	0.815578	3.455	-0.738
12:00 PM	3.914578	0.997462	0.605	0.806498	3.453	-0.75
12:15 PM	3.919995	0.997427	0.664	0.815713	3.457	-0.712
12:30 PM	4.101412	0.997259	0.664	0.812989	3.468	-0.776
12:45 PM	4.056972	0.997299	0.664	0.814437	3.455	-0.771
1:00 PM	3.966532	0.997371	0.664	0.816897	3.491	-0.765
1:15 PM	3.842742	0.99742	0.664	0.820296	3.461	-0.765
1:30 PM	3.674952	0.997498	0.664	0.823389	3.479	-0.747
1:45 PM	3.714734	0.997492	0.628	0.828489	3.288	-0.912
2:00 PM	3.955517	0.997329	0.64	0.816379	3.245	-0.81
2:15 PM	3.950746	0.997315	0.606	0.82181	3.293	-0.998
2:30 PM	4.009976	0.997236	0.612	0.810544	3.309	-0.866
2:45 PM	3.97976	0.99727	0.612	0.809078	3.345	-0.831
3:00 PM	3.967543	0.997291	0.612	0.807399	3.31	-0.793
3:15 PM	3.809377	0.997326	0.612	0.811103	3.296	-0.79
3:30 PM	3.768211	0.997274	0.612	0.809919	3.29	-0.778
3:45 PM	3.905968	0.997195	0.612	0.815236	3.314	-0.918
4:00 PM	4.060726	0.997087	0.612	0.807151	3.349	-0.887
4:15 PM	4.00491	0.997117	0.599	0.803481	3.329	-0.851
4:30 PM	4.036095	0.997084	0.612	0.798766	3.354	-0.765
4:45 PM	3.979296	0.997057	0.612	0.798722	3.409	-0.765
5:00 PM	3.984498	0.99698	0.579	0.792286	3.402	-0.818
5:15 PM	4.101119	0.996876	0.612	0.791623	3.477	-0.769
5:30 PM	4.12674	0.996842	0.612	0.7922	3.589	-0.812

Time	Summer Low Day (4-4-10)					
	Cayetano 2111				Cayetano 2109	
	Real Load Demand (P_{LD}) [MW}	Real Deficit Factor (DF_P)	Reactive Load Demand (Q_{LD}) [MVAR]	Reactive Deficit Factor (DF_Q)	Real Load Demand (P) [MW]	Reactive Load Demand (P) [MW]
5:45 PM	4.203991	0.996735	0.612	0.785436	3.592	-0.777
6:00 PM	4.183243	0.996689	0.541	0.762982	3.695	-0.787
6:15 PM	4.265121	0.996618	0.6	0.771016	3.805	-0.712
6:30 PM	4.325	0.99657	0.638	0.779644	3.752	-0.712
6:45 PM	4.378	0.996529	0.638	0.776927	3.807	-0.712
7:00 PM	4.525	0.996415	0.615	0.761591	3.908	-0.712
7:15 PM	4.866	0.99621	0.71	0.796776	3.981	-0.712
7:30 PM	5.047	0.996069	0.743	0.793915	4.151	-0.697
7:45 PM	5.08	0.996082	0.743	0.809949	4.199	-0.633
8:00 PM	4.966	0.996168	0.743	0.81401	4.193	-0.626
8:15 PM	4.875	0.996238	0.743	0.817925	4.193	-0.633
8:30 PM	4.889	0.996228	0.743	0.817556	4.177	-0.633
8:45 PM	4.868	0.996248	0.743	0.820237	4.138	-0.657
9:00 PM	4.828	0.996275	0.691	0.813299	4.038	-0.659
9:15 PM	4.83	0.996269	0.638	0.802744	3.959	-0.659
9:30 PM	4.774	0.996314	0.652	0.809147	3.879	-0.659
9:45 PM	4.747	0.996338	0.665	0.8141	3.776	-0.659
10:00 PM	4.668	0.996396	0.638	0.813434	3.61	-0.659
10:15 PM	4.64	0.996393	0.677	0.806625	3.457	-0.753
10:30 PM	4.577	0.996457	0.638	0.813721	3.272	-0.914
10:45 PM	4.542	0.996485	0.507	0.924148	3.161	-1.117
11:00 PM	4.461	0.99654	0.686	0.945794	2.991	-1.16
11:15 PM	4.448	0.996552	0.686	0.946142	2.849	-1.16
11:30 PM	4.378	0.996606	0.686	0.947827	2.753	-1.16
11:45 PM	4.355	0.996624	0.686	0.948376	2.714	-1.16

Table 70. Commercial (Cayetano) model Summer Low day (4-4-10) time resolved load demand.

Time	Winter High Day (11-8-10)					
	Cayetano 2111				Cayetano 2109	
	Real Load Demand (P_{LD}) [MW}	Real Deficit Factor (DF_P)	Reactive Load Demand (Q_{LD}) [MVAR]	Reactive Deficit Factor (DF_Q)	Real Load Demand (P) [MW]	Reactive Load Demand (P) [MW]
12:00 AM	8.614	0.993443	1.822	0.946449	2.69	-0.686
12:15 AM	8.55	0.993493	1.826	0.947993	2.529	-0.686
12:30 AM	8.475	0.99356	1.785	0.949162	2.479	-0.686
12:45 AM	8.592	0.993474	1.771	0.94662	2.479	-0.686
1:00 AM	8.61	0.99344	1.859	0.947202	2.479	-0.686
1:15 AM	8.439	0.993571	1.859	0.95055	2.479	-0.686
1:30 AM	8.462	0.993554	1.859	0.950103	2.479	-0.686
1:45 AM	8.651	0.993409	1.86	0.946484	2.415	-0.686
2:00 AM	8.566	0.993457	1.94	0.949082	2.268	-0.686
2:15 AM	8.545	0.993473	1.938	0.949461	2.268	-0.686
2:30 AM	8.479	0.993523	1.938	0.950624	2.329	-0.686

Time	Winter High Day (11-8-10)					
	Cayetano 2111				Cayetano 2109	
	Real Load Demand (P_{LD}) [MW}	Real Deficit Factor (DF_P)	Reactive Load Demand (Q_{LD}) [MVAR]	Reactive Deficit Factor (DF_Q)	Real Load Demand (P) [MW]	Reactive Load Demand (P) [MW]
2:45 AM	8.414	0.993581	1.909	0.951693	2.268	-0.686
3:00 AM	8.323	0.993669	1.833	0.952859	2.268	-0.686
3:15 AM	8.279	0.993702	1.833	0.953709	2.268	-0.686
3:30 AM	8.469	0.993557	1.833	0.950007	2.268	-0.686
3:45 AM	8.565	0.993469	1.893	0.948681	2.268	-0.686
4:00 AM	8.577	0.993432	2.005	0.949423	2.268	-0.686
4:15 AM	8.664	0.993361	2.018	0.947849	2.343	-0.686
4:30 AM	8.738	0.993302	2.018	0.946319	2.479	-0.686
4:45 AM	8.812	0.993245	2.018	0.944943	2.479	-0.686
5:00 AM	9.167	0.993028	2.329	0.96905	2.479	-0.686
5:15 AM	9.279	0.992884	1.846	0.955832	2.479	-0.686
5:30 AM	9.35	0.992829	1.846	0.954104	2.479	-0.686
5:45 AM	9.503	0.992711	1.846	0.95034	2.479	-0.686
6:00 AM	10.132	0.992212	2.054	0.934945	2.479	-0.686
6:15 AM	10.49231	0.991959	2.549	0.940271	3.231	-0.686
6:30 AM	10.27362	0.992104	2.705	0.943762	3.431	-0.686
6:45 AM	10.22742	0.992275	2.479	0.945897	3.578	-0.686
7:00 AM	10.33321	0.992287	2.492	0.945006	3.539	-0.686
7:15 AM	10.35391	0.992401	2.558	0.945628	3.745	-0.686
7:30 AM	10.47762	0.992446	2.558	0.944916	3.745	-0.686
7:45 AM	10.71209	0.992389	2.702	0.941918	3.745	-0.686
8:00 AM	10.96657	0.99233	2.774	0.93944	3.477	-0.686
8:15 AM	10.86854	0.992552	2.693	0.943004	3.422	-0.686
8:30 AM	10.95552	0.992613	2.701	0.943113	3.323	-0.686
8:45 AM	11.20722	0.992519	2.723	0.939714	3.309	-0.686
9:00 AM	11.38892	0.99246	2.869	0.937809	3.218	-0.686
9:15 AM	11.49741	0.992455	2.9	0.936749	3.27	-0.686
9:30 AM	11.57789	0.992461	2.984	0.936348	3.248	-0.686
9:45 AM	11.59237	0.992523	2.968	0.93695	3.218	-0.686
10:00 AM	11.79486	0.99252	3.001	0.945527	3.218	-0.686
10:15 AM	11.65236	0.992685	2.978	0.948571	3.252	-0.686
10:30 AM	11.96887	0.992459	3.121	0.943224	3.282	-0.686
10:45 AM	11.65925	0.992711	3.024	0.948592	3.313	-0.686
11:00 AM	11.61363	0.99273	3.062	0.94906	3.323	-0.686
11:15 AM	11.58312	0.992692	3.09	0.948806	3.323	-0.686
11:30 AM	11.65961	0.992567	3.132	0.946745	3.323	-0.686
11:45 AM	11.74013	0.992377	3.177	0.944105	3.323	-0.686
12:00 PM	11.60866	0.992388	3.051	0.945501	3.323	-0.686
12:15 PM	11.55541	0.992328	3.239	0.945021	3.323	-0.686
12:30 PM	11.74615	0.992126	3.211	0.941363	3.264	-0.686
12:45 PM	11.77347	0.992225	3.208	0.942302	3.218	-0.686
1:00 PM	11.77479	0.992351	3.165	0.943685	3.218	-0.686
1:15 PM	11.44415	0.99258	3.165	0.948751	3.225	-0.686
1:30 PM	11.53251	0.992477	3.196	0.947019	3.159	-0.686
1:45 PM	11.55188	0.992331	3.212	0.945352	3.128	-0.686

Time	Winter High Day (11-8-10)					
	Cayetano 2111				Cayetano 2109	
	Real Load Demand (P_{LD}) [MW}	Real Deficit Factor (DF_P)	Reactive Load Demand (Q_{LD}) [MVAR]	Reactive Deficit Factor (DF_Q)	Real Load Demand (P) [MW]	Reactive Load Demand (P) [MW]
2:00 PM	11.66525	0.992092	3.293	0.941838	3.184	-0.686
2:15 PM	11.81319	0.99184	3.316	0.938041	3.218	-0.686
2:30 PM	11.37913	0.992072	3.24	0.944001	3.174	-0.686
2:45 PM	11.45151	0.991775	3.24	0.940418	3.155	-0.686
3:00 PM	11.5609	0.991465	3.167	0.936228	3.112	-0.686
3:15 PM	11.90425	0.991135	3.26	0.930016	3.151	-0.686
3:30 PM	11.71959	0.991256	3.227	0.932681	3.222	-0.686
3:45 PM	11.70144	0.991224	3.184	0.932208	3.323	-0.686
4:00 PM	11.69928	0.991167	3.191	0.931638	3.351	-0.686
4:15 PM	11.60141	0.991256	3.068	0.93844	3.37	-1.057
4:30 PM	11.62954	0.991158	3.138	0.93884	3.473	-1.187
4:45 PM	11.93227	0.990905	3.104	0.932596	3.769	-1.187
5:00 PM	11.883	0.990932	3.02	0.931695	3.946	-1.116
5:15 PM	12.387	0.99051	3.059	0.920915	4.237	-1.081
5:30 PM	12.567	0.990357	3.059	0.916465	4.414	-1.051
5:45 PM	12.557	0.990344	3.059	0.914692	4.726	-0.976
6:00 PM	12.273	0.990566	3.059	0.91976	4.917	-0.976
6:15 PM	12.179	0.990642	3.059	0.921624	4.897	-0.976
6:30 PM	12.089	0.990717	3.042	0.923189	4.936	-0.976
6:45 PM	12.03	0.990764	3.047	0.924485	4.876	-0.976
7:00 PM	11.956	0.990837	2.98	0.925516	4.948	-0.976
7:15 PM	12.005	0.99079	3.023	0.924944	4.853	-0.976
7:30 PM	11.938	0.99085	2.996	0.926149	4.853	-0.976
7:45 PM	12.002	0.990805	2.98	0.925112	4.755	-0.976
8:00 PM	11.805	0.99096	2.98	0.92868	4.845	-0.976
8:15 PM	11.614	0.99114	2.871	0.932679	4.651	-0.976
8:30 PM	11.495	0.991274	2.674	0.935086	4.555	-0.976
8:45 PM	11.377	0.991378	2.616	0.937696	4.489	-0.976
9:00 PM	11.03	0.9916	2.24	0.930903	4.431	-0.976
9:15 PM	10.819	0.99173	2.353	0.932952	4.207	-0.799
9:30 PM	10.646	0.991874	2.151	0.934278	4.114	-0.686
9:45 PM	10.519	0.991989	1.966	0.937097	3.92	-0.666
10:00 PM	10.304	0.992148	2.109	0.942727	3.756	-0.659
10:15 PM	10.297	0.992169	1.947	0.943881	3.505	-0.659
10:30 PM	10.119	0.992311	1.899	0.948879	3.396	-0.659
10:45 PM	9.9	0.992318	1.918	0.910494	3.177	-0.659
11:00 PM	9.829	0.992427	2.079	0.924769	3.165	-0.659
11:15 PM	9.683	0.992529	2.126	0.928685	3.044	-0.659
11:30 PM	9.656	0.992556	2.117	0.929367	2.82	-0.659
11:45 PM	9.596	0.992596	2.149	0.931199	2.697	-0.659

Table 71. Commercial (Cayetano) model Winter High day (11-8-10) time resolved load demand.

Time	Winter Low Day (2-14-10)

	Cayetano 2111				Cayetano 2109	
	Real Load Demand (P_{LD}) [MW}	Real Deficit Factor (DF_P)	Reactive Load Demand (Q_{LD}) [MVAR]	Reactive Deficit Factor (DF_Q)	Real Load Demand (P) [MW]	Reactive Load Demand (P) [MW]
12:00 AM	4.332	0.996593	0.549	1.016431	2.883	-1.187
12:15 AM	4.224	0.996666	0.49	1.030127	2.611	-1.187
12:30 AM	4.167	0.996704	0.462	1.037505	2.548	-1.187
12:45 AM	4.177	0.996713	0.549	1.02559	2.438	-1.187
1:00 AM	4.167	0.996723	0.567	1.023569	2.491	-1.187
1:15 AM	4.167	0.996723	0.567	1.023482	2.505	-1.187
1:30 AM	4.167	0.996724	0.567	1.024678	2.308	-1.187
1:45 AM	4.167	0.996725	0.567	1.024755	2.295	-1.187
2:00 AM	4.162	0.996728	0.567	1.024747	2.328	-1.187
2:15 AM	4.062	0.996803	0.567	1.028683	2.295	-1.187
2:30 AM	4.062	0.996803	0.567	1.028683	2.295	-1.187
2:45 AM	4.062	0.996803	0.567	1.028683	2.295	-1.187
3:00 AM	4.062	0.996786	0.474	1.042386	2.251	-1.187
3:15 AM	4.062	0.996796	0.525	1.034817	2.189	-1.187
3:30 AM	4.121	0.99676	0.567	1.027108	2.189	-1.187
3:45 AM	4.281	0.99664	0.567	1.021034	2.189	-1.187
4:00 AM	4.378	0.996568	0.567	1.017013	2.229	-1.187
4:15 AM	4.378	0.996568	0.567	1.017165	2.204	-1.187
4:30 AM	4.446	0.996516	0.567	1.013964	2.286	-1.187
4:45 AM	4.484	0.996488	0.567	1.012384	2.295	-1.187
5:00 AM	4.484	0.996488	0.567	1.012384	2.295	-1.187
5:15 AM	4.484	0.996485	0.567	1.010445	2.33	-1.16
5:30 AM	4.484	0.996476	0.567	1.004846	2.419	-1.081
5:45 AM	4.642	0.996356	0.567	0.997781	2.505	-1.081
6:00 AM	4.754	0.99628	0.658	0.988416	2.505	-1.081
6:15 AM	4.8	0.996237	0.673	0.981499	2.552	-1.001
6:30 AM	4.8	0.996236	0.673	0.980882	2.611	-0.996
6:45 AM	4.768819	0.996229	0.65	1.391533	2.626	-1.101
7:00 AM	4.602637	0.995887	0.664	1.098034	2.746	-1.095
7:15 AM	4.469599	0.99603	0.633	1.114744	2.812	-1.1
7:30 AM	4.44156	0.996108	0.633	1.10151	2.782	-0.947
7:45 AM	4.494851	0.996263	0.633	1.117159	2.927	-1.08
8:00 AM	4.566141	0.996375	0.633	1.102594	3.01	-0.942
8:15 AM	4.442084	0.996571	0.633	1.109717	3.072	-0.93
8:30 AM	4.427027	0.996692	0.633	1.105547	3.182	-0.866
8:45 AM	4.494281	0.996793	0.633	1.133283	3.196	-1.11
9:00 AM	4.588536	0.99684	0.633	1.113167	3.191	-0.931
9:15 AM	4.634728	0.996908	0.55	1.162779	3.195	-1.08
9:30 AM	4.63792	0.997024	0.561	1.142092	3.265	-0.923
9:45 AM	4.592181	0.997095	0.554	1.151783	3.266	-0.946
10:00 AM	4.517443	0.99721	0.597	1.145011	3.256	-0.985
10:15 AM	4.626595	0.997204	0.608	1.152086	3.182	-1.102
10:30 AM	4.636748	0.997239	0.618	1.145849	3.13	-1.066
10:45 AM	4.638314	0.997298	0.607	1.159718	3.127	-1.133
11:00 AM	4.66888	0.997341	0.607	1.160262	3.166	-1.134
11:15 AM	4.653012	0.997333	0.607	1.156243	3.191	-1.101

Time	Winter Low Day (2-14-10)					
	Cayetano 2111				Cayetano 2109	
	Real Load Demand (P_{LD}) [MW}	Real Deficit Factor (DF_P)	Reactive Load Demand (Q_{LD}) [MVAR]	Reactive Deficit Factor (DF_Q)	Real Load Demand (P) [MW]	Reactive Load Demand (P) [MW]
11:30 AM	4.641144	0.99735	0.663	1.132896	3.116	-1.059
11:45 AM	4.702974	0.997318	0.69	1.125104	3.161	-1.095
12:00 PM	4.739804	0.997268	0.675	1.12589	3.185	-1.081
12:15 PM	4.722612	0.99729	0.633	1.137035	3.115	-1.035
12:30 PM	4.64742	0.997433	0.737	1.117346	3.096	-1.103
12:45 PM	4.860482	0.997291	0.704	1.114027	3.117	-1.059
1:00 PM	4.618544	0.997429	0.716	1.108859	3.112	-0.949
1:15 PM	4.597358	0.997417	0.731	1.109671	3.112	-1
1:30 PM	4.557172	0.997393	0.711	1.104842	3.087	-0.891
1:45 PM	4.52296	0.997364	0.738	1.103799	3.025	-0.952
2:00 PM	4.551747	0.997265	0.719	1.099745	2.96	-0.883
2:15 PM	4.483153	0.997199	0.717	1.118633	2.996	-1.085
2:30 PM	4.387558	0.99713	0.712	1.11792	3.007	-1.065
2:45 PM	4.443401	0.997052	0.71	1.119128	3.007	-1.106
3:00 PM	4.452243	0.996971	0.681	1.111118	3.004	-0.964
3:15 PM	4.463566	0.996903	0.757	1.098481	2.901	-1.056
3:30 PM	4.468889	0.996777	0.765	1.08015	2.918	-0.912
3:45 PM	4.528181	0.996607	0.765	1.084208	2.983	-1.025
4:00 PM	4.486472	0.996492	0.762	1.089388	2.926	-1.091
4:15 PM	4.510327	0.996336	0.678	1.109756	3.023	-1.136
4:30 PM	4.561182	0.996228	0.765	1.07233	3.144	-1.021
4:45 PM	4.647865	0.996086	0.756	1.074887	3.229	-1.101
5:00 PM	4.819547	0.995858	0.719	1.074779	3.34	-1.134
5:15 PM	4.872274	0.995763	0.744	1.053207	3.494	-1.019
5:30 PM	4.938	0.995654	0.72	1.055528	3.595	-1.057
5:45 PM	5.143	0.995453	0.659	1.02405	3.85	-0.782
6:00 PM	5.289	0.995408	0.698	1.042021	4.109	-0.686
6:15 PM	5.305	0.99538	0.659	1.047377	4.167	-0.686
6:30 PM	5.246	0.995418	0.659	1.049678	4.223	-0.686
6:45 PM	5.251	0.995426	0.679	1.047311	4.111	-0.686
7:00 PM	5.221	0.995455	0.701	1.045204	4.088	-0.686
7:15 PM	5.252	0.995417	0.659	1.0514	4.088	-0.686
7:30 PM	5.2	0.995452	0.659	1.054625	4.056	-0.686
7:45 PM	5.243	0.995423	0.659	1.052206	4.066	-0.686
8:00 PM	5.169	0.995473	0.659	1.056164	4.062	-0.686
8:15 PM	5.145	0.995472	0.62	1.066346	4.034	-0.686
8:30 PM	5.079	0.995486	0.554	1.089036	3.946	-0.686
8:45 PM	5.064	0.995497	0.554	1.091279	3.868	-0.686
9:00 PM	5.064	0.9955	0.554	1.094065	3.848	-0.705
9:15 PM	5.046	0.995521	0.554	1.105382	3.721	-0.768
9:30 PM	5.013	0.995549	0.554	1.11494	3.637	-0.816
9:45 PM	4.933	0.995592	0.554	1.111217	3.565	-0.741
10:00 PM	4.866	0.995593	0.535	1.085217	3.414	-0.88
10:15 PM	4.856	0.995635	0.554	1.108953	3.277	-1.088
10:30 PM	4.774	0.995678	0.51	1.145452	3.146	-1.187

Time	Winter Low Day (2-14-10)					
	Cayetano 2111				Cayetano 2109	
	Real Load Demand (P_{LD}) [MW}	Real Deficit Factor (DF_P)	Reactive Load Demand (Q_{LD}) [MVAR]	Reactive Deficit Factor (DF_Q)	Real Load Demand (P) [MW]	Reactive Load Demand (P) [MW]
10:45 PM	4.654	0.996268	0.319	0.982944	2.996	-1.187
11:00 PM	4.597	0.996338	0.462	0.979805	2.901	-1.187
11:15 PM	4.587	0.996347	0.462	0.981165	2.803	-1.187
11:30 PM	4.549	0.996376	0.462	0.98389	2.711	-1.187
11:45 PM	4.441	0.996458	0.462	0.989921	2.64	-1.187

Table 72. Commercial (Cayetano) model Winter Low day (2-14-10) time resolved load demand.

Time	Summer High Day (10-14-10)						
	Bus 3 [kW]	Bus 8 [kW]	Bus 16 [kW]	Bus 23 [kW]	Bus 25 [kW]	Bus 27 [kW]	Bus 29 [kW]
12:00 AM	0	0	0	0	0	0	0
12:15 AM	0	0	0	0	0	0	0
12:30 AM	0	0	0	0	0	0	0
12:45 AM	0	0	0	0	0	0	0
1:00 AM	0	0	0	0	0	0	0
1:15 AM	0	0	0	0	0	0	0
1:30 AM	0	0	0	0	0	0	0
1:45 AM	0	0	0	0	0	0	0
2:00 AM	0	0	0	0	0	0	0
2:15 AM	0	0	0	0	0	0	0
2:30 AM	0	0	0	0	0	0	0
2:45 AM	0	0	0	0	0	0	0
3:00 AM	0	0	0	0	0	0	0
3:15 AM	0	0	0	0	0	0	0
3:30 AM	0	0	0	0	0	0	0
3:45 AM	0	0	0	0	0	0	0
4:00 AM	0	0	0	0	0	0	0
4:15 AM	0	0	0	0	0	0	0
4:30 AM	0	0	0	0	0	0	0
4:45 AM	0	0	0	0	0	0	0
5:00 AM	0	0	0	0	0	0	0
5:15 AM	0	0	0	0	0	0	0
5:30 AM	0	0	0	0	0	0	0
5:45 AM	0	0	0	0	0	0	0
6:00 AM	0	0	0	0	0	0	0
6:15 AM	0.123598	0.039996	7.060558	0.786826	0	0.050183	5.172708
6:30 AM	0.247197	0.079993	14.12112	1.573652	0	0.100365	10.34542
6:45 AM	0.788239	0.173429	36.44777	2.767799	0	0.343185	35.4835
7:00 AM	1.329281	0.266865	58.77442	3.961946	0	0.586006	60.62159
7:15 AM	2.274971	0.506491	84.42977	11.57639	0	0.949403	111.0322
7:30 AM	3.220661	0.746117	110.0851	19.19083	0	1.3128	161.4428

Time	Summer High Day (10-14-10)						
	Bus 3 [kW]	Bus 8 [kW]	Bus 16 [kW]	Bus 23 [kW]	Bus 25 [kW]	Bus 27 [kW]	Bus 29 [kW]
7:45 AM	4.206203	0.791965	156.9843	31.12671	0	1.428271	229.9704
8:00 AM	5.191745	0.837813	203.8836	43.06259	0	1.543743	298.498
8:15 AM	5.605364	1.148153	231.6101	49.01622	0	1.614434	338.8708
8:30 AM	6.018982	1.458492	259.3367	54.96985	0	1.685125	379.2437
8:45 AM	6.115848	1.662375	280.4679	69.23613	0	2.168219	411.8178
9:00 AM	6.212713	1.866257	301.5991	83.5024	0	2.651314	444.392
9:15 AM	7.306299	1.964008	293.6949	87.5231	0	2.741358	445.1248
9:30 AM	8.399885	2.061758	285.7907	91.5438	0	2.831402	445.8576
9:45 AM	8.654566	2.110743	310.8102	102.2145	0	2.239558	482.3049
10:00 AM	8.909246	2.159727	335.8297	112.8852	0	1.647715	518.7522
10:15 AM	9.250478	2.23943	354.8446	118.5623	0	2.558768	542.8009
10:30 AM	9.59171	2.319134	373.8596	124.2393	0	3.469822	566.8495
10:45 AM	9.502264	2.364998	368.0918	128.0224	0	3.505166	569.9945
11:00 AM	9.412817	2.410863	362.3239	131.8055	0	3.540511	573.1396
11:15 AM	9.347819	2.409969	353.1629	130.7161	0	3.420537	559.0303
11:30 AM	9.28282	2.409075	344.0018	129.6266	0	3.300563	544.921
11:45 AM	9.210467	2.385154	345.3873	131.8209	0	3.388664	552.5785
12:00 PM	9.138113	2.361234	346.7728	134.0152	0	3.476765	560.2359
12:15 PM	8.951513	2.324565	331.8874	136.81	0	3.350064	557.798
12:30 PM	8.764914	2.287897	317.0019	139.6049	0	3.223363	555.3601
12:45 PM	8.430926	2.222502	310.8736	136.5907	0	3.151584	535.9985
1:00 PM	8.096938	2.157107	304.7454	133.5764	0	3.079804	516.637
1:15 PM	7.956568	2.058363	285.5852	131.5363	0	2.895044	493.6387
1:30 PM	7.816198	1.959618	266.425	129.4961	0	2.710283	470.6404
1:45 PM	7.381742	1.847373	254.918	124.7812	0	2.59952	447.416
2:00 PM	6.947286	1.735127	243.4109	120.0662	0	2.488756	424.1917
2:15 PM	6.484085	1.614206	219.2006	112.1885	0	2.276921	387.9276
2:30 PM	6.020884	1.493284	194.9903	104.3108	0	2.065085	351.6635
2:45 PM	5.416457	1.348827	175.6608	95.03976	0	1.853029	319.6543
3:00 PM	4.81203	1.204369	156.3314	85.76868	0	1.640972	287.6451
3:15 PM	3.784663	1.031428	131.1362	77.65855	0	1.37739	248.0679
3:30 PM	2.757296	0.858486	105.9409	69.54841	0	1.113808	208.4907
3:45 PM	2.254359	0.656493	72.22309	55.01116	0	0.902113	149.8196
4:00 PM	1.751422	0.4545	38.50523	40.47391	0	0.690419	91.14841
4:15 PM	1.050889	0.278435	27.58391	29.98363	0	0.436254	55.68657
4:30 PM	0.350356	0.102371	16.66259	19.49335	0	0.18209	20.22473
4:45 PM	0.185938	0.054586	9.869993	11.80444	0	0.092395	11.32919
5:00 PM	0.021519	0.0068	3.077399	4.115536	0	0.0027	2.43365
5:15 PM	0.01076	0.0034	1.538699	2.057768	0	0.00135	1.216825
5:30 PM	0	0	0	0	0	0	0
5:45 PM	0	0	0	0	0	0	0
6:00 PM	0	0	0	0	0	0	0
6:15 PM	0	0	0	0	0	0	0
6:30 PM	0	0	0	0	0	0	0
6:45 PM	0	0	0	0	0	0	0
7:00 PM	0	0	0	0	0	0	0
7:15 PM	0	0	0	0	0	0	0

Time	Summer High Day (10-14-10)						
	Bus 3 [kW]	Bus 8 [kW]	Bus 16 [kW]	Bus 23 [kW]	Bus 25 [kW]	Bus 27 [kW]	Bus 29 [kW]
7:30 PM	0	0	0	0	0	0	0
7:45 PM	0	0	0	0	0	0	0
8:00 PM	0	0	0	0	0	0	0
8:15 PM	0	0	0	0	0	0	0
8:30 PM	0	0	0	0	0	0	0
8:45 PM	0	0	0	0	0	0	0
9:00 PM	0	0	0	0	0	0	0
9:15 PM	0	0	0	0	0	0	0
9:30 PM	0	0	0	0	0	0	0
9:45 PM	0	0	0	0	0	0	0
10:00 PM	0	0	0	0	0	0	0
10:15 PM	0	0	0	0	0	0	0
10:30 PM	0	0	0	0	0	0	0
10:45 PM	0	0	0	0	0	0	0
11:00 PM	0	0	0	0	0	0	0
11:15 PM	0	0	0	0	0	0	0
11:30 PM	0	0	0	0	0	0	0
11:45 PM	0	0	0	0	0	0	0

Table 73. Commercial (Cayetano) model Summer High day (10-14-10) time resolved PV site estimation.

Time	Summer Low Day (4-4-10)						
	Bus 3 [kW]	Bus 8 [kW]	Bus 16 [kW]	Bus 23 [kW]	Bus 25 [kW]	Bus 27 [kW]	Bus 29 [kW]
12:00 AM	0	0	0	0	0	0	0
12:15 AM	0	0	0	0	0	0	0
12:30 AM	0	0	0	0	0	0	0
12:45 AM	0	0	0	0	0	0	0
1:00 AM	0	0	0	0	0	0	0
1:15 AM	0	0	0	0	0	0	0
1:30 AM	0	0	0	0	0	0	0
1:45 AM	0	0	0	0	0	0	0
2:00 AM	0	0	0	0	0	0	0
2:15 AM	0	0	0	0	0	0	0
2:30 AM	0	0	0	0	0	0	0
2:45 AM	0	0	0	0	0	0	0
3:00 AM	0	0	0	0	0	0	0
3:15 AM	0	0	0	0	0	0	0
3:30 AM	0	0	0	0	0	0	0
3:45 AM	0	0	0	0	0	0	0
4:00 AM	0	0	0	0	0	0	0
4:15 AM	0	0	0	0	0	0	0
4:30 AM	0	0	0	0	0	0	0
4:45 AM	0	0	0	0	0	0	0
5:00 AM	0	0	0	0	0	0	0
5:15 AM	0	0	0	0	0	0	0
5:30 AM	0	0	0	0	0	0	0

Time	Summer Low Day (4-4-10)						
	Bus 3 [kW]	Bus 8 [kW]	Bus 16 [kW]	Bus 23 [kW]	Bus 25 [kW]	Bus 27 [kW]	Bus 29 [kW]
5:45 AM	0.123184	0.02722	4.911228	1.410547	0	0.041086	6.797036
6:00 AM	0.246368	0.054441	9.822456	2.821094	0	0.082173	13.59407
6:15 AM	0.462698	0.115318	22.55635	6.56525	0	0.187173	34.17303
6:30 AM	0.679027	0.176196	35.29025	10.30941	0	0.292173	54.75198
6:45 AM	0.955134	0.244316	39.39351	13.04199	0	0.337432	65.88551
7:00 AM	1.231241	0.312437	43.49677	15.77458	0	0.382691	77.01903
7:15 AM	1.322155	0.357667	71.55795	23.46123	0	0.508348	105.2324
7:30 AM	1.41307	0.402896	99.61912	31.14787	0	0.634005	133.4457
7:45 AM	1.501345	0.366935	82.21416	28.36483	0	0.585338	123.6996
8:00 AM	1.58962	0.330975	64.80919	25.58179	0	0.536671	113.9534
8:15 AM	2.536838	0.577653	105.6729	38.95132	0	0.886298	180.2798
8:30 AM	3.484055	0.824331	146.5365	52.32085	0	1.235924	246.6062
8:45 AM	3.996684	0.929659	165.1572	58.86604	0	1.41179	271.4235
9:00 AM	4.509312	1.034987	183.778	65.41124	0	1.587656	296.2408
9:15 AM	3.681935	0.924818	164.9582	60.24957	0	1.406951	271.8844
9:30 AM	2.854559	0.814649	146.1384	55.0879	0	1.226246	247.5279
9:45 AM	2.993726	0.78555	147.2394	56.73705	0	1.147971	242.2662
10:00 AM	3.132894	0.756451	148.3404	58.3862	0	1.069695	237.0045
10:15 AM	3.367703	0.877257	183.5447	68.21309	0	1.351247	291.3083
10:30 AM	3.602512	0.998063	218.749	78.03997	0	1.632799	345.612
10:45 AM	2.982335	0.844425	180.8827	65.8561	0	1.306853	281.7624
11:00 AM	2.362159	0.690788	143.0164	53.67224	0	0.980907	217.9127
11:15 AM	2.114626	0.659912	119.8397	46.22094	0	0.873839	195.6963
11:30 AM	1.867094	0.629036	96.66299	38.76965	0	0.766772	173.4799
11:45 AM	2.208619	0.689916	104.289	40.38114	0	0.812677	183.9953
12:00 PM	2.550143	0.750796	111.9149	41.99264	0	0.858583	194.5106
12:15 PM	2.394852	0.731461	110.6645	39.41661	0	0.778282	173.0092
12:30 PM	2.23956	0.712125	109.4141	36.84058	0	0.697982	151.5078
12:45 PM	2.317991	0.686306	109.2678	37.89825	0	0.713954	155.0878
1:00 PM	2.396422	0.660487	109.1216	38.95592	0	0.729925	158.6677
1:15 PM	2.123852	0.548509	95.50996	35.03577	0	0.68664	149.8372
1:30 PM	1.851281	0.436531	81.89833	31.11562	0	0.643354	141.0068
1:45 PM	1.859521	0.481323	86.53156	32.11426	0	0.648431	145.0991
2:00 PM	1.867761	0.526115	91.1648	33.1129	0	0.653508	149.1914
2:15 PM	1.711448	0.492462	89.29199	31.30493	0	0.621987	137.3234
2:30 PM	1.555135	0.458809	87.41919	29.49696	0	0.590466	125.4553
2:45 PM	1.76186	0.40762	82.74272	30.49446	0	0.678955	137.674
3:00 PM	1.968585	0.356431	78.06625	31.49196	0	0.767445	149.8927
3:15 PM	2.100352	0.415114	64.6686	25.02464	0	0.592501	121.5761
3:30 PM	2.23212	0.473797	51.27095	18.55731	0	0.417556	93.25943
3:45 PM	1.677191	0.347665	57.4685	19.52661	0	0.432322	91.51615
4:00 PM	1.122262	0.221533	63.66605	20.49591	0	0.447087	89.77287
4:15 PM	1.475302	0.311907	50.55104	20.52322	0	0.370297	98.6785
4:30 PM	1.828342	0.402281	37.43603	20.55054	0	0.293508	107.5841
4:45 PM	1.476572	0.305952	29.51784	17.74876	0	0.227468	78.01964
5:00 PM	1.124801	0.209624	21.59965	14.94698	0	0.161428	48.45515
5:15 PM	0.910592	0.190785	14.11827	12.3242	0	0.132882	47.44209

Time	Summer Low Day (4-4-10)						
	Bus 3 [kW]	Bus 8 [kW]	Bus 16 [kW]	Bus 23 [kW]	Bus 25 [kW]	Bus 27 [kW]	Bus 29 [kW]
5:30 PM	0.696384	0.171947	6.636893	9.701418	0	0.104336	46.42903
5:45 PM	0.424207	0.104742	2.961039	6.012221	0	0.063989	28.42528
6:00 PM	0.15203	0.037538	-0.71482	2.323024	0	0.023641	10.42152
6:15 PM	0.076015	0.018769	-0.35741	1.161512	0	0.011821	5.210762
6:30 PM	0	0	0	0	0	0	0
6:45 PM	0	0	0	0	0	0	0
7:00 PM	0	0	0	0	0	0	0
7:15 PM	0	0	0	0	0	0	0
7:30 PM	0	0	0	0	0	0	0
7:45 PM	0	0	0	0	0	0	0
8:00 PM	0	0	0	0	0	0	0
8:15 PM	0	0	0	0	0	0	0
8:30 PM	0	0	0	0	0	0	0
8:45 PM	0	0	0	0	0	0	0
9:00 PM	0	0	0	0	0	0	0
9:15 PM	0	0	0	0	0	0	0
9:30 PM	0	0	0	0	0	0	0
9:45 PM	0	0	0	0	0	0	0
10:00 PM	0	0	0	0	0	0	0
10:15 PM	0	0	0	0	0	0	0
10:30 PM	0	0	0	0	0	0	0
10:45 PM	0	0	0	0	0	0	0
11:00 PM	0	0	0	0	0	0	0
11:15 PM	0	0	0	0	0	0	0
11:30 PM	0	0	0	0	0	0	0
11:45 PM	0	0	0	0	0	0	0

Table 74. Commercial (Cayetano) model Summer Low day (4-4-10) time resolved PV site estimation.

Time	Winter High Day (11-8-10)						
	Bus 3 [kW]	Bus 8 [kW]	Bus 16 [kW]	Bus 23 [kW]	Bus 25 [kW]	Bus 27 [kW]	Bus 29 [kW]
12:00 AM	0	0	0	0	0	0	0
12:15 AM	0	0	0	0	0	0	0
12:30 AM	0	0	0	0	0	0	0
12:45 AM	0	0	0	0	0	0	0
1:00 AM	0	0	0	0	0	0	0
1:15 AM	0	0	0	0	0	0	0
1:30 AM	0	0	0	0	0	0	0
1:45 AM	0	0	0	0	0	0	0
2:00 AM	0	0	0	0	0	0	0
2:15 AM	0	0	0	0	0	0	0
2:30 AM	0	0	0	0	0	0	0
2:45 AM	0	0	0	0	0	0	0
3:00 AM	0	0	0	0	0	0	0
3:15 AM	0	0	0	0	0	0	0
3:30 AM	0	0	0	0	0	0	0
3:45 AM	0	0	0	0	0	0	0

Time	Winter High Day (11-8-10)						
	Bus 3 [kW]	Bus 8 [kW]	Bus 16 [kW]	Bus 23 [kW]	Bus 25 [kW]	Bus 27 [kW]	Bus 29 [kW]
4:00 AM	0	0	0	0	0	0	0
4:15 AM	0	0	0	0	0	0	0
4:30 AM	0	0	0	0	0	0	0
4:45 AM	0	0	0	0	0	0	0
5:00 AM	0	0	0	0	0	0	0
5:15 AM	0	0	0	0	0	0	0
5:30 AM	0	0	0	0	0	0	0
5:45 AM	0	0	0	0	0	0	0
6:00 AM	0	0	0	0	0	0	0
6:15 AM	0.012856	0.015467	0.905921	0.08178	0	0.024108	0.271601
6:30 AM	0.025712	0.030934	1.811842	0.163561	0	0.048216	0.543201
6:45 AM	0.623487	0.172945	27.28874	1.801958	0	0.270584	27.25771
7:00 AM	1.221261	0.314955	52.76565	3.440355	0	0.492952	53.97223
7:15 AM	2.079006	0.527652	82.82341	10.11878	0	0.812124	97.55344
7:30 AM	2.93675	0.740349	112.8812	16.79721	0	1.131296	141.1347
7:45 AM	3.744142	0.932429	146.2885	26.06088	0	1.41694	184.6505
8:00 AM	4.551534	1.124509	179.6959	35.32455	0	1.702584	228.1663
8:15 AM	5.218058	1.29081	205.8189	45.00759	0	1.946087	268.2622
8:30 AM	5.884582	1.457111	231.9418	54.69063	0	2.189589	308.3582
8:45 AM	6.402427	1.59759	252.5717	63.44199	0	2.390823	342.8187
9:00 AM	6.920271	1.73807	273.2016	72.19335	0	2.592056	377.2792
9:15 AM	7.352072	1.848899	287.8546	79.63399	0	2.7542	406.9631
9:30 AM	7.783873	1.959727	302.5077	87.07463	0	2.916345	436.647
9:45 AM	8.046401	2.050882	316.7371	91.78668	0	3.038717	459.7131
10:00 AM	8.308929	2.142037	330.9665	96.49873	0	3.161089	482.7792
10:15 AM	8.687127	2.157464	337.3895	105.3424	0	3.244088	498.5424
10:30 AM	9.065325	2.172891	343.8125	114.1861	0	3.327087	514.3057
10:45 AM	9.15305	2.19814	328.9715	112.9874	0	3.368271	523.5717
11:00 AM	9.240775	2.223388	314.1304	111.7886	0	3.409455	532.8376
11:15 AM	8.916631	1.900973	300.3511	102.1776	0	3.393034	520.3783
11:30 AM	8.592487	1.578558	286.5718	92.56651	0	3.376612	507.9191
11:45 AM	8.773263	1.888909	301.306	105.5886	0	3.287097	415.2905
12:00 PM	8.954039	2.199261	316.0402	118.6107	0	3.197582	322.6619
12:15 PM	8.91984	2.175473	254.158	103.4321	0	3.173994	355.5479
12:30 PM	8.88564	2.151686	192.2758	88.25359	0	3.150406	388.434
12:45 PM	8.594334	2.058518	230.6022	99.85892	0	2.949941	412.4069
1:00 PM	8.303028	1.96535	268.9287	111.4642	0	2.749476	436.3797
1:15 PM	7.901923	1.833181	255.8266	113.4048	0	2.669076	429.5141
1:30 PM	7.500818	1.701011	242.7245	115.3453	0	2.588676	422.6484
1:45 PM	6.648633	1.537343	203.3993	111.6298	0	2.348491	387.3143
2:00 PM	5.796448	1.373674	164.0741	107.9143	0	2.108306	351.9802
2:15 PM	5.616676	1.249692	149.3865	94.41159	0	1.94446	305.5783
2:30 PM	5.436903	1.12571	134.699	80.90893	0	1.780614	259.1763
2:45 PM	4.723875	0.67895	88.97228	52.37746	0	1.521692	194.2391
3:00 PM	4.010846	0.232189	43.24558	23.846	0	1.26277	129.3018
3:15 PM	2.880686	0.325806	39.40554	27.47517	0	1.03262	112.1272
3:30 PM	1.750525	0.419423	35.56551	31.10434	0	0.80247	94.95256

Time	Winter High Day (11-8-10)						
	Bus 3 [kW]	Bus 8 [kW]	Bus 16 [kW]	Bus 23 [kW]	Bus 25 [kW]	Bus 27 [kW]	Bus 29 [kW]
3:45 PM	1.326733	0.345801	29.31399	29.07108	0	0.590979	73.78864
4:00 PM	0.902942	0.272178	23.06247	27.03782	0	0.379489	52.62472
4:15 PM	0.523172	0.162827	13.07816	16.96599	0	0.220223	30.46066
4:30 PM	0.143402	0.053476	3.093847	6.894165	0	0.060957	8.296598
4:45 PM	0.071701	0.026738	1.546923	3.447083	0	0.030479	4.148299
5:00 PM	0	0	0	0	0	0	0
5:15 PM	0	0	0	0	0	0	0
5:30 PM	0	0	0	0	0	0	0
5:45 PM	0	0	0	0	0	0	0
6:00 PM	0	0	0	0	0	0	0
6:15 PM	0	0	0	0	0	0	0
6:30 PM	0	0	0	0	0	0	0
6:45 PM	0	0	0	0	0	0	0
7:00 PM	0	0	0	0	0	0	0
7:15 PM	0	0	0	0	0	0	0
7:30 PM	0	0	0	0	0	0	0
7:45 PM	0	0	0	0	0	0	0
8:00 PM	0	0	0	0	0	0	0
8:15 PM	0	0	0	0	0	0	0
8:30 PM	0	0	0	0	0	0	0
8:45 PM	0	0	0	0	0	0	0
9:00 PM	0	0	0	0	0	0	0
9:15 PM	0	0	0	0	0	0	0
9:30 PM	0	0	0	0	0	0	0
9:45 PM	0	0	0	0	0	0	0
10:00 PM	0	0	0	0	0	0	0
10:15 PM	0	0	0	0	0	0	0
10:30 PM	0	0	0	0	0	0	0
10:45 PM	0	0	0	0	0	0	0
11:00 PM	0	0	0	0	0	0	0
11:15 PM	0	0	0	0	0	0	0
11:30 PM	0	0	0	0	0	0	0
11:45 PM	0	0	0	0	0	0	0

Table 75. Commercial (Cayetano) model Winter High day (11-8-10) time resolved PV site estimation.

Time	Winter Low Day (2-14-10)						
	Bus 3 [kW]	Bus 8 [kW]	Bus 16 [kW]	Bus 23 [kW]	Bus 25 [kW]	Bus 27 [kW]	Bus 29 [kW]
12:00 AM	0	0	0	0	0	0	0
12:15 AM	0	0	0	0	0	0	0
12:30 AM	0	0	0	0	0	0	0
12:45 AM	0	0	0	0	0	0	0
1:00 AM	0	0	0	0	0	0	0
1:15 AM	0	0	0	0	0	0	0
1:30 AM	0	0	0	0	0	0	0
1:45 AM	0	0	0	0	0	0	0
2:00 AM	0	0	0	0	0	0	0

Time	Winter Low Day (2-14-10)						
	Bus 3 [kW]	Bus 8 [kW]	Bus 16 [kW]	Bus 23 [kW]	Bus 25 [kW]	Bus 27 [kW]	Bus 29 [kW]
2:15 AM	0	0	0	0	0	0	0
2:30 AM	0	0	0	0	0	0	0
2:45 AM	0	0	0	0	0	0	0
3:00 AM	0	0	0	0	0	0	0
3:15 AM	0	0	0	0	0	0	0
3:30 AM	0	0	0	0	0	0	0
3:45 AM	0	0	0	0	0	0	0
4:00 AM	0	0	0	0	0	0	0
4:15 AM	0	0	0	0	0	0	0
4:30 AM	0	0	0	0	0	0	0
4:45 AM	0	0	0	0	0	0	0
5:00 AM	0	0	0	0	0	0	0
5:15 AM	0	0	0	0	0	0	0
5:30 AM	0	0	0	0	0	0	0
5:45 AM	0	0	0	0	0	0	0
6:00 AM	0	0	0	0	0	0	0
6:15 AM	0	0	0	0	0	0	0
6:30 AM	0	0	0	0	0	0	0
6:45 AM	0.10975	0.035852	3.67091	-0.02595	0	0.024796	4.003371
7:00 AM	0.219499	0.071704	7.34182	-0.0519	0	0.049592	8.006742
7:15 AM	0.714944	0.206368	24.04875	0.862671	0	0.258227	33.50795
7:30 AM	1.210389	0.341033	40.75567	1.777243	0	0.466862	59.00916
7:45 AM	2.175591	0.514456	74.89826	11.77461	0	0.804517	117.6831
8:00 AM	3.140792	0.687879	109.0409	21.77197	0	1.142172	176.357
8:15 AM	3.998461	0.885037	135.9108	28.10662	0	1.308213	219.8747
8:30 AM	4.85613	1.082194	162.7807	34.44126	0	1.474255	263.3925
8:45 AM	5.366368	1.321278	192.9401	45.16815	0	1.698117	303.7873
9:00 AM	5.876606	1.560362	223.0994	55.89505	0	1.92198	344.1821
9:15 AM	6.66918	1.680724	260.1849	69.08226	0	2.322671	385.7882
9:30 AM	7.461754	1.801086	297.2703	82.26947	0	2.723361	427.3942
9:45 AM	8.093663	1.961515	306.0293	90.54638	0	2.887059	446.6635
10:00 AM	8.725571	2.121945	314.7883	98.82328	0	3.050756	465.9328
10:15 AM	9.022134	2.192438	324.9308	103.6909	0	3.255478	481.5035
10:30 AM	9.318696	2.262931	335.0734	108.5586	0	3.4602	497.0743
10:45 AM	9.537376	2.324991	345.3302	113.1735	0	3.486652	530.4612
11:00 AM	9.756055	2.387051	355.5869	117.7885	0	3.513103	563.8481
11:15 AM	9.949003	2.285864	344.1043	115.7656	0	3.596457	563.3104
11:30 AM	10.14195	2.184678	332.6216	113.7428	0	3.679811	562.7728
11:45 AM	9.798275	2.32974	334.527	124.0482	0	3.46342	537.807
12:00 PM	9.454601	2.474802	336.4324	134.3536	0	3.247028	512.8413
12:15 PM	9.672267	2.429497	333.9558	135.5774	0	3.343032	544.6341
12:30 PM	9.889932	2.384192	331.4792	136.8012	0	3.439036	576.4269
12:45 PM	9.659366	2.361104	333.6847	140.0924	0	3.421868	571.2629
1:00 PM	9.4288	2.338016	335.8901	143.3836	0	3.404699	566.0989
1:15 PM	9.220288	2.268793	330.8665	141.7608	0	3.315813	545.926
1:30 PM	9.011776	2.199569	325.8428	140.138	0	3.226926	525.7531
1:45 PM	8.605276	2.100472	306.9949	134.7441	0	3.016432	496.4987

Time	Winter Low Day (2-14-10)						
	Bus 3 [kW]	Bus 8 [kW]	Bus 16 [kW]	Bus 23 [kW]	Bus 25 [kW]	Bus 27 [kW]	Bus 29 [kW]
2:00 PM	8.198775	2.001376	288.147	129.3501	0	2.805938	467.2442
2:15 PM	7.570328	1.853849	253.1932	118.0659	0	2.614974	422.8546
2:30 PM	6.94188	1.706323	218.2393	106.7817	0	2.424009	378.4651
2:45 PM	6.359433	1.60223	207.1605	103.923	0	2.230599	358.125
3:00 PM	5.776986	1.498137	196.0818	101.0644	0	2.037189	337.7849
3:15 PM	4.938974	1.318534	167.4316	93.62162	0	1.773009	296.4823
3:30 PM	4.100962	1.138932	138.7815	86.17886	0	1.50883	255.1797
3:45 PM	3.133426	0.938698	102.9773	74.73867	0	1.258196	210.1342
4:00 PM	2.16589	0.738464	67.17322	63.29848	0	1.007562	165.0887
4:15 PM	1.767282	0.587484	53.66155	52.38951	0	0.780789	128.1407
4:30 PM	1.368674	0.436504	40.14988	41.48054	0	0.554016	91.19265
4:45 PM	1.015608	0.281963	27.22228	25.245	0	0.277008	65.8229
5:00 PM	0.662543	0.127423	14.29468	9.009458	0	0	40.45314
5:15 PM	0.331271	0.063711	7.147342	4.504729	0	0	20.22657
5:30 PM	0	0	0	0	0	0	0
5:45 PM	0	0	0	0	0	0	0
6:00 PM	0	0	0	0	0	0	0
6:15 PM	0	0	0	0	0	0	0
6:30 PM	0	0	0	0	0	0	0
6:45 PM	0	0	0	0	0	0	0
7:00 PM	0	0	0	0	0	0	0
7:15 PM	0	0	0	0	0	0	0
7:30 PM	0	0	0	0	0	0	0
7:45 PM	0	0	0	0	0	0	0
8:00 PM	0	0	0	0	0	0	0
8:15 PM	0	0	0	0	0	0	0
8:30 PM	0	0	0	0	0	0	0
8:45 PM	0	0	0	0	0	0	0
9:00 PM	0	0	0	0	0	0	0
9:15 PM	0	0	0	0	0	0	0
9:30 PM	0	0	0	0	0	0	0
9:45 PM	0	0	0	0	0	0	0
10:00 PM	0	0	0	0	0	0	0
10:15 PM	0	0	0	0	0	0	0
10:30 PM	0	0	0	0	0	0	0
10:45 PM	0	0	0	0	0	0	0
11:00 PM	0	0	0	0	0	0	0
11:15 PM	0	0	0	0	0	0	0
11:30 PM	0	0	0	0	0	0	0
11:45 PM	0	0	0	0	0	0	0

Table 76. Commercial (Cayetano) model Winter Low day (4-4-10) time resolved PV site estimation.

Bus	NP (MVAR)	Control	Temp Thr [^{o}F]		Time Thr [HH:MM]		Voltage Thr [V_{120}]			
			High (On)	**Low (Off)**	**On**	**Off**	**Low (On)**	**High (Off)**	**Mgn**	**Over-ride [min]**

4	1.8	Temp	125	115	(8:15)	(18:45)	-	-	-	-
10	1.2	Temp	125	115	(8:15)	(18:00)	-	-	-	-
15	1.2	Temp	130	120	(5:45)	(21:45)	-	-	-	-
20	1.2	TC w/ VO	-	-	21:00	5:00	120	126	2	60
21	1.2	TC w/ VO	-	-	21:30	5:30	118	125	2	60
22	1.2	Time	-	-	6:45	22:45	-	-	-	-
30	1.8	Temp w/ VO	125	115	-	-	118	125	1.5	60

Table 77. Cayetano Summer High capacitor settings.

Bus	NP (MVAR)	Control	Temp Thr [^{o}F]		Time Thr [HH:MM]		Voltage Thr [V_{120}]			
			High (On)	**Low (Off)**	**On**	**Off**	**Low (On)**	**High (Off)**	**Mgn**	**Over-ride [min]**
4	1.8	Temp	125	115	(8:15)	(18:45)	-	-	-	-
10	1.2	Temp	125	115	(8:15)	(18:00)	-	-	-	-
15	1.2	Temp	130	120	(5:45)	(21:45)	-	-	-	-
20	1.2	TC w/ VO	-	-	21:00	5:00	120	123.5	1.5	60
21	1.2	TC w/ VO	-	-	21:30	5:30	120	123.5	1.5	60
22	1.2	Time	-	-	6:45	22:45	-	-	-	-
30	1.8	Temp w/ VO	125	115	-	-	118	125	1.5	60

Table 78. Cayetano Summer Low capacitor settings.

Bus	NP (MVAR)	Control	Temp Thr [^{o}F]		Time Thr [HH:MM]		Voltage Thr [V_{120}]			
			High (On)	**Low (Off)**	**On**	**Off**	**Low (On)**	**High (Off)**	**Mgn**	**Over-ride [min]**
4	1.8	Off	-	-	-	-	-	-	-	-
10	1.2	Off	-	-	-	-	-	-	-	-
15	1.2	Temp	130	120	(5:45)	(21:45)	-	-	-	-
20	1.2	TC w/ VO	-	-	21:00	5:00	120	126	2.5	60
21	1.2	TC w/ VO	-	-	23:59	6:45	118	124	2.25	60
22	1.2	Time	-	-	6:45	22:45	-	-	-	-
30	1.8	Off	-	-	-	-	-	-	-	-

Table 79. Cayetano Winter High capacitor settings.

Bus	NP [MVAR]	Control	Temp Thr [^{o}F]		Time Thr [HH:MM]		Voltage Thr [V_{120}]			
			High (On)	**Low (Off)**	**On**	**Off**	**Low (On)**	**High (Off)**	**Mgn**	**Over-ride [min]**
4	1.8	Off	-	-	-	-	-	-	-	-
10	1.2	Off	-	-	-	-	-	-	-	-
15	1.2	Temp	130	120	(5:45)	(21:45)	-	-	-	-
20	1.2	TC w/ VO	-	-	21:00	5:00	121	126	2.5	60
21	1.2	TC w/ VO	-	-	21:30	5:30	118	124	2. 5	60
22	1.2	Time	-	-	6:45	22:45	-	-	-	-
30	1.8	Off	-	-	-	-	-	-	-	-

Table 80. Cayetano Winter Low capacitor settings.

Parameter	**Summer High**	**Summer Low**	**Winter High**	**Winter Low**
Nameplate [MVA]	27	27	27	27
Impedance [Ω%]	j0.09	j0.5	j0.25	j0.4
Regulation [%]	±10	±10	±10	±10
Steps	32	32	32	32
V_{LC} [V_{120}]	122	122	122	122
R [Ω]	4	7	2.75	2
X [Ω]	0	0	0	0
Band [V_{120}]	±1.5	±1.75	±1. 5	±1. 5
CT ratio	1300:1	1300:1	1300:1	1300:1
PT ratio	100:1	100:1	100:1	100:1

Table 81. Cayetano sub-station Load Tap Changer with Load Drop Compensator settings.

10.3 Appendix C: Residential (Menlo 1102) Model Settings

Time	Summer High Day (9-28-10)					
	Menlo 1102				Menlo 1101	
	Real Load Demand (P_{LD}) [MW}	Real Deficit Factor (DF_P)	Reactive Load Demand (Q_{LD}) [MVAR]	Reactive Deficit Factor (DF_Q)	Real Load Demand (P) [MW]	Reactive Load Demand (P) [MW]
12:00 AM	4.093	0.989266	1.638	0.972386	3.028	0.473
12:15 AM	4.093	0.989552	1.48	0.972254	3.028	0.459
12:30 AM	4.093	0.989584	1.463	0.972356	3.028	0.432
12:45 AM	4.093	0.989627	1.442	0.972759	3.028	0.345
1:00 AM	3.574	0.990618	1.419	0.981542	3.028	0.311
1:15 AM	3.481	0.990841	1.402	0.984426	3.028	0.258
1:30 AM	3.481	0.990783	1.433	0.984287	3.028	0.25
1:45 AM	3.481	0.990781	1.433	0.984166	3.028	0.274
2:00 AM	3.481	0.990844	1.402	0.984652	3.028	0.214
2:15 AM	3.481	0.99091	1.367	0.984978	2.598	0.205
2:30 AM	3.481	0.990782	1.382	0.978571	2.395	0.173
2:45 AM	3.481	0.990769	1.388	0.978499	2.395	0.185
3:00 AM	3.356	0.99097	1.413	0.981534	2.395	0.235
3:15 AM	3.175	0.99138	1.389	0.986599	2.395	0.178
3:30 AM	3.175	0.991453	1.353	0.986962	2.395	0.159
3:45 AM	3.175	0.991503	1.327	0.987173	2.395	0.156
4:00 AM	3.175	0.991618	1.267	0.987854	2.395	0.116
4:15 AM	3.175	0.991727	1.206	0.988328	2.395	0.119
4:30 AM	3.175	0.991709	1.213	0.987881	2.395	0.186
4:45 AM	3.175	0.991629	1.257	0.987367	2.395	0.217
5:00 AM	3.175	0.99153	1.309	0.986781	2.395	0.254
5:15 AM	3.175	0.991568	1.286	0.986562	2.395	0.324
5:30 AM	3.175	0.991382	1.383	0.986009	2.395	0.302
5:45 AM	3.17872	0.991363	1.395	0.985509	2.395	0.387
6:00 AM	3.182441	0.990595	1.453	1.639761	2.395	0.504
6:15 AM	3.218241	0.990706	1.472	1.631466	2.395	0.468
6:30 AM	3.589042	0.991016	1.393	2.12063	2.508	0.546
6:45 AM	4.29838	0.989886	1.612	1.654198	3.36	0.057
7:00 AM	4.355719	0.990373	1.703	1.088368	3.36	-0.382
7:15 AM	4.408994	0.99049	1.737	1.085841	3.36	-0.376
7:30 AM	4.462269	0.99061	1.754	1.084425	3.419	-0.353
7:45 AM	4.509303	0.990771	1.612	1.095299	3.671	-0.292
8:00 AM	4.556337	0.990448	2.015	1.129592	3.671	-0.278
8:15 AM	5.055899	0.989525	2.116	1.106889	3.671	-0.237
8:30 AM	4.939462	0.989935	2.12	1.110122	3.671	-0.169
8:45 AM	5.160256	0.989663	2.173	1.10018	3.671	-0.118
9:00 AM	5.32305	0.989468	2.252	1.091289	3.671	-0.13
9:15 AM	5.35406	0.989457	2.367	1.082932	3.671	-0.082
9:30 AM	5.385069	0.989513	2.378	1.081561	3.671	-0.027
9:45 AM	5.410289	0.989563	2.387	1.080161	3.789	0.036
10:00 AM	5.435509	0.989752	2.39	1.098959	4.309	-0.049

Time	Summer High Day (9-28-10)					
	Menlo 1102				Menlo 1101	
	Real Load Demand (P_{LD}) [MW}	Real Deficit Factor (DF_P)	Reactive Load Demand (Q_{LD}) [MVAR]	Reactive Deficit Factor (DF_Q)	Real Load Demand (P) [MW]	Reactive Load Demand (P) [MW]
10:15 AM	5.453683	0.989761	2.392	1.098249	4.309	-0.004
10:30 AM	5.471857	0.989659	2.614	1.082304	4.309	0.13
10:45 AM	5.483368	0.989662	2.633	1.080849	4.416	0.154
11:00 AM	5.49488	0.989667	2.593	1.082136	4.61	0.222
11:15 AM	5.497746	0.989703	2.59	1.082263	4.61	0.227
11:30 AM	5.500613	0.989775	2.477	1.087328	4.61	0.365
11:45 AM	6.2938	0.988432	2.879	1.071399	4.61	0.347
12:00 PM	6.418988	0.988089	2.791	1.070771	4.785	0.442
12:15 PM	6.406548	0.988079	2.897	1.065837	4.911	0.393
12:30 PM	6.394108	0.988051	2.933	1.063556	4.911	0.429
12:45 PM	6.385874	0.988153	3.035	1.074192	4.911	0.45
1:00 PM	6.37764	0.988104	3.116	1.068469	4.911	0.593
1:15 PM	6.387661	0.987996	3.136	1.067509	4.911	0.524
1:30 PM	7.088682	0.986352	3.198	1.044423	4.911	0.637
1:45 PM	7.040293	0.986278	3.258	1.040599	4.911	0.784
2:00 PM	7.171904	0.985989	3.276	1.050014	4.911	0.818
2:15 PM	7.133977	0.985896	3.316	1.048558	5.391	0.768
2:30 PM	7.09605	0.985793	3.335	1.046658	5.536	0.849
2:45 PM	7.053132	0.985694	3.253	1.048299	5.676	0.965
3:00 PM	7.010214	0.985581	3.303	1.046601	5.676	0.924
3:15 PM	6.972048	0.985495	3.308	1.046447	5.676	0.912
3:30 PM	7.177882	0.985009	3.394	1.050525	5.633	0.978
3:45 PM	7.553122	0.983968	3.434	1.038671	5.38	0.879
4:00 PM	7.507363	0.983867	3.415	1.039864	5.38	0.821
4:15 PM	7.457712	0.983768	3.391	1.041051	5.38	0.784
4:30 PM	7.408062	0.983672	3.3	1.043598	5.38	0.852
4:45 PM	7.362	0.983515	3.362	1.040408	5.616	0.89
5:00 PM	7.315938	0.98342	3.291	1.043968	5.518	0.806
5:15 PM	7.303256	0.98339	3.326	1.043118	5.444	0.766
5:30 PM	7.685575	0.982467	3.352	0.831892	5.444	0.777
5:45 PM	7.917287	0.981941	3.387	0.826234	5.444	0.782
6:00 PM	7.917	0.98193	3.405	0.826479	5.444	0.812
6:15 PM	7.917	0.981941	3.403	0.827031	5.444	0.749
6:30 PM	7.917	0.981942	3.378	0.825954	5.314	0.791
6:45 PM	7.917	0.981967	3.343	0.82585	5.138	0.704
7:00 PM	7.917	0.981969	3.349	0.826221	5.138	0.685
7:15 PM	8.03	0.981736	3.328	0.823066	5.138	0.598
7:30 PM	7.945	0.981931	3.329	0.825944	5.138	0.567
7:45 PM	7.923	0.981986	3.326	0.826803	5.138	0.537
8:00 PM	7.923	0.982011	3.291	0.826779	5.138	0.431
8:15 PM	7.923	0.982035	3.217	0.82507	4.962	0.378
8:30 PM	7.629	0.982711	3.139	0.832575	4.837	0.275
8:45 PM	7.546	0.982697	3.076	0.819517	4.75	0.279
9:00 PM	7.246	0.983377	2.97	0.826077	4.536	0.177
9:15 PM	6.957	0.983942	2.936	0.828867	4.536	0.618

Time	Summer High Day (9-28-10)					
	Menlo 1102				Menlo 1101	
	Real Load Demand (P_{LD}) [MW}	Real Deficit Factor (DF_P)	Reactive Load Demand (Q_{LD}) [MVAR]	Reactive Deficit Factor (DF_Q)	Real Load Demand (P) [MW]	Reactive Load Demand (P) [MW]
9:30 PM	6.678	0.984473	2.769	1.028806	4.536	1.02
9:45 PM	6.539	0.984791	2.729	1.035051	4.536	0.984
10:00 PM	6.06	0.985421	2.324	0.996876	4.154	0.874
10:15 PM	5.734	0.986083	2.505	1.003347	3.935	0.847
10:30 PM	5.468	0.986696	2.416	1.014389	3.935	0.737
10:45 PM	5.165	0.987363	2.313	1.026688	3.935	0.706
11:00 PM	4.8	0.988007	2.019	1.178593	3.389	0.613
11:15 PM	4.608	0.987745	1.464	1.16072	3.328	0.499
11:30 PM	4.412	0.987996	1.675	1.142913	3.328	0.471
11:45 PM	4.193	0.988445	1.626	1.155819	3.328	0.403

Table 82. Residential (Menlo) model Summer High day (9-28-10) time resolved load demand.

Time	Summer Low Day (7-2-10)					
	Menlo 1102				Menlo 1101	
	Real Load Demand (P_{LD}) [MW}	Real Deficit Factor (DF_P)	Reactive Load Demand (Q_{LD}) [MVAR]	Reactive Deficit Factor (DF_Q)	Real Load Demand (P) [MW]	Reactive Load Demand (P) [MW]
12:00 AM	3.708	0.990723	1.392	0.925423	2.289	-0.022
12:15 AM	3.263	0.991647	1.324	0.929095	2.289	-0.041
12:30 AM	3.102	0.991918	1.348	0.933595	2.289	0.002
12:45 AM	3.102	0.991994	1.303	0.931706	2.289	0.057
1:00 AM	3.102	0.991897	1.359	0.933866	2.289	0.006
1:15 AM	3.102	0.991893	1.359	0.933642	2.289	0.029
1:30 AM	3.102	0.991896	1.36	0.934	2.289	-0.005
1:45 AM	3.102	0.991879	1.369	0.934287	2.289	-0.009
2:00 AM	3.102	0.991868	1.378	0.934953	2.289	-0.053
2:15 AM	3.102	0.991998	1.309	0.93299	2.289	-0.052
2:30 AM	2.883	0.99244	1.3	0.937893	2.289	-0.018
2:45 AM	2.796	0.992619	1.294	0.939805	2.289	-0.016
3:00 AM	2.796	0.992645	1.281	0.939521	2.289	-0.021
3:15 AM	2.796	0.992688	1.257	0.938622	2.289	0.004
3:30 AM	2.796	0.9927	1.209	0.93015	2.289	-0.009
3:45 AM	2.796	0.992703	1.207	0.930067	2.289	-0.008
4:00 AM	2.796	0.992619	1.252	0.931633	2.289	-0.009
4:15 AM	2.796	0.992644	1.242	0.931801	2.289	-0.057
4:30 AM	2.796	0.992625	1.252	0.93208	2.289	-0.052
4:45 AM	2.797755	0.992553	1.286	0.932333	2.289	0.03
5:00 AM	2.799509	0.992603	1.26	0.931075	2.289	0.071
5:15 AM	3.047605	0.992094	1.281	0.926288	2.289	0.002
5:30 AM	3.1057	0.992196	1.161	0.91979	2.289	0.007
5:45 AM	3.13193	0.992209	1.197	0.921511	2.289	0.007
6:00 AM	3.158159	0.992222	1.228	0.922433	2.289	0.052
6:15 AM	3.19836	0.99252	1.112	0.917113	2.289	0.066

Time	Summer Low Day (7-2-10)					
	Menlo 1102				Menlo 1101	
	Real Load Demand (P_{LD}) [MW}	Real Deficit Factor (DF_P)	Reactive Load Demand (Q_{LD}) [MVAR]	Reactive Deficit Factor (DF_Q)	Real Load Demand (P) [MW]	Reactive Load Demand (P) [MW]
6:30 AM	3.27256	0.992638	1.688	0.952831	2.407	0.04
6:45 AM	3.583956	0.992334	1.516	0.950033	2.616	-0.832
7:00 AM	3.628352	0.992226	1.745	0.954016	2.616	-0.757
7:15 AM	3.673554	0.992295	1.76	0.952498	2.616	-0.705
7:30 AM	3.740756	0.992339	1.952	0.951505	2.616	-0.756
7:45 AM	4.395199	0.991252	1.664	0.933396	2.616	-0.64
8:00 AM	4.438642	0.990793	2.404	0.946085	2.616	-0.562
8:15 AM	4.48039	0.990844	2.411	0.94742	2.616	-0.618
8:30 AM	4.522137	0.990965	2.469	0.941459	2.616	-0.412
8:45 AM	4.561171	0.991038	2.538	0.941523	2.616	-0.448
9:00 AM	4.600205	0.991111	2.567	0.940097	2.616	-0.401
9:15 AM	4.634108	0.991178	2.565	0.939096	2.616	-0.355
9:30 AM	4.668011	0.991218	2.64	0.937495	2.871	-0.34
9:45 AM	4.693585	0.991242	2.699	0.935701	3.592	-0.339
10:00 AM	4.719159	0.991272	2.75	0.935117	3.592	-0.336
10:15 AM	4.740314	0.991308	2.768	0.935181	3.592	-0.345
10:30 AM	4.761469	0.991334	2.794	0.934173	3.592	-0.311
10:45 AM	4.77562	0.991348	2.805	0.931947	3.592	-0.207
11:00 AM	4.534771	0.991903	2.769	0.939379	3.592	-0.286
11:15 AM	4.495865	0.992008	2.76	0.939907	3.592	-0.263
11:30 AM	4.502959	0.992055	2.685	0.94052	3.592	-0.246
11:45 AM	4.421569	0.992199	2.712	0.941972	3.592	-0.254
12:00 PM	4.19118	0.992628	2.713	0.945312	3.592	-0.206
12:15 PM	4.183119	0.992633	2.665	0.946157	3.592	-0.212
12:30 PM	4.175058	0.992592	2.734	0.946264	3.592	-0.263
12:45 PM	4.159695	0.992572	2.703	0.945755	3.592	-0.222
1:00 PM	4.144333	0.992546	2.698	0.946258	3.592	-0.242
1:15 PM	4.124121	0.992466	2.767	0.944191	3.592	-0.199
1:30 PM	4.103909	0.992434	2.746	0.944577	3.592	-0.205
1:45 PM	4.076571	0.992405	2.702	0.94685	3.592	-0.278
2:00 PM	4.049233	0.992339	2.715	0.945823	3.592	-0.245
2:15 PM	4.015516	0.99227	2.715	0.946453	3.592	-0.276
2:30 PM	3.9818	0.992176	2.751	0.945117	3.592	-0.245
2:45 PM	3.943981	0.992123	2.689	0.946276	3.592	-0.259
3:00 PM	3.906162	0.99203	2.703	0.945919	3.592	-0.257
3:15 PM	3.863183	0.991961	2.635	0.946506	3.592	-0.242
3:30 PM	3.820204	0.991851	2.659	0.945867	3.592	-0.235
3:45 PM	3.775486	0.991749	2.647	0.94584	3.592	-0.231
4:00 PM	3.730768	0.991664	2.624	0.945426	3.592	-0.203
4:15 PM	3.687482	0.991554	2.505	0.945751	3.592	-0.149
4:30 PM	3.937197	0.990857	2.6	0.940133	3.592	-0.223
4:45 PM	3.899082	0.990696	2.595	0.93863	3.592	-0.169
5:00 PM	3.852966	0.990566	2.596	0.938666	3.592	-0.177
5:15 PM	4.055704	0.99008	2.548	0.935192	3.592	-0.239
5:30 PM	4.091442	0.98945	2.203	0.922938	3.592	-0.221

Time	Summer Low Day (7-2-10)					
	Menlo 1102				Menlo 1101	
	Real Load Demand (P_{LD}) [MW}	Real Deficit Factor (DF_P)	Reactive Load Demand (Q_{LD}) [MVAR]	Reactive Deficit Factor (DF_Q)	Real Load Demand (P) [MW]	Reactive Load Demand (P) [MW]
5:45 PM	4.067712	0.989353	2.182	0.921431	3.592	-0.163
6:00 PM	4.131982	0.98919	2.246	0.919436	3.592	-0.19
6:15 PM	4.341375	0.98872	2.179	0.913933	3.592	-0.216
6:30 PM	4.337767	0.988712	2.167	0.916134	3.592	-0.3
6:45 PM	4.334996	0.988693	2.163	0.915142	3.592	-0.263
7:00 PM	4.332225	0.9886	2.051	0.919918	3.42	-0.425
7:15 PM	4.331613	0.988649	2.086	0.922262	3.286	-0.503
7:30 PM	4.331	0.988642	2.074	0.923446	3.286	-0.545
7:45 PM	4.331	0.988624	2.059	0.923188	3.286	-0.534
8:00 PM	4.331	0.988645	2.075	0.923773	3.286	-0.557
8:15 PM	4.489	0.988369	2.092	0.918989	3.286	-0.566
8:30 PM	4.636	0.98809	2.096	0.913591	3.286	-0.542
8:45 PM	4.636	0.98815	2.163	0.91372	3.286	-0.544
9:00 PM	4.636	0.988128	2.161	0.910663	3.286	-0.429
9:15 PM	4.636	0.988289	2.429	0.906628	3.286	0.434
9:30 PM	4.636	0.988113	1.742	0.870081	3.286	0.415
9:45 PM	4.636	0.988147	2.074	0.881736	3.286	0.384
10:00 PM	4.636	0.987744	1.988	0.903358	3.286	0.378
10:15 PM	4.372	0.988309	1.895	0.908987	3.068	0.34
10:30 PM	4.32	0.988443	1.863	0.911087	2.985	0.212
10:45 PM	4.057	0.988951	1.811	0.917805	2.809	0.17
11:00 PM	3.85	0.99029	1.457	0.921658	2.68	0.148
11:15 PM	3.703	0.990585	1.467	0.926823	2.68	0.069
11:30 PM	3.629	0.990813	1.427	0.928091	2.444	0.037
11:45 PM	3.397	0.991188	1.422	0.927816	2.368	0.037

Table 83. Residential (Menlo) model Summer Low day (7-2-10) time resolved load demand.

Time	Menlo 1102 Summer High day (P**art 1) [kW]**											
	B2	B3	B4	B6	B9	B11	B15	B16	B17	B18	B19	B20
12:00 AM	0.00	0.00	0.00	0.00	0.00	0.00	0.00	0.00	0.00	0.00	0.00	0.00
12:15 AM	0.00	0.00	0.00	0.00	0.00	0.00	0.00	0.00	0.00	0.00	0.00	0.00
12:30 AM	0.00	0.00	0.00	0.00	0.00	0.00	0.00	0.00	0.00	0.00	0.00	0.00
12:45 AM	0.00	0.00	0.00	0.00	0.00	0.00	0.00	0.00	0.00	0.00	0.00	0.00
1:00 AM	0.00	0.00	0.00	0.00	0.00	0.00	0.00	0.00	0.00	0.00	0.00	0.00
1:15 AM	0.00	0.00	0.00	0.00	0.00	0.00	0.00	0.00	0.00	0.00	0.00	0.00
1:30 AM	0.00	0.00	0.00	0.00	0.00	0.00	0.00	0.00	0.00	0.00	0.00	0.00
1:45 AM	0.00	0.00	0.00	0.00	0.00	0.00	0.00	0.00	0.00	0.00	0.00	0.00
2:00 AM	0.00	0.00	0.00	0.00	0.00	0.00	0.00	0.00	0.00	0.00	0.00	0.00
2:15 AM	0.00	0.00	0.00	0.00	0.00	0.00	0.00	0.00	0.00	0.00	0.00	0.00
2:30 AM	0.00	0.00	0.00	0.00	0.00	0.00	0.00	0.00	0.00	0.00	0.00	0.00
2:45 AM	0.00	0.00	0.00	0.00	0.00	0.00	0.00	0.00	0.00	0.00	0.00	0.00
3:00 AM	0.00	0.00	0.00	0.00	0.00	0.00	0.00	0.00	0.00	0.00	0.00	0.00
3:15 AM	0.00	0.00	0.00	0.00	0.00	0.00	0.00	0.00	0.00	0.00	0.00	0.00

Time	Menlo 1102 Summer High day (P**art 1) [kW]**											
	B2	B3	B4	B6	B9	B11	B15	B16	B17	B18	B19	B20
3:30 AM	0.00	0.00	0.00	0.00	0.00	0.00	0.00	0.00	0.00	0.00	0.00	0.00
3:45 AM	0.00	0.00	0.00	0.00	0.00	0.00	0.00	0.00	0.00	0.00	0.00	0.00
4:00 AM	0.00	0.00	0.00	0.00	0.00	0.00	0.00	0.00	0.00	0.00	0.00	0.00
4:15 AM	0.00	0.00	0.00	0.00	0.00	0.00	0.00	0.00	0.00	0.00	0.00	0.00
4:30 AM	0.00	0.00	0.00	0.00	0.00	0.00	0.00	0.00	0.00	0.00	0.00	0.00
4:45 AM	0.00	0.00	0.00	0.00	0.00	0.00	0.00	0.00	0.00	0.00	0.00	0.00
5:00 AM	0.00	0.00	0.00	0.00	0.00	0.00	0.00	0.00	0.00	0.00	0.00	0.00
5:15 AM	0.00	0.00	0.00	0.00	0.00	0.00	0.00	0.00	0.00	0.00	0.00	0.00
5:30 AM	0.00	0.00	0.00	0.00	0.00	0.00	0.00	0.00	0.00	0.00	0.00	0.00
5:45 AM	0.03	0.02	0.03	0.00	0.07	0.38	1.13	0.20	0.60	0.06	0.21	0.12
6:00 AM	0.06	0.03	0.05	0.00	0.13	0.75	2.26	0.40	1.20	0.12	0.41	0.23
6:15 AM	0.56	0.29	0.49	0.00	0.76	5.30	10.21	1.67	4.97	0.48	3.56	0.97
6:30 AM	1.06	0.55	0.93	0.00	1.39	9.84	18.17	2.94	8.74	0.84	6.70	1.70
6:45 AM	1.62	0.85	1.43	0.00	2.17	17.43	38.04	4.71	14.00	1.34	10.52	2.70
7:00 AM	2.19	1.15	1.93	0.00	2.96	25.02	57.92	6.48	19.26	1.84	14.34	3.70
7:15 AM	2.82	1.48	2.48	0.00	3.79	31.74	73.99	8.18	24.31	2.37	18.20	4.76
7:30 AM	3.45	1.81	3.03	0.00	4.62	38.47	90.06	9.88	29.35	2.90	22.07	5.82
7:45 AM	4.05	2.13	3.56	0.00	5.32	44.67	103.23	11.44	33.97	3.33	25.77	6.70
8:00 AM	4.66	2.44	4.10	0.00	6.03	50.88	116.40	12.99	38.59	3.77	29.48	7.58
8:15 AM	5.09	2.67	4.47	0.00	6.38	53.22	130.34	14.24	42.30	4.16	32.33	8.36
8:30 AM	5.51	2.89	4.84	0.00	6.74	55.56	144.28	15.49	46.01	4.55	35.19	9.14
8:45 AM	5.78	3.03	5.08	0.00	7.65	63.35	155.43	16.86	50.10	4.93	38.07	9.90
9:00 AM	6.05	3.17	5.32	0.00	8.57	71.14	166.59	18.24	54.18	5.31	40.95	10.66
9:15 AM	6.66	3.49	5.86	0.00	9.12	76.03	174.95	19.15	56.89	5.65	43.47	11.35
9:30 AM	7.27	3.81	6.39	0.00	9.68	80.92	183.31	20.06	59.60	5.99	45.99	12.03
9:45 AM	7.55	3.96	6.63	0.00	9.87	83.40	191.09	20.90	62.09	6.22	47.77	12.48
10:00 AM	7.83	4.10	6.88	0.00	10.07	85.87	198.87	21.74	64.58	6.44	49.55	12.94
10:15 AM	8.02	4.20	7.05	0.00	10.44	88.03	204.32	22.38	66.48	6.63	50.72	13.32
10:30 AM	8.21	4.30	7.21	0.00	10.82	90.19	209.77	23.02	68.39	6.82	51.90	13.70
10:45 AM	8.47	4.44	7.44	0.00	10.90	90.26	214.41	23.54	69.94	6.89	52.48	13.85
11:00 AM	8.73	4.57	7.67	0.00	10.99	90.34	219.04	24.06	71.49	6.95	53.06	14.00
11:15 AM	8.75	4.58	7.69	0.00	11.02	91.97	218.73	24.02	71.37	6.98	53.34	14.05
11:30 AM	8.77	4.60	7.71	0.00	11.04	93.59	218.42	23.98	71.25	7.00	53.61	14.10
11:45 AM	8.67	4.54	7.62	0.00	11.10	93.11	206.86	23.68	70.34	6.93	53.13	13.94
12:00 PM	8.57	4.49	7.53	0.00	11.15	92.63	195.31	23.37	69.43	6.86	52.65	13.78
12:15 PM	8.51	4.46	7.48	0.00	10.92	90.87	191.08	23.15	68.78	6.73	51.68	13.53
12:30 PM	8.45	4.43	7.43	0.00	10.69	89.11	186.85	22.93	68.13	6.61	50.71	13.28
12:45 PM	8.23	4.31	7.23	0.00	10.59	88.27	190.52	21.81	64.79	6.50	50.12	13.06
1:00 PM	8.00	4.19	7.03	0.00	10.49	87.43	194.20	20.69	61.45	6.39	49.53	12.84
1:15 PM	7.63	4.00	6.71	0.00	9.98	82.88	190.06	20.53	60.98	6.19	47.44	12.45
1:30 PM	7.26	3.80	6.38	0.00	9.46	78.34	185.92	20.37	60.51	6.00	45.35	12.05
1:45 PM	6.86	3.60	6.03	0.00	8.94	75.16	172.88	19.16	56.91	5.63	42.94	11.32
2:00 PM	6.46	3.39	5.68	0.00	8.42	71.98	159.84	17.95	53.32	5.27	40.53	10.59
2:15 PM	6.03	3.16	5.30	0.00	7.73	64.22	150.19	16.89	50.18	4.86	37.86	9.77
2:30 PM	5.59	2.93	4.91	0.00	7.04	56.45	140.53	15.84	47.04	4.45	35.18	8.94
2:45 PM	5.19	2.72	4.56	0.00	6.60	53.93	128.93	14.00	41.58	4.00	30.59	8.04
3:00 PM	4.78	2.51	4.20	0.00	6.15	51.40	117.32	12.16	36.12	3.55	25.99	7.13
3:15 PM	4.27	2.24	3.75	0.00	5.39	45.52	104.69	11.20	33.27	3.26	24.55	6.55

Time	Menlo 1102 Summer High day (Part 1) [kW]											
	B2	B3	B4	B6	B9	B11	B15	B16	B17	B18	B19	B20
3:30 PM	3.76	1.97	3.30	0.00	4.63	39.64	92.06	10.24	30.41	2.97	23.11	5.96
3:45 PM	3.17	1.66	2.79	0.00	4.02	33.73	78.52	8.67	25.74	2.57	19.39	5.17
4:00 PM	2.58	1.35	2.27	0.00	3.42	27.81	64.97	7.10	21.08	2.17	15.67	4.37
4:15 PM	2.01	1.05	1.77	0.00	2.53	20.47	50.88	5.22	15.51	1.67	12.14	3.36
4:30 PM	1.44	0.76	1.27	0.00	1.64	13.14	36.78	3.35	9.94	1.17	8.62	2.36
4:45 PM	0.91	0.48	0.80	0.00	1.00	8.13	22.35	2.21	6.57	0.73	5.46	1.47
5:00 PM	0.38	0.20	0.33	0.00	0.36	3.11	7.93	1.08	3.21	0.29	2.31	0.57
5:15 PM	0.19	0.10	0.17	0.00	0.19	1.59	4.03	0.55	1.65	0.15	1.19	0.30
5:30 PM	0.01	0.01	0.01	0.00	0.01	0.06	0.12	0.03	0.09	0.01	0.07	0.02
5:45 PM	0.00	0.00	0.00	0.00	0.00	0.03	0.06	0.01	0.04	0.00	0.03	0.01
6:00 PM	0.00	0.00	0.00	0.00	0.00	0.00	0.00	0.00	0.00	0.00	0.00	0.00
6:15 PM	0.00	0.00	0.00	0.00	0.00	0.00	0.00	0.00	0.00	0.00	0.00	0.00
6:30 PM	0.00	0.00	0.00	0.00	0.00	0.00	0.00	0.00	0.00	0.00	0.00	0.00
6:45 PM	0.00	0.00	0.00	0.00	0.00	0.00	0.00	0.00	0.00	0.00	0.00	0.00
7:00 PM	0.00	0.00	0.00	0.00	0.00	0.00	0.00	0.00	0.00	0.00	0.00	0.00
7:15 PM	0.00	0.00	0.00	0.00	0.00	0.00	0.00	0.00	0.00	0.00	0.00	0.00
7:30 PM	0.00	0.00	0.00	0.00	0.00	0.00	0.00	0.00	0.00	0.00	0.00	0.00
7:45 PM	0.00	0.00	0.00	0.00	0.00	0.00	0.00	0.00	0.00	0.00	0.00	0.00
8:00 PM	0.00	0.00	0.00	0.00	0.00	0.00	0.00	0.00	0.00	0.00	0.00	0.00
8:15 PM	0.00	0.00	0.00	0.00	0.00	0.00	0.00	0.00	0.00	0.00	0.00	0.00
8:30 PM	0.00	0.00	0.00	0.00	0.00	0.00	0.00	0.00	0.00	0.00	0.00	0.00
8:45 PM	0.00	0.00	0.00	0.00	0.00	0.00	0.00	0.00	0.00	0.00	0.00	0.00
9:00 PM	0.00	0.00	0.00	0.00	0.00	0.00	0.00	0.00	0.00	0.00	0.00	0.00
9:15 PM	0.00	0.00	0.00	0.00	0.00	0.00	0.00	0.00	0.00	0.00	0.00	0.00
9:30 PM	0.00	0.00	0.00	0.00	0.00	0.00	0.00	0.00	0.00	0.00	0.00	0.00
9:45 PM	0.00	0.00	0.00	0.00	0.00	0.00	0.00	0.00	0.00	0.00	0.00	0.00
10:00 PM	0.00	0.00	0.00	0.00	0.00	0.00	0.00	0.00	0.00	0.00	0.00	0.00
10:15 PM	0.00	0.00	0.00	0.00	0.00	0.00	0.00	0.00	0.00	0.00	0.00	0.00
10:30 PM	0.00	0.00	0.00	0.00	0.00	0.00	0.00	0.00	0.00	0.00	0.00	0.00
10:45 PM	0.00	0.00	0.00	0.00	0.00	0.00	0.00	0.00	0.00	0.00	0.00	0.00
11:00 PM	0.00	0.00	0.00	0.00	0.00	0.00	0.00	0.00	0.00	0.00	0.00	0.00
11:15 PM	0.00	0.00	0.00	0.00	0.00	0.00	0.00	0.00	0.00	0.00	0.00	0.00
11:30 PM	0.00	0.00	0.00	0.00	0.00	0.00	0.00	0.00	0.00	0.00	0.00	0.00
11:45 PM	0.00	0.00	0.00	0.00	0.00	0.00	0.00	0.00	0.00	0.00	0.00	0.00

Table 84. Residential (Menlo) model Summer High day (9-28-10) time resolved PV site estimation (Part 1 of 2).

Time	Menlo 1102 Summer High day (Part 2) [kW]											
	B24	B26	B28	B29	B31	B32	B33	B34	B35	B38	B39	B41
12:00 AM	0.00	0.00	0.00	0.00	0.00	0.00	0.00	0.00	0.00	0.00	0.00	0.00
12:15 AM	0.00	0.00	0.00	0.00	0.00	0.00	0.00	0.00	0.00	0.00	0.00	0.00
12:30 AM	0.00	0.00	0.00	0.00	0.00	0.00	0.00	0.00	0.00	0.00	0.00	0.00
12:45 AM	0.00	0.00	0.00	0.00	0.00	0.00	0.00	0.00	0.00	0.00	0.00	0.00
1:00 AM	0.00	0.00	0.00	0.00	0.00	0.00	0.00	0.00	0.00	0.00	0.00	0.00
1:15 AM	0.00	0.00	0.00	0.00	0.00	0.00	0.00	0.00	0.00	0.00	0.00	0.00
1:30 AM	0.00	0.00	0.00	0.00	0.00	0.00	0.00	0.00	0.00	0.00	0.00	0.00

Time	Menlo 1102 Summer High day (P**art 2) [kW]**											
	B24	B26	B28	B29	B31	B32	B33	B34	B35	B38	B39	B41
1:45 AM	0.00	0.00	0.00	0.00	0.00	0.00	0.00	0.00	0.00	0.00	0.00	0.00
2:00 AM	0.00	0.00	0.00	0.00	0.00	0.00	0.00	0.00	0.00	0.00	0.00	0.00
2:15 AM	0.00	0.00	0.00	0.00	0.00	0.00	0.00	0.00	0.00	0.00	0.00	0.00
2:30 AM	0.00	0.00	0.00	0.00	0.00	0.00	0.00	0.00	0.00	0.00	0.00	0.00
2:45 AM	0.00	0.00	0.00	0.00	0.00	0.00	0.00	0.00	0.00	0.00	0.00	0.00
3:00 AM	0.00	0.00	0.00	0.00	0.00	0.00	0.00	0.00	0.00	0.00	0.00	0.00
3:15 AM	0.00	0.00	0.00	0.00	0.00	0.00	0.00	0.00	0.00	0.00	0.00	0.00
3:30 AM	0.00	0.00	0.00	0.00	0.00	0.00	0.00	0.00	0.00	0.00	0.00	0.00
3:45 AM	0.00	0.00	0.00	0.00	0.00	0.00	0.00	0.00	0.00	0.00	0.00	0.00
4:00 AM	0.00	0.00	0.00	0.00	0.00	0.00	0.00	0.00	0.00	0.00	0.00	0.00
4:15 AM	0.00	0.00	0.00	0.00	0.00	0.00	0.00	0.00	0.00	0.00	0.00	0.00
4:30 AM	0.00	0.00	0.00	0.00	0.00	0.00	0.00	0.00	0.00	0.00	0.00	0.00
4:45 AM	0.00	0.00	0.00	0.00	0.00	0.00	0.00	0.00	0.00	0.00	0.00	0.00
5:00 AM	0.00	0.00	0.00	0.00	0.00	0.00	0.00	0.00	0.00	0.00	0.00	0.00
5:15 AM	0.00	0.00	0.00	0.00	0.00	0.00	0.00	0.00	0.00	0.00	0.00	0.00
5:30 AM	0.00	0.00	0.00	0.00	0.00	0.00	0.00	0.00	0.00	0.00	0.00	0.00
5:45 AM	0.25	0.01	0.01	0.01	0.03	0.01	0.20	0.05	0.10	0.05	0.07	0.11
6:00 AM	0.51	0.02	0.03	0.01	0.06	0.02	0.40	0.10	0.21	0.09	0.14	0.21
6:15 AM	3.05	0.18	0.17	0.13	0.61	0.19	4.25	1.07	2.22	0.36	0.88	0.88
6:30 AM	5.59	0.33	0.31	0.25	1.17	0.37	8.10	2.03	4.22	0.64	1.63	1.55
6:45 AM	9.11	0.52	0.50	0.39	1.82	0.58	12.67	3.18	6.61	0.99	2.72	2.47
7:00 AM	12.62	0.70	0.69	0.52	2.46	0.78	17.25	4.33	9.00	1.35	3.82	3.39
7:15 AM	16.21	0.88	0.89	0.66	3.15	1.00	22.06	5.54	11.51	1.73	4.86	4.36
7:30 AM	19.80	1.06	1.09	0.81	3.84	1.22	26.88	6.76	14.02	2.12	5.90	5.33
7:45 AM	22.85	1.24	1.26	0.94	4.44	1.43	31.36	7.89	16.36	2.46	6.77	6.14
8:00 AM	25.90	1.41	1.42	1.06	5.04	1.63	35.84	9.02	18.70	2.81	7.64	6.94
8:15 AM	28.85	1.58	1.59	1.17	5.55	1.79	39.30	9.88	20.50	3.08	8.41	7.66
8:30 AM	31.80	1.76	1.75	1.28	6.05	1.94	42.75	10.74	22.30	3.36	9.17	8.38
8:45 AM	33.81	1.88	1.86	1.38	6.64	2.12	46.66	11.73	24.34	3.61	9.96	9.07
9:00 AM	35.83	2.00	1.97	1.48	7.23	2.30	50.58	12.71	26.38	3.86	10.75	9.77
9:15 AM	38.08	2.13	2.09	1.56	7.57	2.40	52.94	13.31	27.62	4.06	11.28	10.40
9:30 AM	40.34	2.25	2.22	1.64	7.90	2.51	55.31	13.90	28.85	4.26	11.82	11.02
9:45 AM	42.18	2.33	2.32	1.71	8.27	2.63	57.83	14.54	30.17	4.45	12.46	11.45
10:00 AM	44.01	2.41	2.42	1.79	8.63	2.74	60.35	15.18	31.48	4.65	13.10	11.87
10:15 AM	45.27	2.48	2.49	1.84	8.87	2.82	62.06	15.60	32.37	4.81	13.26	12.21
10:30 AM	46.53	2.55	2.56	1.89	9.11	2.90	63.76	16.02	33.26	4.97	13.42	12.56
10:45 AM	46.78	2.61	2.57	1.92	9.17	2.95	65.06	16.35	33.94	5.06	13.65	12.68
11:00 AM	47.03	2.67	2.59	1.95	9.23	3.01	66.36	16.68	34.62	5.16	13.88	12.81
11:15 AM	47.68	2.67	2.62	1.96	9.35	3.02	66.53	16.73	34.70	5.17	13.97	12.85
11:30 AM	48.33	2.67	2.66	1.98	9.47	3.03	66.70	16.78	34.79	5.17	14.06	12.90
11:45 AM	48.31	2.66	2.66	1.96	9.40	3.00	65.93	16.58	34.39	5.13	14.11	12.76
12:00 PM	48.29	2.64	2.66	1.95	9.32	2.96	65.16	16.38	33.99	5.08	14.16	12.63
12:15 PM	47.48	2.59	2.61	1.90	9.19	2.91	63.98	16.08	33.38	5.00	13.86	12.40
12:30 PM	46.66	2.53	2.57	1.86	9.05	2.85	62.80	15.78	32.76	4.91	13.55	12.17
12:45 PM	45.20	2.46	2.49	1.81	8.88	2.79	61.33	15.42	31.99	4.84	13.28	11.97
1:00 PM	43.74	2.39	2.41	1.76	8.70	2.72	59.87	15.06	31.23	4.77	13.00	11.76
1:15 PM	42.22	2.31	2.32	1.70	8.38	2.61	57.43	14.44	29.96	4.51	12.53	11.40
1:30 PM	40.70	2.24	2.24	1.65	8.05	2.50	55.00	13.82	28.69	4.25	12.06	11.04

Time	Menlo 1102 Summer High day (Part 2) [kW]											
	B24	B26	B28	B29	B31	B32	B33	B34	B35	B38	B39	B41
1:45 PM	38.81	2.11	2.13	1.57	7.65	2.37	52.08	13.09	27.17	4.07	11.46	10.37
2:00 PM	36.91	1.97	2.03	1.50	7.25	2.23	49.16	12.36	25.64	3.88	10.86	9.70
2:15 PM	34.20	1.87	1.88	1.38	6.63	2.10	46.37	11.65	24.19	3.66	9.93	8.95
2:30 PM	31.49	1.76	1.73	1.27	6.00	1.98	43.58	10.94	22.74	3.44	9.01	8.20
2:45 PM	28.76	1.58	1.58	1.16	5.56	1.76	38.74	9.73	20.21	3.15	8.42	7.37
3:00 PM	26.03	1.39	1.43	1.05	5.11	1.54	33.90	8.52	17.68	2.86	7.82	6.54
3:15 PM	23.54	1.28	1.29	0.95	4.57	1.38	30.43	7.65	15.87	2.50	6.90	6.00
3:30 PM	21.04	1.16	1.16	0.85	4.02	1.22	26.95	6.77	14.06	2.14	5.98	5.46
3:45 PM	17.48	0.98	0.96	0.72	3.37	1.07	23.46	5.89	12.24	1.82	4.98	4.73
4:00 PM	13.92	0.80	0.77	0.60	2.71	0.91	19.96	5.02	10.41	1.50	3.99	4.00
4:15 PM	11.32	0.59	0.62	0.47	2.22	0.71	15.68	3.94	8.18	1.08	3.20	3.08
4:30 PM	8.72	0.38	0.48	0.35	1.73	0.52	11.40	2.86	5.95	0.66	2.41	2.16
4:45 PM	4.36	0.25	0.24	0.22	1.03	0.31	6.90	1.73	3.60	0.45	1.46	1.34
5:00 PM	0.00	0.12	0.00	0.09	0.32	0.11	2.39	0.60	1.25	0.25	0.51	0.53
5:15 PM	0.00	0.07	0.00	0.05	0.17	0.06	1.22	0.31	0.63	0.14	0.26	0.27
5:30 PM	0.00	0.01	0.00	0.01	0.01	0.00	0.04	0.01	0.02	0.02	0.02	0.02
5:45 PM	0.00	0.01	0.00	0.00	0.00	0.00	0.02	0.01	0.01	0.01	0.01	0.01
6:00 PM	0.00	0.00	0.00	0.00	0.00	0.00	0.00	0.00	0.00	0.00	0.00	0.00
6:15 PM	0.00	0.00	0.00	0.00	0.00	0.00	0.00	0.00	0.00	0.00	0.00	0.00
6:30 PM	0.00	0.00	0.00	0.00	0.00	0.00	0.00	0.00	0.00	0.00	0.00	0.00
6:45 PM	0.00	0.00	0.00	0.00	0.00	0.00	0.00	0.00	0.00	0.00	0.00	0.00
7:00 PM	0.00	0.00	0.00	0.00	0.00	0.00	0.00	0.00	0.00	0.00	0.00	0.00
7:15 PM	0.00	0.00	0.00	0.00	0.00	0.00	0.00	0.00	0.00	0.00	0.00	0.00
7:30 PM	0.00	0.00	0.00	0.00	0.00	0.00	0.00	0.00	0.00	0.00	0.00	0.00
7:45 PM	0.00	0.00	0.00	0.00	0.00	0.00	0.00	0.00	0.00	0.00	0.00	0.00
8:00 PM	0.00	0.00	0.00	0.00	0.00	0.00	0.00	0.00	0.00	0.00	0.00	0.00
8:15 PM	0.00	0.00	0.00	0.00	0.00	0.00	0.00	0.00	0.00	0.00	0.00	0.00
8:30 PM	0.00	0.00	0.00	0.00	0.00	0.00	0.00	0.00	0.00	0.00	0.00	0.00
8:45 PM	0.00	0.00	0.00	0.00	0.00	0.00	0.00	0.00	0.00	0.00	0.00	0.00
9:00 PM	0.00	0.00	0.00	0.00	0.00	0.00	0.00	0.00	0.00	0.00	0.00	0.00
9:15 PM	0.00	0.00	0.00	0.00	0.00	0.00	0.00	0.00	0.00	0.00	0.00	0.00
9:30 PM	0.00	0.00	0.00	0.00	0.00	0.00	0.00	0.00	0.00	0.00	0.00	0.00
9:45 PM	0.00	0.00	0.00	0.00	0.00	0.00	0.00	0.00	0.00	0.00	0.00	0.00
10:00 PM	0.00	0.00	0.00	0.00	0.00	0.00	0.00	0.00	0.00	0.00	0.00	0.00
10:15 PM	0.00	0.00	0.00	0.00	0.00	0.00	0.00	0.00	0.00	0.00	0.00	0.00
10:30 PM	0.00	0.00	0.00	0.00	0.00	0.00	0.00	0.00	0.00	0.00	0.00	0.00
10:45 PM	0.00	0.00	0.00	0.00	0.00	0.00	0.00	0.00	0.00	0.00	0.00	0.00
11:00 PM	0.00	0.00	0.00	0.00	0.00	0.00	0.00	0.00	0.00	0.00	0.00	0.00
11:15 PM	0.00	0.00	0.00	0.00	0.00	0.00	0.00	0.00	0.00	0.00	0.00	0.00
11:30 PM	0.00	0.00	0.00	0.00	0.00	0.00	0.00	0.00	0.00	0.00	0.00	0.00
11:45 PM	0.00	0.00	0.00	0.00	0.00	0.00	0.00	0.00	0.00	0.00	0.00	0.00

Table 85. Residential (Menlo) model Summer High day (9-28-10) time resolved PV site estimation (Part 2 of 2).

Time	Menlo 1102 Summer Low day (Part 1) [kW]											
	B2	B3	B4	B6	B9	B11	B15	B16	B17	B18	B19	B20

Time	Menlo 1102 Summer Low day (P**art 1) [kW]**											
	B2	B3	B4	B6	B9	B11	B15	B16	B17	B18	B19	B20
12:00 AM	0.00	0.00	0.00	0.00	0.00	0.00	0.00	0.00	0.00	0.00	0.00	0.00
12:15 AM	0.00	0.00	0.00	0.00	0.00	0.00	0.00	0.00	0.00	0.00	0.00	0.00
12:30 AM	0.00	0.00	0.00	0.00	0.00	0.00	0.00	0.00	0.00	0.00	0.00	0.00
12:45 AM	0.00	0.00	0.00	0.00	0.00	0.00	0.00	0.00	0.00	0.00	0.00	0.00
1:00 AM	0.00	0.00	0.00	0.00	0.00	0.00	0.00	0.00	0.00	0.00	0.00	0.00
1:15 AM	0.00	0.00	0.00	0.00	0.00	0.00	0.00	0.00	0.00	0.00	0.00	0.00
1:30 AM	0.00	0.00	0.00	0.00	0.00	0.00	0.00	0.00	0.00	0.00	0.00	0.00
1:45 AM	0.00	0.00	0.00	0.00	0.00	0.00	0.00	0.00	0.00	0.00	0.00	0.00
2:00 AM	0.00	0.00	0.00	0.00	0.00	0.00	0.00	0.00	0.00	0.00	0.00	0.00
2:15 AM	0.00	0.00	0.00	0.00	0.00	0.00	0.00	0.00	0.00	0.00	0.00	0.00
2:30 AM	0.00	0.00	0.00	0.00	0.00	0.00	0.00	0.00	0.00	0.00	0.00	0.00
2:45 AM	0.00	0.00	0.00	0.00	0.00	0.00	0.00	0.00	0.00	0.00	0.00	0.00
3:00 AM	0.00	0.00	0.00	0.00	0.00	0.00	0.00	0.00	0.00	0.00	0.00	0.00
3:15 AM	0.00	0.00	0.00	0.00	0.00	0.00	0.00	0.00	0.00	0.00	0.00	0.00
3:30 AM	0.00	0.00	0.00	0.00	0.00	0.00	0.00	0.00	0.00	0.00	0.00	0.00
3:45 AM	0.00	0.00	0.00	0.00	0.00	0.00	0.00	0.00	0.00	0.00	0.00	0.00
4:00 AM	0.00	0.00	0.00	0.00	0.00	0.00	0.00	0.00	0.00	0.00	0.00	0.00
4:15 AM	0.00	0.00	0.00	0.00	0.00	0.00	0.00	0.00	0.00	0.00	0.00	0.00
4:30 AM	0.00	0.00	0.00	0.00	0.00	0.00	0.00	0.00	0.00	0.00	0.00	0.00
4:45 AM	0.01	0.01	0.01	0.00	0.04	0.32	0.73	0.03	0.10	0.02	0.07	0.05
5:00 AM	0.02	0.01	0.02	0.00	0.08	0.64	1.46	0.07	0.20	0.05	0.14	0.10
5:15 AM	0.06	0.03	0.05	0.00	0.11	0.91	2.13	0.20	0.60	0.07	0.40	0.14
5:30 AM	0.10	0.05	0.09	0.00	0.15	1.19	2.79	0.34	1.01	0.09	0.67	0.18
5:45 AM	0.35	0.18	0.31	0.00	0.47	3.89	11.32	1.27	3.77	0.36	2.76	0.73
6:00 AM	0.60	0.32	0.53	0.00	0.79	6.58	19.85	2.20	6.52	0.63	4.85	1.27
6:15 AM	1.07	0.56	0.94	0.00	1.40	11.70	31.60	3.47	10.32	1.02	7.83	2.04
6:30 AM	1.54	0.81	1.35	0.00	2.02	16.82	43.34	4.75	14.12	1.40	10.81	2.81
6:45 AM	2.08	1.09	1.82	0.00	2.73	22.73	56.51	6.21	18.44	1.83	14.06	3.67
7:00 AM	2.62	1.37	2.30	0.00	3.44	28.64	69.68	7.66	22.76	2.26	17.31	4.53
7:15 AM	3.18	1.67	2.79	0.00	4.17	34.75	83.25	9.15	27.18	2.69	20.32	5.41
7:30 AM	3.74	1.96	3.29	0.00	4.91	40.86	96.83	10.63	31.59	3.13	23.32	6.29
7:45 AM	4.29	2.25	3.77	0.00	5.64	46.86	109.12	12.00	35.65	3.53	26.78	7.10
8:00 AM	4.84	2.54	4.26	0.00	6.36	52.86	121.41	13.36	39.70	3.93	30.24	7.91
8:15 AM	5.35	2.81	4.71	0.00	7.04	58.49	134.25	14.57	43.29	4.31	33.06	8.67
8:30 AM	5.87	3.08	5.16	0.00	7.71	64.12	147.08	15.78	46.88	4.69	35.88	9.43
8:45 AM	6.29	3.30	5.53	0.00	8.24	68.46	158.65	17.27	51.29	5.08	38.99	10.21
9:00 AM	6.72	3.52	5.90	0.00	8.78	72.79	170.22	18.75	55.71	5.47	42.11	10.99
9:15 AM	7.09	3.72	6.23	0.00	9.31	77.91	179.95	19.79	58.80	5.80	44.62	11.66
9:30 AM	7.46	3.91	6.56	0.00	9.85	83.02	189.68	20.84	61.90	6.13	47.14	12.33
9:45 AM	7.85	4.11	6.90	0.00	10.25	85.76	197.21	21.72	64.52	6.39	49.13	12.85
10:00 AM	8.23	4.31	7.23	0.00	10.66	88.50	204.75	22.60	67.14	6.65	51.13	13.37
10:15 AM	8.43	4.42	7.41	0.00	10.99	91.39	210.96	23.29	69.19	6.86	52.69	13.78
10:30 AM	8.62	4.52	7.58	0.00	11.33	94.28	217.18	23.98	71.25	7.06	54.26	14.19
10:45 AM	8.85	4.64	7.78	0.00	11.57	96.28	221.39	24.40	72.50	7.19	55.16	14.46
11:00 AM	9.07	4.76	7.97	0.00	11.82	98.28	225.59	24.82	73.75	7.32	56.07	14.73
11:15 AM	9.16	4.80	8.05	0.00	11.92	99.39	227.58	25.05	74.41	7.39	56.62	14.87
11:30 AM	9.25	4.85	8.13	0.00	12.02	100.50	229.56	25.27	75.07	7.47	57.18	15.01
11:45 AM	9.22	4.83	8.11	0.00	11.84	98.77	231.56	25.23	74.96	7.45	57.08	14.96

Time	Menlo 1102 Summer Low day (P**art 1) [kW]**											
	B2	B3	B4	B6	B9	B11	B15	B16	B17	B18	B19	B20
12:00 PM	9.20	4.82	8.08	0.00	11.66	97.04	233.57	25.20	74.85	7.42	56.99	14.92
12:15 PM	9.12	4.78	8.01	0.00	11.69	97.33	229.07	24.98	74.23	7.36	56.52	14.79
12:30 PM	9.04	4.74	7.95	0.00	11.72	97.62	224.57	24.77	73.60	7.29	56.04	14.66
12:45 PM	8.81	4.62	7.75	0.00	11.48	95.62	220.07	24.28	72.12	7.15	54.79	14.38
1:00 PM	8.59	4.50	7.55	0.00	11.24	93.62	215.57	23.78	70.64	7.01	53.54	14.09
1:15 PM	8.37	4.39	7.36	0.00	10.95	91.37	209.72	23.09	68.59	6.80	52.10	13.66
1:30 PM	8.15	4.27	7.16	0.00	10.66	89.12	203.87	22.40	66.54	6.60	50.67	13.24
1:45 PM	7.79	4.08	6.85	0.00	10.26	85.50	195.90	21.50	63.86	6.33	48.65	12.71
2:00 PM	7.43	3.89	6.53	0.00	9.86	81.88	187.93	20.59	61.17	6.06	46.64	12.19
2:15 PM	7.06	3.70	6.21	0.00	9.26	77.40	177.84	19.50	57.94	5.74	44.11	11.55
2:30 PM	6.70	3.51	5.89	0.00	8.66	72.93	167.75	18.41	54.70	5.43	41.59	10.91
2:45 PM	6.24	3.27	5.48	0.00	8.13	68.21	156.47	17.17	51.01	5.06	38.83	10.17
3:00 PM	5.77	3.03	5.08	0.00	7.61	63.50	145.18	15.93	47.32	4.69	36.08	9.43
3:15 PM	5.28	2.77	4.65	0.00	6.94	57.04	132.69	14.57	43.28	4.27	32.97	8.59
3:30 PM	4.80	2.51	4.22	0.00	6.26	50.58	120.19	13.21	39.23	3.86	29.87	7.75
3:45 PM	4.24	2.22	3.73	0.00	5.52	45.02	106.79	11.73	34.86	3.44	26.54	6.91
4:00 PM	3.69	1.94	3.25	0.00	4.77	39.45	93.38	10.26	30.48	3.02	23.20	6.07
4:15 PM	3.11	1.63	2.73	0.00	4.10	34.06	79.59	8.76	26.01	2.64	20.30	5.31
4:30 PM	2.53	1.33	2.22	0.00	3.44	28.67	65.79	7.25	21.55	2.27	17.40	4.55
4:45 PM	2.04	1.07	1.79	0.00	2.63	22.41	51.63	5.69	16.90	1.84	14.08	3.70
5:00 PM	1.54	0.81	1.36	0.00	1.83	16.14	37.47	4.13	12.26	1.42	10.77	2.84
5:15 PM	1.18	0.62	1.03	0.00	1.28	10.97	28.68	3.13	9.30	1.02	7.83	2.06
5:30 PM	0.81	0.42	0.71	0.00	0.74	5.81	19.89	2.13	6.34	0.63	4.90	1.27
5:45 PM	0.49	0.26	0.43	0.00	0.46	3.64	12.12	1.30	3.86	0.39	2.94	0.78
6:00 PM	0.17	0.09	0.15	0.00	0.19	1.47	4.35	0.46	1.38	0.14	0.98	0.29
6:15 PM	0.12	0.06	0.10	0.00	0.14	1.12	2.95	0.35	1.05	0.10	1.00	0.19
6:30 PM	0.06	0.03	0.05	0.00	0.10	0.77	1.54	0.24	0.71	0.05	1.02	0.10
6:45 PM	0.04	0.02	0.03	0.00	0.06	0.45	0.91	0.15	0.44	0.03	0.62	0.06
7:00 PM	0.01	0.01	0.01	0.00	0.02	0.14	0.28	0.06	0.17	0.01	0.22	0.02
7:15 PM	0.01	0.00	0.01	0.00	0.01	0.07	0.14	0.03	0.09	0.00	0.11	0.01
7:30 PM	0.00	0.00	0.00	0.00	0.00	0.00	0.00	0.00	0.00	0.00	0.00	0.00
7:45 PM	0.00	0.00	0.00	0.00	0.00	0.00	0.00	0.00	0.00	0.00	0.00	0.00
8:00 PM	0.00	0.00	0.00	0.00	0.00	0.00	0.00	0.00	0.00	0.00	0.00	0.00
8:15 PM	0.00	0.00	0.00	0.00	0.00	0.00	0.00	0.00	0.00	0.00	0.00	0.00
8:30 PM	0.00	0.00	0.00	0.00	0.00	0.00	0.00	0.00	0.00	0.00	0.00	0.00
8:45 PM	0.00	0.00	0.00	0.00	0.00	0.00	0.00	0.00	0.00	0.00	0.00	0.00
9:00 PM	0.00	0.00	0.00	0.00	0.00	0.00	0.00	0.00	0.00	0.00	0.00	0.00
9:15 PM	0.00	0.00	0.00	0.00	0.00	0.00	0.00	0.00	0.00	0.00	0.00	0.00
9:30 PM	0.00	0.00	0.00	0.00	0.00	0.00	0.00	0.00	0.00	0.00	0.00	0.00
9:45 PM	0.00	0.00	0.00	0.00	0.00	0.00	0.00	0.00	0.00	0.00	0.00	0.00
10:00 PM	0.00	0.00	0.00	0.00	0.00	0.00	0.00	0.00	0.00	0.00	0.00	0.00
10:15 PM	0.00	0.00	0.00	0.00	0.00	0.00	0.00	0.00	0.00	0.00	0.00	0.00
10:30 PM	0.00	0.00	0.00	0.00	0.00	0.00	0.00	0.00	0.00	0.00	0.00	0.00
10:45 PM	0.00	0.00	0.00	0.00	0.00	0.00	0.00	0.00	0.00	0.00	0.00	0.00
11:00 PM	0.00	0.00	0.00	0.00	0.00	0.00	0.00	0.00	0.00	0.00	0.00	0.00
11:15 PM	0.00	0.00	0.00	0.00	0.00	0.00	0.00	0.00	0.00	0.00	0.00	0.00
11:30 PM	0.00	0.00	0.00	0.00	0.00	0.00	0.00	0.00	0.00	0.00	0.00	0.00
11:45 PM	0.00	0.00	0.00	0.00	0.00	0.00	0.00	0.00	0.00	0.00	0.00	0.00

Table 86. Residential (Menlo) model Summer Low day (7-2-10) time resolved PV site estimation (Part 1 of 2).

Time	Menlo 1102 Summer Low day (Part 2) [kW]											
	B24	B26	B28	B29	B31	B32	B33	B34	B35	B38	B39	B41
12:00 AM	0.00	0.00	0.00	0.00	0.00	0.00	0.00	0.00	0.00	0.00	0.00	0.00
12:15 AM	0.00	0.00	0.00	0.00	0.00	0.00	0.00	0.00	0.00	0.00	0.00	0.00
12:30 AM	0.00	0.00	0.00	0.00	0.00	0.00	0.00	0.00	0.00	0.00	0.00	0.00
12:45 AM	0.00	0.00	0.00	0.00	0.00	0.00	0.00	0.00	0.00	0.00	0.00	0.00
1:00 AM	0.00	0.00	0.00	0.00	0.00	0.00	0.00	0.00	0.00	0.00	0.00	0.00
1:15 AM	0.00	0.00	0.00	0.00	0.00	0.00	0.00	0.00	0.00	0.00	0.00	0.00
1:30 AM	0.00	0.00	0.00	0.00	0.00	0.00	0.00	0.00	0.00	0.00	0.00	0.00
1:45 AM	0.00	0.00	0.00	0.00	0.00	0.00	0.00	0.00	0.00	0.00	0.00	0.00
2:00 AM	0.00	0.00	0.00	0.00	0.00	0.00	0.00	0.00	0.00	0.00	0.00	0.00
2:15 AM	0.00	0.00	0.00	0.00	0.00	0.00	0.00	0.00	0.00	0.00	0.00	0.00
2:30 AM	0.00	0.00	0.00	0.00	0.00	0.00	0.00	0.00	0.00	0.00	0.00	0.00
2:45 AM	0.00	0.00	0.00	0.00	0.00	0.00	0.00	0.00	0.00	0.00	0.00	0.00
3:00 AM	0.00	0.00	0.00	0.00	0.00	0.00	0.00	0.00	0.00	0.00	0.00	0.00
3:15 AM	0.00	0.00	0.00	0.00	0.00	0.00	0.00	0.00	0.00	0.00	0.00	0.00
3:30 AM	0.00	0.00	0.00	0.00	0.00	0.00	0.00	0.00	0.00	0.00	0.00	0.00
3:45 AM	0.00	0.00	0.00	0.00	0.00	0.00	0.00	0.00	0.00	0.00	0.00	0.00
4:00 AM	0.00	0.00	0.00	0.00	0.00	0.00	0.00	0.00	0.00	0.00	0.00	0.00
4:15 AM	0.00	0.00	0.00	0.00	0.00	0.00	0.00	0.00	0.00	0.00	0.00	0.00
4:30 AM	0.00	0.00	0.00	0.00	0.00	0.00	0.00	0.00	0.00	0.00	0.00	0.00
4:45 AM	0.06	0.00	0.00	0.01	0.01	0.00	0.09	0.02	0.05	0.03	0.02	0.05
5:00 AM	0.13	0.01	0.01	0.01	0.03	0.01	0.18	0.05	0.10	0.07	0.04	0.09
5:15 AM	0.33	0.02	0.02	0.02	0.08	0.03	0.57	0.14	0.30	0.14	0.10	0.13
5:30 AM	0.54	0.04	0.03	0.02	0.14	0.04	0.96	0.24	0.50	0.21	0.16	0.16
5:45 AM	1.72	0.14	0.09	0.08	0.49	0.16	3.47	0.87	1.81	0.32	0.72	0.67
6:00 AM	2.89	0.24	0.16	0.13	0.83	0.27	5.98	1.50	3.12	0.43	1.28	1.17
6:15 AM	6.20	0.38	0.34	0.26	1.36	0.43	9.54	2.40	4.98	0.58	2.05	1.87
6:30 AM	9.52	0.52	0.52	0.39	1.89	0.60	13.11	3.29	6.84	0.73	2.82	2.58
6:45 AM	12.45	0.69	0.68	0.51	2.46	0.78	17.10	4.30	8.92	0.88	3.67	3.37
7:00 AM	15.38	0.85	0.85	0.63	3.04	0.96	21.09	5.30	11.00	1.03	4.52	4.15
7:15 AM	18.06	1.01	0.99	0.75	3.63	1.15	25.22	6.34	13.15	1.32	5.42	4.96
7:30 AM	20.74	1.18	1.14	0.87	4.21	1.33	29.35	7.38	15.31	1.62	6.31	5.77
7:45 AM	23.82	1.33	1.31	0.98	4.75	1.50	33.11	8.32	17.27	2.17	7.13	6.51
8:00 AM	26.90	1.48	1.48	1.09	5.29	1.67	36.88	9.27	19.24	2.72	7.94	7.25
8:15 AM	29.59	1.63	1.63	1.20	5.85	1.85	40.77	10.25	21.27	3.11	8.77	7.94
8:30 AM	32.27	1.78	1.77	1.31	6.40	2.03	44.65	11.22	23.29	3.50	9.60	8.64
8:45 AM	34.94	1.93	1.92	1.42	6.90	2.18	48.11	12.09	25.10	3.62	10.30	9.35
9:00 AM	37.62	2.07	2.07	1.53	7.40	2.34	51.56	12.96	26.90	3.74	10.99	10.07
9:15 AM	39.79	2.19	2.19	1.60	7.81	2.48	54.54	13.71	28.45	4.11	11.69	10.68
9:30 AM	41.96	2.31	2.31	1.68	8.21	2.61	57.51	14.45	30.00	4.47	12.38	11.30
9:45 AM	43.74	2.41	2.41	1.76	8.58	2.72	59.75	15.03	31.17	4.66	12.90	11.78
10:00 AM	45.51	2.50	2.50	1.84	8.95	2.82	61.99	15.60	32.34	4.84	13.43	12.25
10:15 AM	46.91	2.58	2.58	1.90	9.22	2.90	63.93	16.08	33.35	4.99	13.84	12.63
10:30 AM	48.30	2.65	2.66	1.95	9.50	2.99	65.86	16.55	34.36	5.14	14.25	13.00
10:45 AM	49.21	2.70	2.71	1.99	9.68	3.05	67.16	16.87	35.03	5.25	14.52	13.24
11:00 AM	50.13	2.76	2.76	2.03	9.86	3.10	68.45	17.18	35.71	5.36	14.78	13.48

Time	Menlo 1102 Summer Low day (P**art 2) [kW]**											
	B24	B26	B28	B29	B31	B32	B33	B34	B35	B38	B39	B41
11:15 AM	50.61	2.78	2.78	2.05	9.95	3.14	69.07	17.36	36.03	5.31	14.92	13.62
11:30 AM	51.09	2.81	2.81	2.07	10.03	3.17	69.70	17.54	36.36	5.27	15.06	13.76
11:45 AM	51.02	2.81	2.81	2.07	10.00	3.16	69.63	17.51	36.32	5.39	15.11	13.71
12:00 PM	50.95	2.81	2.80	2.06	9.96	3.16	69.57	17.49	36.29	5.51	15.16	13.67
12:15 PM	50.42	2.77	2.77	2.04	9.89	3.13	68.98	17.34	35.98	5.43	14.93	13.55
12:30 PM	49.90	2.74	2.74	2.02	9.81	3.11	68.39	17.19	35.68	5.34	14.70	13.43
12:45 PM	48.90	2.69	2.69	1.98	9.61	3.05	67.06	16.86	34.98	5.23	14.41	13.17
1:00 PM	47.90	2.64	2.63	1.94	9.41	2.98	65.73	16.52	34.29	5.12	14.11	12.91
1:15 PM	46.47	2.56	2.56	1.88	9.14	2.89	63.75	16.02	33.25	4.97	13.70	12.53
1:30 PM	45.03	2.48	2.48	1.82	8.86	2.80	61.76	15.52	32.22	4.82	13.29	12.15
1:45 PM	43.25	2.38	2.38	1.75	8.51	2.69	59.30	14.91	30.94	4.63	12.75	11.66
2:00 PM	41.48	2.28	2.28	1.68	8.16	2.58	56.85	14.29	29.66	4.44	12.20	11.17
2:15 PM	39.30	2.16	2.16	1.59	7.68	2.45	53.87	13.54	28.10	4.21	11.56	10.58
2:30 PM	37.12	2.04	2.04	1.50	7.21	2.31	50.89	12.79	26.54	3.98	10.92	9.99
2:45 PM	34.56	1.90	1.90	1.40	6.76	2.15	47.43	11.92	24.74	3.71	10.15	9.32
3:00 PM	31.99	1.77	1.76	1.29	6.31	2.00	43.98	11.05	22.94	3.44	9.38	8.64
3:15 PM	29.28	1.61	1.61	1.18	5.77	1.83	40.21	10.11	20.97	3.15	8.54	7.87
3:30 PM	26.58	1.46	1.46	1.08	5.23	1.65	36.44	9.16	19.01	2.85	7.70	7.10
3:45 PM	23.62	1.30	1.30	0.96	4.71	1.47	32.38	8.14	16.89	2.53	6.84	6.33
4:00 PM	20.67	1.14	1.14	0.84	4.19	1.29	28.33	7.12	14.78	2.22	5.99	5.56
4:15 PM	18.08	0.96	0.99	0.73	3.62	1.12	24.73	6.22	12.90	1.87	5.15	4.87
4:30 PM	15.49	0.79	0.85	0.63	3.04	0.96	21.12	5.31	11.02	1.52	4.31	4.17
4:45 PM	12.62	0.66	0.69	0.51	2.47	0.78	17.23	4.33	8.99	1.28	3.35	3.39
5:00 PM	9.75	0.53	0.54	0.39	1.90	0.61	13.34	3.35	6.96	1.04	2.40	2.61
5:15 PM	6.41	0.35	0.35	0.26	1.39	0.44	9.66	2.43	5.04	0.69	1.69	1.89
5:30 PM	3.07	0.17	0.17	0.13	0.87	0.27	5.99	1.51	3.13	0.34	0.97	1.16
5:45 PM	2.01	0.11	0.11	0.08	0.53	0.17	3.66	0.92	1.91	0.22	0.60	0.71
6:00 PM	0.95	0.05	0.05	0.04	0.19	0.06	1.33	0.33	0.69	0.10	0.23	0.26
6:15 PM	0.73	0.04	0.04	0.03	0.13	0.04	0.99	0.25	0.52	0.08	0.17	0.18
6:30 PM	0.50	0.02	0.03	0.01	0.07	0.03	0.66	0.16	0.34	0.05	0.12	0.09
6:45 PM	0.28	0.01	0.02	0.01	0.04	0.02	0.37	0.09	0.19	0.03	0.07	0.05
7:00 PM	0.07	0.00	0.00	0.00	0.01	0.00	0.09	0.02	0.05	0.01	0.02	0.02
7:15 PM	0.03	0.00	0.00	0.00	0.01	0.00	0.05	0.01	0.02	0.00	0.01	0.01
7:30 PM	0.00	0.00	0.00	0.00	0.00	0.00	0.00	0.00	0.00	0.00	0.00	0.00
7:45 PM	0.00	0.00	0.00	0.00	0.00	0.00	0.00	0.00	0.00	0.00	0.00	0.00
8:00 PM	0.00	0.00	0.00	0.00	0.00	0.00	0.00	0.00	0.00	0.00	0.00	0.00
8:15 PM	0.00	0.00	0.00	0.00	0.00	0.00	0.00	0.00	0.00	0.00	0.00	0.00
8:30 PM	0.00	0.00	0.00	0.00	0.00	0.00	0.00	0.00	0.00	0.00	0.00	0.00
8:45 PM	0.00	0.00	0.00	0.00	0.00	0.00	0.00	0.00	0.00	0.00	0.00	0.00
9:00 PM	0.00	0.00	0.00	0.00	0.00	0.00	0.00	0.00	0.00	0.00	0.00	0.00
9:15 PM	0.00	0.00	0.00	0.00	0.00	0.00	0.00	0.00	0.00	0.00	0.00	0.00
9:30 PM	0.00	0.00	0.00	0.00	0.00	0.00	0.00	0.00	0.00	0.00	0.00	0.00
9:45 PM	0.00	0.00	0.00	0.00	0.00	0.00	0.00	0.00	0.00	0.00	0.00	0.00
10:00 PM	0.00	0.00	0.00	0.00	0.00	0.00	0.00	0.00	0.00	0.00	0.00	0.00
10:15 PM	0.00	0.00	0.00	0.00	0.00	0.00	0.00	0.00	0.00	0.00	0.00	0.00
10:30 PM	0.00	0.00	0.00	0.00	0.00	0.00	0.00	0.00	0.00	0.00	0.00	0.00
10:45 PM	0.00	0.00	0.00	0.00	0.00	0.00	0.00	0.00	0.00	0.00	0.00	0.00
11:00 PM	0.00	0.00	0.00	0.00	0.00	0.00	0.00	0.00	0.00	0.00	0.00	0.00

Time	Menlo 1102 Summer Low day (Part 2) [kW]											
	B24	B26	B28	B29	B31	B32	B33	B34	B35	B38	B39	B41
11:15 PM	0.00	0.00	0.00	0.00	0.00	0.00	0.00	0.00	0.00	0.00	0.00	0.00
11:30 PM	0.00	0.00	0.00	0.00	0.00	0.00	0.00	0.00	0.00	0.00	0.00	0.00
11:45 PM	0.00	0.00	0.00	0.00	0.00	0.00	0.00	0.00	0.00	0.00	0.00	0.00

Table 87. Residential (Menlo) model Summer Low day (7-2-10) time resolved PV site estimation (Part 2 of 2).

Bus	NP [MVAR]	Control	Temp Thr [°F]		Time Thr [HH:MM]		Voltage Thr [V_{120}]			
			High (On)	**Low (Off)**	**On**	**Off**	**Low (On)**	**High (Off)**	**Mgn**	**Over-ride [min]**
5	0.6	On	-	-	-	-	-	-	-	-
10	0.9	TC w/ VO	-	-	8:00	22:00	117.5	127	3	1
13	0.6	TC w/ VO	-	-	7:00	17:30	118.25	127	3.5	2
27	0.3	Off	-	-	-	-	-	-	-	-
30	0.3	TC w/ VO	-	-	17:00	23:00	117	126	4.5	3
40	0.9	TC w/ VO	-	-	6:30	23:15	121	127	2.25	3

Table 88. Menlo Summer High capacitor settings.

Bus	NP [MVAR]	Control	Temp Thr [°F]		Time Thr [HH:MM]		Voltage Thr [V_{120}]			
			High (On)	**Low (Off)**	**On**	**Off**	**Low (On)**	**High (Off)**	**Mgn**	**Over-ride [min]**
5	0.6	On	-	-	-	-	-	-	-	-
10	0.9	TC w/ VO	-	-	8:00	22:00	118	125	2	1
13	0.6	TC w/ VO	-	-	7:00	17:30	119	126	2	2
27	0.3	Off	-	-	-	-	-	-	-	-
30	0.3	TC w/ VO	-	-	17:30	23:00	118	128	4.5	5
40	0.9	TC w/ VO	-	-	6:30	21:30	121	127	2.5	1

Table 89. Menlo Summer Low capacitor settings.

Parameter	Summer High	Summer Low
Nameplate [MVA]	16	16
Impedance [Ω%]	j0.08	j0.15
Regulation [%]	±10	±10
Steps	32	32

Parameter	Summer High	Summer Low
V_{LC} [V_{120}]	117	122
R [Ω]	1.875	2.375
X [Ω]	0	0
Band [V_{120}]	±1.4	±2
CT ratio	800:5	1300:1
PT ratio	60:1	100:1

Table 90. Menlo sub-station Load Tap Changer with Load Drop Compensator settings.

10.4 Appendix D: Acronyms

abC/DQ0	Alpha-beta/direct-quadrature
AC	Alternating Current
ACSR	Aluminum conductor steel reinforced
APEP	Advanced Power and Energy Program
APF	Active Power Filter
Band	Regulation bandwidth around V_{ideal} [$\pm V_{120}$]
BEP	Break-even point
BW	Bandwidth
C	Capacitance
CAISO	California Independent System Operator
Cayetano	Commercial high penetration PV
CPUC	California Public Utilities Commission
CT	Current transformer turns-ratio
CT	Current transformer
D_{BUS}	Percentage of System DG penetration located at the bus
DC	Direct Current
DER	Distributed Energy Resources
DF	Deficit Factor
DG	Distributed Generation
DG	Distributed Generation
DHI	Diffused horizontal irradiance
d_i	Normalized line distance of bus
DNI	Direct Normal Irradiance
E_{bus} [kWh]	Total bus energy usage
$E_{bus\ customer}$ [kWh]	Seasonal energy usage for each customer
$E_{LD,i}$	Total day energy consumed by bus
$E_{PV,i}$	Total day energy generated by bus
GC	Generation Center
GHI	Global Horizontal Irradiance
High-Pen PV	High Penetration PV
I	Current
I	Measured line current at LTC [A]
I/CT	Sub-station current measurement
I_{CAP}	Capacitor current
I_{DG}	Load generation current
I_{DS}	Downstream current
IEEE	Institute of Electrical and Electronic Engineers
IGBTs	Insulated gate bipolar transistors
I_{LD}	Load Current
I_{LD}	Complex load demand current
I_{PV}	PV generation current
I_R	Real current component
I_R	In-phase current

I_X	Reactive current component
I_X	Out-of-phase current
$j_{S/S}$	Sub-station upstream index
K	X/R transformer impedance ratio
LC	Load Center
LC/GC→0	Load distribution is upstream from the generation
LC/GC→1	Load distribution is closer to the generation during extended RPF
LC/GC→∞	Load distribution is located downstream of the generation
LDAF	Load Demand Allocation Factor
LDAF	Load demand allocation factor
LDC**	Load Drop Compensation
LD_E	Total load demand energy for a typical day
$LD_{E,HIGH}$	Load demand energy of a characteristic High day
$LD_{E,LOW}$	Load demand energy of a characteristic Low day
LL_E	Interpolated loss of typical day
$LL_{E,HIGH}$	Line loss energy of a characteristic High day
$LL_{E,LOW}$	Line loss energy of a characteristic High day
LTC	Load tap changing
LTC	Load Tap Changing
LVR	Local voltage regulation
Menlo	Residential high penetration PV
MIMO	Multiple-input, multiple-output
MOSFETs	Metal-oxide semiconductor field effect transistors
NOTC	Normal Operations Temperature Celsius
NPF	Normal power flow
NRMSE	Normalized Root Mean Square Error
P	Real power
P_{CAP}	Capacitor real power
P_{DG}	Generation capacity
P_{EC}	Excess generation capacity
$P_{EC,USj}$	Excess capacity at each upstream bus
PEN	DG bus penetration
PF	Power factor
PFC	Power Factor Correction
PG&E	Pacific Gas & Electric
PI	Proportional-integral
P_{LD}	Load demand real power
P_{ld}	Real power load demand
P_{LD} [W], Q_{LD} [var]	Total system LD
$P_{LD,bus}$ [W], $Q_{LD,bus}$ [var]	LD for each bus
$P_{LD,DG}$	DG bus load demand
$P_{LD,DS}$	DG bus load demand downstream
$P_{LD,init}$	Power initial estimate
$P_{LD,lcl}$	Local DG load demand

$P_{ld,sim}$	Simulation load power
P_{LL}	power consumed by the line and turned into heat; real component
PLL	Phase-locked loop
P_{loss}	Power loss component
P_{max} %/^{o}C	Power de-rating temperature coefficient
P_{PK}	circuit-wide peak real power load demand
P_{PV}	PV generation real power
P_{PV}	PV generation real power
PR	Proportional-resonant
PT	Potential Transformer turns-ratio
PT	Potential transformer
PV	Photovoltaic
PWM	Pulse-width modulation
Q	Reactive power
Q_{CAP}	Reactive capacitive power
Q_{CAP}	3-phase rating of capacitor bank [kVAR]
Q_{CAP}	3-phase rating of capacitor bank [kVAR]
Q_{CAP}	Capacitor reactive power
QCLCD	Quality Controlled Local Climatology Database
Q_{LD}	Load demand reactive power
Q_{ld}	Reactive power load demand
Q_{PV}	PV generation reactive power
R	Resistance
R	Transformer resistance [Ω]
R	Resistance to load center [Ω]
Regulation	Total voltage regulation percentage [±%]
RPF	Reverse power flow
RPF_{PEN}	DG penetration to induce reverse power flow
RPF_{PEN}	RPF penetration
RPF_{PT}	Upstream index of the farthest upstream bus experiencing reverse power flow to from the DG bus
RPF_{R}	Line resistance between the DG bus and upstream bus at the RPF_{pt} index
$RPF_{R,0}$	DG's upstream distribution current
$RPF_{R,NORM}$, $RPF_{R0,NORM}$	Normalization factors
$R_{S/S}$	Resistive impedance
S	Apparent power
$S_{3\phi}$	Three-phase nameplate transformer rating [VA]
SCADA	Supervisory Control and Data Acquisition
SISO	Single-input, single-output
S_{LD}	Complex load demand power
S_{PQ}	Apparent power calculated using real and reactive power
S_{PV}	PV generation complex power
STATCOM	Reactive power compensation

Steps	Total allowable taps of LTC
SVC	Static variable compensator
S_{VI}	Apparent power calculated using voltage and current
Tap	Regulation coil tap position in LTC
Tap_{Range}	Tap range of LTC
TC	Time-clock
Temp	Temperature
$Thr_{High\ VAR}$	High VAR threshold [kVAR]
$Thr_{Low\ VAR}$	Low VAR threshold [kVAR]
UCI	University of California, Irvine
UL	Underwriters Laboratories
V	Measured line-to-neutral voltage at LTC [V]
VAR	Volt-amp reactive
V_{base}	System voltage
V_{DG}	DG bus voltage
V_I	Reactive voltage component
V_{ideal}	Ideal LTC voltage to achieve VLC [V_{120}]
V_L	Load
V_{LC}	Load Center Voltage [V_{120}]
VLC	Load center voltage
V_{LL}	Line-to-Line voltage [kV]
$V_{LL,H}$	Transformer high-voltage line-to-line nameplate voltage rating [V]
$V_{LL,X}$	Transformer low-voltage line-to-line nameplate rating [V]
V_{LN}	Line-to-neutral voltage
VO	Voltage override
VO	Voltage override
V_{pu}	Per unit voltage
V_R	Real voltage component
V_{rise}	The estimate percentage voltage rise from capacitor [%]
VRS	Voltage rise score
V_S	Sub-station
V_{Step}	Voltage per tap step [V_{120}]
V_{US}	Upstream voltage
V_{US}	Upstream bus voltage
X	Reactance
X	Transformer reactance [Ω]
X	Reactance to load center [Ω]
X_L	Positive Sequence impedance from source to capacitor [Ω]
$x_{SCADA,max}$	The day maximum SCADA measurement
$x_{SCADA,min}$	The day minimum SCADA measurement
$x_{SCADA,t}$	The SCADA measurement at time “t”
$x_{SIM,t}$	The simulation result at time “t”
Z	Transformer impedance magnitude [Ω]
Z%	Percentage transformer voltage drop at full load

Z_{LN}	Line impedance
Z_{LN}	Line impedance
δ	Phase angle
ΔV	Voltage drop
ΔV	Voltage drop
ΔV_{DG}	Percentage of voltage rise at the DG bus over the adjacent upstream bus
$-\theta$	Inductive
σ_{GC}	Standard deviation of the generation center
σ_{LC}	Standard deviation of the Load Center